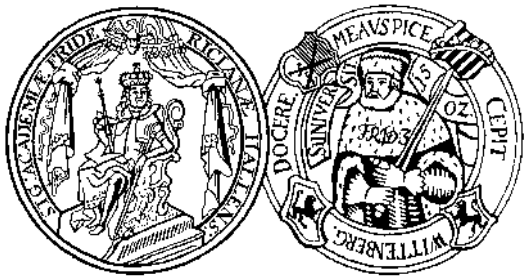

Controlling the location of polymer functionalized (CdSe) nanoparticles in mixed lipid/polymer membranes

Dissertation

Zur Erlangung des akademischen Grades
Doctor rerum naturalium (Dr. rer. nat.)

vorgelegt der

Naturwissenschaftlichen Fakultät II
der Martin-Luther-Universität Halle-Wittenberg

von

Adekunle A. Olubummo

ausgeführt unter der Leitung von

Prof. Dr. Wolfgang Binder
Professor für Makromolekulare Chemie
Martin-Luther-Universität Halle-Wittenberg

Gutachter:
1. Prof. Dr. Wolfgang H. Binder
2. Prof. Robson F. Storey

Verteidigungstermin: 18.07.2014 Halle (Saale), den 15.01.2014

Abbreviations

AIBN	- Azobisisobutyronitrile
AuNPs	- gold nanoparticles
BCPs	- block copolymers
BPB	- bromo propoxy benzene
CdSe	- cadmium selenide
CdTe	- cadmium telluride
$CHCl_3$	- chloroform
DCM	- dichloromethane
DCTB	- *trans*-2-(3-(4-*tert*-butylphenyl)-2-methyl-2-propenylidene) malononitrile
DIPEA	- *N*,*N*-diisopropylamine
Dithranol	- 1,8-dihydroxy-10*H*-anthracen-9-on
DMA	- *N*,*N*-dimethylacetamide
DMAP	- 4-(dimethylamino) pyridine
DMF	- dimethyl formamide
DMPC	- 1,2-dimyristoyl-sn-glycero-3-phosphocholine
DOPC	- 1,2-dioleoyl-sn-glycero-3-phosphocholine
DPPC	- 1,2-dipalmitoyl-sn-glycero-3-phosphocholine
DPPG	- 1,2-Dipalmitoyl-sn-glycero-3-phospho-rac-(1-glycerol)
DtBp	- 2,6-di-*tert*-butylpyridine
EDC.HCl	- 1-ethyl-3-(3-dimethyllaminopropyl)carbodiimide hydrochloride
Et_2O	- diethyl ether
LiTFA	- lithium triflouroacetate
MCPBA	- meta-chloroperbenzoic acid
MeOH	- methanol
MSE	- methyl styrene epoxide
NaTFA	- sodium triflouroacetate
NHS	- N-hydroxysuccinimide
NPs	- nanoparticles
PBr_3	- phosphorus tribromide
PEO	- poly(ethylene oxide)
PIB	- poly(isobutylene)
PO	- phosphine oxide
QDs	- quantum dots
SLBs	- supported lipid bilayers
TBTA	- tris[(1-benzyl-1*H*-1,2,3-triazol-4-yl)methyl]amine
THF	- tetrahydrofuran
THY	- thymine moiety
TOPO	- trioctylphosphine oxide
TRI	- triazine moiety
USPIO	- ultra small superparamagnetic iron oxide

1.0 Introduction

1.1 Lipid and polymer membranes

1.1.1 Introduction to lipid and polymer membranes

Amphiphilic compounds (such as lipids or block copolymers) in their structural morphology feature at least a fraction or a block which is hydrophilic (*i.e. having affinity towards water)* whereas the other fraction or block is hydrophobic which *segregates* itself from water.[1] The preparation of vesicular structures from amphiphilic block copolymers in selective solvents (which was pioneered by Eisenberg and Discher) are frequently referred to as polymersomal membranes,[2] whereas vesicles fabricated from the self-assembly of lipids in water or buffer solutions are called liposomal membranes[3] as shown in **Figure 1**.

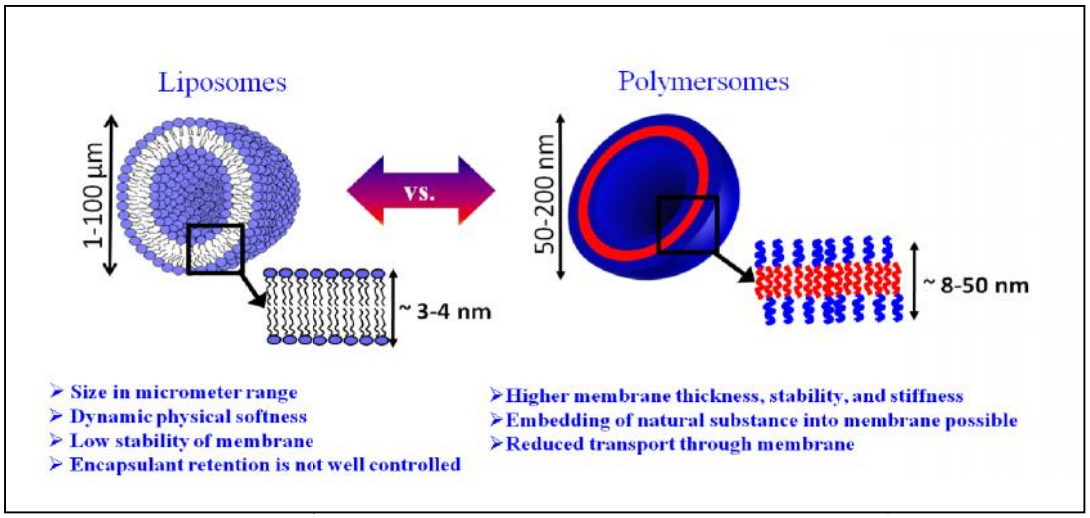

Figure 1. Schematic diagram comparing the properties of liposomes and polymersomes.

Lipid membranes (e.g. liposomes) which function as barriers between subcellular compartments as well as between the cell and its surrounding environment is made up of aggregation of more than 100,000 small amphiphiles (having molecular weight less than 1 kD) into a molecularly thin membrane. Thereby manifesting itself in a dynamic, physical softness. Consequently, lipid vesicle properties such as encapsulant retention, membrane stability are not well controlled. Due to this limitation, scientists have synthesized and studied artificial membranes made of synthetic block copolymers (so called polymersomes). As illustrated in **Figure 1**, block copolymers (BCPs) displaying a similar amphiphilic character as lipid molecules,[4] allow similar chemical properties of a membrane, further expanded by chemically tuning the respective blocks of the

block copolymer. When compared to liposomes, polymersomes show a higher mechanical and thermal stability within their curved membrane, and thereby enable the embedding and precise positioning of significant amount of hydrophobic molecules like nanoparticles into their hydrophobic membrane interior.[5-7]

Depending on their molecular architecture and on other parameters, such as temperature, hydrophobic to hydrophilic balance, pressure, pH and the presence of non-amphiphilic additives such as metal ions, numerous morphologies of amphiphilic molecules such as micelles, vesicles, tubules have been found.[3] The shape (geometry) of self-assembled polymersomes is determined by the size of the hydrophobic block and described by a packing parameter $P = v/al_c$, where v is the volume of the densely packed hydrophobic segment, a is the area occupied by the hydrophilic group, and l_c is the chain length of the hydrophobic segment.[8] When P is less than 1/3, spherical micelles are formed, and when P is between 1/3 and 1/2, cylindrical micelles are observed, whereas when P is between 1/2 and 1 vesicles are formed.

Over the years, research performed on liposomes and polymersomes have shown them to emerge as important materials for mimicking natural cellular membrane, and as a consequence, they are interesting tools for the understanding of various cellular processes like therapeutic encapsulation, delivery of active ingredients[9,10] and in the design of artificial cells and organelles.

1.2 Interaction of nanoparticles with lipid membranes

The interaction of functional nanoparticles with lipid or polymer membranes can influence such important aspects as intercellular uptake,[11] drug and gene delivery,[12] localization of the nanoparticles at specific positions of the membrane or within cellular compartment[6] and their biological/biomedical application with minimal cytotoxicity. Because of their flexibility and high elasticity, lipid membranes can easily be deformed when nanoparticles interact with them, either by insertion or *via* adsorption onto their surface **Figure 2A** to **C**. Interaction between nanoparticles and lipid membranes induces chain stretching of the lipids near the site of interaction,[13] nanoparticle induced spontaneous curvature of the membrane,[14] changes in lipid packing[15] and other macroscopic effects such as pearling[16] **Figure 2D**.[17]

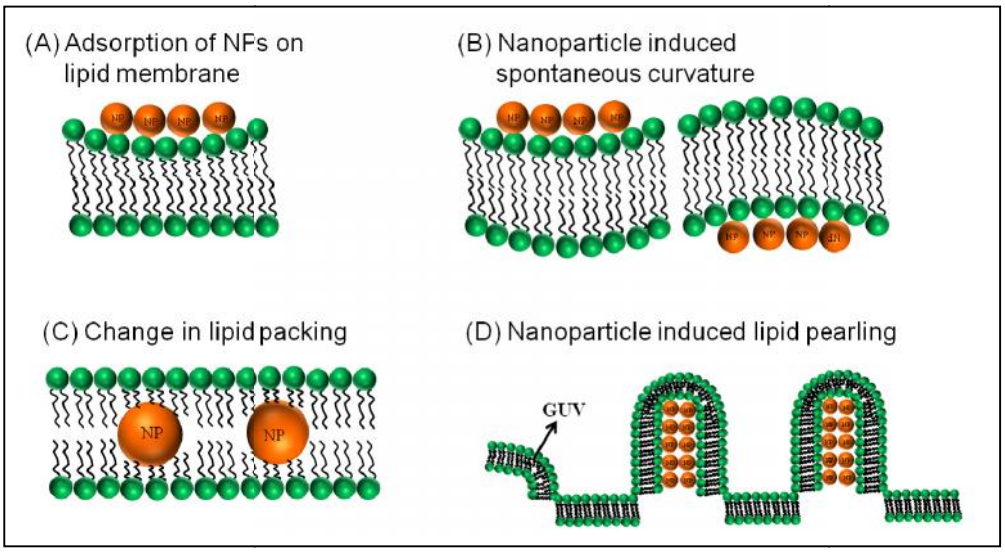

Figure 2. The interaction of nanoparticle with lipid membranes (A) adsorption of nanoparticles on lipid membrane (B) nanoparticle induced spontaneous membrane curvature (C) change in lipid packing (D) nanoparticle induced lipid pearling

1.2.1 Interaction of hydrophobic nanoparticles with lipid membranes

The degree of membrane disruption caused by nanoparticles (e.g. hole formation, and membrane thinning), can be measured by the level of enzyme leakage,[18] dye diffusion, cytotoxicity, nanoparticle uptake (measured *in vitro*)[19] and the degree of nonselective tissue uptake.[20] The following sections will focus on how nanoparticles interact with lipid membranes with regards to nanoparticles surface hydrophobicity, effect of the nanoparticles charge, size effect, and their shape (i.e. being round shaped or tubular).[17]

Hydrophobicity plays a very important role when dealing with the interaction of nanomaterials with lipid membranes, as nanoparticles assembly and lipid stabilization is essentially driven by hydrophobic/hydrophilic (interfacial) effects.[21] Upon interaction of NPs with lipid membranes, numerous theoretical studies and computer simulation have found that morphological reorganization and hole formation strongly depend on the surface hydrophobicity or hydrophilicity of the interacting NPs.[22,23] In principle, a nanoparticle can be encapsulated into a liposome, being either trapped within the aqueous vesicle core or embedded within the hydrophobic lipid bilayer part. Embedding of functional hydrophobic nanoparticles within a lipid bilayer provides a plethora of different applications for controlling bilayer permeabilization, biocompatibility and liposomal release, also useful for investigating

biochemical reactions *in vitro*[17]. In order to embed NPs into the hydrophobic membrane interior, the nanoparticles must fulfil two requirements. Firstly, the NP must be small enough (<8 nm) to fit within the bilayer dimension and secondly, it must possess a hydrophobic surface. Modifying the surface of nanoparticles with a hydrophobic or hydrophilic moiety will thus direct the location of the nanoparticles either onto the surface or within a specific compartment of the membrane.[6] In one of the first successful examples of NP incorporation into lipid membrane,[24] lipid/hydrophobic CdSe nanoparticle hybrid vesicles were prepared using the solvent rehydration method, where a solution of trioctylphosphine oxide (TOPO) coated CdSe QDs and lipids in chloroform was dried to form a multilamellar lipid film, from which vesicles are spontaneously formed by hydration with water[17]. Embedding of such hydrophobic nanoparticles into DPPC lipids vesicles can suppress their pretransition temperature (T_p = 36 °C describes the transition from ordered gel (L_b) to rippled gel (P_b) phase) by shifting it to higher temperatures,[25] and also lead to a controlled release of liposomal content, having more prominence with increased nanoparticle loading. As a result of the reduction in lipid ordering caused by the embedded nanoparticles, the melting temperature of the liposomal membrane can be lowered with an additional increase in the bilayer fluidity at high lipid to nanoparticle ratio (more than 15:1 w/w).[26]

The enrichment of hydrophobic nanoparticle within the lipid bilayer interior has been explained as a result of nanoparticle interaction with the hydrophobic tails of the lipid molecules **Figure 3A**.[27] Hydrophobic nanoparticles can cause the bilayer to "unzip'' when they are located at the center, leading to changes in lipid packing and disruption of lipid-lipid interactions between the head groups and/or acyl tails[17]. When two nanoparticles are present in the bilayer, the total membrane curvature is reduced as a result of the present nanoparticles as shown in **Figure 3B**.[28] This unzipping creates void space around the nanoparticle resulting in nanoparticle clustering and minimization of the free energy of deformation **figure 3C.**

As it remains unknown how and to what extent NP surface hydrophobicity induces disruption and pore formation of the lipid bilayers, it can be explained[29] that the disruption of supported lipid bilayer was noticed above a critical NP hydrophobicity and concentration (c* ~ 3 nM). Semi hydrophobic nanoparticles (cPS-NPs with hydrophobic polystyrene displaying an ionizable end-group) were found to readily adsorb on α-PC bilayers and drag lipids from the bilayer leading to the formation and growth of lipid-poor regions referred to as pores or holes. Hydrophobic attraction can facilitate the formation of patched lipid bilayers on large NPs which can further enhanced the formation and growth of lipid-poor regions on SLBs.[17]

Proof to this observation was obtained by theoretical coarse-grained lipid models,[30] where 10 nm hydrophobic nanoparticles were included into lipid membranes leading to a lateral distribution of lipids around the nanoparticle inclusion, which is generally referred to as hydrophobic "mismatch". In contrast semi-hydrophilic (apolar) nanoparticles were observed to adsorb on the surface of the lipid bilayer because of the substantial energy barrier needed to be subdued for the wrapping process.[17]

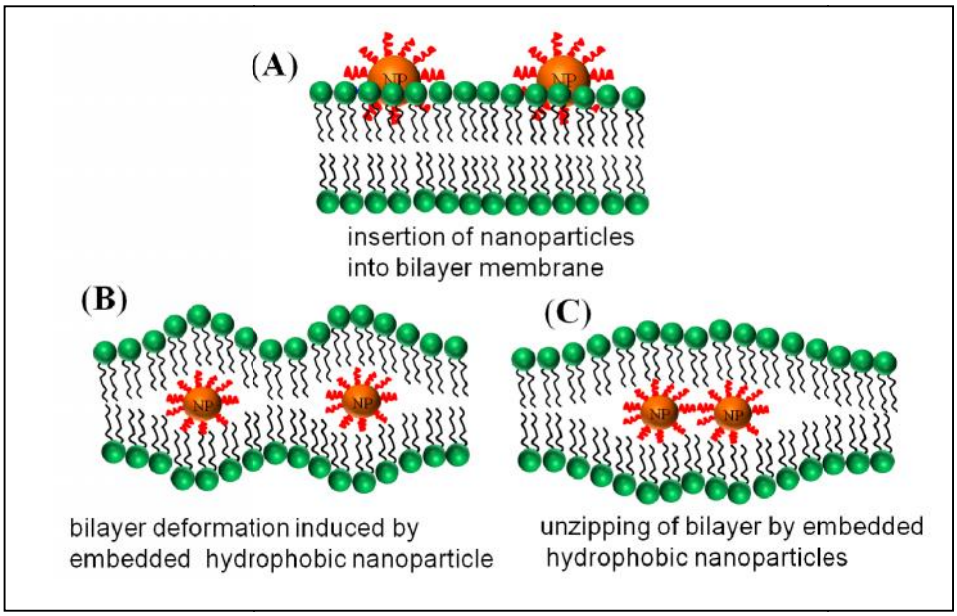

Figure 3. Membrane-interaction with hydrophobic nanoparticles (A) insertion of a hydrophobic nanoparticle into a lipid bilayer (B) induced membrane deformation and (C) ''unzipping'' of the bilayer.

1.2.2 Interaction of surface charged nanoparticles with lipid membranes

Besides adsorption of nanoparticles on lipid membranes, the exposure of membranes to nanocrystals like iron oxide, CdSe and gold bearing a significant surface charge can lead to severe membrane disruption effects induced by such charged nanoparticles, which in turn can result in enhanced porosity of the cellular membrane.[31] Disruption events, namely nanoscale hole formation, membrane thinning and differences in the packing density of lipids in close proximity to regions where the nanoparticles are adsorbed are some of the main described disruption effect of charged nanoparticles see **Figure 4**. In model membrane, such disruption events have been explored by using oriented circular dichroism,[32] molecular modeling[33] and atomic force microscopy.[34] Disruption events of living cells by charged nanoparticles are analyzed using cytosolic enzyme leakages, dye diffusion assays and fluoresence micropcopy.

As a consequence of the nanoparticle interactions with lipid membrane, the molecular packing of the bilayer is disrupted. The lipid chains respond to this disruption by stretching in order to maintain the molecular space filing requirement of the lipid bilayer and eliminate voids. Membrane thinning is an energetically unfavorable processes, which at higher nanoparticle dosage, may result in the formation of pores.[17]

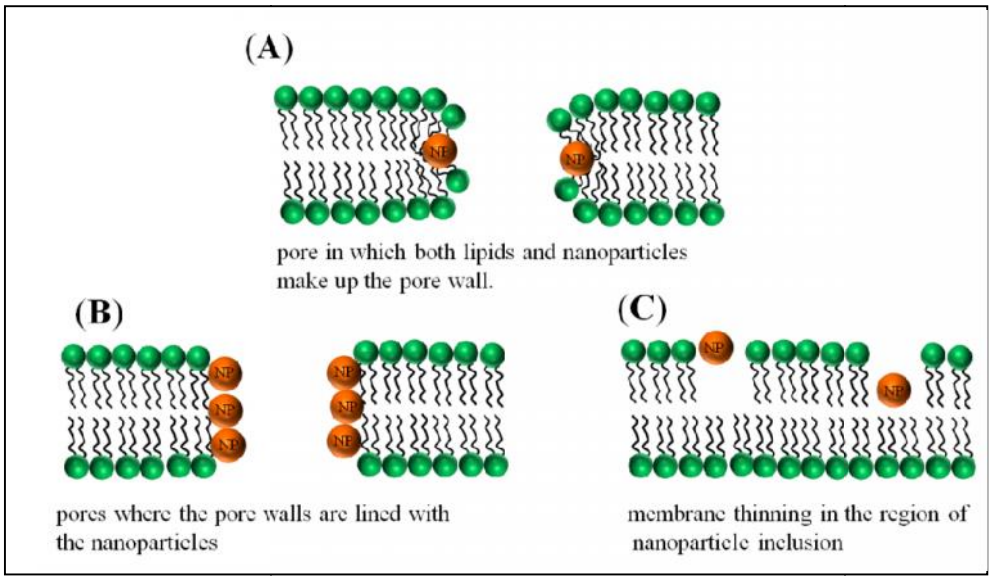

Figure 4. Illustration of the interaction of lipid membranes with charged nanoparticles (A) pore formation in lipid membrane by cationic nanoparticles where both, the lipids and the nanoparticles forms the pore wall. (B) pore formation in lipid membrane by nanoparticles where the pore walls are lined with the nanoparticles. (C) lipid membrane thinning at regions of nanoparticle inclusion.

In contrast to uncharged particles (which prefer to remain in the aqueous phase), charged nanoparticles induce membrane deformation and influence the density distribution of the lipid head groups driven by electrostatic interactions.[35] Cationic nanoparticles interact with the phosphate terminus of the lipid by increasing the tilt angle, thus enlarging the area of the head groups and altering the bilayer surface texture. As a result, cationic nanoparticles (AuNPs) are more disruptive to negatively charged lipid vesicles than their anionic counterparts.[36] This disruptive effect of cationic nanoparticles depends on the number of positive charges on the nanoparticles surface.

Positively charged nanoparticles can also induce flipping of membrane areas leading to particle inclusion and membrane depolarization (*i.e.* decrease in membrane potential).[37] The extent of

membrane depolarization caused by nanoparticle is dependent on nanoparticle concentration with minimal depolarization at 10 nM and substantial depolarization at 1.2 μM. The presence of functional groups (e.g silanol) on the surface of cationic nanoparticles can significantly contribute to the driving force responsible for their strong attraction with giant unilamellar vesicle membrane.[38] The increased affinity of the nanoparticles to the membrane as a result of the silanol groups could increase the tilt angle of the membrane head group which in turn leads to an enhancement of phospholipid density and subsequently to membrane stiffening. In contrast to cationic nanoparticles, experiments[35] have shown that anionically charged nanoparticles induce the formation of increased densities of the lipids around the nanoparticles by interacting with the positively charged head group of the lipid, thereby causing a reduction in the tilt angle of the lipid's head group.[17]

In addition to the above mentioned effects, membrane fusion is another effect caused by charged nanoparticles. When liposomes are aggregated by oppositely charged NPs, the interliposomal contact ensures that they can cling and fuse to form larger vesicles, also inducing membrane fusion.[39] Simulation, as well as calorimetric and fluorescence studies have demonstrated that membranes formed from single component phospholipid bilayer can switch their local phase state upon binding of charged nanoparticles.[40] Anionic (negatively charged) carboxyl-modified nanoparticles induce local gelation as a result of shrinkage of initially fluidic liposomes.[17]

1.2.3 Effect of nanoparticle size on interaction with lipid membranes

Despite the intense research effort into the field of cellular uptake of nanoparticles, it remains uncertain how NP's size relates to the extent of membrane disruption or the structure and morphology of nanoparticles lipid assemblies. Smaller dodecanethiol capped gold nanoparticles (~ 5.7 nm) in the proximity of a lipid bilayer can embed directly within the bilayer, while larger gold particles were capped and dispersed in the aqueous phase by a lipid monolayer bringing the alkyl tails of the lipid in contact with the decanethiol tails.[26] To further study the effect of nanoparticle size on lipid membranes Roiter and his group members[41] investigated the interaction of DMPC with small (< 22 nm) and large (> 22 nm) nanostructured silica nanoparticles formed on a silica surface using AFM. They observed that small nanoparticles form a hole in the lipid bilayer, whereas larger nanoparticles are mostly covered with the lipid bilayers as a whole. A critical particle diameter $d_0 \approx 22$ nm was defined for a transition between

the envelopment and the free state of a particle (with $d_0 \approx 3\lambda$ where λ is a specific length of the membrane as defined by the bending modulus and the adhesion constant). This size effect has been determined by measuring the bilayer current in the presence of nanoparticles,[42] using 50 nm and 500 nm aminated silica nanospheres in contact with DOPC bilayer. The bilayer disruption effect of these silica nanospheres was significantly more pronounced for the 500 nm sized particles.[17]

As demonstrated by calculations,[43] smaller, interacting nanoparticles will cause a curving-away of the membrane from the nanoparticles, whereas in the case of small, non-interacting nanoparticles the membrane will curve towards the nanoparticles. Non-anchored particles may be repelled from or attracted towards the membrane surfaces. If these particles are repelled from the membranes, depletion layers are formed in front of these membranes which increase the excess free energies of the membrane/water interfaces. In such a situation, the membranes bend towards the particle solution in order to decrease the size of the depletion zone.

On the other hand, if relatively small particles are adsorbed onto the membrane, the Gibbs adsorption equation implies that the membrane tends to bend away from the particle solution in order to increase its area.[44] With larger nanoparticles, inclusion effects and the formation of fission and budding structures[45] could be derived. Based on the bilayer phase behavior, it was demonstrated that it may be possible to embed nanoparticles that have a diameter in proximity to, or exceeding the thickness of the bilayer, which is consistent with the numerical simulation.[22]

When dendrimers (which can be seen as small nanoparticles) in noncytotoxic concentrations were interacting with lipids an enhanced porosity with important implication for drug and gene delivery was observed. Using AFM and conductance measurements,[46,47] it was shown that generation 5(G5) and generation 7(G7) amine terminated dendrimers induce holes in the membrane and/or expands the already existing holes, while uncharged (hydrophobic) dendrimers can only absorbs onto the outer membrane surface. It was further observed that such created holes led to dendrimer internalization into cells and diffusion of cytosolic proteins out of cells. Interaction of cationic phosphorous containing dendrimer (CPD) with DMPC/DPPG was also studied using differential scanning calorimetry.[48] It was observed that CPDs alter the thermotropic behavior of the bilayer by reducing the cooperativity of phospholipids which depends on the surface charge of the membrane (i.e. the incorporation of a negative charge into the membrane makes the dendrimer interact with only the hydrophilic part of the membrane.[17]

1.2.4 The effect of carbon nanoparticles (fullerene, carbon nanotubes) on lipid membranes

Since the discovery of fullerene (C_{60}) in 1985,[49] lots of research activities have been directed towards its use in biomedical technology, such as x-ray contrast agents,[50] inhibitors to allergic responses,[51] transport of electrons across the host lipid membranes,[52] and as robust ant-HIV drugs.[53] It is therefore important to fully understand how fullerene interacts with the bilayer membrane in order to habituate them for the above mentioned biomedical applications. Toxicology studies on fullerene molecular aggregates suggest that they can enter cells, alter their functions and also cross the blood brain barrier. However, the mechanisms by which fullerenes penetrate and disrupt cell membranes are still poorly understood.[54] Coarse grained and molecular dynamic simulation[55, 56] have been employed for studying the interactions of both hydrophobic pristine C_{60} and its various derivatives with a DPPC bilayer. It was shown that the number of polar groups on the surface of C_{60} affects the nature of fullerene/bilayer interaction which in turn can range from partitioning into the bilayer to adsorption onto the bilayer surface.[17] The pure C_{60} enters the hydrophobic bilayer core and remains inside. In contrast, more polar derivatives of fullerenes enter rapidly into the bilayer from the aqueous phase, but were found to be partitioned close to the head group/tail interface of the bilayer. The amphiphilic C_{60}-molecule is oriented such that the hydrophobic surface interacts with lipid tails, while its polar surface interacts with the lipid head group.

Fullerene has been reported to suppress the phase transition of DPPC bilayers, resulting in a ripple-like in-plane bilayer ordering across the lipid bilayer with an enhanced correlation along the bilayer plane.[57] The bilayer ordering indicates that C_{60} can be better accommodated into the host bilayer in the liquid crystalline state. Unlike small, hydrophobic solutes, it has been shown[58] that larger, non-hydrophobic fullerene prefers to be situated off the center plane of a hydrated DMPC membrane, which optimizes the dispersion interactions between the atomically denser fullerene surface and the relatively dense atomic environment. This tendency to be situated off the bilayer center was mediated by the distortion of the bilayer structure by the fullerene, which is induced as the fullerenes begin to aggregate.

1.3 Location and interaction of nanoparticles within polymer membranes

Polymersomes as synthetic analogues to liposomes have attracted considerable attention due to their increased thickness, rigidity and stability.[3,59] In general, the interaction of nanoparticles and block copolymer vesicles has been shown to offer a convenient way to control the arrangement of nanoparticles in polymer films by segregating nanoparticles into a favorably interacting polymer domain or at the interface between two polymers.[60,61] Morphological changes of block copolymer assemblies can be induce by the incorporation of nanoparticles which play an active role in the self assembly of block copolymers into membranes than rather being passively incorporated in the polymer matrix.[62] This nanoparticle induced self assembly structure of the polymer is generally controlled by solvent-nanoparticle and polymer–nanoparticle interactions. Thus, NP interaction is enabled to occur in one of three ways: either the NPs are internalized into the central hydrophobic position of the membrane, or they aggregate a the interface (core-shell polymersomes), or they form purely micellar aggregates.[63] Two main approaches have been reported in the literature for the incorporation of nanoparticles into block copolymer aggregates. The first involves an *in-situ* process where transition-metal ions are bound or adsorbed onto monomer that can subsequently be polymerized via a living mechanism e.g (norbonene via ROMP),[64] or binding of nanoparticle precursors to preformed block copolymers followed by a chemical reaction that will induce the growth of the nanoparticles after the block copolymer has been formed into a micelle or a vesicle.[65] The second involves an *ex-situ* process where nanoparticles are synthesized with specific organic chains on the surface via the grafting from or grafting to method followed by the co-assembly of the nanoparticles and the block copolymers.[66,6] In the literature,[67,68,69] hydrophobic nanoparticles were successfully enclosed inside the hydrophobic compartment of vesicle prepared from poly(butadiene)-*b*-poly(ethylene oxide) or polyisobutylene in a PIB_{75}-*b*-PEO_{52} block copolymer, having affinity to the hydrophobic polyisobutylene domain. The quantum dots located between the hydrophobic poly(butadiene) layers introduced curvature of the copolymer layer around the guest particles (**Figure 5A**). Eisenberg and Mai[70] have shown that nanoparticles can be selectively incorporated into the central portion of block copolymer vesicle walls by coating the particles with diblock copolymers of a structure similar to that of the diblock copolymers used in forming the polymersomes, which allows the particles to be preferentially localized in the central portion of the walls (**Figure 5C**).

To prepare stable polymersomes containing embedded nanoparticles, it has been found[71] that the mass ratio $r = m_n/m_p$ of nanoparticles m_n, to polymer, m_p should be less than acritical ratio $r^* \approx$ 0.2 to 0.3, otherwise polymer/nanoparticle agglomerates will be formed. This aggregation effect was observed by Lecommandoux[72] when investigating the incorporation of hydrophobic iron oxide nanoparticles into vesicle-forming polybutadiene-*b*-poly(glutamic acid) block copolymers. A rather aggregated but still hollow, vesicle-like structure was observed, which was deformable in external magnetic fields. Several factors such as the nanoparticle surface functionality and the hydrophobic/lipophilic balance determined the location of the nanoparticles in the polymersomal membrane. Hydrophobic nanoparticles with a hydrophilic/lipophilic balance (HLB) between that of the hydrophobic phase (PI) and the hydrophilic phase (PEO/water) will preferentially segregate to the hydrophilic/hydrophilic interface with a penetration depth into the hydrophobic domain depending on its HLB value.[71] The nanoparticles decorate the interface of the polymersomal membrane, which can induce the formation of bridges from one bilayer to an adjacent bilayer, leading to bilayer pairing (see **Figure 5B**).

It has been reported[73] that BCP vesicular bilayers composed of nanoparticles can undergo a morphological transition into the coexistence of spherical micelles and bilayers in water depending on the NP volume fraction. This structural transformation occurs through the budding process caused by clustering of the embedded nanoparticles. The driving force for this budding process was attributed to the increased entropy of polymer strands surrounding the nanoparticle aggregates due to the excessive stretching of polymers at the edge of NP aggregates.

Hydrophobic surface functionalized nanoparticles have been reported to increase membrane thickness (from 2.4 nm to 6.1±1.3 nm) of polymersomes prepared from PEO-*b*-PBO because they interact with the hydrophobic domain of the polymer during the self assembly.[74] Increased functionality and enhanced mechanical strength of polymersomes can be introduced by embedding of nanoparticles into their curved membrane.[66] The surface of positively charged polymer vesicles was covered with negatively charged (~ 24 nm) silica nanoparticles using electrostatic attractions as the driving force.[75] The nanoparticles adhered to the outer surface of polymersomes made of poly (n-butylmethacrylate)-*b*-poly(ethylene oxide) without affecting the hollow bilayer, thereby increasing the overall rigidity and altering the permeability of the polymersomes rendering them potentially useful for the uptake and release of drugs.[17]

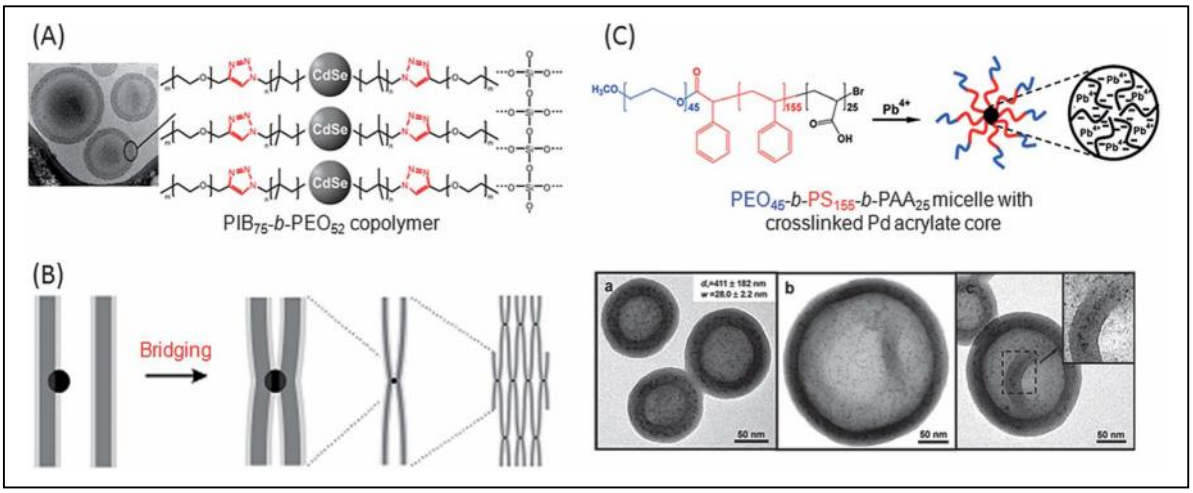

Figure 5. (A) The inclusion of CdSe nanoparticles into the central portion of vesicles made from PIB-*b*-PEO. (C) Schematic illustration of the preparation of diblock copolymer coated nanoparticles and TEM micrographs of vesicles with the incorporated nanoparticles prepared from the combined solution of the PS_{235}-*b*-PEO_{45} copolymer (0.5 wt%) and PEO_{45}-*b*-PS_{155}-*b*-$P(APb)_{25}$ micelles (0.5 wt%). In (a) small vesicles; (b) a large vesicle; (c) an indented vesicle with the magnified indentation of the vesicle membrane is shown. (B) Scheme of nanoparticle-induced bilayer pairing and bridging. The nanoparticles are located in the hydrophobic/hydrophilic interface[17]. (A) Reprinted from ref. [7], copyright 2008, Wiley-VCH Verlag GMbH & Co. KGaA, Weinheim. (B) Reprinted with permission from ref. [71], copyright 2008, American Chemical Society. (C) Reprinted with permission from ref. [70], copyright 2010, American Chemical Society.

1.4 Biological impact of nanoparticle/membrane interactions

The interaction of nanoparticles with biological systems has become one of the most significant areas of research in material science, because the exposure of human beings to nanoparticles is inevitable and therefore a deeper comprehension of the potential risk and hazard is necessary. The dissertation will not go into a detailed discussion about nanoparticle interactions with cell and the eventual toxicological impact of nanoparticles, as this issue has been reviewed by different authors, such as Stellacci,[76] Brayner,[77] Ren,[78] and Drezek.[79] However, it should be emphasized that smaller nanoparticles with a diameter of tens of nanometres or less are consistently more toxic than larger analogues with a diameter of hundreds of nanometers. Thus various authors have shown that the cytotoxicity effect of nanoparticles primarily depends on their size.[80,81] The entrance of nanoparticles into cellular membranes has been described[82] to follow the route of either endocytosis or direct penetration. Research has suggested the latter mechanism to have potential adverse effects to human health because of its potential to induce

membrane disruption and lipid peroxidation.[83] Systematic studies include the work by Napierska et al.[84] who investigated the viability of endothelial cells in the presence of monodisperse silica nanospheres with seven different diameters (ranging from 14 to 335 nm). LDH and mitochondrial activity assays have demonstrated that a reduction in diameter leads to an increase in toxicity. It has been shown[85] that the presence of polymer-coated AuNPs causes destruction and increases the permeability of mannitol across epithelial Caco-2 monolayers by up to 4-fold. The increased permeability was caused by loosening of tight junction connecting the epithelial cells thereby allowing small molecules such as mannitol to pass through the monolayer via the paracellular route. This result was also shown by Minchin et al.[86] where they demonstrated that poly(acrylic acid) coated Au-NPs can bind to and induce unfolding of the fibrinogen in plasma leading to an inflammatory response.[17]

1.5 Nanotechnology and nanoparticles

One of the most prominent fields of nanotechnology is the synthesis of *nanomaterials* which was engendered by the need of electronic manufacturers (in optoelectronics)[87-90] and bioengineers (in health care and drug delivery)[91-93] to understand, synthesize and control substances that have at least one dimension less than 100 nanometers. One particular type of nanoparticle, ‘’semiconductor nanocrystals’’ which includes: quantum dots (QDs), Q-particles, nanoclusters or artificial atoms) have been shown to be of significant importance in the fields of electronics[87] and health care delivery[94] because of their typical dimensions ranging between 1 to 20 nanometers which induces unique physical, photophysical, photochemical, photoelectronic and photocatalytic properties when compared to that of bulk semiconductor.[95,96]

The unique properties that semiconductor nanocrystals possess can be attributed to *quantum confinement* which could be explained as the inability of charge carriers (generated when the nanoparticles absorb light) to move freely as a result of the confinement of electrons within the nanometer-size particle. This occurs when the dimensions of the nanocrystals are the same or smaller than the exciton Bohr radius of a bulk crystalline material.[97,98] The quantum confinement causes a change in the structural, electronic and optical properties which in turn generates other novel properties that dominate the behavior of these nanocrystals, causing their significantly difference properties when compared to those of bulk materials.[99] As the nanocrystal gets smaller, the surface to volume ratio increases. This large surface to volume ratio of smaller nanocrystals causes a large fraction of the atoms to be situated at the surface thereby inducing an increase in surface specific active sites for chemical reactions and contributing to their enhanced properties

when compared to those of larger nanocrystals. For example a nanocrystal sized ~ 2 nm will have 80% of its atoms on the nanoparticle surface when compared to a six nanometer nanocrystal which will have 30% of its atoms on the nanoparticle surface (**see Figure 6A**).

In semiconductor nanocrystals, the energy difference between the highest occupied (*HOMO*) and the lowest unoccupied (*LUMO*) electron energy state (conduction and valence band, respectively) is a material constant called the *''band gap''* (E_g). In a nanocrystal, the band gap of the nanoparticle increases with decreasing size, thereby resulting into discrete and quantized splitting of the energy levels unlike the continuous band that is observed in the bulk material see **Figure 6C.**

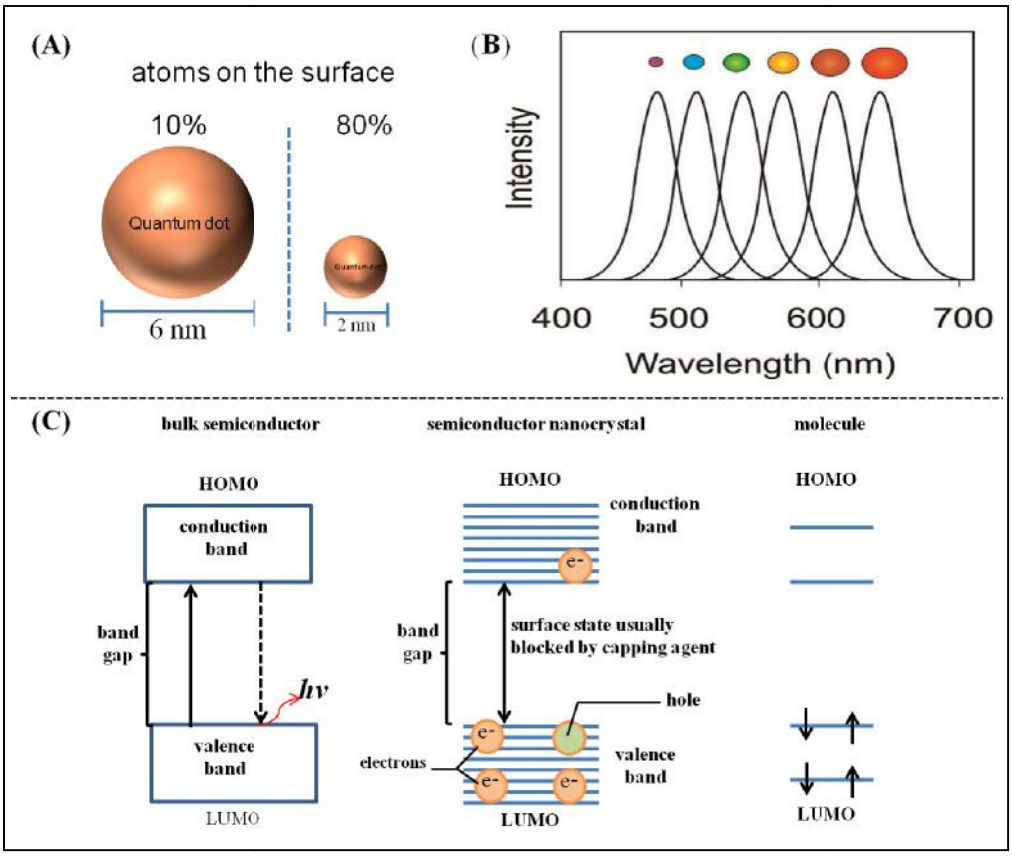

Figure 6. (A) The fraction of surface molecules as a function of nanoparticle size for a spherical nanoparticle. (B) Graph showing the shift in the wavelength with increase in the nanoparticle size. (C) Schematic illustration of the spatial electronic state for bulk semiconductor, semiconductors nanocrystal and a molecule. Picture (B) taken from ref.[100]

As the diameter of the nanocrystal decreases (*i.e* approaches the exciton Bohr diameter), its electronic properties start to change. The energy of the exciton is increased due to the

confinement of the electron and a hole within the crystal, thereby shifting the exciton to a lower wavelength and increasing the band gap. The band gap of a nanocrystal can be tuned from 1.7 eV (deep red) to 2.4 eV (green) by reducing the particle diameter from 20 nm to 2 nm. In the visible light spectrum, the wavelengths at which quantum dots fluoresce are directly dependent on the size of the dots[101] *i.e.* smaller dots fluoresce starting in the blue range of visible light, and as the quantum dots grow, they gradually move into the red range **Figure 6B.**

1.6 Synthesis and surface functionalization of semiconductor nanocrystals

Semiconductor nanocrystals are composed of an inorganic core (made up of between a few hundred to a few thousand atoms) surrounded by an organic outer layer of surfactant molecules (ligands). The quest of researchers to synthesize nanocrystals with high quality and well defined properties (e.g monodispersed, predictable particle size, high crystallinity, and high photoluminescence) was preceded by the use of various method which include Na_2S salts as precursors,[102] high energy ball milling of metals,[103,104] solid state methathesis,[105,106] reaction of H_2Se gas and Cd^{2+},[107-108] microwave assisted synthesis,[109] sonochemical method,[110,111] and photochemical method.[112,113] Most of these mentioned methods are characterized by slow kinetics, low photoluminescence quantum yields, lack of sharp absorption features, long reaction times, toxic, explosive starting material and high cost of production. In the late 80s and early 90s, experiments pioneered by Steigerwald[114] and Murray[115] lead to the development of the hot-injection solvothermal method (high temperature pyrolysis of organometallic precursors in surfactant like TOPO, alkylamines, phosphonic or fatty acids). The hot injection method was conducted by utilizing dimethylcadmium $(CH_3)_2Cd$ and trioctylphosphine (TOP)-Se as the organometallic precursor in a coordinating high boiling point alkyl solution such as technical-grade trioctylphosphine oxide (technical grade TOPO). However, because $(CH_3)_2Cd$ is air sensitive, pyrophoric, toxic and explosive at high temperature, researchers were motivated to explore greener synthetic methodologies by replacing dimethylcadmium with cadmium oxide (CdO)[116] or cadmium acetate ($Cd(CH_3CO_2)_2$.[117] The greener synthetic methodologies provides avenue towards the synthesis of high quality monodispersed nanoparticles and the ability to control important parameters such as their size and structure.

In a typical synthetic route reported in the literature[118] nanocrystals were chemically synthesized by the thermal decomposition of organometallic precursors, in an organic surfactant that not only passivates the surface, but can also control the growth rate of the nanocrystals and their size and

shape[119]. The surfactant molecules (*i.e* TOPO) are heated to a high temperatures (~330 °C); then the precursor molecules ($Cd(CH_3CO_2)_2$ are injected thereby initiating the nucleation of the nanocrystals. To obtain satisfactory control over the size and shape of the nanocrystal during the nanoparticle synthesis, a fast nucleation event should occur first, followed by a much slower growth process of the initially formed nuclei. In general, isotropic growth of nanocrystals into the thermodynamically favored equilibrium morphologies is preferred under a thermodynamically controlled regime; whereas anisotropic growth of nanocrystals into a shape which deviates from the equilibrium morphology is facilitated under a kinetically controlled regime.[120] The controlled growth of the nanoparticles can be achieved when the surfactant molecules form a complex with the atoms on the surface of the nanoparticles as well as with the precursor atoms thereby reducing the rate at which the precursor is decomposed.[121] The nucleation and growth of the nanoparticles only occurs at elevated temperatures; hence the growth of the nanoparticles can be stopped once the desired size is attained by removing the heating source. After the nanoparticles have been grown to the desired size, they are purified from the excess TOPO ligand by repeated precipitation in methanol.

After synthesizing the nanoparticles, the organic shell (ligands) of the as-synthesized nanoparticles provides a colloidal dispersion, and overall stability of the nanocrystal in solution determines their chemical behavior (*i.e* polar or charged ligand molecules provide solubility in polar or aqueous solvents while nanoparticles with apolar ligand molecules such as hydrocarbon chains are only soluble in apolar organic solvents, e.g. in hexane, toluene or chloroform). Since the ligand shell may not be suitable for the further end use of the nanocrystal, and being loosely bonded to the inorganic nanocrystal core, it can be easily manipulated and even completely exchanged thereby modifying the original surface cap with other ligands giving the possibility of tailoring the properties of the nanoparticles depending on their end-use or desired application.

Some examples of tailoring the ligand shell for specific end-use applications include stabilization of the nanoparticles in a medium (in a solvent or a polymer melt) where the nanoparticles are to be dispersed, passivating the surface of very reactive or toxic nanoparticles for biological use such as biolabelling and intracellular delivery,[122] creating a stable dispersion of the nanoparticles in water, functionalizing the nanoparticles for applications such as molecular recognition,[123] and selectively positioning the nanoparticles in the hydrophobic or hydrophilic portions of lipid or polymersomes.[70, 124] As the ligand can interact with the surface of the nanoparticles and influences their properties, it is therefore critical to choose the modifying ligands and the modification method with care. These capping ligand molecules are responsible for stabilizing colloidal

solutions of nanoparticles, preventing irreversible aggregation, coagulation, and fusion of the NPs due to van der Waals interactions.[125-131]

Usually, the stabilizing ligand molecule that is formed on the nanoparticles surface during synthesis are not suitable enough for the end application of the nanoparticles, or they can easily desorb from the nanoparticles surface by competition with another molecule able to bind to the quantum dot surface. It is therefore required to exchange the original ligand on the surface with the desired ligand by a process called ligand exchange see **Figure 7.**

In the ligand exchange procedure, the original hydrophobic ligand formed during the nanoparticle synthesis is replaced with another ligand which normally possess a terminal functionality reactive toward the surface atoms of the nanoparticle. The new ligand binds more strongly to the inorganic nanoparticles surface, and furnishes the nanoparticles with new surface properties or functionality. For example CdSe nanoparticles have be made water soluble by replacing the phosphine-based hydrophobic TOPO ligands formed on the inorganic nanoparticle surface during synthesis with a poly(propyleneimine),[132] hydrophilic thiol-based molecules like thiolated poly(amido amine) dendrimer[133] and mercaptocarboxylic acids[134] in order to apply the nanocrystals for biomedical application. **Table 1** shows some of the used hydrophobic and hydrophilic ligands that have been introduced to the surface of nanocrystals via ligand exchange. As mentioned earlier, nanoparticles are synthesized in hydrophobic organic solvent through high temperature routes thereby preventing their water solubility and biocompatibility **Figure 7A**. To engender their water solubility, biocompatibility and bio-stability, scientists have employed polymers with low toxicity and biocompatibility for the passivation of quantum dot surface to develop engineered nanocrystals which can be used for various biomedical applications.[135,136] **Table 2** shows the list of biocompatible polymers that have been utilized for the fabrication of water soluble biocompatible polymers. Different synthetic routes have been employed to attach such biocompatible polymers to quantum dots, including grafting polymer from quantum dots, grafting polymer to quantum dots and capping polymers on the passivating ligands of the quantum dots as shown in **Figure 7B-D**

Table 1. Example of ligand introduced to the surface of nanocrystals during synthesis

Entry	Ligand	nanocrystal	citation
1	dihydrolipoic acid (DHLA)	CdSe/ZnS, Au	137,138
2	dithiothreitol (DTT)	CdSe, CdSe/ZnS, Au	139,140
3	mercaptoacetic acid (MMA)	Fe_2O_3, Ag	141,142
4	macrocyclic polyammonium (MPA)	Ag, Au	143,144
5	triphenylphosphine oxide (TPPO)	CO, CdSe	145,146
6	oleic acid (OA)	Fe_2O_3, Au	147,148
7	trioctylphosphine oxide (TOPO)	CdSe, EuF_3	149,150,151
8	dimecaptosuccinic acid (DMSA)	Fe_2O_4, CdS	152,153
9	aminoethanethiol (AET)	Au, CdSe, CdSe/Zns, CdS	154,155,156
10	tetraoctylammonium bromide (TOAC)	Au	157
11	dodecanethiol (DDT)	Au	158,159
12	multidentate ligand	Au	160,161
13	carboxylioc acid (CA)	Fe_2O_3, Ag	162,163
14	mercaptoundecanoic acid (MUA)	CdSe/ZnS, Au	164,165
15	thioglycolic acid (TGA)	CdTe, CdSe	166,167
16	mercaptobenzoic acid (MBA)	CdSe, Ag	168,169

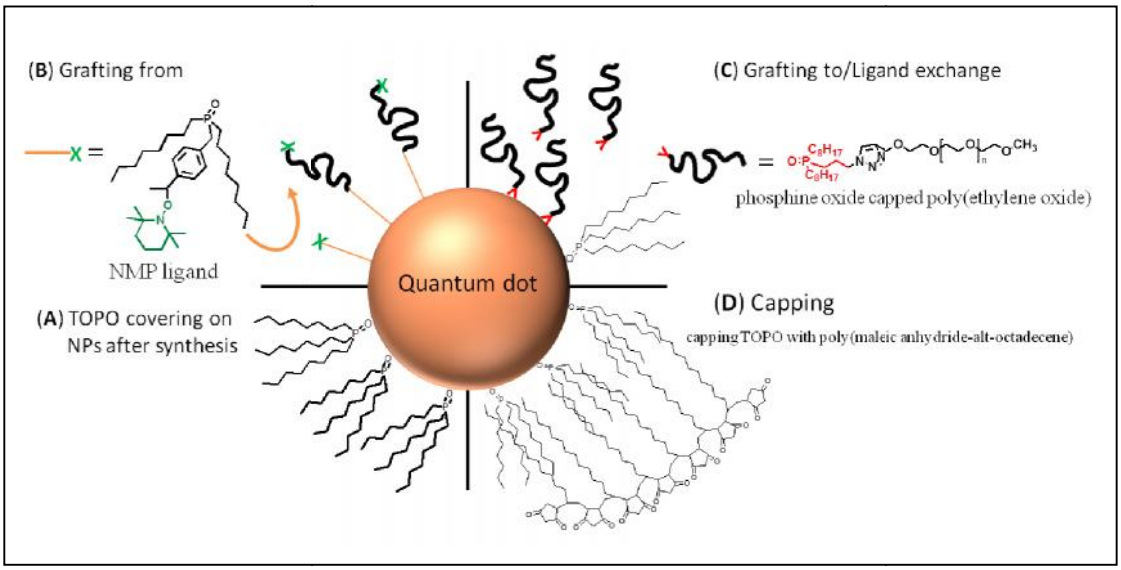

Figure 7. Schematic representation for the functionalization of nanoparticles with biocompatible polymer (A) TOPO Ligand formed after nanoparticle synthesis (B) grafting polymer from QDs (C) QDs grafting polymer to QDs (D) capping polymer onto QDs.

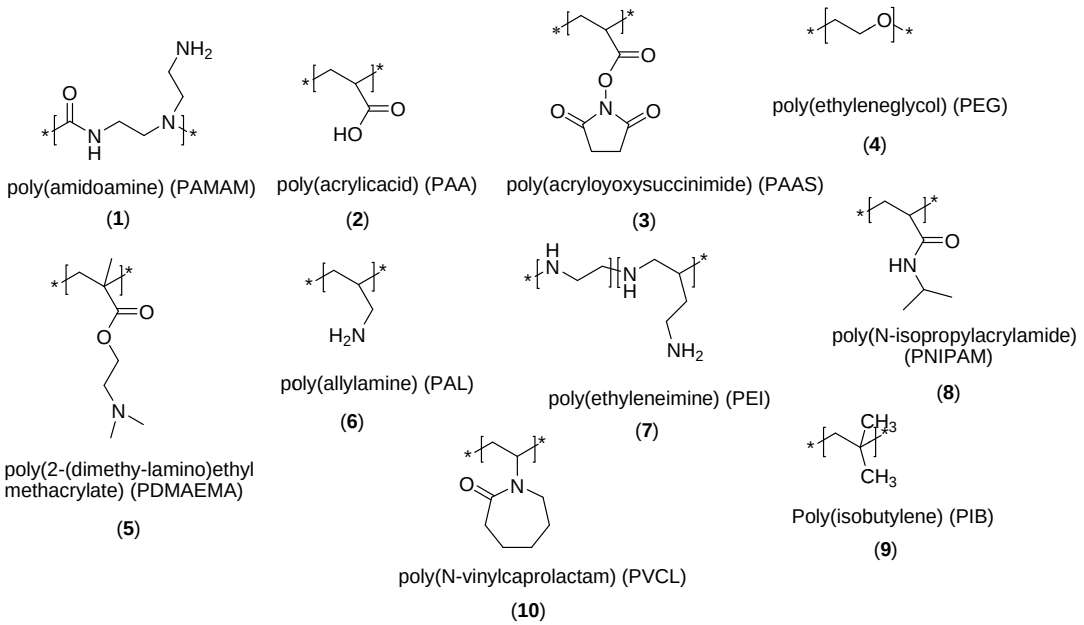

Scheme 1. Chemical structures of polymers utilized for the synthesis of water soluble or biocompatible nanocrystals.

Table 2. Example of polymer attached to the surface of nanocrystals for biological applications

entry	Polymer attached	nanocrystal	citation
1	poly(amidoamine) (PAMAM)	CdSe	[170]
2	poly(acrylicacid) (PAA)	CdTe	[171]
3	poly(acryloyoxysuccinimide) (PAAS)	CdSe/ZnS	[172]
4	poly(ethyleneglycol) (PEG)	CdSe, CdS	[173]
5	poly(2-(dimethy-lamino)ethyl methacrylate) (PDMAEMA)	CdSe/ZnS, CdSe	[174]
6	poly(allylamine) (PAL)	CdSe	[175]
7	poly(ethyleneimine) (PEI)	CdSe, CdS/ZnS	[176]
8	poly(*N*-isopropylacrylamide) (PNIPAM)	CdSe	[177]
9	poly(isobutylene) (PIB)	CdSe	[124]
10	poly(N-vinylcaprolactam) (PVCL)	CdSe/ZnS	[178]

1.6.1 Grafting polymer from quantum dots

In the *grafting from* approach to functionalize nanocrystals with polymers, polymers are usually grown directly from the surface of the NPs that have been pre-functionalized with small initiator molecules (like disulfide initiator or active groups such as hydroxyl, carboxylic acid, amine and bromine) via a living surface initiated polymerization. To synthesize the polymers, various polymerization techniques have been reported. The most prevalent techniques are living radical polymerizations such as atom transfer radical polymerization (ATRP)[179], reversible addition fragmentation chain transfer (RAFT)[180], and nitroxide mediated polymerization (NMP)[181] due to their simplicity, versatility, the ability to yield polymer with controlled molecular weight and potential for high surface grafting densities of the polymer brush see **Table 3.** Atom transfer radical polymerization (ATRP) has been problematic with CdSe QDs because of the loss of the

QD photoluminescence (PL) emission during the polymerization possibly due to reaction of the nanoparticles with the copper ions used in the ATRP process.[182] Emrick and coworker used a mild, palladium-catalyzed Heck-type coupling reaction to grow poly(p-paraphenylene vinylene) from CdSe QD surfaces[183]. Other grafting from polymerization methods include ring-opening metathesis polymerization (ROMP)[184] and ring-opening polymerization (ROP)[185]. The main advantage of "grafting from" method where the polymer brushes grow from the initiators on the surface of NPs, is that high grafting density of polymer brush can be obtained.

1.6.2 Grafting polymer to quantum dots

The *grafting to* method involves covalently linking of functional polymers that has been independently synthesized to the active anchor groups like azide or amine at the surface of quantum dot.[186-187] Grafting polymer to the nanoparticle could also be performed by independently synthesizing the polymers to contain a group that can bind to the nanocrystals, subsequently followed by the well established ligand exchange process with alkyl or pyridine capped quantum dots.[124, 188] A large number of ligand exchange procedures with different ligands have been reported in the literature.[155, 167-168, 174, 178] The most common strategy involves mixing the nanocrystals with excess of the new ligand to be grafted to the surface of the nanoparticles, followed by intensive stirring at moderate temperatures, depending on the used solvent.[189] The grafting density of polymers on the nanoparticles may be relatively low due to steric hindrance that arises by the placement of each successive polymer chain onto the nanoparticles surface. However, in some applications, very high density of polymer on the nanoparticles surface may not be required,[190] therefore the grafting density achieved by ligand exchange procedure is sufficient to provide the desired property and/or functionality of the nanoparticles surface. Grafting to method is also a useful technique to couple biopolymers (e.g., protein, peptide and DNA) onto QDs, since biopolymers mostly contain a number of amino groups along the chains which can react with COOH functionalized QDs through EDC/NHS chemistry. For example, antibody proteins have been covalently "grafted to" highly luminescent CdSe/ZnS core/shell QDs for biological detection.[136]

Table 3: Examples of polymerization methods to graft polymer from the surface of nanocrystals.

entry	polymerization method	Polymer	nanocrystal	citation
1	ATRP	poly(methylmetacrylate) (PMMA), poly(butylacrylate) PBA	CdS	[179,191]
2	RAFT	poly(styrene) (PS), poly(methylmetacrylate) (PMMA)	CdSe	[180,192]
3	NMP	poly(styrene) (PS)	CdSe	[181]
4	ROP	poly(caprolactone) (PCL)	CdS	[185]
5	ROMP	poly(cyclooctene) (PCO)	CdSe	[193]
6	LCCP	poly(isobutylene) (PIB)	SiO_2	[194]
7	OAVP	poly(2-(dimethylamino)ethyl methacrylate) (PDMAEMA)	CdTe	[195]

ATRP : Atom Transfer Radical Polymerization, RAFT : Reversible Addition Fragmentation Chain Transfer, NMP: Nitroxide Mediated Chain Transfer, ROP: Ring Opening Polymerization, LCCP: Living Carbocationic Polymerization, OAVP: Oxyanionic Vinyl Polymerization

1.6.3 Capping polymers on the nanocrystal passivating ligand

In the capping approach (see **Figure 7C)**, an additional layer of organic amphiphilic molecules is used in capping the original ligand that was formed during the nanoparticles synthesis. The side chain (hydrophobic segments) of the polymer adsorbs via hydrophobic interaction to the original hydrophobic ligand molecules of the nanoparticles while the hydrophilic part promotes the dispersion and solubility of the nanocrystals in aqueous media. The main advantage of the capping method is that it does not depend on the composition of the inorganic core material,

since the adsorption is predominantly based on hydrophobic interaction of hydrocarbon chains and van der Waals forces between the molecules. Amphiphiles such as phospholipids,[196,197] α-cyclodextrin,[198,199] and cetyl-trimethylammonium bromide[200] have been employed to render nanoparticles water soluble. However, due their relatively weak hydrophobic interactions, they are normally not sufficiently stable when used in biological applications. More effectively, nanoparticles can be capped with amphiphilic block copolymers consisting of a hydrophilic backbone and long hydrophobic alkyl side chains, amphiphilic polymers such as poly(maleic anhydride-alt-octadecene)[201], polystyrene-*b*-poly(acrylic acid),[202] poly(methyl methacrylate)-*b*-poly(ethyleneoxide)[203] and poly(ethyleneglycol-*b*-poly (N,N-dimethyl-aminoethyl methacrylate)[204] have been used to solubilize semiconductor nanoparticles in water for biological applications via ligand exchange. Poly(acrylic acid) was modified with hydrophobic alkyl amine via an amide bond using DCC coupling.[205] This branched PAA was used for coating TOPO covered CdSe for biological application. Poly(acrylic acid) having octylacrylamide and isopropylacrylamide as side groups have also been used.[206] Poly (maleic anhydride-alt-1-octadecene) block primary amine-terminated PEG (PMAO-*b*-PEG) coated QDs were found to have excellent solubility in water and to be capable of recognizing cancer cells having a Her2 receptor. The capping method has also been employed to attach charged polymers onto nanocrystals through electrostatic interaction. Poly (acrylamide) (PAM) was used to modify CdSe/ZnS QDs through electrostatic interaction between the positively charged side chains of PAM and the negatively charged ligands on QDs.[207]

2.0 Aim of the Thesis

The aim of this thesis was to investigate and control the specific interaction and location of surface modified functionalized CdSe nanoparticles within hybrid lipid/polymer membranes utilizing the monolayer and bilayer technique as shown in **Figure 8**. The interaction should include hybrid lipid/polymer membranes where either monolayers (DOPC or DPPC in mixture with block copolymers (BCPs) composed of PIB_n-*b*-PEO_m) or bilayer membranes should be studied, probing the interaction of CdSe NPs with different surface modifications (hydrophobic, hydrophilic and amphiphilic). Aspects of the interaction of hydrophobic, hydrophilic and amphiphilic CdSe-NPs with phase separated or mixed lipid/block copolymer membranes should be investigated, as understanding the specific location of nanoparticles and their interaction within hybrid lipid/polymer membranes have interesting implications for medical imaging, drug delivery, nanotoxicology and critical for the rational design of nanocarrier agents.

To this purpose, monodispersed CdSe nanoparticles (~ 2 nm) should be synthesized and the functionalization of their surface with hydrophobic polyisobutylene (PIB), hydrophilic poly (ethylene oxide) (PEO) and amphiphilic polyisobutylene-*b*-polyethylene oxide) biocompatible polymers using the ligand exchange approach should be accomplished.

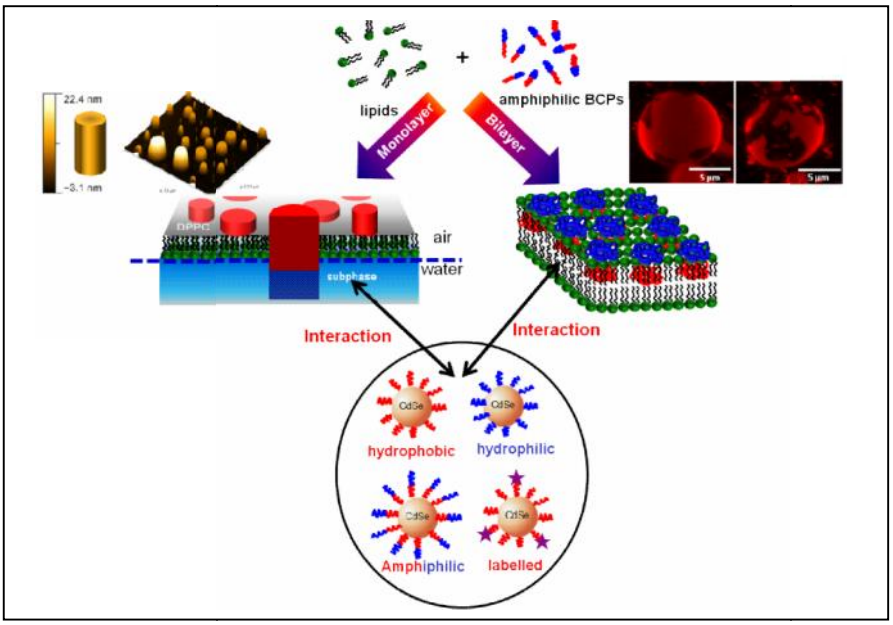

Figure 8: Interaction and specific localization of polymer functionalized CdSe nanoparticles with phase separate hybrid lipid/polymer membrane on monolayer- and bilayer- membranes.

3.0 Concept

To study the interaction and specific localization of polymer functionalized nanoparticles with hybrid lipid/polymer membrane, small (~2 nm) and monodispersed CdSe nanoparticles should be synthesized using the conventional hot injection method **Scheme 2**. In order to functionalize the CdSe nanoparticles with biocompatible polymers, nonsymmetric α, ω functionalized polyisobutylenes (PIBs) should be prepared able to functionalize CdSe NPs by introducing appropriate surface binding groups. Thus on one chain end of the polymer, a phosphine oxide ligand will be attached (to facilitate their attachment to the surface of the nanoparticles), whereas the other chain end can be substituted by either a hydrogen bonding moiety (thymine/2,4-diaminotriazine) (to enable their use in selective supramolecular recognition), rhodamine-B (to enable easy visualization of the nanoparticles) or poly (ethylene oxide) (to generate an amphiphilic block copolymer).

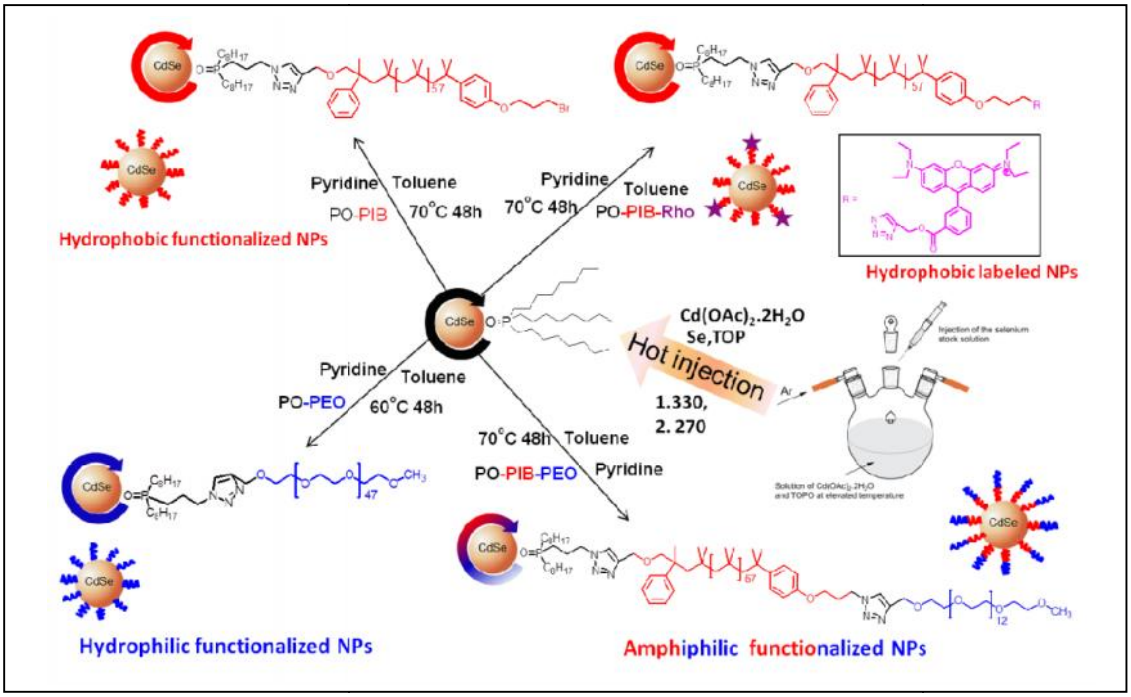

Scheme 2 : Schematic diagram showing the synthesis of hydrophobic-, amphiphilic- and hydrophilic- water soluble CdSe- nanoparticles.

Nonsymmetric PIBs (with molecular weights M_n ~ 4000 g·mol^{-1} and low polydispersities (M_w/M_n = 1.3) will be synthesized via living cationic polymerization using methyl-styrene epoxide as initiator, followed by quenching reaction with 3-bromopropoxybenzene.

Subsequent bromide/azide exchange and the use of the azide/alkyne click reaction will be employed to attach different moieties (*i.e.* supramolecular recognition-moieties (such as thymine or 2,4-diaminotriazine), dyes (rhodamine-B) or simple hydrophilic moieties (poly(ethylene oxide)) to the chain end of the poly(isobutylene). The chemical identity of the final structures will be proven by extensive ^{1}H NMR investigations and matrix-assisted laser desorption-ionization mass spectroscopy (MALDI).

Furthermore, a water soluble nanoparticle engineered to carry a long PEO_{47}-thymine polymer on the surface will be synthesized in order to effect a controlled supramolecular recognition onto bi- and mono-layers composed of a hybrid lipid/polymer mixture **Figure 9**.

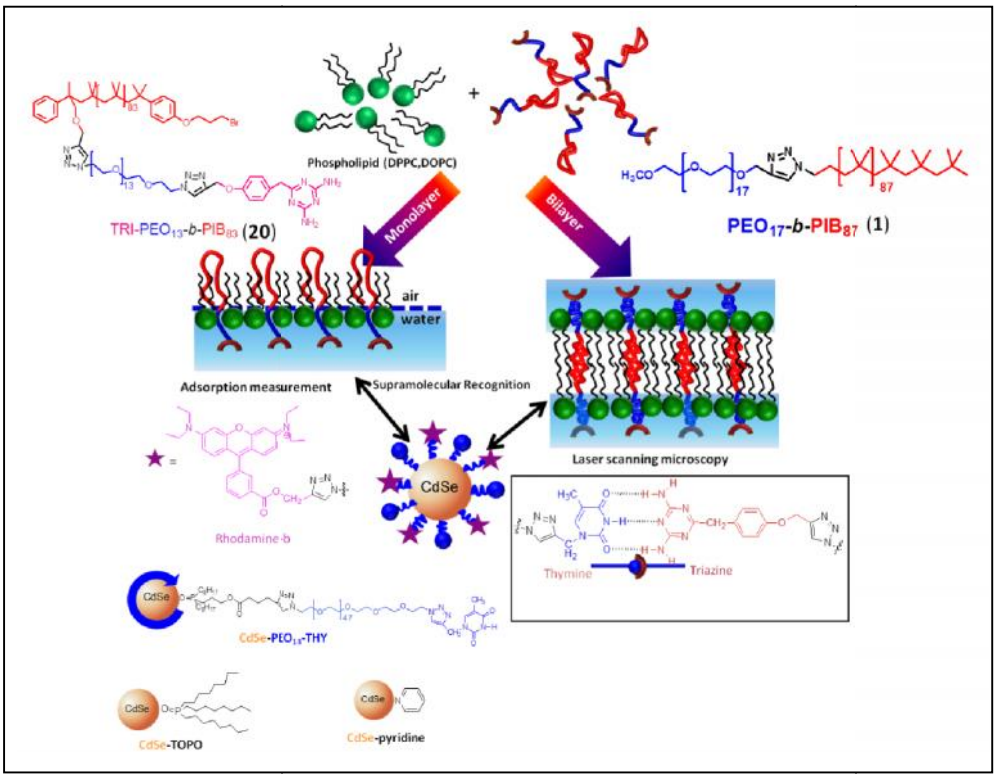

Figure 9. Schematic diagram for studying the supramolecular recognition between thymine functionalized CdSe nanoparticles (labeled with rhodamine-B) and a triazine-functionalized hybrid lipid/BCP mono- and bilayer membranes, which are composed of either DPPC or DOPC in mixture with BCP **(20)** and/or BCP **(1)**

The lipid/polymer membrane will be constructed from DPPC or DOPC and a biocompatible amphiphilic block copolymer carrying a triazine moiety (TRI-PEO_{13}-*b*-PIB_{83}). The thymine moiety attached to the surface of the nanoparticles can recognize the triazine moiety

covalently connected to the block copolymer incorporated into a mixed lipid/polymer membrane. Subsequent supramolecular recognition between the PEO_{47}-thymine functionalized nanoparticles and the triazine functionalized polymer in the mixed membrane can induce a change in the morphology of the hybrid lipid/polymer mixture as a result of the selective removal of the polymer component similar to results reported for cholesterol and cyclodextrine.[208] These effects will be subsequently investigated using Langmuir-film-techniques as well as confocal laser microscopy using giant unilameller vesicles (GUVs).

4.0 Synthesis of nonsymmetric chain end functionalized poly (isobutylene)

Olubummo Adekunle, Florian Herbst, Katharina Hackethal, Wolfgang H. Binder

Part of this chapter was published in the Journal of Polymer Science Part A: Polymer Chemistry Volume 49, Issue 13, pages 2931–2940, 1 July 2011.

4.1 Introduction

Poly(isobutylene), a biocompatible polymer with high chain mobility has found increased use in areas of supramolecular polymer science,[209,210] amphiphilic conetworks,[211-213] and self-healing materials.[214] In many of these applications, a significant quest for polymers with a highly defined endgroup-structure is demanded, requiring the presence of hydrogen-bonding moieties,[215-218] metal-complexes, or ligands for nanoparticle and surface attachment[194,219] to achieve the desired effects of chain ordering, supramolecular organization, or self-healing. To this endeavor, a large variety of monobivalent and symmetric bivalent polyisobutylenes (PIBs) have been prepared,[220] in the latter case featuring symmetrical endgroups on both chain ends. This chapter describes the synthesis of functionalized poly(isobutylene) chains, where two different functional supramolecular endgroups are affixed to the ‘‘initiating α’’ and ‘‘terminal ω’’ chain end of a poly(isobutylene) chain, thus, generating nonsymmetric α, ω-functionalized PIB. Often prohibitive for the direct synthesis of such α, *ω*-functionalized polymers is the use of a functional initiator equipped with a supramolecular moiety before the living cationic polymerization (LCCP) of isobutylene. As LCCP is highly sensitive toward polar moieties, only few initiators enabling subsequent attachment of functional (polar) entities have been reported, such as the 3,3,5-trimethyl-5-chlorohexyl acetate initiator by Storey and coworkers,[221,222] who introduced an acetyl moiety for a subsequent attachment of an atom transfer radical polymerization (ATRP) initiator onto the α- initiating part of the PIB-chain. Recently, another highly useful initiator is represented by styrene epoxides as discussed by Puskas *et al.*,[223,224] introducing a hydroxymethyl moiety onto the α-end of the PIB-chain as residual part of the initiator- moiety. Lange *et al.*[225] have used 3-chloropentene followed by a hydrosilylation reaction to achieve a differentiation between the α-chain and ω-chain end via moderately selective hydrosilylation chemistry. However, most of the aforementioned initiators have not been exploited for subsequent chemistry, as only a

reduced reactivity of the endgroups allowed the introduction of appropriate functional moieties and the attachment of more complex, supramolecular entities has not been accomplished up to now.

4.2 Result and Discussion

The approach towards the preparation of α-ω-functionalized PIBs relies on the combination of methyl-styrene epoxide (**4**) as initiator for LCCP and azide/alkyne-‘‘click’’-chemistry[226-229] for further modification of the α- and ω-endgroup after quenching the polymerization with a well known bromo phenoxy benzene (BPB).[230] Initiating isobutylene with initiator (**4**) and subsequent quenching reaction with BPB afforded the α-hydroxymethyl-ω-bromo telechelic PIB (**5**) in high yield and with a complete endgroup efficiency as judged by excessive NMR (**Figure 10a** (^{1}H) and appendix 1, **Figure S3 (**^{13}C), GPC, and MALDI-investigations. It should be noted that in accordance with the results of Puskas *et al.*,[224,223] only about ~ 30 % of the epoxide initiator (**4**) acts as an active initiator for the polymerization, concomitant with in situ kinetic measurements (appendix 1, **Figure S23**) indicating the completion of the polymerization after ~30 min (see appendix 1, **Table S1** for details). A final quenching reaction with BPB similar to Morgan and Storey[230] was achieved after ~2 h at a temperature of -70 °C. Critical for the success of the generation of α, ω-functionalized chains in polymer (**5**) is conducting the polymerization at -60 °C and the quenching reaction at lower temperatures (-70 to -75 °C). Relevant data for the polymerization (**Table 4**) indicate an excellent match between the endgroup of either side as judged by comparison of M_n(GPC) with M_n(NMR) and the ratio on integration of both endgroups. Furthermore, the chemical identity of the (α)-hydroxymethyl-(ω)-bromo telechelic PIB (**5**) could be proven via MALDI (appendix 1, **Figure S21**), showing one main series, where each series of ions were separated by 56 Da, the mass of the isobutylene repeating unit. This series could be assigned to the PIB having both the initiating head group and the terminal bromide endgroup ionized as $[M \cdot Na]^+$ ($C_{190}H_{365}O_2BrNa$). The signal at 2786.375 Da agrees with the calculated value of 2784.754 Da for 42 units of isobutylene.

As the further synthetic strategy relies on the use of the highly yielding azide/alkyne click chemistry, the propargylation of the hydroxyl head group was achieved with the use of propargyl bromide to furnish α-alkynyl-ω-bromotelechelic PIB (**6**) in yields of 90% ($M_{n(GPC)}$ = 4300 g·mol^{-1} and $M_{n(NMR)}$ = 4250 g·mol^{-1}). The resonance of the newly formed alkyne

moiety at ~2.35 ppm and the overlap of the triplet form the proton adjacent to the oxygen (O-CH_2) of the head alkoxy-moiety and that of the proton adjacent to the oxygen (O-CH_2) of the quencher at ~4.06 ppm confirms the formation of alkyne **Figure 10b.**

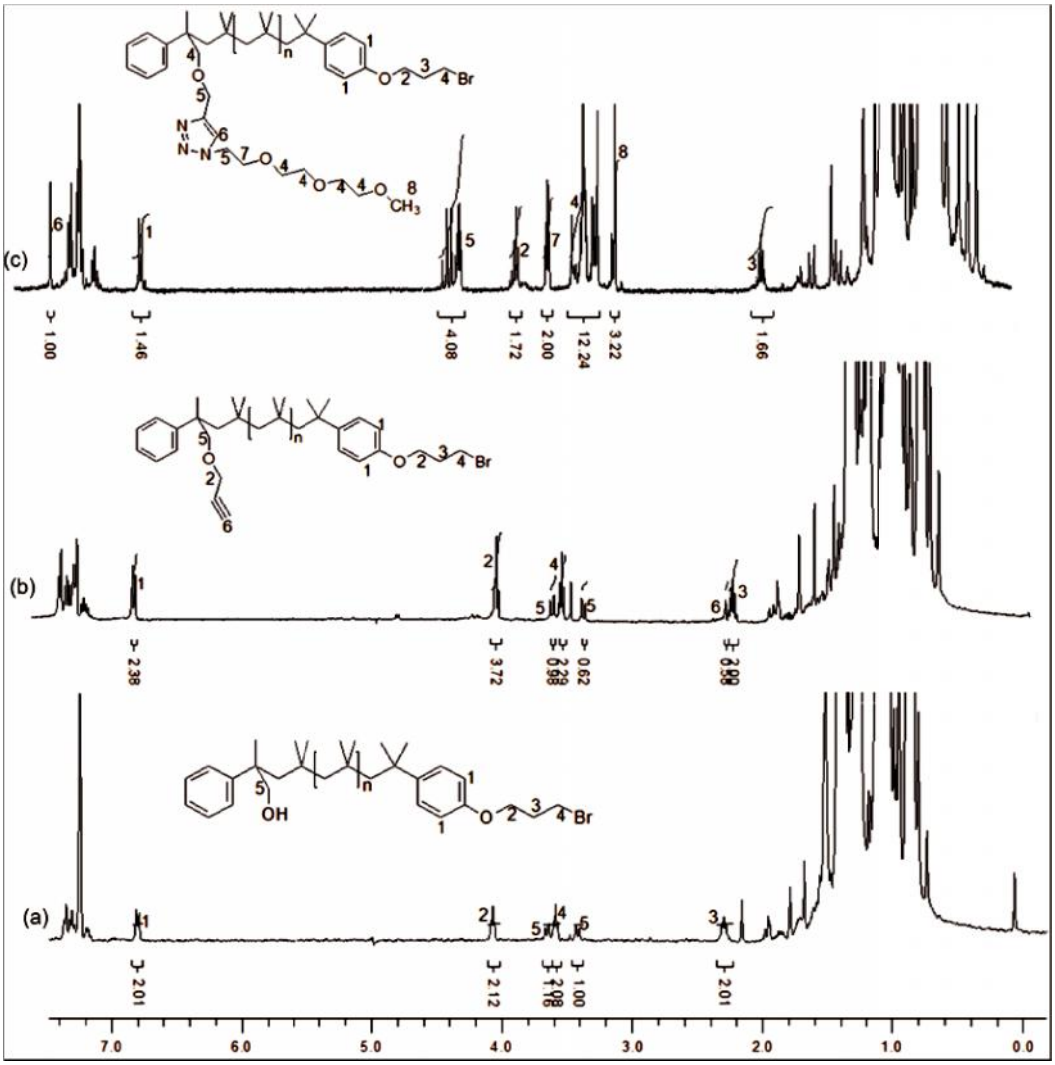

Figure 10. (a) ^{1}H NMR spectrum of α-hydroxymethyl-ω-bromo telechelic PIB (**5**), (b) a-alkinyl-x-bromo telechelic PIB (**6**), and (c) α -TEO- ω -bromo telechelic PIB (**14**).

Subsequent azide/alkyne click reaction between the α-alkynyl-ω-bromo telechelic PIB (**6**) and the azido-telechelic TEO (**9a**) was conducted in the presence of Cu^I yielding α-TEO-ω-bromo telechelic PIB (**14**) as judged by NMR spectroscopy (**Figure 10c** entry 3 in **Table 4**), M_w/M_n = 1.29; $M_{n(GPC)}$ = 4600 g mol^{-1}; and $M_{n(NMR)}$ = 4400 g mol^{-1}. The resonance of the newly formed triazole moiety at ~7.45 ppm as well as the newly formed triplet at ~4.47 ppm and a diastereotopic proton together with a newly formed triplet at ~3.83 (triazol-CH_2- CH_2-

O-TEO) confirms the structure of the α-TEO-ω-bromo telechelic PIB (**14**) **Figure 10c**. In MALDI-analysis, one major and one minor series were observed: the major series could be assigned to the species ionized with Ag^+ [M· Ag^+] ($C_{156}H_{294}N_3O_5BrAg_1$) (found: 2480.579 Da

Table 4. Molecular weights of polymers **2-7**, **10-13** obtained by GPC-analysis, NMR-integration as well as MALDI-analysis.

Entry	Polymer	PDI	$M_{n(calculated)}$ [g/mol]	$M_{n(GPC)}$ [g/mol]	$M_{n(NMR)}$ [g/mol]	Headgroup/ End group	Yield [%]
1	**5**	1.31	4,000	4,200	4,400	1.2:2.4[a)]	98
2	**6**	1.32	4,039	4,300	4,250	1.2:2.3:2.0[b)]	95
3	**14**	1.29	4,228	4,600	4,400	3.2:2.4:1.7[c)]	50
4	**15**	1.24	4,228	4,700	4,800	3.2:2.4:3.4[d)]	90
5	**18**	1.30	4,434	4,800	4,850	3.1:2.3:1.7[e)]	70
6	**19**	1.24	4,495	3,700	4,465	2.9:1.2:2.6[f)]	75
7	**27**	1.21	4,396	4,100	3,900	4.3:1.2:1.6[g)]	50
8	**28**	1.21	4,396	4,100	4,050	4.3:1.2:1.6[h)]	90
9	**30**	1.21	4,616	5,600	4,494	1.7:4.0:1.7[i)]	75

[a)] NMR integration of the triplet at ~7.14 ppm (aromatic head group proton) and that of the end group at ~3.58 ppm (*CH_2*-Br). [b)] NMR integration of the multiplet at ~2.35 ppm (alkyne proton), the triplet at ~7.14 ppm (aromatic head group proton) and the end group at ~3.58 ppm (*CH_2*-Br). [c)] NMR integration of the singlet at ~3.36 ppm (terminal *CH_3* group of the TEO), the triplet at ~7.14 ppm (aromatic head group proton) and the end group at ~2.29 ppm (*CH_2*-Br). [d)] NMR integration of the singlet at ~3.36 ppm (terminal *CH_3* group of the TEO), the triplet at ~7.14 ppm (aromatic head group proton) and the end group at ~2.02 ppm (*CH_2*-N_3). [e)] NMR integration of the singlet at ~3.36 ppm (terminal *CH_3* group of the TEO), the triplet at ~7.14 ppm (aromatic head group proton) and the thymine end group at ~4.93 ppm (triazol-*CH_2*-thymine). [f)] NMR integration of the singlet at ~3.36 ppm (terminal *CH_3* group of the TEO), the triplet at ~7.14 ppm (aromatic head group proton) and the triazine end group at ~5.1 ppm (*NH_2*) [g)]NMR integration of the proton at ~4.5/4.3 ppm (*CH_2*-triazol-*CH_2*), the triplet at ~7.14 ppm (aromatic head group proton) and the end group at ~2.29 ppm (*CH_2*-Br) .[h)] NMR integration of the proton at ~4.5/4.3 ppm (*CH_2*-triazol-*CH_2*), the triplet at ~7.14 ppm (aromatic head group proton) and the end group at ~4.0 ppm (O-*CH_2*). [i)] NMR integration of triplet at ~7.14 ppm (aromatic head group proton), the phosphine oxide end group at ~2.15 and thymine end group at ~4.93 ppm (triazol-*CH_2*-thymine).

calculated 2479.111 Da for n = 31), the minor series can be assigned to species ionized with Na^+ [M·Na^+] ($C_{160}H_{302}N_3O_5BrNa_1$) (found: 2466.789 Da; calculated 2467.232 Da; for n = 32 units; **Figure 11**).

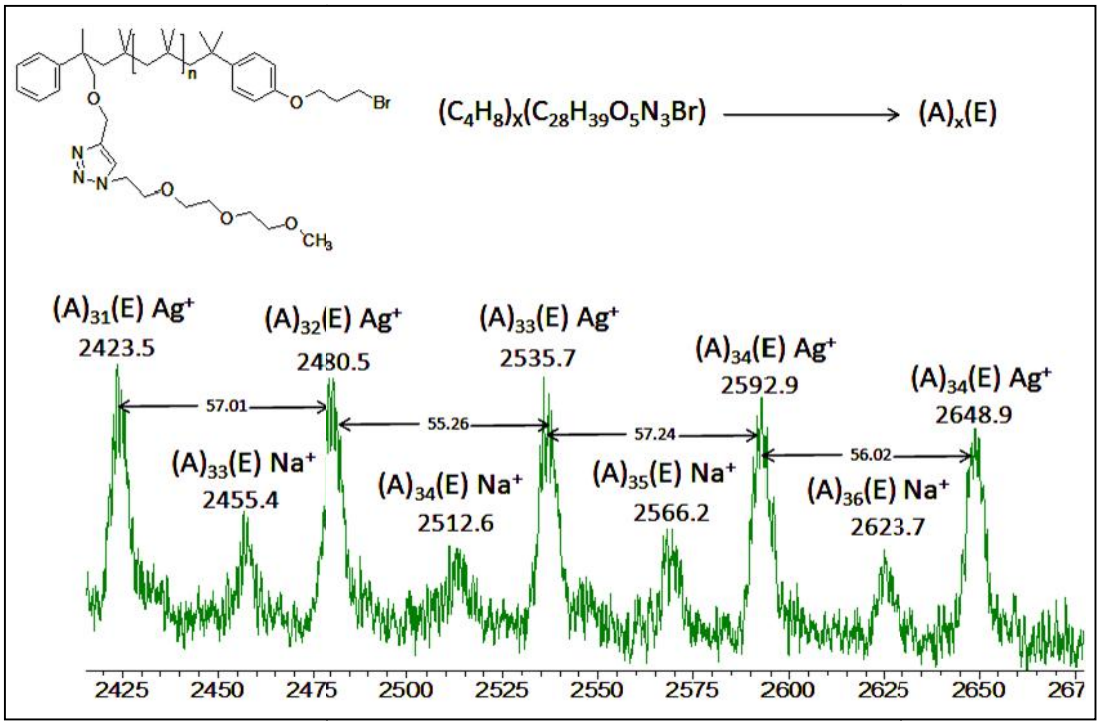

Figure 11. MALDI-TOF-MS of α-TEO-ω-bromo-telechelic PIB (**14**)

Subsequent bromide/azide-exchange is then achieved by NaN_3 exchange in DMF and proven via a shift of the resonance at ~2.28 ppm (-CH_2-CH_2-Br) in (**14**) to ~2.02 ppm (-CH_2-CH_2-N_3) in the α-TEO-ω-azido telechelic PIB (**15**) for NMR data (see **Figure 12a** (^{1}H) and appendix 1, **Figure S10** (^{13}C). For the (α)-TEO-(ω)-azido telechelic PIB (**15**), the MALDI-mass spectrum shows one major and one minor series, thus proving the final structure by assigning both the major species as [M·Ag^+] [($C_{264}H_{510}N_6O_5Ag_1$); found: 3956.67 Da; calculated: 3956.897 Da; n = 58 units] and the minor series [M·Na^+] [($C_{268}H_{518}N_6O_5Na_1$); found: 3929.333 Da; calculated: 3927.042 Da; n = 59 units] **Figure 13d**. The second click reaction on the ω-side of α-TEO-ω- azido telechelic PIB (**15**) using two different hydrogen bonding moieties (thymine and triazine) was also complete (as judged via IR-spectroscopy by the complete loss of the azide-band) to yield the α-ω-nonsymmetric PIBs (**18, 19**). Thus, the thymine residue was attached to α-TEO-ω-azido telechelic PIB (**15**) via the azide/alkyne

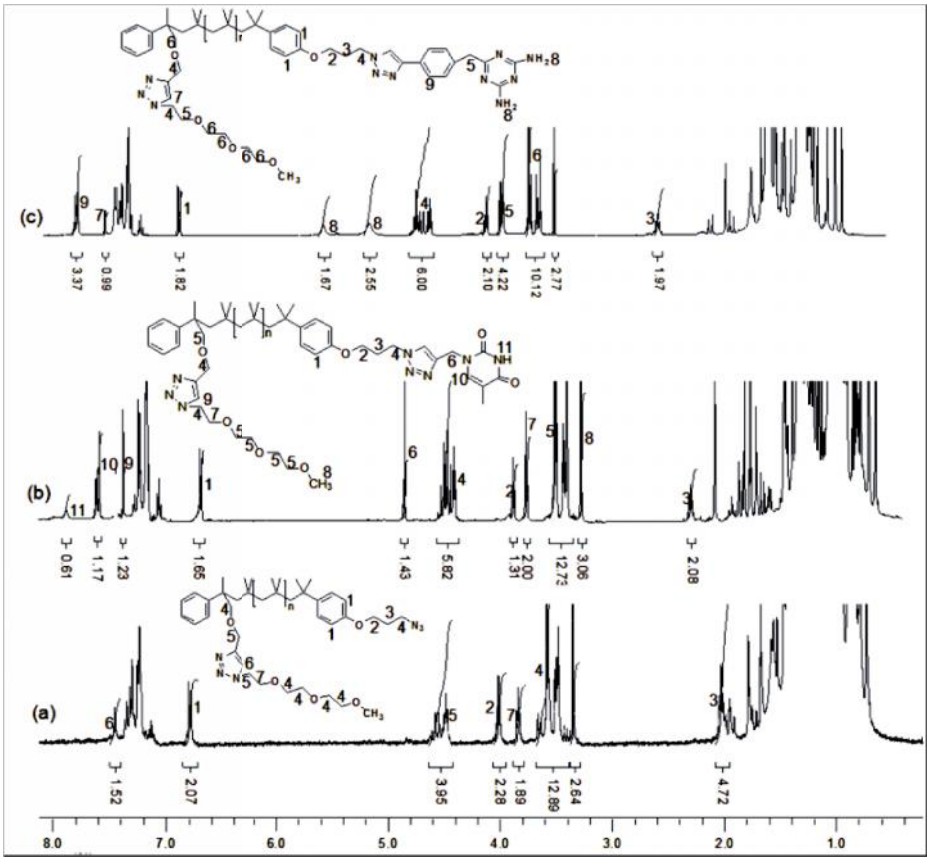

Figure 12. ^{1}H-NMR spectra of (a) α-TEO-ω-azido telechelic PIB (**15**) (b) α-TEO-ω-thymine telechelic PIB (**18**), (c) α-TEO-ω-triazine telechelic PIB (**19**).

click reaction to furnish α-TEO-ω-thymine-telechelic PIB (**18**), whose structure could be proven unambiguously by ^{1}H NMR-spectroscopy due to the emergence of new peaks at approximately 7.90, 7.61, and 4.87 ppm resulting from the attachment of the thymine moiety (see **Figure 12b** and appendix 1, **Figure S12** (^{13}C) NMR). A similar picture was achieved for the (α)-TEO-(ω)-triazine telechelic PIB (**19**). New peaks at approximately 7.78 ppm, 5.47–5.05 ppm, and 3.63–3.47 ppm proved that triazine-moiety has been attached (see **Figure 12c** and appendix 1, **Figure S15** (^{13}C) NMR). Extensive MALDI-spectra were accumulated for the nonsymmetric α-TEO-ω-thymine telechelic PIB (**18**) and the α-TEO-ω-triazine-telechelic PIB (**19**) to prove their chemical identity see **Figure 13b,c**. In contrast to previous MALDI-investigations,[217] where the best desorption results were achieved via ionization with Ag^{+}-salts, the α-TEO-ω-thymine telechelic PIB (**18**) gave the best ionization with lithium ions (dithranol:LiTFA:(**18**) = 100:1:10). Thus, the MALDI-mass spectrum shows one important and one minor series, where each series of ions were separated by 56 Da, the mass of the

repeating unit [main series: found 3233.242 Da; calculated for $[M \cdot Li]^+$ ($C_{216}H_{406}N_8O_7Li_1$; n = 44) 3234.189 Da]; first minor series: 3136.849 Da; calculated for $[M \cdot Na]^+$ ($C_{208}H_{390}N_8O_7Na_1$; n = 42) 3138.037 Da see **Figure 13b**. Similar to (**18**), the α-TEO-ω-triazine telechelic PIB (**19**) gave the best ionization with silver ions with (DCTB: AgTFA:(**19**) = 100:1:10) showing only one major series with 4967.111 Da as $[M \cdot Ag]^+$ ($C_{332}H_{633}N_{11}O_5Ag_1$; n = 72);calculated: 4966.877 Da see **Figure 13c**.

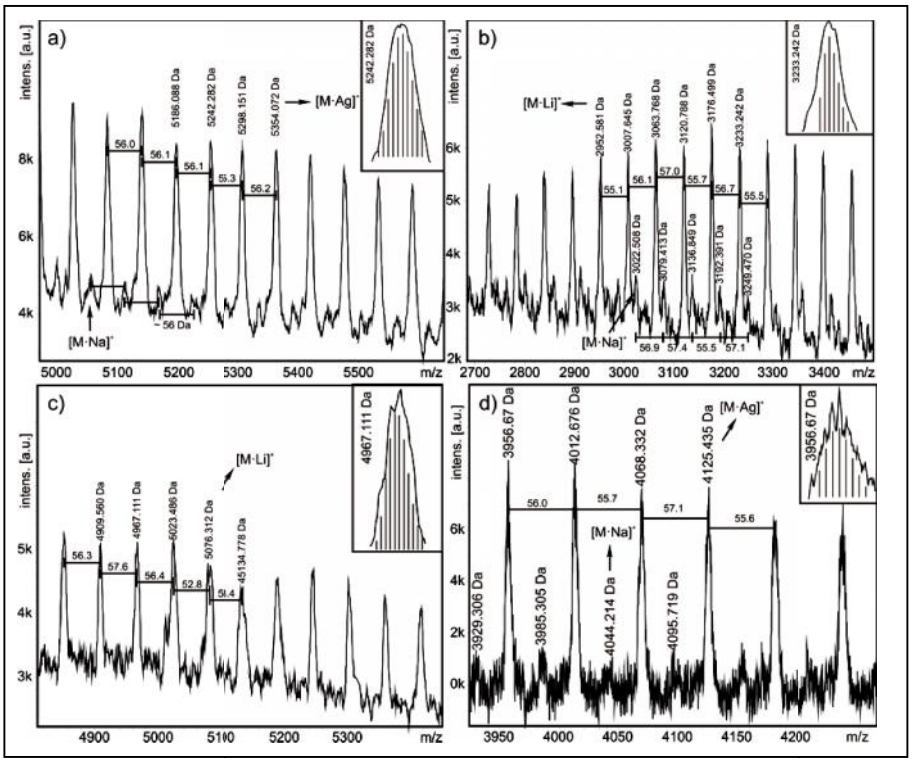

Figure 13. MALDI-mass spectra of (a) α-phosphinoxide-ω-thymine-telechelic PIB (**30**). (b) α-TEO-ω-thymine-telechelic PIB (**18**), (c) α-TEO-ω-2,4-diaminotriazine telechelic PIB **(19)** (d) α-TEO-ω-azido telechelic PIB (**15**). Inserts shows the simulated peaks.

Finally, the anchoring of a more complex molecule for attachment of PIB-chains onto CdSe-nanoparticle surfaces (namely the phosphinoxide (**25**)) was probed, starting with the azide/alkyne-click-reaction between the phosphinoxide (**25**) and the α-alkinyl-ω-bromo telechelic PIB (**6**). Conducting a two-step synthetic sequence, furnishing first α-phosphinoxide-ω-bromo telechelic PIB (**27**) see **Figure 14a**, followed by bromide/azide-exchange toward α-phosphinoxide-ω-azido telechelic PIB (**28**) see **Figure 14b**, and subsequent azide/alkyne-click-reaction with the thymine derivative furnished the final α-phosphinoxide-ω-thymine telechelic PIB (**30**). Again, the final structure of (**30**) was proven

by ^{1}H NMR, ^{13}C NMR, and ^{31}P NMR spectroscopy (see **Figure 14c** and appendix 1, **Figure S19** (^{13}C) and **Figure S20** (^{31}P) NMR) as well as MALDI-MS (**Figure 14a**). The α-phosphinoxide-ω-thymine telechelic PIB (**30**) contains a nanoparticle attachment site via the phosphine oxide moiety as well as a supramolecular recognition site via the thymine moiety.

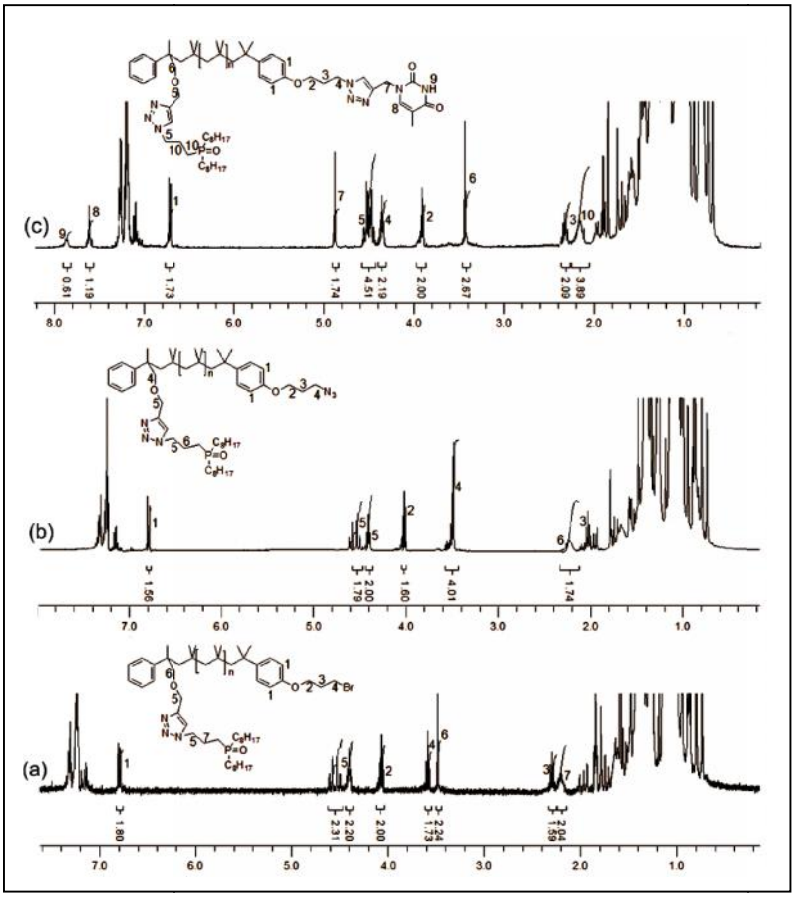

Figure 14. (a) ^{1}H NMR spectrum of α-phosphineoxide-ω-bromo-telechelic (**27**), (**b)** ^{1}H NMR spectrum of α-phosphineoxide-ω-azido-telechelic (**28**), (**c)** ^{1}H NMR spectrum of α-phosphine oxide-ω-thymine-telechelic PIB (**30**).

4.3 Conclusions

Summed up, the method to use a functional initiator (MSE, **4**) as well as BPB as quencher, followed by a series of azide/alkyne-‘‘click’’-reaction furnishes an excellent approach toward nonsymmetrically substituted α,ω–functionalized PIB. The so obtained PIBs contain hydrogen-bonded moieties as recognition units on one side of the PIB polymer as well as a second functional moiety (TEO or phosphine oxide) on the other side of the PIB polymer.

Therefore, this method for the first time opens the possibility to engineer the supramolecular recognition of PIB on its two different telechelic sides of the polymer.

5.0 Controlling the localization of polymer-functionalized nanoparticles in mixed lipid/polymer membranes

Adekunle Olubummo, Matthias Schulz, Bob-Dan Lechner, Peggy Scholtysek, Kirsten Bacia, Alfred Blume, Jörg Kressler, and Wolfgang H. Binder

Part of this chapter was published in ACS Nano 2012, Volume 6, Issue 10, Pages 8713–8727.

5.1 Introduction

Research in understanding the interaction between functional surface modified nanoparticles with lipid or polymer membranes has grown significantly over the past years,[6, 24, 231] aiming to use nanoparticle/lipid hybrid systems for broad biomedical applications and nanotechnology and as therapeutic agents with minimal cytotoxicity. These applications can be achieved only with a tailored control over nanoparticles' interaction with lipid or polymer membranes. Thus, the nanoparticles' surface chemistry plays an important role together with other unique nanoparticle properties such as size, shape, surface charge, and chemical composition.[17, 61, 232-233] Both vesicular lipid membranes (liposomes[234]) and polymer membranes (polymersomes[3]) feature a membrane bilayer that differentiates the hydrophilic properties inside their aqueous cavity from the hydrophobic properties within their bilayer interior.[235] This clear-cut difference provides possibilities of selective location, dispersing or concentration of nanoparticles via encapsulation, binding, or specific interfacial interactions. Liposomes are a construct of naturally occurring phospholipids with low molecular weight, whereas polymersomes in contrast are constructed solely from amphiphilic diblock copolymers with a molecular weight up to 100 kg/mol, thus offering a chance to tune the dimensions as well as the chemical properties of the membrane. As a result, polymersomes show a higher mechanical and thermal stability within their curved membrane and have thus gained significant use in biomedical applications.[3, 236-237] Hydrophobicity[22-23] in particular plays a very important role when dealing with the interaction between NPs and liposomes, as nanoparticle assembly and lipid stabilization are essentially driven by hydrophobic/ hydrophilic (interfacial) effects,[21] entrapping nanoparticles within the aqueous vesicle core or into the hydrophobic part of the lipid bilayer. Embedding functional hydrophobic nanoparticles provides a plethora of different applications for controlling bilayer permeability, biocompatibility, and liposomal release, also useful for investigating

biochemical reactions in vitro. In order to embed NPs into the hydrophobic membrane interior of a lipid bilayer, the nanoparticle must fulfill two requirements: first, it must be small enough (diameter less than 8 nm) to fit within the lipid bilayer dimension (<4 nm), and second, it must possess a hydrophobic surface. Thus, a plethora of hydrophobic nanoparticles such as fullerene (C_{60}),[238-239] gold,[6, 240] silver,[241-242] SiO_2,[243] and quantum dots[5, 244-246] have been comfortably embedded within lipid bilayers without significantly compromising the liposome structure. The enrichment of surface-functionalized hydrophobic nanoparticles within the lipid bilayer interior has been explained by Korgel et al.[28] as a result of NP interaction with the hydrophobic tail of the lipid molecules. Thus, hydrophobic nanoparticles can cause the bilayer to "unzip" when they are located at the center, leading to changes in lipid packing and disruption of lipid-lipid interactions between the lipid head groups and/or the lipid alkyl tails. This unzipping creates void space around the nanoparticles, resulting in nanoparticle clustering and minimization of the free energy of deformation. The incorporation of nanoparticles forming a hydrophobic or hydrophilic shell has been further reported in the literature to induce some secondary effects such as reduced lipid ordering with increasing nanoparticle loading,[25] formation of holes,[247] curving effects to or from the membrane,[43, 248] and fission and budding of vesicles.[249] The interaction of surface-functionalized nanoparticles with block copolymer (BCP) vesicles (polymersomes) has been shown to offer a convenient way of controlling the arrangement of nanoparticles in polymer vesicles by segregating nanoparticles into a more favorable interacting polymer domain or at the interface between two polymers.[60-61] Polymer/nanoparticle interactions can induce a morphological change of block copolymer assemblies,[73, 250] thus enabling the segregation of the NPs into the central hydrophobic position of either the membrane or its interface.[63] Eisenberg et al.[70] have shown that nanoparticles can selectively be incorporated into the central portion of block copolymer vesicle walls by coating the particles with a diblock copolymer having a similar structure to that of the diblock copolymers used in forming the polymersomal membrane. This allows the particles to be preferentially localized in the central portion of the membrane wall. The localization of surface-functionalized nanoparticles into a specific portion of the polymersomal membrane has also been shown to induce vesicle aggregation.[71, 251]

Recently, we have demonstrated the formation of truly biocompatible hybrid mono- and bilayer membranes[252] composed of an amphiphilic PEO_{17}-*b*-PIB_{88} BCP (**1**) (PEO = poly(ethylene oxide); PIB = poly(isobutylene) and a natural lipid (1,2-dipalmitoyl-sn-

glycerol-3-phosphocholine, DPPC). In general, the incorporation of such amphiphilic polymers into lipid membranes has been shown to influence transport properties and membrane stability and curvature, and to induce channels in the lipid membranes.[124, 253] Only a few examples[254-257] have been reported in the literature until now demonstrating a mixture between amphiphilic block copolymers and biological phospholipids within a bilayer membrane. It was observed that the incorporation of biocompatible polymers into DPPC monolayers using different amphiphilic PIB-PEO BCPs to DPPC ratios leads to remarkable effects on the lipid bilayer organization (i.e., the formation of a demixed system forming lipid- and polymer-rich domains from 20 to 28 mol% of the diblock copolymer). Thus, we were interested in investigating the selective localization of hydrophobic/ hydrophilic surface-functionalized nanoparticles in this demixed system, which may open a new prospective for subtle engineering of membranes and their nanoporosity, nanophased structure, and mechanical properties, serving as a model system in designing functional nanomaterials for effective nanomedicine or drug delivery.

In this chapter, we report the synthesis of polymer-grafted hydrophobic, hydrophilic, and amphiphilic surface-functionalized CdSe NPs, aiming at controlling their selective localization in a binary lipid/ polymer mixture via a direct assembly method on a Langmuir monolayer (see **Figure 15**).

As the now controllable interaction between the nanoparticle surfaces and the lipid/polymer part should allow a selective location, the synthesis of appropriately surface-functionalized nanoparticles with grafted polymer chains was envisioned. In order to further investigate the nanoparticle location within the monolayer, atomic force microscopy (AFM) and fluorescence monolayer studies were performed, also probing the selective interaction of the water-soluble hydrophilic NPs in the binary mixed system via adsorption measurements. The selective interaction between functionalized NPs and polymer domains in mixed monolayers can enhance the incorporation and localization of hydrophobic NPs into hybrid bilayer membranes. Furthermore, we were able to demonstrate the selective incorporation of PIB-modified CdSe NPs into the BCP phase of the phase-separated hybrid bilayer membrane composed of DPPC and the PEO_{17}-*b*-PIB_{87} BCP (**1**).

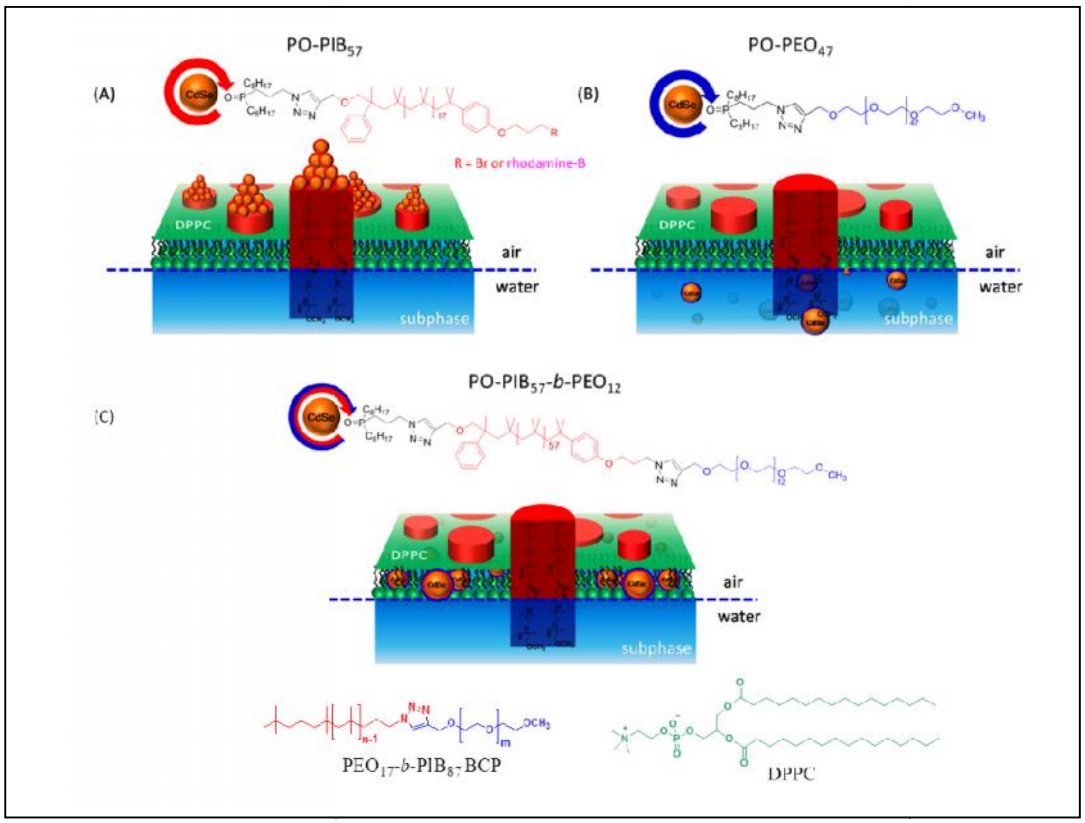

Figure 15: General concept for the location of polymer functionalized CdSe nanoparticles in mixed DPPC/ PEO_{17}-*b*-PIB_{87} BCP monolayers. (A) Specific location of hydrophobic modified NPs on top of the polymer-domains, (B) interaction of water-soluble NPs with mixed lipid/polymer monolayers within the subphase and (C) unspecific location of amphiphilic NPs in mixed monolayers at the air/water interface.

5.2 Result and Discussion

As part of the concept to investigate the controlled nanoparticle location in mixed lipid/polymer membranes, different nanoparticles with grafted polymer chains were investigated, featuring either purely hydrophobic, purely hydrophilic, or amphiphilic surface properties. As quantum dots can be prepared easily and their ligand exchange has been investigated intensely, CdSe nanoparticles (sized ~ 2 nm) were chosen as inorganic cores, together with phosphine oxides as ligands binding tightly but still exchangeable onto the quantum-dot surface. With poly(isobutylene) as hydrophobic and poly(ethylene oxide) as hydrophilic polymer a simple methodology of generating all three types of nanoparticles can be executed, using block copolymers composed of PIB-PEO in the case of amphiphilic nanoparticles. The following parts describe the synthesis of such polymer-covered quantum

dots, as well as their interaction with lipid monolayers in different, mixed, or phase-separated conditions.

5.2.1 Synthesis of polymer functionalized CdSe NPs

CdSe NPs, covered with either hydrophobic PIB_{57} (**NP3**), hydrophilic PEO_{47} (**NP4**), or the amphiphilic block copolymer PIB_{57}-*b*-PEO_{12} (**NP5**) were synthesized by exchanging the passivating trioctylphosphine oxide (TOPO) on **NP1** with a weak bonding pyridine to furnish **NP2**, followed by ligand exchange with either α-phosphineoxide-ω-bromo telechelic PIB (M_n(GPC) = 3200 g·mol^{-1}; M_w/M_n = 1.3) (**27**), α-phosphineoxide-ω-methylene telechelic PEO (M_n(GPC) = 2100 g·mol^{-1}, M_w/M_n = 1.2) (**31**), or α-phosphineoxide-ω-poly(ethylene oxide) telechelic polyisobutylene (M_n(GPC) = 3560 g·mol^{-1}; M_w/M_n = 1.3) (**29**),[258] yielding polymer-functionalized nanoparticles **NP3, NP4,** and **NP5,** respectively. All polymers were prepared via living polymerization methods, thus ensuring low polydispersity and controlled molecular weights, and subsequently attached to the nanoparticles via the phosphine oxide ligand as explained in the literature,[258] forming a highly stable bond. UV-vis measurements of the TOPO (**NP1**) and polymer-covered nanoparticles (**NP3, NP4,** and **NP5**) were conducted to ensure that no oxidation or aggregation had taken place during the pyridine treatment[259] (see appendix 2 **Figure S24**). According to the size and wavelength equation proposed by Peng *et al*.,[260] the first exciton peak at 512 nm corresponds to a 2.4 nm core diameter of the nanoparticles. After ligand exchange with polymers **27**, **31**, and **29** the first exciton peak of **NP1** still remained at around 512 nm, indicating the absence of aggregation or oxidation of the NPs during the process of ligand exchange. NMR spectroscopy showed that the signals coming from the part of the ligands being in the direct neighborhood or bound to the NP surface were strongly broadened or shifted in comparison to the free unbounded ligand. This can especially be observed in the broadening of the proton peak at 1.6 - 2.2 ppm in the phosphine oxide ligand bound to the NP surface (see appendix 2 Figure **S25**), which is in agreement with literature values.[261-263] The IR spectrum of **NP3**, **NP4**, and **NP5** showed peaks matching all the polymer peaks in frequency and relative intensity, except for the P-O stretching vibration in the region 1200 - 900 cm^{-1}, which is shifted about 20 cm^{-1} and broadened, confirming the direct attachment of the polymer to the NP surface (see appendix 2 **Figure S28**). These results are in good agreement with IR measurements performed on triphenylphosphine oxide ligand complexing to CdI_2 and other metal salts,[264] which typically show a shift in the P-O vibrational frequency between 20 and 60 cm^{-1} upon complexation.

The change in size of the nanoparticles as a result of replacing the TOPO ligand in **NP1** with the polymers **27**, **31**, and **29** was monitored by dynamic light scattering (DLS), which shows that replacing TOPO with α-phosphineoxide-ω-bromotelechelic PIB (PO-PIB_{56}-Br) (**27**), α-phosphineoxide-ω-methylene telechelic PEO (PO-PEO_{47}) (**31**), or α-phosphineoxide-ω-polyethylene oxide telechelic PO-PIB_{57}-*b*-PEO_{12} (**29**) induced an increase in the hydrodynamic diameter from 2.4 nm to 6.4 nm for the hydrophobic PO-PIB_{56}-Br-covered CdSe-NPs (**NP3**), to 9.9 nm for the hydrophilic PO-PEO_{47}-covered CdSe NPs (**NP4**), and to about 11 nm for the amphiphilic PO-PIB_{57}-*b*-PEO_{12} (**NP5**) (see **Table 5**).

Table 5. Characterization data for **NP3, NP4, NP5** and **NP6** *via* DLS, TGA, and UV-Vis and fluorescence spectroscopy.

NP	size before ligand exchange (nm)	size after ligand exchange (nm)[a]	grafting density (chains·nm^{-2})[b]	absorption maximum after ligand exchange (nm)[c]	emission maximum after ligand exchange (nm)[c]
NP3	2.4	6.4	0.5	513	625
NP4	2.4	9.9	0.47	513	570
NP5	2.4	11	0.53	513	540
NP6	2.4	6.3	0.52	513	585

[a]determined by dynamic light scattering (DLS), [b]determined by TGA, [c]determined by fluorescence spectroscopy

Thermogravimetric (TGA) measurements were conducted to evaluate the amount of polymer chains attached to the nanoparticles' surface. Thus, the grafting density of chains was obtained by relating the weight loss to the NP surface area using equation S1 according to ref [265] (see Supporting Information), resulting in a grafting density of 0.5 chains·nm^{-2} for the hydrophobic PIB_{57}-covered CdSe nanoparticles (**NP3**), 0.47 chains·nm^{-2} for the hydrophilic PEO_{47}-covered CdSe NPs (**NP4**), and 0.53 chains·nm^{-2} for the amphiphilic PO-PIB_{57}-*b*-PEO_{12}-covered nanoparticles (**NP5**). According to UV-vis measurements, an average of three chains of rhodamine-B labeled PIB (**38**) was calculated to be attached to each nanoparticle, furnishing the fluorescently-labeled **NP6**. The UV-vis intensity at a known concentration of rhodamine-B labeled PIB (**38**) was compared with that of a known concentration of the labeled **NP6**. As the amount of NPs at this concentration is known, the amount of polymer equaling the number of polymer chains attached to each nanoparticle was easily determined (see appendix 2 **Figure S33**).

5.2.2 *Interaction and location of hydrophobic CdSe NPs (NP3) in hybrid monolayers*

Effects of differently surface-modified NPs (**NP3** and **NP5**) on the phase behavior of hybrid DPPC:PEO_{17}-*b*-PIB_{87} monolayers were extensively studied by Langmuir monolayer measurements, serving as a model for half a bilayer membrane. In comparison to the isotherms of the pure DPPC and PEO_{17}-*b*-PIB_{87} BCP (**1**), which have been reported in the literature,[252, 266] the first significant increase in surface pressure of the hydrophobic PIB-covered CdSe NPs (**NP3**) was observed at a mean molecular area (mmA) of 1900 $Å^2$ (see **Figure 16A**, black curve). In an attempt to generate the full nanoparticle isotherm, increased amounts of NP were deposited at the air/water interface. Regardless of the amount of material deposited, we did not observe any monolayer collapse in which particle movement out of the monolayer was apparent. In all cases the barrier moved into the minimum area position without the monolayer showing any collapse point. This demonstrates that the particles are unable to form a two-dimensional rigid phase, which would break upon sufficient compression. Such behavior might be a result of a NP multilayer stack formation, which could be clearly seen by comparing the AFM height image of a transferred NP monolayer at 30 mNm^{-1} with that at 20 mNm^{-1} (see appendix 2 **Figure S29**).

The interaction of hydrophobic PIB-covered CdSe NPs (**NP3**) with hybrid DPPC:PEO_{17}-*b*-PIB_{87} (80:20 or 60:40 mol %) membranes was first investigated using a monolayer that mimics half a bilayer membrane. The effect of an increased nanoparticle loading on mixed DPPC:PEO_{17}-*b*-PIB_{87} monolayers was investigated, as shown in **Figure 16B** and **C**. In the 80:20 mol % mixture without nanoparticles (red curve), it can be seen that the amphiphilic PEO_{17}-*b*-PIB_{87} (**1**) copolymer molecule impacts the rearrangement behavior of the lipid molecules at the air/water interface, which results in the disturbance of the lipid packing, leading to a shift of the LE/LC transition plateau of DPPC to higher surface pressures (compare DPPC isotherm, black curve). A flattening of the isotherm of the 80:20 mol % mixture was observed in the low-pressure region between 0 and 8 mNm^{-1}, as the BCP chains support the persistence of the expanded phase of the lipid monolayer.

In the 80:20 mol % mixture with increasing amount of nanoparticles, 1:1000 (blue), 1:500 (green), and 1:50 (purple), with respect to PEO_{17}-*b*-PIB_{87} (**1**), the nanoparticles shift the isotherm of the 80:20 mixture to higher areas per molecule. This indicates that the incorporation of the polyisobutylene-covered CdSe NPs (**NP3**) into the 80:20 mol% mixed

monolayer reduces the free area of the DPPC and PEO_{17}-*b*-PIB_{87} (**1**), showing a lift-off at higher areas per molecule.

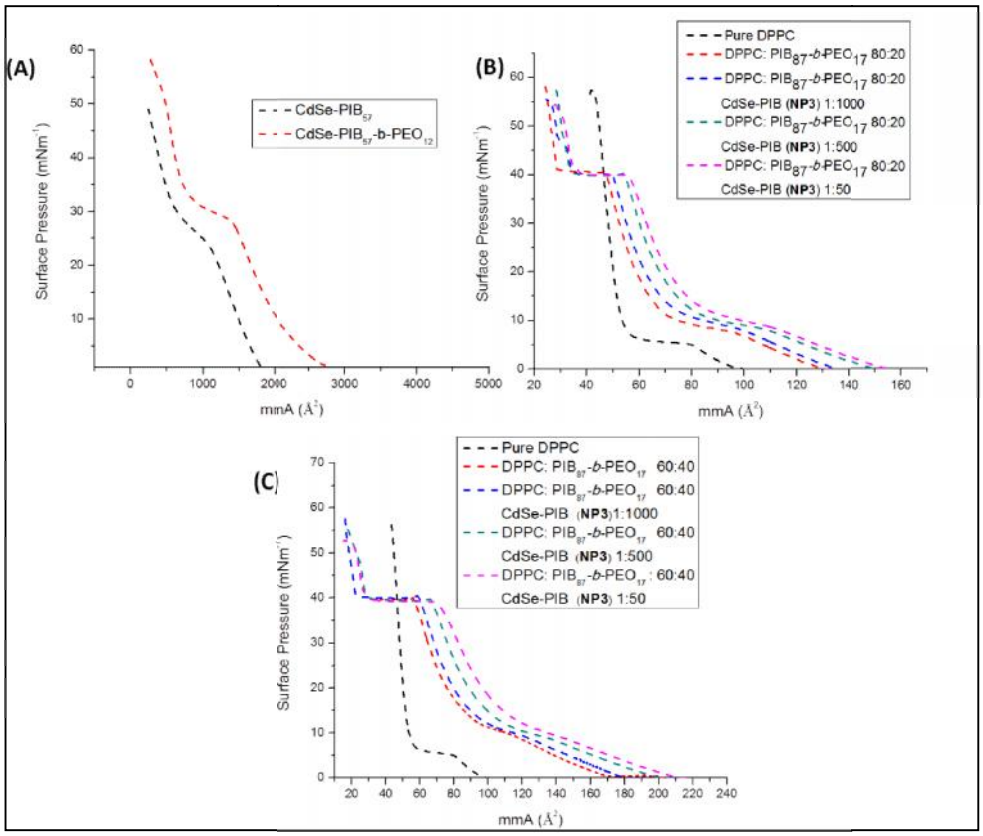

Figure 16. Langmuir monolayer isotherms of DPPC: PEO_{17}-*b*-PIB_{87} and NPs mixture (A) CdSe-PIB_{57} (**NP3**) (black) and CdSe-PIB_{57}-*b*-PEO_{12} (**NP5**) (red). (B) Mixture of DPPC: PEO_{17}-*b*-PIB_{87} in the ratio 80:20 mol% with hydrophobic PIB covered CdSe NPs **(NP3)** at different ratios. (C) Mixture of DPPC: PEO_{17}-*b*-PIB_{87} in the ratio 60:40 mol% with hydrophobic PIB covered CdSe NPs **(NP3)** at different ratios.

As a result of the NP penetration into the mixed monolayer, the lift-off in the isotherm related to the compression of the liquid expanded (LE) phase occurs at a higher area per molecule as the amount of nanoparticles increases. Considering the LE/liquid-condensed (LC) coexistence phase, incorporation of the PIB-covered CdSe NPs makes the LE/LC coexistence phase less flattened with increasing NP amounts. This might be interpreted as a result of hindering of the phase transition. A similar behavior was observed for the hydrophobic nanoparticles (**NP3**) interacting with mixed 60:40 mol % monolayer (see **Figure 16C**).

In order to locate the position of the hydrophobic NPs (**NP3**) in phase-separated DPPC:PEO_{17}-*b*-PIB_{87} monolayers,[252] where we know that the copolymer domains are getting larger with increasing copolymer content, AFM investigations were performed using the Langmuir Blodgett (LB) technique. Thus, monolayers of DPPC:PEO_{17}-*b*-PIB_{87} 80:20 or 60:40 mol % with hydrophobic PIB-covered CdSe NPs (**NP3**) (NP/ PEO_{17}-*b*-PIB_{87} = 1:1000) were transferred onto silicon substrates at 30 mNm^{-1} (comparable to the internal pressure of biological membranes).[267] Interestingly, the 80:20 mol % mixture without nanoparticles shows cylindrical-shaped mesomorphic PIB domains surrounded by the lipid monolayer, mostly dominated with a height of ∼11 nm, which scales exactly with a single-folded PIB chain, and other columns with a ∼22 nm height, corresponding to a fully stretched PIB chain, as explained in the literature[268] (see **Figure 17A**). The incorporation of **NP3** induces a morphological change of the cylindrical-shaped PIB columns into a cone-like structure with increased total heights up to ∼65 nm. These findings match with a hierarchical assembly in which the NPs are found to be selectively located on top of the PIB columns, forming three to eight NP stacks, as illustrated in **Figure 17B**. In contrast, the observed cone-like polymer domains in a 60:40 mixture (**Figure 18**) (DPPC:PEO_{17}-*b*-PIB_{87}) have heights up to ∼130 nm. A change in height of about 100 nm observed in the 60:40 mol % DPPC:PEO_{17}-*b*-PIB_{87} mixtures can be explained by the higher absolute amount of polymer in comparison to the 80:20 mixture. As the domain sizes and the number of domains are the same in both mixtures (80:20 and 60:40) and the fraction of the NPs/polymer stays constant (1:1000), the formation of higher NP stacks in comparison to the 80:20 mixture (DPPC:PEO_{17}-*b*-PIB_{87}) results. Additional interfacial effects could be responsible for the same number of domains in both cases.

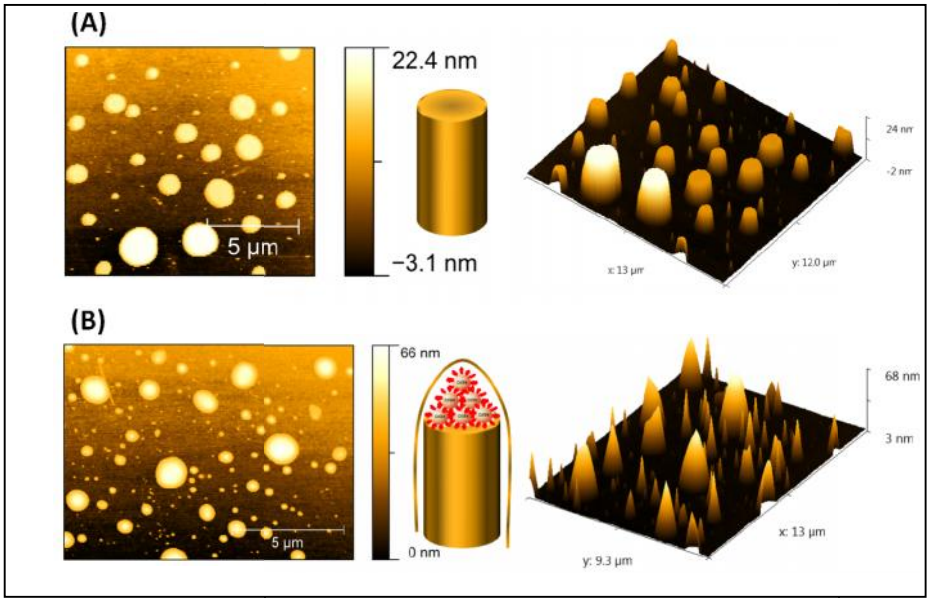

Figure 17. AFM height image of a mixed DPPC:PEO_{17}-*b*-PIB_{87} monolayer in the ratio 80:20 mol% transferred at a surface pressure of 30 mNm^{-1} (A) without NPs; (B) with hydrophobic PIB covered CdSe NPs (**NP3**).

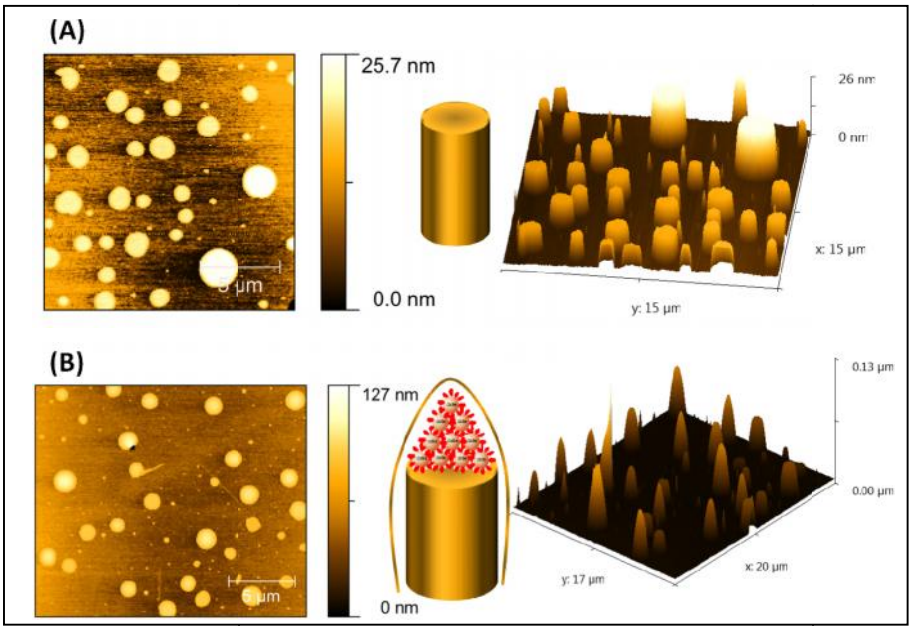

Figure 18. AFM height image of a mixed DPPC:PEO_{17}-*b*-PIB_{87} monolayer in the ratio 60:40 mol% transferred at a surface pressure of 30 mNm^{-1} (A) without NPs; (B) with hydrophobic PIB covered CdSe NPs **(NP3)**.

5.2.3 Interaction and location of amphiphilic CdSe NPs (NP5) in hybrid monolayers

When compared to the isotherm of PIB-covered CdSe NPs (**NP3**), the isotherms of the amphiphilic PIB_{57}-*b*-PEO_{12} covered CdSe NPs (**NP5**) showed a first significant rise in surface pressure at mmA of 2800 $Å^2$, which might be considered as a gas-to-liquid transition or sponge phase, followed by a continuous increase in the surface pressure and a pseudoplateau at 30 mNm^{-1} (**Figure 16A** (red)). The isotherm also did not show any collapse as the barrier moved into the minimum area position without the monolayer showing any collapse point.

Incorporation of amphiphilic nanoparticles (**NP5**) into mixed DPPC:PEO_{17}-*b*-PIB_{87} (80:20 or 60:40 mol %) membranes resulted in a significant disturbance of the lipid packing, shifting the isotherms of both the 80:20 and the 60:40 mol % mixtures to higher areas per molecule with increasing **NP5** ratio. This favors an earlier molecule packing at higher mmA values. The LE/LC coexistence region was less pronounced and shifted to higher surface pressure with increased **NP5** ratio as observed before in the case of **NP3** (see **Figure 19A** and **B**).

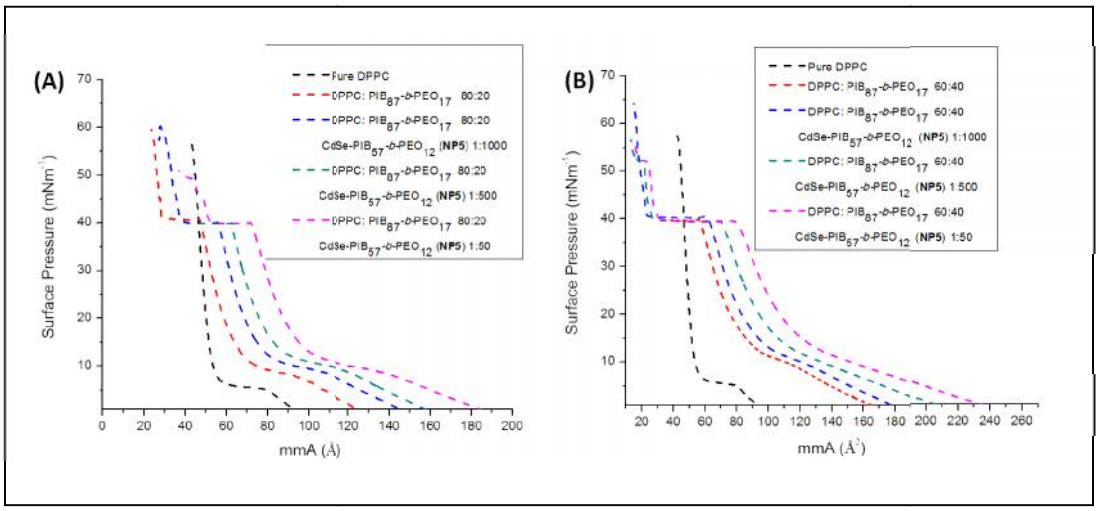

Figure 19. Langmuir monolayer isotherms of DPPC:PEO_{17}-*b*-PIB_{87} and NPs mixtures (A) mixture of DPPC:PEO_{17}-*b*-PIB_{87} in the ratio 80:20 mol % with amphiphilic PIB_{57}-*b*-PEO_{12} covered CdSe NPs (**NP5**) at different ratios. (B) Mixture of DPPC and PEO_{17}-*b*-PIB_{87} in the ratio 60:40 with amphiphilic PIB_{57}-*b*-PEO_{12} covered CdSe NPs (**NP5**) at different ratios.

This can be explained by the fact that the PEO block length (12 units) of the amphiphilic **NP5** is able to anchor the NPs to the air/water interface, but is not long enough to induce further effects on the phase transition state of the mixed monolayer, thus leading to a similar

isothermal behavior when using **NP3**. A monolayer of the ternary mixture of 80:20 mol % DPPC:PEO_{17}-*b*-PIB_{87} and amphiphilic NPs (**NP5**) was transferred onto silicon substrates and scanned with AFM. The AFM result (**Figure 20B**) revealed that amphiphilic NPs (**NP5**) induce a morphological change of the cylindrical-shaped PIB columns into cone-like structures with height increases from 24 nm up to 51 nm, similar to that observed for **NP3**. It should be noticed that the amphiphilic covered CdSe NPs could be located in the polymer-rich areas as well as in the lipid-rich areas of the monolayer. The small cone-like domains, as seen in the 3D height image of **Figure 20B**, are nearly homogeneously distributed in the transferred monolayer, which might be nanoscopic stacks of amphiphilic NPs being anchored to the silicon substrate by their short PEO chains.

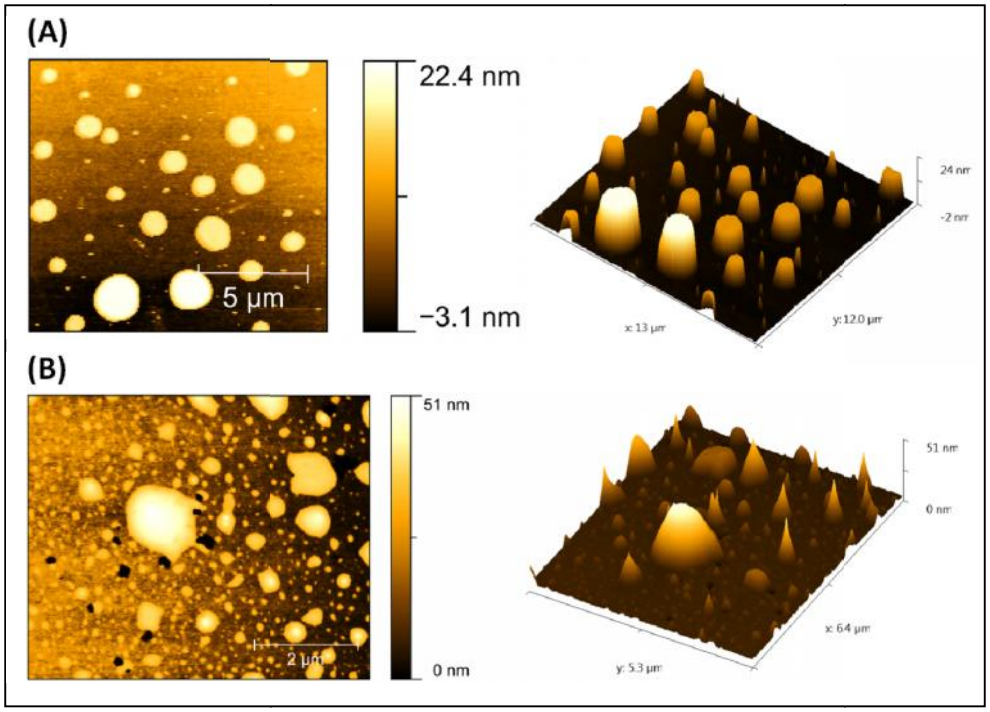

Figure 20. AFM height image of mixed DPPC:PEO_{17}-*b*-PIB_{87} monolayers in the ratio 80:20 mol% transferred at a surface pressure of 30 mNm^{-1}(A) without NPs; (B) with amphiphilic PIB_{57}-*b*-PEO_{12} covered CdSe NPs (**NP5**) transferred at the surface pressure of 30 mNm^{-1}.

5.2.4 Fluorescence microscopy of hydrophobic rhodamine-B labeled CdSe NPs (NP6) within hybrid monolayers

To prove the AFM results of transferred hybrid monolayers (composed of lipid, polymer and functionalized NPs), the morphology of these ternary mixed monolayers at the air/water

interface was monitored by fluorescence microscopy using fluorescent labeled hydrophobic CdSe NPs, similar to the morphology studies of binary mixed monolayers consisting of DPPC and PEO_{17}-*b*-PIB_{87} BCP, which was reported previously.[252] It was shown that mixed monolayers from 10 to 40 mol % of the diblock copolymer component demonstrate phase separation phenomena over the whole compression range. Initially, at low surface pressures ($\pi \leq 4$ mNm^{-1}) polymer-rich domains appeared completely round surrounded by the LE phase of DPPC showing a uniform fluorescence intensity signal of the rhodamine-B labeled lipid. Further compression of the film passing the well-known plateau region of DPPC (LE/LC transition)[266] forms pure LC domains of the lipid molecules.

An increase in the polymer content of mixed monolayers showed that the DPPC transition plateau was shifted to higher surface pressures, attributed to the BCP molecules, which support the persistence of the liquid-expanded phase of the lipid monolayer. Typically with increasing polymer content, we also observed that the separation process between the lipid and polymer molecules led to an increase in size of the polymer-rich domains.[252] In the present study, the goal of our work was to investigate the location of functionalized NPs in phase-separated lipid/polymer films depending on the monolayer compression state.

We therefore have labeled hydrophobic NPs (**NP3**) with rhodamine-B, thus generating **NP6**, which allowed the simultaneous monitoring of the localization of the labeled NPs in the phase-separated film. Fluorescence monolayer microscopy of lipid/polymer mixtures (80:20 mol %) treated with fluorescent labeled hydrophobic NPs (**NP6**) (NP to polymer ratio of 1 to 1000) revealed essentially the same hierarchical morphologies as observed by transferred monolayers (AFM studies). **Figure 21** presents fluorescence microscopy images of ternary mixed monolayers recorded at different surface pressures.

At low surface pressures (below 6 mNm^{-1}), we found only slight differences in the grayscale level of the monolayer images, corresponding to the formation of round polymer-rich domains (dark gray spots) in the liquid-expanded DPPC film (light gray). The observed small differences in brightness indicate that the NPs are nearly homogenously distributed in the lipid/polymer monolayer, showing no preferential location at low compression states of the films. With further compression of the monolayer passing the LC/LE phase transition of DPPC the nucleation and growth of pure DPPC LC domains occurred (see **Figure 21C-E**). These completely black-colored domains indicate a change of the NP miscibility with the lipid-rich areas so that the NPs are excluded from the LC monolayer regions. At higher surface pressures (above 12mNm^{-1}) the NPs start to move on top of the polymer-rich

domains, as clearly visible in **Figure 21F**, by displaying a very bright edge of the polymer domains. Obviously, the attractive interaction between the PIB columns formed by the PEO_{17}-*b*-PIB_{87} and the PIB corona of the NPs leads to such hierarchical ordering at the air/water interface. Fluorescence microscopy images at higher compression states of the ternary mixed monolayers (~30 mNm^{-1}) demonstrated that the NPs (**NP6**) are selectively located on top of the polymer-rich domains, showing a nearly homogeneous fluorescence intensity signal (polymer domains perceptibly increased in brightness; **Figure 21H**).

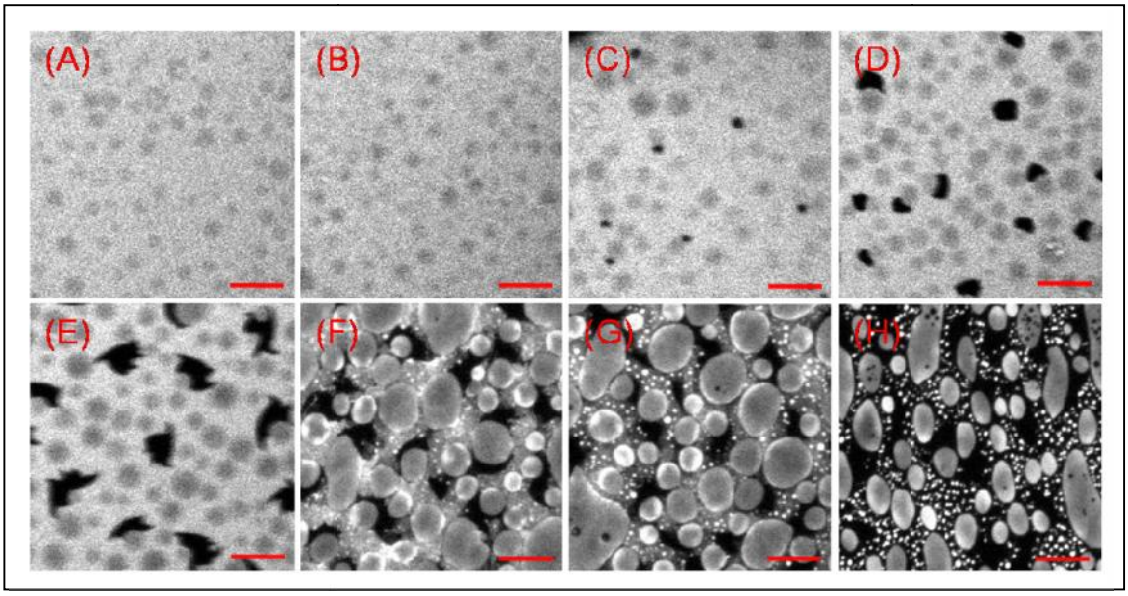

Figure 21. Fluorescence microscopy images of mixed DPPC:PEO_{17}-*b*-PIB_{87} monolayers 80:20 mol% at the air/water interface (20°C) mixed with fluorescently labeled NPs (**NP6**) to monitor their location and behavior depending on the compression state of the film. The images were recorded at surface pressures of 2.7 mN/m (A), 6.1 mN/m (B), 8.2 mN/m (C), 8.7 mN/m (D), 9.4 mN/m (E), 11.5 mN/m (F), 12.4 mN/m (G) and 30.1 mN/m (H). The scale bars represent 16 µm.

The initial homogeneous distribution of hydrophobic NPs in lipid/polymer monolayers varies strongly with increasing surface pressure. As mentioned earlier, the formation of pure DPPC (LC phase) domains already in the low surface pressure region (12 mNm^{-1}) leads to the selective location of the hydrophobic NPs in the polymer-rich areas of the phase-separated film, which demonstrates their attractive interaction. The final increase in brightness of the polymer domains at high surface pressures (30 mNm^{-1} and above), indicated by a nearly homogenously bright color of the polymer domains, confirms the result of our AFM studies

revealing the hierarchical ordering of the NPs on top of the BCP chains at the air/water interface.

5.2.5 Monolayer adsorption experiments of hydrophilic CdSe NPs (NP4) on pure and mixed DPPC/PEO_{17}-b-PIB_{87} monolayers

Since the interaction of hydrophilic PEO_{47}-covered NPs (**NP4**) with the mixed DPPC:PEO_{17}-*b*-PIB_{87} BCP (**1**) monolayer could not be investigated via Langmuir film balance measurements due to their excellent water solubility preventing any determination of a stable Langmuir isotherm, we have decided to investigate the effect of water-soluble CdSe NPs on pure DPPC, pure PEO_{17}-*b*-PIB_{87} BCP (**1**), and mixed DPPC:PEO_{17}-*b*-PIB_{87} monolayers by conducting monolayer adsorption measurements. Changes in the surface pressure as a function of time after injecting hydrophilic PEO-covered CdSe NPs (**NP4**) into the subphase below the spread monolayers of pure DPPC (black curve) (see **Figure 22**), pure PEO_{17}-*b*-PIB_{87} BCP (red curve), or binary mixtures (DPPC:PEO_{17}-*b*-PIB_{87} with 20 mol % (blue curve) or 40 mol % BCP (green curve)) caused by the surface adsorption of **NP4** are shown in **Figure 22**. The starting surface pressure (π_0) values were determined at time zero, which corresponds to the injection time of the NPs into the subphase. From the adsorption measurement, it is obvious that immediately after injection of the PEO covered CdSe NPs (**NP4**) the surface pressure starts to increase until an equilibrium value (π_{eq}) is reached, where a significant increase in the surface pressure could no longer be observed. The change in the surface pressure ($\Delta\pi$ ($\Delta\pi = \pi_{eq} - \pi_0$)) of all samples indicates that the PEO covered NPs (**NP4**) were rapidly adsorbed onto the hydrophilic portion of the monolayer at the air/water interface (*i.e*. displaying surface activity), where they can interact with the DPPC head groups and compete for area to occupy.

Changes in surface pressure, $\Delta\pi$, that were observed for pure PEO_{17}-*b*-PIB_{87} BCP (**1**) monolayers were not as large as compared to pure DPPC films at the same starting surface pressure, π_0. This could be explained by the fact that the PEO chains of the BCPs are dissolved and stretched into the subphase, which forms a barrier, thus preventing the hydrophilic NPs from coming up to the interface, which has an effect on the rearrangement behavior of the BCP chains (see schematic illustrations in **Figure 22**). Interestingly, the binary mixture of DPPC and the PEO_{17}-*b*-PIB_{87} BCP (**1**) using either 20 or 40 mol % of the polymer component showed that with increasing polymer content the changes in the surface pressure ($\Delta\pi$) decrease drastically, which implies less interaction of the NPs with the

molecules at the interface. This is in good agreement with the observations as obtained for pure polymer films, which showed minimal influence on the molecule organization by surface-adsorbed **NP4**, demonstrating attractive interactions between the PEO chains of the BCP and the functionalized NP shell, which keep the water-soluble NPs away from the air/water interface. The high affinity of the PEO-functionalized NPs (**NP4**) towards the hydrophilic portion of the BCP molecules is clearly seen by comparing the changes in surface pressure with increasing polymer content (see appendix 2 **Table S2**), assuming that the PEO chains of the BCP in phase-separated lipid/polymer monolayers submerged into the subphase might serve as an attractive barrier for the PEO-covered NPs (**NP4**), preventing interactions with DPPC domains. The starting pressure at which the NPs were injected (compare **Figure 23**, measurements at 10 and 20 mN m^{-1}) influences the magnitude of surface pressure changes ($\Delta\pi$) when nanoparticles were injected, demonstrating that the molecule packing density at the air/water interface regulates regulates the penetration ability of the hydrophilic CdSe NPs.

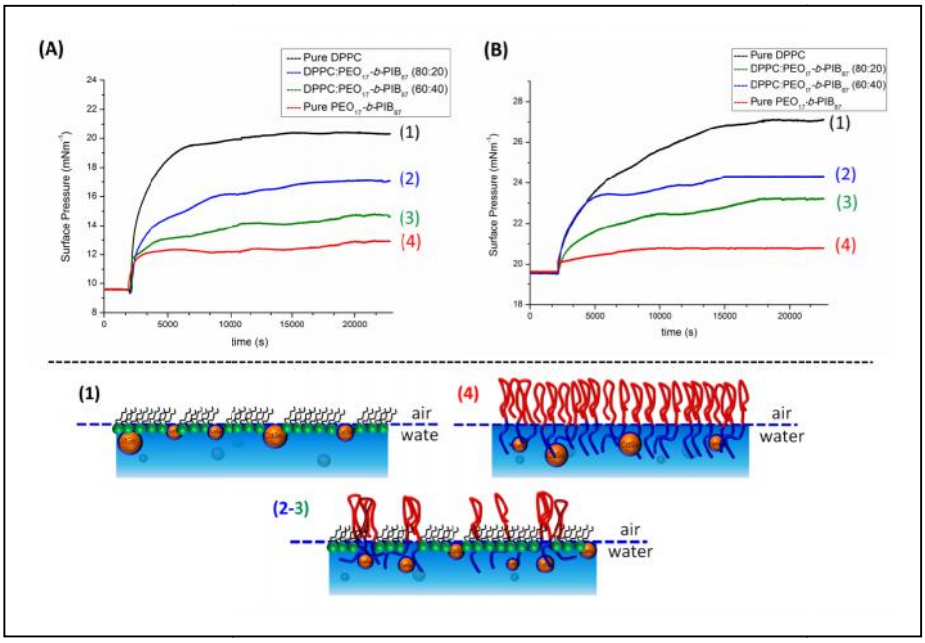

Figure 22. Time dependent Langmuir adsorption isotherms of **NP4** injected into the subphase at 20 °C of monolayers of pure DPPC (black curve), pure PEO_{17}-*b*-PIB_{87} (red curve) and mixtures of DPPC: PEO_{17}-*b*-PIB_{87} at 20 mol% (blue) and 40 mol% (green) PEO_{17}-*b*-PIB_{87} BCP at an initial surface pressures of (A) 10 mNm^{-1} and (B) 20 mNm^{-1}.

5.2.6 Bilayer investigations: Incorporation of hydrophobic NPs into hybrid bilayer membranes

As the monolayer studies of hydrophobic (PIB), hydrophilic (PEO), and amphiphilic (PIB-PEO) functionalized CdSe NPs with mixed lipid/polymer membranes composed of DPPC and the PEO_{17}-*b*-PIB_{87} block copolymer (**1**) have shown selective interactions depending on the NP surface hydrophobicity, the controlled localization of hydrophobic PIB modified CdSe NPs within the polymer domains was extended into a bilayer system using giant unilamellar vesicles (GUVs) consisting of DPPC and the PEO_{17}-*b*-PIB_{87} BCP (**1**). Such a designed amphiphilic block copolymer, when incorporated into gel-phase vesicles of DPPC, has been shown to induce different membrane morphologies by varying the lipid to polymer composition.[252] The membrane morphology of these hybrid vesicles appears uniform when prepared from mixtures below 20 mol % and above 30 mol % of the BCP component. In contrast, we have observed a phase-separated membrane morphology in the narrow compositional range between 20 and 28 mol % of BCP, resulting in the formation of lipid- and polymer-rich domains. Since NPs with diameters smaller than 8 nm are not expected to induce disruption of DPPC bilayer membranes,[17,22] we investigated the incorporation of hydrophobic CdSe NPs into the well-investigated hybrid membrane system, addressing the specific NP location with respect to the lipid/polymer mixing ratio and the resulting membrane morphology. Additionally, the size (~ 6 nm) of the NPs was expected to further drive a selective localization of the NPs into the BCP phase. Hybrid GUVs with incorporated **NP6** were formed by a modified electroformation method as originally reported by Angelova *et al*.[269] using a NP to lipid ratio of 1 to 1500. Since we expected that the incorporation of hydrophobic NPs will basically depend on the prevailing membrane morphology, a selective incorporation of the PIB-modified NPs into the polymer-rich phases should be observed. Therefore, we have chosen two different lipid/polymer mixing ratios, one showing a mixed (16 mol% BCP) and the other a phase-separated membrane morphology (20 mol % BCP), as shown in **Figure 23**.

For the 84:16 mol % mixture of lipid with BCP, the obtained hybrid GUVs with incorporated hydrophobic NPs (NP to lipid ratio = 1 to 1500) clearly demonstrate a uniform membrane morphology, which is visualized by monitoring the excited **NP6** (excited at a wavelength of 561 nm). The obtained hybrid GUVs remain stable, and no disruption of the bilayer membrane was observed at this NP to lipid ratio. As depicted in **Figure 23B** and **C**, the PIB-modified CdSe NPs are uniformly embedded within the whole hybrid bilayer, showing a

single-phase membrane. In contrast, we observed for the 80:20 mol % mixture of DPPC with PEO_{17}-*b*-PIB_{87} upon cooling to room temperature the formation of phase-separated membrane morphologies (**Figure 23D** to **F**).

Monitoring the fluorescent-labeled NPs **(NP6),** which are preferentially incorporated into one of the two prevailing phases (green-colored domains; see over view image in **Figure 24D**) we can attribute these domains to the polymer-rich phases. This is most likely, considering the fact that the polymer-functionalized NPs (**NP6**) exhibit a brush of polyisobutylene chains on their surface and should therefore be selectively incorporated into the polymer-rich domains. Consequently, we drew the conclusion that the dark domain in the hybrid GUV membrane, as shown in **Figure 23F**, is the lipid-rich phase showing no fluorescence signal of the **NP6**.

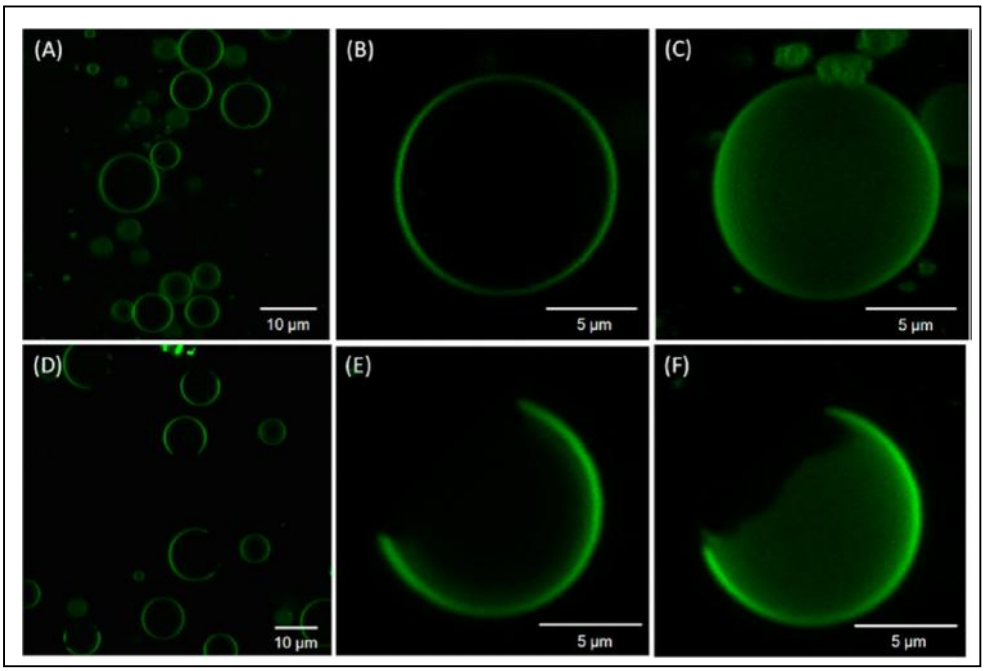

Figure 23. Confocal microscopy images of mixed (A-C) and phase-separated hybrid GUVs (D-F) composed of DPPC and the PEO_{17}-*b*-PIB_{87} BCP (**1**) with incorporated hydrophobic CdSe NPs (**NP6**) (NP to lipid ratio of 1 to 1500), demonstrating differences in the phase labeling behavior of the monitored fluorescent-labeled NPs by varying the lipid to BCP composition. Panels (A), (B), and (C) show an overview and single GUV images of mixed hybrid GUVs at RT, which were obtained from a 84:16 mol % mixture of DPPC with BCP, proving that the incorporated fluorescent CdSe NPs (**NP6**) (green, excited at 561 nm) are localized in the whole vesicle membrane. In panel (C), the 3D reconstruction of an axial series of confocal slices from the single GUV in (B) clearly demonstrates the uniform fluorescent intensity signal of the labeled NPs (green) in the hybrid GUV membrane.

Panels (D), (E), and (F) depict an overview and single GUV images of phase-separated hybrid GUVs at RT obtained from a 80:20 mol% mixture of DPPC with BCP, monitoring the fluorescent-labeled NPs. The fluorescent CdSe NPs preferentially partition into one of the two prevailing phases (black and green patches), as clearly shown in the 3D reconstruction of a single GUV in panel (F).

These domains appear upon cooling to room temperature below the transition temperature of DPPC (T_m = 41.6 °C), indicating that at room temperature (RT) the demixing process leads to the formation of more ordered lipid-rich domains,[270] which are depleted of polymer molecules. In contrast, at high temperatures (above T_m of DPPC) the hybrid bilayer is in a fluid state showing complete mixing.

5.3 Conclusions

We have thoroughly investigated the interaction of surface-grafted nanoparticles (CdSe, size 2 nm) with mixed monolayers, thus probing the different states of interaction between nanoparticles and mixed lipid/polymer membranes. As surface hydrophobicity plays a significant role in controlling the interaction between nanoparticles and lipid membranes, we demonstrate the preparation and characterization of polymer-functionalized CdSe NPs, based on ligand exchange of pyridine-covered CdSe nanoparticles with end group functionalized polymers, bearing phosphine oxide ligands for polymer chain attachment. As proven by DLS, TGA, NMR, and IR experiments, grafting of either hydrophobic (PIB), hydrophilic (PEO), or amphiphilic (PEO-PIB) chains onto the nanoparticles with grafting densities of ~0.5 chains·nm^{-2} can be achieved. Thus, the selective interaction of nanoparticles with mixed lipid/polymer membranes from 1,2-dipalmitoyl-sn-glycero-3-phophocholine and PEO_{17}-*b*-PIB_{87} block copolymer was demonstrated, depending purely on the type of NP surface. It was observed that hydrophobic PIB-modified CdSe NPs can be selectively located within polymer domains in a mixed lipid/polymer monolayer at the air/water interface by changing their typical domain morphology, while amphiphilic PIB-PEO-modified CdSe NPs showed no specific localization in phase-separated lipid/polymer films. As a result, AFM experiments of transferred monolayers could clearly demonstrate the specific “piling up” of the nanoparticles **NP3** on top of the separated PIB columns formed upon compression of the mixed monolayer. In addition, hydrophilic water-soluble PEO-modified CdSe NPs can readily adsorb onto spread monolayers, showing a larger effect on the molecular packing at the air/water interface in the case of pure lipid films compared to mixed monolayers. On the basis of attractive interactions between the polymer shell of the NPs and the hydrophilic block copolymer

chains, the NPs were shielded from lipid domains being merged with the BCP PEO chains in the subphase. Bilayer investigations using hybrid GUVs demonstrate that PIB-modified CdSe NPs were selectively incorporated into polymer-rich phases when incorporated into a DPPC:PEO_{17}-*b*-PIB_{87} mixture, which by itself initially formed phase-separated membrane morphologies. Preferential incorporation is a result of the formation of PIB brushes on the polymer functionalized NP surfaces (**NP6**), which leads to the specific location within the PIB phase of the BCP. Consequently, we could prove that the selective interactions between functionalized NPs and polymer domains in mixed lipid/polymer mono- and bilayers are possible by simply tuning the appropriate interfacial energies between the NP surfaces and the interacting membrane components. Thus, understanding the incorporation of nanoparticles into specific parts of bilayer membranes open a new prospect for subtle engineering of membranes, their nanoporosity, (nano-) domain structure, and mechanical properties serving as a model system in designing functional nanomaterials for effective nanomedicine or drug delivery.

6.0 Phase changes in mixed lipid/polymer membranes by multivalent nanoparticle recognition

Adekunle Olubummo, Matthias Schulz, Regina Schöps, Jörg Kressler, and Wolfgang H. Binder

Part of this chapter was published in Langmuir 2014, Volume **30***, Issue 1, Pages 259–267*

6.1 Introduction

Supramolecular recognition in the form of hydrogen bonds between a guest and a host molecule is one of the most important processes for spontaneous association of molecules under equilibrium conditions into stable structures, well defined aggregates and highly organized systems.[271-278] So far, many hydrogen-bonding systems have been often studied in organic solvents since hydrogen bonds tend to be weakened considerably in aqueous solution as a result of the competitive binding of water molecules in turn disrupting many hydrogen bonds.[279] However, due to their high specificity, hydrogen bonds exert a significant and still strong binding at interfaces, especially the air/water interface, given that they are affixed to amphiphilic compounds able to guide their interfacial assembly. Thus, Langmuir monolayers at the air/water interface have served extensively as a model system for one of the two coupled monolayers in a bilayer membrane to mimic the recognition of hydrogen bonds,[280-282] allowing to specifically study this molecular recognition between a dissolved guest and host component.[283-284] A significant number of hydrogen bonding interactions at the air/water interface have been studied (*e.g.* those between diaminotriazine (TRI) and thymine (THY) derivatives,[280] amphiphilic orate and adenine,[285] barbituric acid and triaminotriazine,[286] barbituric acid and melamine,[287] adenine and thymine,[288] guanidine and carboxylic-acids,[289-290] azobenzene and cyclodextrin[291] or β-cyclodextrin and cholesterol [292]) revealing the tendency to form relatively complex aggregates with such “simple” molecules. When the interaction between two supramolecular moieties is strong, removal of membrane components is evident showing distinct effects on the membrane organization. For example, when β-cyclodextrin (β-CD) interacts with cholesterol in mono-[293-295] and bi-layer membranes[292, 296-298] the ability of methyl-β-CD to remove cholesterol and/or phospholipids with high efficiency was demonstrated, also explaining their toxicity (membrane rupture) in cellular systems.

Significantly more complex structures with highly specific and selective interactions were formed when mixed monolayers were used, still allowing to selectively recognize soluble

analytes with the exactly matching hydrogen bonding pattern e.g. the recognition of flavine-adenine-dinucleotide by mixed thymine/guanidine amphiphiles at the air/water interface[299-301] or the recognition of a dipeptide by a mixed guanidinium/amide monolayer.[302-303]

The strength of molecular recognition at the air/water interface can be significantly enhanced which also leads to an increase in the association constant when compared to that of the respective interaction in bulk or in aqueous solution.[290,304-308] Additionally, multivalent molecular recognition at the air/water interface has been demonstrated in order to mimic the multiple cooperating functional units of biological molecules like enzymes, proteins and antibodies.[281, 301, 309] We[252, 310-311] and others[254-256, 312] have recently studied hybrid vesicles and monolayers as a result of blending natural lipids with synthetic polymer molecules forming hybrid membranes.[313-321] Depending on the composition and choice of lipids/polymers, either phase segregated or homogeneously mixed membrane surfaces were observed.[311, 314-315, 317] The formation of biocompatible hybrid DPPC/PEO_{17}-*b*-PIB_{87} **BCP 1** bilayer membranes reported in our group,[252] showed that their surface morphologies can be controlled by the lipid/**BCP 1** mixing ratio (see **Figure 9** on page 26). Thus, GUVs prepared from mixtures with 0 to 14 mol% of **BCP 1** showed a multifaceted vesicular surface typical for the gel phase behavior of DPPC-liposomes, whereas GUVs from mixtures above 14 mol% of **BCP 1** featured a completely closed membrane and a uniformly smooth surface. Furthermore, it was demonstrated that the composition of hybrid lipid/block copolymer membranes composed of **BCP 1** clearly influences the biological recognition between a membrane incorporated receptor-molecule (ganglioside) and a water soluble protein (cholera-toxin).[322]

This chapter investigates the supramolecular recognition between an amphiphilic **BCP 20** in mixtures with a lipid (DPPC or DOPC) and a multivalent nanoparticle (**NP7** and **NP8)**. To address a specific supramolecular interaction, the amphiphilic **BCP 20** was engineered to carry a 2,4-diaminotriazine (TRI) moiety on the hydrophilic PEO chain, thereby positioning the diaminotriazine at the vesicular surface of the mixed lipid/polymer membrane. In turn supramolecular recognition between a rhodamine-B labeled thymine-functionalized CdSe nanoparticle (**NP8**) and a triazine- (TRI) functionalized **BCP 20** was investigated using laser scanning microscopy and adsorption monolayer measurement.

6.2 Results and Discussion

In order to investigate the supramolecular recognition between the multivalent THY-functionalized nanoparticles (**NP7** and **NP8**) and mixed lipid/polymer membranes composed of DPPC or DOPC as lipid component in mixture with TRI-PEO_{13}-*b*-PIB_{83} (**20**) or PEO_{17}-*b*-PIB_{87} (**1**) as polymer component, hydrophilic CdSe nanoparticles (sized ~2 nm) with grafted PEO_{47}-THY chains on their surface were synthesized via a ligand exchange approach as reported earlier in our group.[124] To monitor the recognition process, **NP7** was further labeled with rhodamine-B to enhance its visualization by laser scanning microscopy. As it is known from literature that unsaturated lipids like DOPC (T_m = -20°C) are more fluid at room temperature than saturated lipids like DPPC (T_m = 41.6 °C),[323] we therefore investigated the role of membrane fluidity in the removal of membrane components by selective recognition and binding of water soluble molecules, similar to what has been reported for cholesterol/cyclodextrin interactions at mono- and bilayer membranes.[292]

6.3 Interaction of NP8 with binary and ternary DPPC/polymer mixtures

Previously, we have demonstrated the formation of biocompatible hybrid bilayer membranes composed of a synthesized amphiphilic PEO_{17}-*b*-PIB_{87} **BCP 1** and a natural lipid (DPPC).[252] To introduce a supramolecular recognition unit into our hybrid lipid/polymer system, we have synthesized an amphiphilic block copolymer TRI-PEO_{13}-*b*-PIB_{83} (**20**) bearing a hydrogen bonding moiety (triazine (TRI)) on the PEO chain, but comparable to the PEO_{17}-*b*-PIB_{87} **BCP 1** in its hydrophobic/hydrophilic chain length ratio (For details see Supplementary). We therefore expect the incorporation of this TRI-PEO_{13}-*b*-PIB_{83} BCP (**20**) into the lipid bilayer, thus functionalizing the GUV surfaces with moieties available to enable supramolecular recognition at the bilayer/water interface. Hybrid GUVs were prepared from a mixture of DPPC and 16 mol% of pure TRI-PEO_{13}-*b*-PIB_{83} **BCP 20**, featuring a completely round and smooth vesicle surface, which was stable when monitored over several hours. The results in **Figure 24A** and **B** are in accordance with previous investigation using PEO_{17}-*b*-PIB_{87} BCP (**1**) to prepare hybrid GUVs,[252] indicating no phase separation with respect to the resolution limit of the microscope (200 to 300 nm). Subsequently, a solution of **NP8** (3 $mg \cdot ml^{-1}$) was added to selectively recognize the triazine moiety of TRI-PEO_{13}-*b*-PIB_{83} BCP (**20**) in the hybrid GUVs. In the initial 5 to10 min after NP addition into the freshly prepared GUV suspension, the thymine-functionalized nanoparticles **NP8** recognize the triazine

moiety of the **BCP 20** within the mixed membrane, which effects the binding of the **NP4** to the membrane surface visible by increased fluorescence intensity of the NPs at the vesicle surface (excited at λ_{max}= 561 nm, rhodamine-B) (see appendix 3 **Figure S42**).

After 15 to 20 min of nanoparticle addition (see **Figure 24C** to **E**) facetation of the vesicle surface typical for pure DPPC or vesicles with less polymer content (< 14 mol %) was observed. This effect could be explained as a result of the removal of the TRI-PEO_{13}-*b*-PIB_{83} BCP (**20**) from the mixed GUVs thereby leaving the DPPC vesicles with reduced polymer content in their gel phase state (stable even after 24 hours **Figure 24F** to **H**).

As reported in the literature,[280] the single association constant (K_a) of thymine/triazine at the air/water interface was found to be $2*10^2$ M^{-1}. This single association between thymine/triazine can be significantly enhanced by the multivalency of the thymine functionalized **NP8** when they undergo supramolecular recognition with the triazine chain end of the membrane incorporated **BCP 20** molecules leading to a much stronger interaction. Thus, a selective removal of the **BCP 20** from the hybrid bilayer membrane can be explained, analogous to the reported selective removal of cholesterol from lipid membranes by cyclodextrin derivates displaying a binding constant of ~$1.7*10^4$ M^{-1}.[324]

To exclude unspecific destruction of the vesicle surface by the added nanoparticles,[29, 47] a control experiment was conducted where GUVs were prepared using a mixture of DPPC and 16 mol% of PEO_{17}-*b*-PIB_{87} BCP (**1**) devoid of any hydrogen bonding moieties; in contrast, the hybrid vesicles remained completely round with a smooth surface even after 24 hours of **NP8** addition (see **Figure 25**). The observed stability of the hybrid GUVs prepared from this mixture (16 mol% of **BCP 1**) shows that the previously observed vesicle facetation in the case of DPPC and 16 mol% of **BCP 20** is not a result of unspecific vesicle destruction by the nanoparticles.

To investigate the ability of the TRI-PEO_{13}-*b*-PIB_{83} **BCP 20** to form phase separated membrane morphologies as reported for PEO_{17}-*b*-PIB_{87} **BCP 1**, [252] we prepared GUVs from DPPC and 24 mol% of TRI-PEO_{13}-*b*-PIB_{83} BCP (**20**). Unexpectedly, in contrast to PEO_{17}-*b*-PIB_{87} **BCP 1**, the obtained vesicles featured a well mixed membrane morphology. Addition of **NP8** also induced vesicle facetation (data not shown). To further mimic biological receptor/ligand binding processes, we studied the selective recognition of **BCP 20** by the **NP8** in hybrid GUVs from a more complex ternary mixture containing DPPC, 11 mol% of PEO_{17}-*b*-PIB_{87} BCP (**1**) and 5 mol% of TRI-PEO_{13}-*b*-PIB_{83} **BCP 20**. As these mixed GUVs

now contain a total amount of 16 mol% of BCP (**1** and **20**) as mentioned earlier, they should display a completely closed membrane and a uniformly smooth surface.

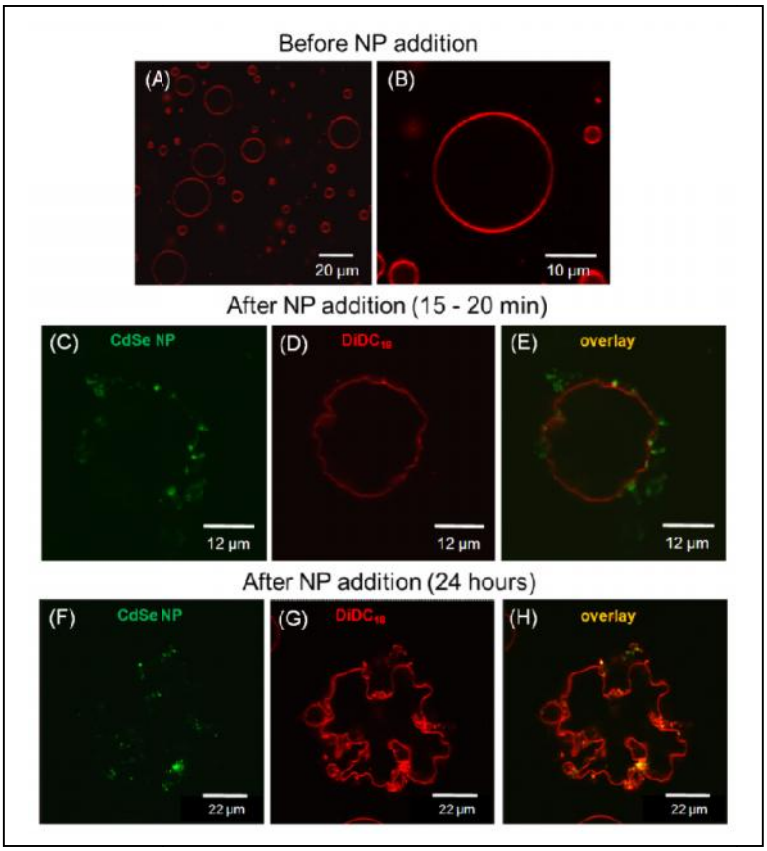

Figure 24. Confocal microscopy images of freshly prepared hybrid GUVs composed of DPPC and 16 mol% TRI-PEO_{13}-*b*-PIB_{83} BCP (**20**) showing the facetation effect of the vesicles upon addition of **NP8**. Panel (A) and (B) shows an overview and a single GUV image of hybrid GUVs, which were obtained from DPPC and 16 mol% TRI-PEO_{13}-*b*-PIB_{83} BCP (**20**) labeled with $DiDC_{18}$. Panel (C), (F) fluorescence of the rhodamine-B labeled PEO_{47}-thymine covered CdSe NP (**NP8**) (green; excited at 561 nm) showing their binding to the mixed GUV. Panel (D), (G) a single faceted GUV after 15 min and 24 h of **NP8** addition (red; excited at 633 nm). Panel (E), (H) overlay images showing the fluorescence of (**NP8**) as they bind to the GUVs after 15 min and 24 h of **NP8** addition.

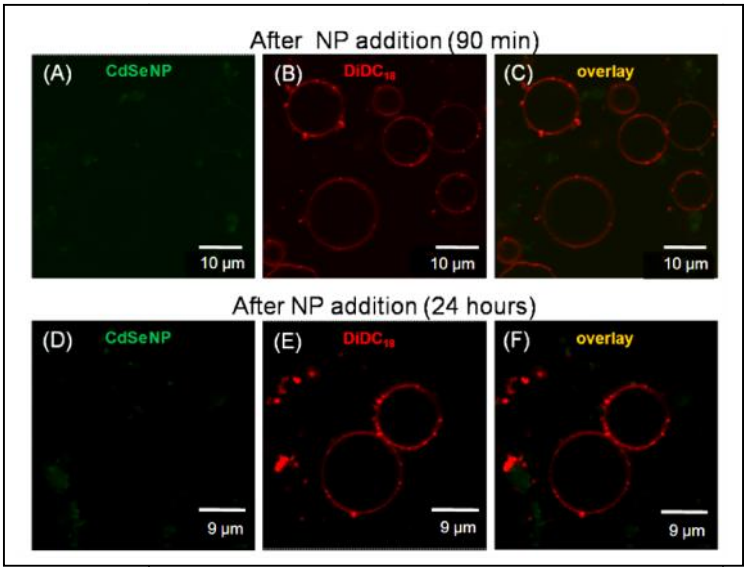

Figure 25. Confocal microscopy images of freshly prepared hybrid GUVs composed of DPPC and 16 mol% PEO_{17}-*b*-PIB_{87} **BCP 1**. Panel (A), (D) shows the fluorescence of the rhodamine-B labeled PEO_{47}-thymine covered CdSe NP (**NP8**) (green; excited at 561 nm). Panel (D), (G) single faceted GUVs after 15 min and 24 h of **NP8** addition (red; excited at 633 nm). Panel (C), (F) overlay images showing the fluorescence of (**NP8**) compared to $DiDC_{18}$ membrane dye.

In **Figure 26A** and **B**, the obtained hybrid GUVs from the now ternary mixture indeed showed a completely closed membrane and a uniformly smooth surface, stable over several hours. Adding **NP8** to the solution of the hybrid GUVs, the hybrid vesicles again became faceted after 20 to 30 min of the NP addition as shown in **Figure 26G** and **H**, which is as a result of the supramolecular interaction between the thymine-functionalized nanoparticles and the triazine of the **BCP 20**, followed by the selective removal of **BCP 20** from the mixed membrane now leaving behind the PEO_{17}-*b*-PIB_{87} (**BCP 1**) devoid of hydrogen bonds. As this remaining amount of **BCP 1** is not sufficient to prevent the formation of extended areas of gel phase in DPPC, the facetation was observed, as explained in the literature.[252]

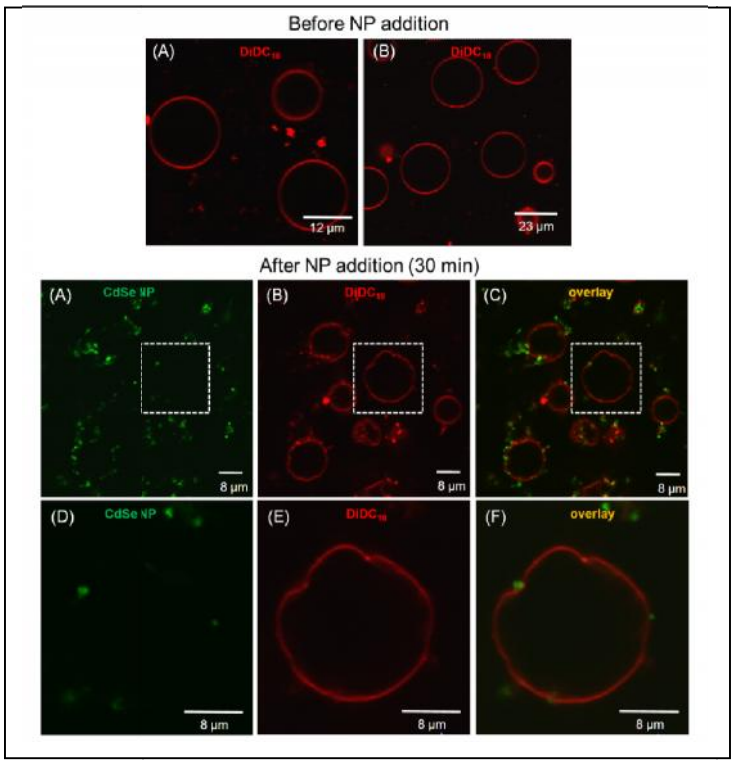

Figure 26. Confocal microscopy images of freshly prepared hybrid GUVs composed of DPPC with 11 mol% PEO_{17}-*b*-PIB_{87} **BCP 1** and 5 mol% of TRI-PEO_{13}-*b*-PIB_{83} **BCP 20**. Panel (A) and (B) shows an overview and a single GUV image of mixed hybrid GUVs. Panel (C), (F) fluorescence of the rhodamine-B labeled PEO_{47}-thymine covered CdSe NP (**NP8**) (green; excited at 561 nm) showing their binding to the mixed GUV. Panel (D), (G) show a single faceted GUVs after 30mins of **NP8** addition (red; excited at 633 nm). Panel (E), (H) overlay images showing the fluorescence of the (**NP8**) after 30 min of NP addition (green; excited at 561 nm) compared to $DiDC_{18}$.

6.4 Interaction of NP8 with binary and ternary DOPC/polymer mixtures

As known from literature unsaturated lipids like DOPC (T_m = -20 °C) are more fluid at room temperature in comparison to saturated lipids like DPPC (T_m = 41.6 °C).[323] We therefore investigated the supramolecular recognition between the triazine-functionalized **BCP 20** and the multivalent **NP8** in a more fluid system (using DOPC), having in mind that DOPC/polymer hybrid vesicles might show a different behavior compared to the facetation observed in DPPC membranes.

GUVs were first prepared from pure DOPC, which is known in literature to feature a completely closed membrane and a uniformly smooth surface. Our prepared DOPC GUVs

featured a completely closed membrane and a uniformly smooth surface separated from each other and stable when monitored over several hours see **Figure 27A**.

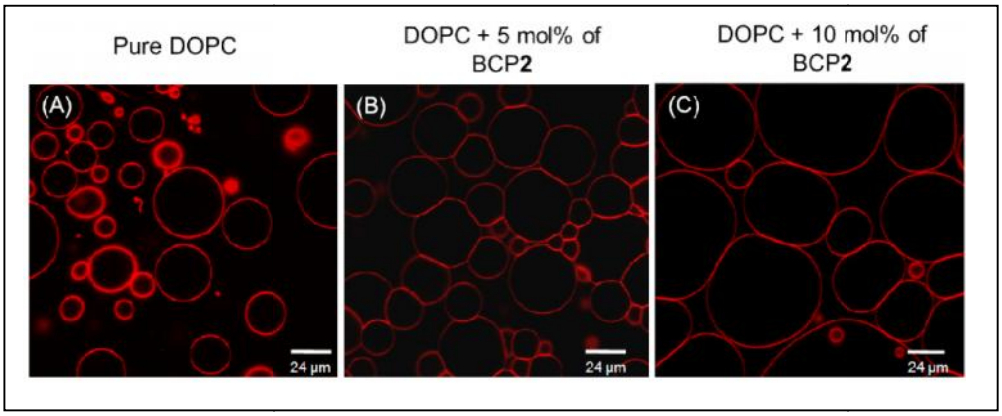

Figure 27. Confocal microscopy images of freshly prepared hybrid GUVs. Panel (A) pure DOPC, panel (B) mixture of DOPC and 5 mol% of TRI-PEO_{13}-*b*-PIB_{83} **BCP 20** and (C) mixtures of DOPC and 10 mol% of TRI-PEO_{13}-*b*-PIB_{83} **BCP 20** showing mixed GUVs which are connected to each other.

The formed hybrid GUVs observed from mixtures of DOPC with either 5 or 10 mol% of TRI-PEO_{13}-*b*-PIB_{83} **BCP 20** displayed the formation of contact areas between the vesicles, as shown in **Figure 27B** and **C**. These contact areas could be a result of the hydrogen bond interaction between the triazine molecules within the hybrid DOPC/BCP membranes, due to the now increased lateral fluidity as compared to hybrid GUVs from DPPC (rigid bilayers at *RT*) and BCPs. By addition of **NP8** to the freshly prepared suspension of hybrid GUVs containing either 5 or 10 mol% **BCP 20** (10 mol% case shown in **Figure 28**), it was observed that the NPs were specifically attracted to the edges of the formed contact areas between the hybrid GUVs where the polymers are concentrated by forming the intervesicular hydrogen bonds (see overview in **Figure 28A** to **C**). The recognition and binding of **NP8** to the triazine-functionalized vesicle surfaces lead to reduction of these intervesicular contact areas (see magnified membrane contact regions in **Figure 28E** to **F).**

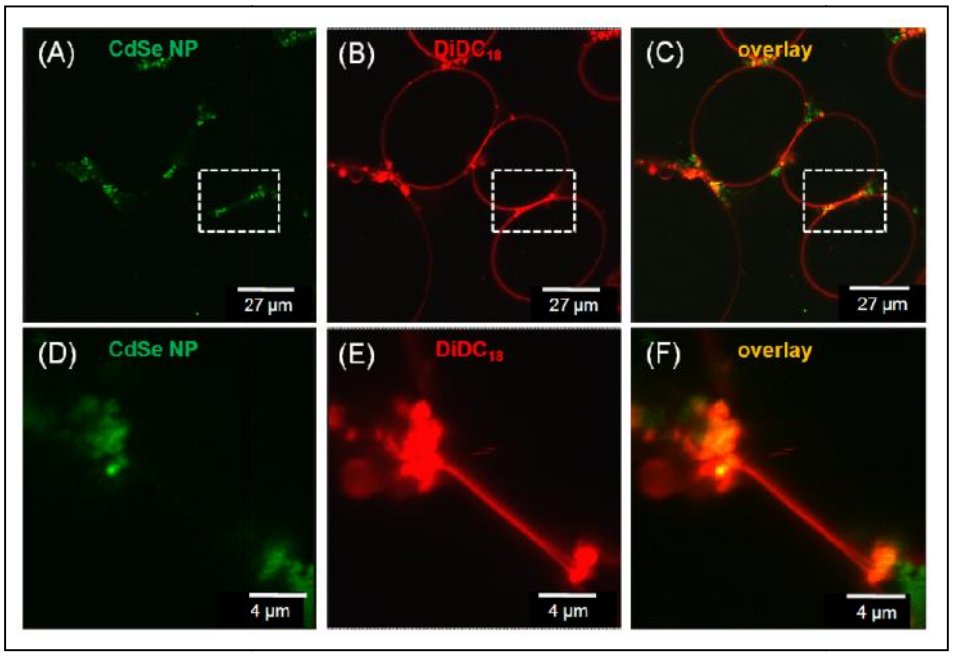

Figure 28. Confocal microscopy images of hybrid GUVs prepared from mixtures of DOPC and 10 mol % of TRI-PEO_{13}-*b*-PIB_{83} BCP (**20**). Panel (A to C) shows the specific attraction of **NP8** at the edges of the observed contact areas (i.e. **BCP 20** rich areas of the vesicular membrane). Panel (D to F) shows the magnified area of the single GUVs as indicated in panel (A to C), the specific recognition of the thymine-functionalized NP4 at the **BCP 20** rich regions of the polymer can be observed.

During that process, the removal of the TRI-PEO_{13}-*b*-PIB_{83} BCP (**20**) was confirmed by the destruction of all hybrid vesicles within minutes (most of all within 30 min) after addition of **NP8** (see also appendix 3 **Figure S43** showing a time series and appendix 3 **Figure S44/45** demonstrating microscopy images of destroyed GUVs). In general, we expected that the more fluid DOPC membrane would be better able to compensate the polymer extraction by the NPs compared to DPPC (highly rigid membranes at *RT*), but the experimental results clearly show that in case of fluid membranes all hybrid GUVs were destroyed by the fast polymer extraction (within minutes). This destruction of giant vesicles might be explained by the bending rigidity concept[326] of fluid membranes (DOPC) allowing high membrane curvatures of the lipid bilayer. Fluid membranes have much smaller bending rigidities (*i.e.* higher flexibilities)[327] compared to gel-phase membranes of DPPC (high bending rigidity) thus during the **BCP 20** extraction from the lipid bilayers, many defects in the membrane were formed resulting, in the case of fluid DOPC, in membrane fragments (nanometer range), which self-close to small unilamellar vesicles (highly curved membrane). Consequently, the

initial hybrid DOPC/BCP GUVs disappeared, and the formed small DOPC-rich vesicles were not detected by LSM due to the resolution limit of the microscope (~200 – 300 nm).

In a control experiment, GUVs were prepared using a mixture of DOPC with 10 or 15 mol % of **BCP1** devoid of hydrogen bonding moieties. The mixed GUVs also exhibited a completely round and smooth surface without the formation of contact areas when monitored for several hours. Addition of **NP 8** did not have any significant effect on the mixed GUVs in the first hours of monitoring (data not shown), which is remarkably different from the result observed in the mixed GUVs with **BCP 20** having hydrogen bonding moieties. After 24 hours, we observed that some of the vesicles from DPPC and **BCP 1** were still stable (round and smooth shape) whereas some were destroyed. Based on the observed removal of the triazine-functionalized polymers (**20**) from the mixed GUVs in the earlier discussed experiments, we decided to prepare GUVs from ternary mixtures of DOPC with 15 mol% of **BCP1** and 5 mol% of **BCP 20**, keeping in mind that if the 5 mol% of TRI-PEO_{13}-*b*-PIB_{83} BCP (**20**) are removed after **NP8** addition the remaining 15 mol% of PEO_{17}-*b*-PIB_{87} BCP (**1**) might be sufficient to maintain stable vesicles. Thus, GUVs prepared from mixtures of DOPC containing 15 mol% of **BCP1** and 5 mol% of **BCP 20** also featured a completely closed membrane and a uniformly smooth surface (see figure S13A in Supplementary). These vesicles were still visible after 60 min of **NP8** addition to the freshly prepared hybrid GUVs (see appendix 3 **Figure S46B to D**). The observed vesicles were stable as a consequence of the remaining 15 mol % of **BCP 1** in the mixed membrane which thus improved significantly the stability of DOPC GUVs during the selective removal of **BCP 20**.

To further investigate the effect of **NP8** on pure DOPC vesicles devoid of any hydrogen bonds, **NP8** was add to freshly prepared DOPC vesicles, which showed no destruction of the vesicles, when monitored over several hours (see appendix 3 **Figure S47**). These observations in contrast to hybrid DOPC/BCP GUVs prove that the observed vesicle destruction in case of DOPC/**BCP20** vesicles was induced by the selective removal of the triazine-functionalized polymer molecules from the hybrid membrane when the multivalent **NP8** was added.

6.5 Monolayer adsorption experiments of hydrophilic CdSe NP (NP7) with binary lipid/polymer mixtures

In order to better understand the nature of the supramolecular interaction observed in the bilayer experiment resulting to a selective removal of **BCP 20** due to the recognition and binding by **NP8**, we have chosen to study the supramolecular interaction by monolayer adsorption measurements. Adsorption experiments were earlier conducted in our laboratory[46] on mixed DPPC/**BCP 1** monolayers with hydrophilic PEO-covered CdSe NPs at the air/water interface. The high affinity of the PEO-functionalized NPs towards the hydrophilic portion of the BCP molecules was clearly seen by comparing the changes in surface pressure of a pure lipid and hybrid monolayer with increasing polymer content, assuming that the submerged PEO chains of the BCPs might serve as a barrier for the PEO-covered NPs (preferred interactions) preventing the NPs from approaching the air/water interface.

Therefore, we investigated the supramolecular recognition between the PEO_{47}-thymine functionalized nanoparticles (**NP3**) and hybrid monolayers from mixture of lipid (DPPC or DOPC) with **BCP20** at the air/water interface. In adsorption monolayer measurements, the lipid/polymer mixture was first spread on the subphase at the air/water interface, followed by injection of the nanoparticles into the subphase after reaching a stable monolayer (constant surface pressure).

Changes in the surface pressure were measured as a function of time after injecting the **NP7** into the subphase, as shown in **Figure 29** and **30.** From the adsorption measurement, it was evident that immediately after injecting the **NP7** (time of injection marked in blue in **Figure 29**) the surface pressure started to increase (as a result of the supramolecular interaction of NPs with the **BCP 20** molecules at the air/water interface and/or due to the surface activity of the NPs) until an equilibrium value π_{eq} was reached, where a significant increase in the surface pressure could no longer be observed. In case of DPPC/TRI-PEO_{13}-*b*-PIB_{83} mixtures higher changes in the surface pressure $\Delta\pi$ ($\Delta\pi = \pi_{eq} - \pi_0$) indicated that the multivalent PEO_{47}-thymine covered NPs can recognize the triazine moiety of **BCP 20** at the air/water interface. Comparing the mixture of DPPC/PEO_{17}-*b*-PIB_{87} (red curve) with DPPC/TRI-PEO_{13}-*b*-PIB_{83} (black curve) in **Figure 29**, it could be clearly seen that the supramolecular recognition between **NP7** and **BCP 20** leads to a significant higher increase in surface pressure as compared to the nonspecifically interacting DPPC/**BCP 1** mixtures.

The higher surface pressure change that was observed in the DPPC/**BCP 20** mixture is a result of the rapid adsorption of the NPs onto the hydrophilic portion of the monolayer supported by the hydrogen bond interactions between thymine and triazine moieties. Additionally as now the C_8H_{17}-chains attached to the **NP7** (see chemical structure of the phosphine oxide ligand in **NP7**) are close to the air/water interface, the strong increase in surface pressure can be the result of the insertion of the C_8H_{17}-chains into the hydrophobic portion of the hybrid monolayer. Based on this argument, we suggest that the much higher increase in surface pressure in case of the triazine-functionalized monolayer (DPPC/**BCP 20**) compared to the DPPC/**BCP 1** is caused by the specific supramolecular recognition between **NP7** and **BCP 20**. Thus, the particles closer to the air/water interface enable a much higher incorporation of the hydrophobic C_8H_{17}-chains rather than in case of the nonspecifically interacting DPPC/**BCP 1** monolayer, where the insertion of the C_8H_{17}-chains is just a statistical event.

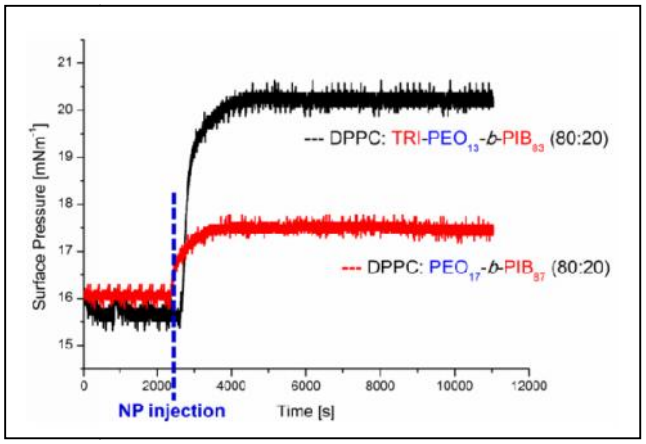

Figure 29. Time dependent Langmuir adsorption isotherms of hybrid monolayers after injection of **NP3** into the subphase below the monolayer, which is composed of a binary mixtures of DPPC (80 mol %)/TRI-PEO_{13}-*b*-PIB_{83} BCP (**20**) (20 mol%) (black curve) or DPPC/PEO_{17}-*b*-PIB_{83} BCP (**1**) (red curve), at 20 °C with an initial surface pressures of 16 mNm^{-1}.

To understand the role of fluidity as earlier explained in the case of bilayer investigations, we studied the interaction of the water soluble thymine-functionalized NPs (**NP3**) with hybrid monolayer from DOPC and **BCP 20** or **BCP 1**. After injection of the NPs into the subphase (see blue mark in **Figure 30**) an initial rise in the surface pressure was only noticed in case of the triazine-functionalized monolayer (DOPC/**BCP 20**) demonstrating the specific supramolecular recognition between the nanoparticles and **BCP 20** molecules. The initial

increase in surface pressure was followed by the drastic drop of the surface pressure, which might be explained by the selective removal of the polymer component (**BCP 20**) from the mixed monolayer into the subphase (see black curve in **Figure 30**). This result is consistent with those observed in the bilayer measurement, where the mixed GUVs prepared form a mixture of DOPC and **BCP 20** were completely destroyed after addition of **NP8** (within minutes). In case of the nonspecifically interacting monolayer (DOPC/**BCP 1**) without any hydrogen bonding moiety, a sudden decrease in surface pressure was observed after injecting **NP7** into the subphase. This drastic decrease in surface pressure might be caused by the diffusion of the nanoparticles to the air/water interface due to their surface activity, thereby inducing the collapse of the hybrid monolayer (see red curve in **Figure 30**) as shown by the strong drop from 19 mNm^{-1} to less than 13 mNm^{-1} within 150 mins.

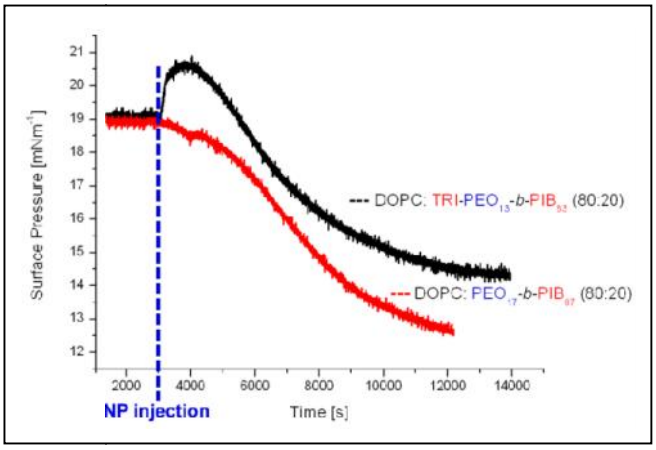

Figure 30. Time dependent Langmuir adsorption isotherms of hybrid monolayers after injection of **NP7** into the subphase below the monolayer, which is composed of either DOPC/TRI-PEO_{13}-*b*-PIB_{83} (black curve) or DPPC/PEO_{17}-*b*-PIB_{83} BCP (red curve), at 20 °C with an initial surface pressures of 19 mNm^{-1}.

6.6 Conclusion

The basic idea of this investigation concerned the recognition between a mixed membrane (lipid/amphiphilic block copolymer (**BCP 1** and/or **BCP 20**)) and a multivalent nanoparticle (**NP7** or **NP8**), with one membrane component (**BCP 20**) being able to recognize a specific hydrogen bond on the NP surface. In detail the supramolecular recognition of a triple-hydrogen bond (TRI/THY) between the amphiphilic **BCP 20** in mixture with either a liquid crystalline (DPPC) or a fluid (DOPC) lipid and a multivalent nanoparticle (**NP7** and **NP8**)

was chosen to effect a specific (multivalent) interaction between one membrane component and the nanoparticle. In a first step, the preparation of the amphiphilic block copolymer TRI-PEO_{13}-*b*-PIB_{83} (**20**) was accomplished carrying a 2,4-diaminotriazine (TRI) moiety on the hydrophilic PEO chain, thereby positioning the diaminotriazine at the vesicular surface of the mixed lipid/polymer membrane. In turn supramolecular recognition between a rhodamine-B labeled thymine-functionalized CdSe nanoparticle (**NP8**) and a triazine-functionalized BCP (**20**) were investigated using laser scanning microscopy and adsorption monolayer measurements.

Using hybrid GUVs as model bilayer membrane, NPs with surface bound THY-moieties (**NP3**) interacted specifically with a mixture of DPPC and 16 mol% of pure TRI-PEO_{13}-*b*-PIB_{83} BCP (**20**), first recognizing the triazine moiety of **BCP 20** within the mixed membrane, followed by removing the polymer component **BCP 20** from the mixed vesicular membrane thus leaving the DPPC GUVs with a now reduced polymer content in their respective gel phase state (stable even after 24 hours). Several experiments (also in ternary mixture from DPPC/**BCP1**/**BCP 20**) proved the selectivity of the interaction and the selective removal of the interacting **BCP 20**. Exchanging DPPC with DOPC as the now fluid lipid component at room temperature, GUVs fabricated from mixtures of DOPC/**BCP 20** indicated a selective interaction between the hydrophilic PEO_{47}-THY-functionalized CdSe-NPs (**NP8**) and **BCP 20** again leading to a selective removal of the polymer component, which finally resulted in destruction of the giant vesicles via membrane rupture. The differences in bending rigidities of fluid DOPC membranes (highly flexible) in contrast to gel-phase membranes of DPPC (high bending rigidity) lead, in case of hybrid DOPC/**BCP 20** membranes to the destruction of the GUVs into small vesicles, whereas the selective removal of **BCP 20** from rigid DPPC membranes results in the formation of highly faceted, giant vesicles as consequence of reducing the defects in the membrane obtained during the polymer extraction.

Adsorption experiments in mixed monolayers fabricated from DPPC/**BCP 20** revealed that hydrophilic THY-functionalized NPs can specifically recognize the triazine-functionalized BCPs (**20**) at the air/water interface inducing significantly higher changes in surface pressure when compared to a monolayer of the nonspecifically interacting DPPC/PEO_{17}-*b*-PIB_{87} mixture.

In summary, the presented method allows to specifically address recognition between membrane components and externally added nanoparticles via a relatively simple (supramolecular) interaction. Surprisingly, the in-water binding efficiency of the weak

THY/TRI-interaction is sufficient to selectively remove one membrane component from the mixed mono- or bilayer membrane. Similar to experiments showing the selective cholesterol-removal by cyclodextrins, the presented investigation demonstrated several phenomena relating to membrane-NP interactions, *e.g.* pore-formation, selective vesicle disintegration, and the specific binding of NPs to membrane receptors. The here demonstrated methodology is applicable to a large number of receptor molecules of similar or even stronger association constants between receptor and ligand. We thus do hope that this basic investigation can spur e.g. the selective capturing and detection of cancer cells via similar principles.

7.0 Experimental

7.1 Solvents and Reagents

All chemicals were purchased from Sigma-Aldrich (Schnelldorf, Germany) and were used as received unless otherwise stated. All solvents, which were used for the synthesis of the diblock copolymer and workup procedures, were distilled prior to use. Toluene and tetrahydrofuran (THF) were predried over potassium hydroxide for several days, refluxed over sodium/benzophenone, and freshly distilled under an argon atmosphere. The PIB-PEO diblock copolymer (PEO_{17}-*b*-PIB_{87} (**1**); M_n(NMR) = 5900 g·mol^{-1} determined by ^{1}H NMR) with a minimal polydispersity (PDI ≤ 1.2), used in this thesis, was synthesized in our laboratory via a combination of a living carbocationic polymerization method and the approach of the azide/alkyne "click" reaction, as reported previously.[252] 1,2-Dipalmitoyl-sn-glycero-3-phophocholine (M_n = 734.05 g·mol^{-1}) was purchased from Avanti Polar Lipids (Alabaster, AL, USA) and used without further purifications.

7.2 Methods

7.2.1 NMR measurement

^{1}H NMR and ^{13}C NMR spectra were obtained on a Gemini 2000 (Varian) FT-NMR spectrometer (200 and 400MHz) using MestRec-C software (vers. 4.9.9.6) for data interpretation. Deuterated chloroform ($CDCl_3$) from Sigma Aldrich was used for NMR investigations. All chemical shifts (δ) are given in parts per million (ppm) relative to Me_4Si (TMS) and referenced to the residual solvent signals [$CDCl_3$: 7.26 ppm (^{1}H) and 77.0 ppm (^{13}C)]. Coupling constants (J) are given in Hertz (Hz). To indicate the hydrogen coupling patterns, standard abbreviations are used (s = singlet; d = doublet; t = triplet; m = multiplet; bs = broad singlet).

7.2.2 GPC analysis

GPC analysis was performed on a Viscotek GPCmax VE2001 system and analyzed using the OmniSec (4.5.6) software. The investigations of polyisobutylene based polymers dissolved in THF were carried out on a Viscotek GPCmax VE2001 module combined with a Viscotek

TDA302 (triple detector array), and polyisobutylene standards were used for conventional external calibration. The polystyrene-divinylbenzene based column set consists of a H_{HR} – HGuard – 17 369 precolumn followed by a GMH_{HR} – N – Mixed Bed 18055 (1 000 to 4 x 10^5 Da) and a $G2500H_{HR}$ – 17,354 (100 to 2 x 10^4 Da) column. The detector/column temperature was 35°C, the flow rate of 1 mL.min^{-1}, and injection volume was 100 µL.

7.2.3 MALDI-TOF analysis

Matrix-assisted laser desorption/ionization time-of-flight mass spectrometry (MALDI-TOF MS) experiments were performed on a Bruker Autoflex III system operating in reflection and linear modes. The data evaluation was carried out on flexAnalysis software (vers. 3.0). Ions were formed by laser desorption (smart beam laser at 355, 532, 808, and 1,064 ± 5 nm; 3 ns pulse width; up to 2,500 Hz repetition rate), accelerated by voltage of 20 kV and detected as positive ions.The matrix solution was prepared by dissolving 1,8,9-anthracenetriol (dithranol) or *trans*-2-[3-(4-tert-butylphenyl)-2-methyl-2-propenylidene]malononitrile (DCTB) in chloroform at a concentration of 20 mg·mL^{-1}. Polymers were dissolved in chloroform at a concentration of 20 mg·mL^{-1}; salt AgTFA and KCl were dissolved at a concentration of 10 mg·mL^{-1} in chloroform and acetone, respectively. Solutions of the matrix, the polymer and the salt were mixed in a volume ratio of 100:10:1 and 1 mL of each mixture was spotted on the MALDI-target plate. Baseline subtraction and smoothing of the recorded spectra were performed using a three point Savitzky–Golay algorithm. The instrument was externally calibrated with poly(ethylene glycol) (PEG) standards (M_p = 2,000 and 4,200 g·mol^{-1}) applying a quadratic calibration method with an error of 1–2 ppm.

7.2.4 Langmuir monolayer measurements

Surface pressure (π) measurements of the pure compounds and of different binary mixed systems of PEO_{17}-*b*-PEO_{87} BCP, TRI-PEO_{13}-*b*-PIB_{83} BCP, DPPC, and NPs at the air/water interface were performed using a Langmuir trough system (KSV, Helsinki, Finland) with a maximum available surface of 76,800 mm^2. To minimize dust, the trough was kept in a closed box. The used subphase (water) was purified by a Pure lab Option system (ELGA Ltd., Celle, Germany). Before each measurement, the trough was purified four times with distilled water and two times with ultrapure water (total organic carbon < 5 ppm; conductivity < 0.055 µS·cm^{-1}). All compression measurements were performed at a constant

temperature (20 °C) achieved by a circulating water bath system. The investigated mixture of copolymers, DPPC, and NPs was dissolved in chloroform (HPLC grade, Sigma Aldrich, Schnelldorf Germany) at a concentration of 1 mM. Defined amounts (50 µL) of the prepared solutions (different molar ratios of DPPC to BCP and NPs) were spread on the subphase using a digital microsyringe (Hamilton, Schnelldorf Germany). Afterward, each surface pressure measurement using a compression rate of 5 $mm \cdot min^{-1}$ was started 15 min after spreading to ensure full evaporation of the solvent and a uniform monolayer formation. Monolayers were transferred at a speed of 1 $mm \cdot min^{-1}$ to silicon wafers that was previously hydrophilized by plasma treatment in the presence of oxygen.

7.2.5 Atomic force microscopy

In other to microscopically investigate the structure of the monolayer at a particular surface pressure, the monolayers were transferred to a solid substrate (silicon wafer or mica). The transfer process was achieved by depositing a solution of the polymer or surfactant onto the air/water interface, followed by steadily compressing the barriers until the transfer surface pressure was attained. The LB trough uses a feedback controller to maintain a constant surface pressure during the transfer process as a result of material loss as the monolayer is being removed.

Surface topography of LB films was studied using an atomic force microscope working in tapping mode with silicon cantilevers. Cantilevers were of type TESPA (NanoWorld, Switzerland) and had a nominal resonance frequency of about 285 kHz and an average spring constant of about 42 $N \cdot m^{-1}$.

7.2.6 UV-Vis spectroscopy

UV-Vis spectra were recorded in chloroform (HPLC-grade purchased from VWR Darmstadt Germany) at a concentration of 0.5 $mg \cdot mL^{-1}$ using a PerkinElmer Lambda 18 UV-vis spectrophotometer with 1 cm path length quartz cells. The absorbance values were used to calculate the nanocrystal diameters and the molar nanocrystal extinction coefficients. Particle size correlated to the color and consequently to the band gap of the particles. Peng *et al.*[260] investigated different particle sizes and found a correlation between size and wavelength leading to the final equation.

$$For\ CdSe: D = (1.6122\ x\ 10^{-9})\lambda^4 - (2.6575\ x\ 10^{-6})\lambda^3 + (1.6242\ x\ 10^{-3})\lambda^2 - (0.4277)\lambda + 41.57$$

In the above equation, D (nm) is the diameter or size of a given nanocrystal sample, and λ (nm) is the wavelength of the first exciton absorption peak of the nanoparticle solution.

7.2.7 TGA analysis

In the nanocrystal characterization, TGA enabled access to information on the grafting density of the ligand shell, as one could observe the presence of stepwise weight loss, which corresponded to organic ligand decomposition. TGA was conducted on a Mettler Toledo (DSC-H22) instrument. The sample was heated in a platinum pan under a nitrogen atmosphere over a temperature range of 25 to 800 °C with a heating rate of 10 $K \cdot min^{-1}$.

7.2.8 Hybrid GUV formation

The formation of hybrid lipid/polymer GUVs was achieved as described previously[252] using an electroformation method originally reported by Angelova *et al*.[269] Ultrapure water that was used for the study was purified via passage through a filtration system by Purelab Option system (ELGA Ltd., Celle, Germany). Briefly, all lipid/polymer mixtures varying in their compositions were prepared in chloroform (HPLC grade, Sigma Aldrich, Schnelldorf, Germany), dried under a continuous N_2-stream, and dissolved in a defined solvent volume, reaching a total concentration of 10 $mg \cdot mL^{-1}$. The final mixtures were used to generate a homogeneous thin film on optically transparent indium tin-oxide (ITO)-coated coverslips (electrodes) via a spin-coating method. Afterward, the coverslips were placed in a capacitor-type configuration at a distance of 2 mm using a home-built flowchamber. Finally, the flow-chamber was filled with water and the electroformation process was started.

7.2.9 Fluorescence microscopy monolayer investigations

Fluorescence microscopy imaging of monolayers at the air/water interface was performed using an "Axio Scope.A1 Vario" epifluorescence microscope (Carl Zeiss MicroImaging, Jena, Germany). The microscope was equipped with a Langmuir Teflon trough with a maximum area of 264 cm^2 and two symmetrically moveable computer-controlled Teflon barriers (Riegler & Kirstein, Berlin, Germany). The trough was positioned on an x-y stage

(Märzhäuser, Wetzlar, Germany) to be able to move the film balance with respect to the objective lens to any desired surface position. The x-y-z motion control was managed by a MAC5000 system (Ludl Electronic Products, Hawthorne, NY, USA). The trough was enclosed with a home-built Plexiglas hood to ensure a dust-free environment; the temperature of 20 °C was maintained with a circulating water bath, and the whole setup was placed on a vibration-damped optical table (Newport, Darmstadt, Germany). The air/water surface was illuminated using a 100 W mercury arc lamp with a long-distance objective (LD EC Epiplan-NEOFLUAR 50), and the respective wavelengths were selected with a filter/beam splitter combination, which is appropriate for the excitation and detection of Rh-DHPE (Zeiss filter set 20: excitation band-pass BP 546/12 nm, beam splitter FT 560 nm, emission band-pass BP 575-640 nm). Images were recorded using an EMCCD camera (Image EM C9100-13, Hamamatsu, Herrsching, Germany). Image analysis and data acquisition were done using AxioVision software (Carl Zeiss MicroImaging, Jena, Germany). All presented images show areas of individually contrast-adjusted raw data.

7.3.0 Adsorption measurements

Monolayer adsorption experiments at the air/water interface were carried out at 20 °C starting with different initial surface pressures of pure lipid, pure diblock copolymer, and lipid/ diblock mixture (with diblock copolymer amounts of 20 and 40 mol %) on a circular Langmuir trough with a diameter of 3 cm, a depth of 1.39 cm, and a subphase volume of 10.25 mL (Riegler & Kirstein, Berlin, Germany). For preparation of the pure and mixed monolayers, a defined amount in HPLC-grade chloroform was spread with a digital Hamilton microsyringe onto the water subphase of Millipore quality (total organic carbon < 5 ppm; conductivity < 0.055 μScm^{-1}). After waiting for 20 min for complete solvent evaporation and uniform dispersion of the monolayer molecules at the air/water interface, 10 µL of the water soluble hydrophilic CdSe nanoparticles (25 or 5 $mgmL^{-1}$) was injected into the subphase below the monolayers through a channel located at the bottom of the Langmuir trough. In order to ensure a homogeneous bulk concentration of NPs in the subphase and in order to avoid large perturbations at the air/water interface, the subphase was gently stirred with a small rolling sphere. The changes of surface pressure (mNm^{-1}) at the air/water interface caused by the injected aqueous solution of NP were monitored as a function of time (seconds) by measuring initial and final surface pressure using a filter paper as a Wilhelmy plate.

7.3.1 Dynamic light scattering

DLS measurements were performed in chloroform solutions of the NPs after dilution by ~ 1/50 with pure solvent on a Viscotek 802 using OmniSIZE software.

7.3.2 FTIR measurement

Infrared measurements were performed on a Bruker Vertex 70 FT-IR spectrometer (Bruker, Leipzig, Germany) from 3500 to 1000 cm^{-1} using an ATR diamond crystal.

7.3.3 Giant vesicle analysis by confocal laser scanning microscopy

Confocal microscopy images were obtained on a commercially available confocal laser scanning microscope (LSM 710/ConfoCor3; Carl-Zeiss, Germany) using a C-Apochromat 40*/1.2 NA water immersion objective. The hydrophobically functionalized NPs, which were fluorescently labeled with rhodamine-B, were excited with a DPSS laser at 561 nm. Lipophilic carbocyanine DiDC18 was also used as membrane label and was excited with a HeNe laser at 633 nm. Furthermore, Rh–DHPE was also used as fluorescence dye, which was excited with an Argon-Ion-laser at 488 or 514 nm. Imaging of all GUV samples was performed after cooling to room temperature unless otherwise stated.

7.3.4 Supramolecular recognition studies with rhodamine-B labeled water soluble CdSe NP (NP8)

All supramolecular recognition studies between **NP8** and hybrid GUVs consisting either of DPPC or DOPC with incorporated TRI-PEO_{13}-*b*-PIB_{83} BCP (**20**) and/or the PEO_{17}-*b*-PIB_{87} BCP (**1**) were conducted at room temperature (20°C). After the electroformation process, the prepared GUVs with incorporated BCP molecules were first cooled down to room temperature, monitored by laser scanning microscopy revealing changes in their membrane morphologies and afterwards incubated with an aqueous solution of nanoparticles (**NP8**). Using a microsyringe, 50 µL (3 $mg \cdot ml^{-1}$) of the water soluble CdSe nanoparticle solution was injected into the flow chamber which contained the freshly prepared vesicles. The recognition process was thereafter monitored by laser scanning microscopy. All recognition studies were performed using fluorescently labeled NP (**NP8**) (excited at 561 nm, green color).

7.4 Synthesis

7.4.1 Synthesis of methyl styrene epoxide (4)[328]

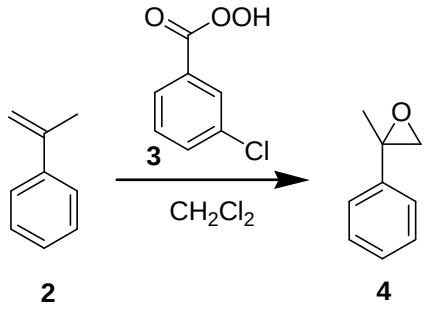

Methyl styrene epoxide (MSE) (**4**) was synthesized by the epoxidation reaction of α-methyl styrene (**2**) with pure 3-chloroperoxybenzoic acid (MCPBA) (**3**) in dichloromethane (CH_2Cl_2) as follows: α-methyl styrene (**2**) (4g, 3.6mL, 0.034mol) was distilled under reduced pressure (40°C, 1bar) prior to use and charged into a 250 ml three neck round bottom flask containing 80 ml of CH_2Cl_2 equipped with a mechanical stirrer and a dropping funnel. The mixture was stirred and cooled down to 0 °C with an ice bath. MCPBA 70% (**3**) (6g, 0.037 mol) dissolved in 70 mL of CH_2Cl_2 was added drop-wise. The resulting mixture was stirred at 0 °C for 3 hours. After 3 hours the mixture was washed with 10% Na_2CO_3 (5 times) till all the excess MCPBA was removed and then washed with saturated NaCl solution. The organic layer was dried with Na_2SO_4 and the solvent was removed with a rotary evaporator. The resulting slight yellow liquid (**4**) (yield 98 %, 3.9 g) was analyzed with NMR.

^{1}H-NMR (400 MHz, $CDCl_3$): δ ppm 7.40-7.31 (m, 5H), 2.95 (d, J = 5.43 Hz, 1H), 2.78 (d, J = 5.43 Hz, 1H), 1.72 (s, 1H); **^{13}C-NMR** (400 MHz, $CDCl_3$) δ ppm 141.1, 128.4, 127.4, 125.3, 57.0, 56.8, 22.0

7.4.2 Synthesis of α-hydroxymethyl-ω-bromo telechelic PIB (5) [230, 329]

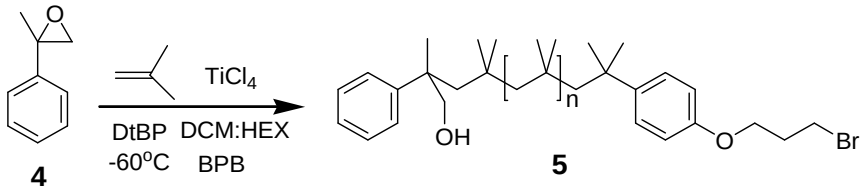

5a; n = 57 (M_n = 3190 gmol^{-1}, PDI= 1.2)

5b; n = 83 (M_n = 4500 gmol^{-1}, PDI= 1.2)

5c; n = 100 (M_n = 5600 gmol^{-1}, PDI= 1.2)

A representative procedure for the synthesis of α-hydroxymethyl-ω-bromo telechelic PIB (**5**) with M_n = 4000 g·mol^{-1} using a combination of methods of Puskas and co workers[329] and Morgan and Storey[230] was as follows: under a nitrogen atmosphere, dichloromethane/olefin-free n-hexane (solvent mixture; 40/60), di-*tert*-butyl pyridine (5 mmol·L^{-1}), and MSE (**4**) initiator (0.049 mol·L^{-1}) were chilled to -60°C in a three-necked round–bottom flask equipped with a septum and a mechanical stirrer. To the mixture was added a prechilled solution of $TiCl_4$ (0.034 mol·L^{-1}). The polymerization was started by charging condensed isobutylene (1 mol·L^{-1}) into the reactor with a syringe. After complete monomer conversion as judged via inline IR spectroscopy (~ 30 min) the polymerization mixture was cooled to -70 °C, and quantitative end-capping was achieved by directly charging an excess (2.5 equiv. per chain end) of 3-bromopropoxybenzene (BPB) to the reaction mixture. After 3 hours, the catalyst was destroyed by addition of excess methanol, and the PIB was isolated by repeated precipitation from hexane into methanol. The resulting α-hydroxymethyl-ω-bromo telechelic PIB (**5**) was obtained in a yield of 98%, 4.9 g.

^{1}H-NMR (400 MHz, $CDCl_3$) δ ppm 7.35 (d, J = 7.74 Hz, 2H), 7.30 (t, J = 7.65 Hz, 2H), (t, J = 6.25 Hz, 1H), 6.82 (d, J = 8.79 Hz, 2H), 4.08 (t, J = 5.78 Hz, 2H), 3.64 (d, J = 10.77 Hz, 1H), 3.58 (t, J = 6.53 Hz, 2H), 3.41 (d, J = 10.78 Hz, 1H), 2.29 (p, J = 6.23 Hz, 2H); **^{13}C-NMR** (400 MHz, $CDCl_3$): δ ppm 154, 148.5, 141.6, 128.4, 125.7, 125.1, 114, 70.1, 67.3, 53.4, 43.8, 32.6, 30, 28, 20.5.

7.4.3 Synthesis of ~ϳalkynyl-μ-bromo telechelic PIB (6)[330]

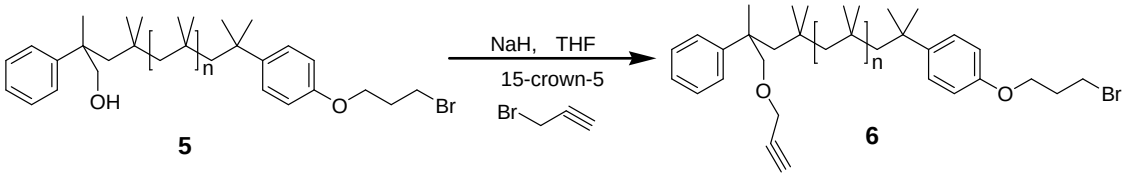

5 **6**

6a; n = 57 (M_n = 3200 gmol^{-1}, PDI= 1.2)

6b; n = 83 (M_n = 4500 gmol^{-1}, PDI= 1.2)

6c; n = 100 (M_n = 5400 gmol^{-1}, PDI= 1.2)

NaH (1.2 equiv. 17 mg 0.71 mmol) was washed three times with dry THF under an argon atmosphere to remove the mineral oil and cooled down to 0 °C in an ice bath. α-Hydroxymethyl-ω-bromo telechelic PIB (**4**) (2.5 g, 0.595 mmol) and 15-crown-5 (1 equiv. 0.131 g, 0.595 mmol) were added drop-wise. The reaction mixture was allowed to stir at 0 °C for 30 min, and propargyl bromide (80% in toluene, 2 equiv. 0.141 g, 1.2 mmol) was added slowly. The ice bath was removed and the reaction was further stirred at 35 °C for 48 hours.

After 48 hours, the THF was removed with a rotary evaporator. The residue was suspended in hexane, washed three times with water, once with brine and dried over Na_2SO_4. The α-alkyne-ω-bromo telechelic PIB (**5**) was isolated by precipitation from hexane into methanol: acetone (1:1) to form a slight yellow product with 95% yield, 2.4 g.

^{1}H-NMR (400 MHz, $CDCl_3$) δ ppm 6.81 (d, J = 8.46 Hz, 2H), 4.08 (m, 4H), 3.64 (d, J = 10.77 Hz, 1H), 3.58 (t, J = 6.53 Hz, 2H), 3.41 (d, J = 10.78 Hz, 1H), 2.35 (m, 1H) 2.29 (p, J = 6.23 Hz, 2H); **^{13}C-NMR** (400 MHz, $CDCl_3$): δ 154, 148.5, 141.6, 128.4, 125.7, 125.1, 114, 82.3, 75.6, 73.4, 71.7, 67.3, 53.4, 43.8, 32.6, 30, 28, 20.5.

7.4.4 Synthesis of α-methoxy-ω-azido telechelic polyethylene oxide (9)[330]

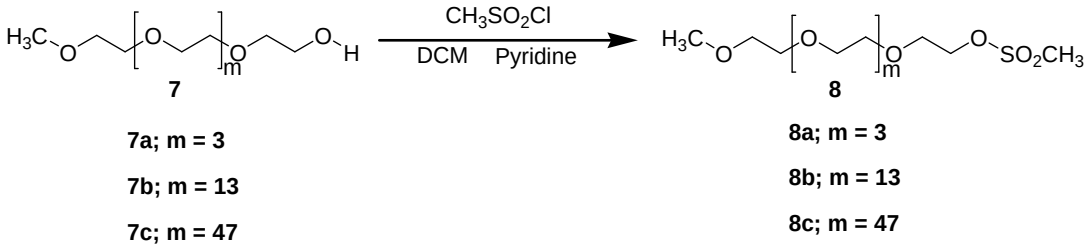

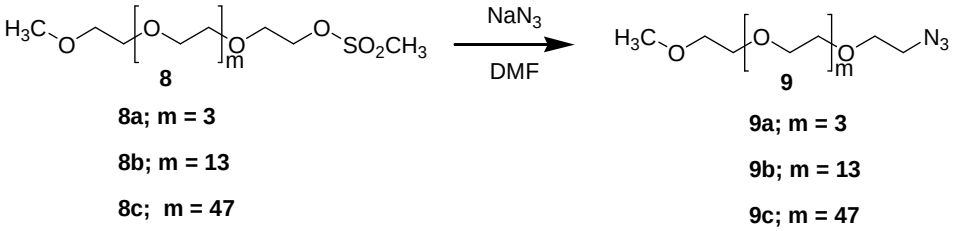

α-Methoxy-ω-azido telechelic triethylene oxide (**9a**) was synthesized according to literature[330] as follows. Methanesulfonyl chloride (5.0 mL, 0.065 mol) solution in 200 ml DCM was added drop-wise to triethylene glycol monomethyl ether (**7a**) (2 g, 0.012 mol) solution in 15 ml of pyridine vigorously stirred and cooled to 0 °C. The reaction mixture was allowed to warm to room temperature and stirred with a magnetic stirrer for 18 h. After the mixture was concentrated using rotary evaporation to ca. 30% of its original volume, the residue was washed with a saturated solution of sodium hydrogen carbonate and extracted with DCM. The organic layer was dried over Na_2SO_4; the solvent was removed with a rotary evaporator and monotosylated triethylene oxide (**8a**) was obtained as a yellow liquid with 90% yield, 1.8 g.

8a, ^{1}H-NMR (400 MHz, $CDCl_3$) δ ppm 4.31 (m, 2H), 3.70-3.40 (m, 10H), 3.30 (s, 3H), 3.01 (s, 3H); **^{13}C-NMR** (400 MHz, $CDCl_3$) δ ppm 71.7, 70.1, 70.4, 69.1, 68.3, 59.0, 37.7.

8b, ^{1}H-NMR (400 MHz, $CDCl_3$) δ ppm 4.31 (m, 2H), 3.70-3.40 (m, 48H), 3.30 (s, 3H), 3.01 (s, 3H); **^{13}C-NMR** (400 MHz, $CDCl_3$) δ ppm 87.7, 72.7, 70.5, 70.2, 66.5, 59.3, 37.9.
8c, ^{1}H-NMR (400 MHz, $CDCl_3$) δ ppm 4.31 (m, 2H), 3.70-3.40 (m, 192H), 3.30 (s, 3H), 3.01 (s, 3H); **^{13}C-NMR** (400 MHz, $CDCl_3$) δ ppm 87.7, 72.7, 70.5, 70.2, 66.5, 59.3, 37.9.

The obtained monotosylated triethylene oxide (**8a**) (1.5 g, 0.0973 mol) was dissolved in DMF (10 mL), and sodium azide (1.5 g, 0.024 mol) was added to the solution. The reaction mixture was stirred for 4 h at 105 °C in a nitrogen atmosphere and for 18 h at room temperature. The reaction mixture was concentrated by rotary evaporator,extracted with DCM and vacuum dried at room temperature to yield α-methoxy-ω-azido telechelic triethylene oxide (**9a**) as a yellow liquid in 95% yield 1.4 g.
9a, ^{1}H-NMR (400 MHz, $CDCl_3$) δ ppm 3.64 (m, 8H), 3.55-3.50 (m, 2H), 3.39-3.33 (m, 5H); **^{13}C-NMR** (400 MHz, $CDCl_3$) δ ppm 71.9, 70.8-70.5, 70.0, 59.01, 50.76; **FTIR:** ν (cm^{-1}) = 3000 – 2700 (C-H), 2110 (N_3).
9b, ^{1}H-NMR (400 MHz, $CDCl_3$) δ ppm 3.64 (m, 48H), 3.55-3.50 (m, 2H), 3.39-3.33 (m, 5H); **^{13}C-NMR** (400 MHz, $CDCl_3$) δ ppm 72.0, 70.8-70.5, 70.0, 59.1, 51.1; **FTIR:** ν (cm^{-1}) = 3000 – 2700 (C-H), 2110 (N_3).
9c, ^{1}H-NMR (400 MHz, $CDCl_3$) δ ppm 3.64 (m, 192H), 3.55-3.50 (m, 2H), 3.39-3.33 (m, 5H); **^{13}C-NMR** (400 MHz, $CDCl_3$) δ ppm 72.0, 70.8-70.6, 70.04, 59.1, 51.1; **FTIR:** ν (cm^{-1}) = 3000 – 2700 (C-H), 2110 (N_3).

7.4.5 Synthesis of α-azido-ω-azido telechelic polyethylene oxide (12)[330]

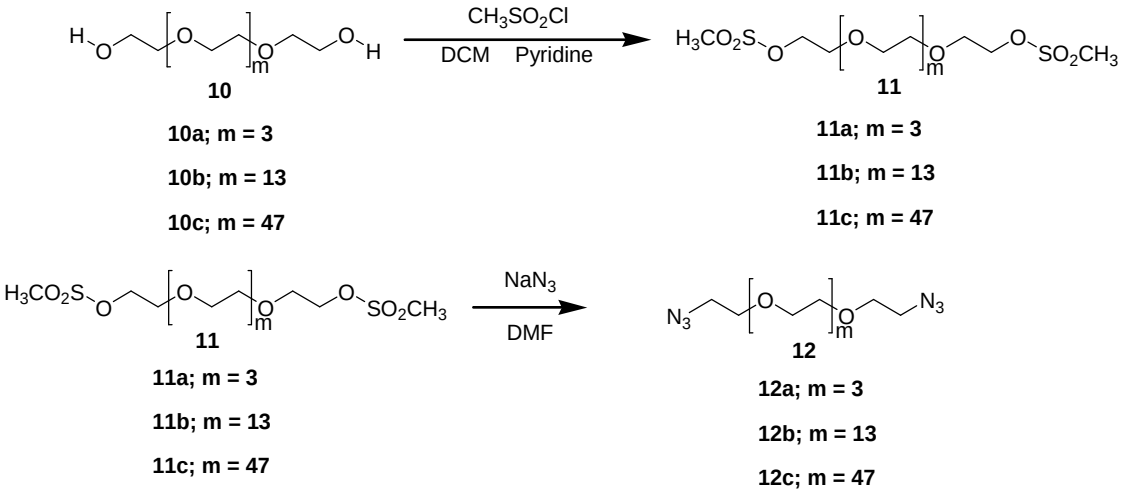

10
10a; m = 3
10b; m = 13
10c; m = 47

11
11a; m = 3
11b; m = 13
11c; m = 47

11
11a; m = 3
11b; m = 13
11c; m = 47

12
12a; m = 3
12b; m = 13
12c; m = 47

Methanesulfonyl chloride (5.0 ml, 0.065 mol) solution in 200 ml DCM was added drop-wise to polyethylene oxide (**10a**) (2 g, 0.013 mol) solution in 15 mL of pyridine vigorously stirred

and cooled to 0 °C. The reaction mixture was allowed to warm to room temperature and stirred with a magnetic stirrer for 18 h. After concentration using rotary evaporator to ca. 30% of its original volume, the residue was washed with a saturated solution of sodium hydrogen carbonate and extracted with DCM. After drying the organic layer over Na_2SO_4, the solvent was removed with a rotary evaporator and monotosylated triethylene oxide (**11**) was obtained as a yellow liquid with 90% yield, 1.8 g.

11a: **^{1}H-NMR** (400 MHz, $CDCl_3$) δ ppm 2.45 (s, 6H), 3.53 (s, 4H), 3.64–3.67 (m, 4H), 4.12–4.15 (m, 4H), 7.34 (d, J = 8.4 Hz, 4H), 7.79 (d, J = 8.4 Hz, 4H); **^{13}C NMR** (400 MHz, $CDCl_3$) δ ppm 21.8, 68.9, 69.4, 70.7, 70.9, 128.2, 130.0, 133.2, 145.0

11b: **^{1}H-NMR** (400 MHz, $CDCl_3$) δ ppm 2.45 (s, 6H), 3.53 (s, 4H), 3.64–3.67 (m, 48H), 4.12–4.15 (m, 4H), 7.34 (d, J = 8.4 Hz, 4H), 7.79 (d, J = 8.4 Hz, 4H); **^{13}C NMR** (400 MHz, $CDCl_3$) δ ppm 21.8, 68.8, 69.4, 70.6-70.9, 128.1, 130.0, 133.1, 145.0.

11c: **^{1}H-NMR** (400 MHz, $CDCl_3$) δ ppm 2.45 (s, 6H), 3.53 (s, 4H), 3.64–3.67 (m, 192H), 4.12–4.15 (m, 4H), 7.34 (d, J = 8.4 Hz, 4H), 7.79 (d, J = 8.4 Hz, 4H); **^{13}C NMR** (400 MHz, $CDCl_3$) δ ppm 21.8, 68.8, 69.4, 70.3,-70.8, 128.1, 130.0, 133.1, 145.0.

The obtained ditosylated polyethylene oxide (**11**) (1.5 g, 0.097 mol) was dissolved in DMF (10 ml), and sodium azide (1.5 g, 0.023 mol) was added to the solution. The reaction mixture was stirred for 5 h at 105 °C in a nitrogen atmosphere and for 18 h at room temperature. The reaction mixture was concentrated by rotary evaporator, extracted with DCM and vacuum dried at room temperature to yield α-azido-ω-azido telechelic polyethylene oxide (**12**) as a yellow liquid in 95% yield, 1.4 g.

12a: **^{1}H-NMR** (400 MHz, $CDCl_3$) δ ppm 3.38-3-41 (m, 4H), 3.68-3.71 (m, 4H); **^{13}C-NMR** (400 MHz, $CDCl_3$) δ ppm 50.8, 70.2-70.8; **FTIR:** ν (cm^{-1}) = 3000 – 2700 (C-H), 2110 (N_3).

12b: **^{1}H-NMR** (400 MHz, $CDCl_3$) δ ppm 3.38-3-41 (m, 48H), 3.68-3.71 (m, 48H); **^{13}C-NMR** (400 MHz, $CDCl_3$) δ ppm 50.8, 70.1-70.9; **FTIR:** ν (cm^{-1}) = 3000 – 2700 (C-H), 2110 (N_3).

12c: **^{1}H-NMR** (400 MHz, $CDCl_3$) δ ppm 3.38-3-41 (m, 192H), 3.68-3.71 (m, 192H); **^{13}C-NMR** (400 MHz, $CDCl_3$) δ ppm 50.7, 70.1-70.9; **FTIR:** ν (cm^{-1}) = 3000 – 2700 (C-H), 2110 (N_3).

7.4.6 Synthesis of α-methoxy-ω-alkyne telechelic triethylene oxide (13)[330]

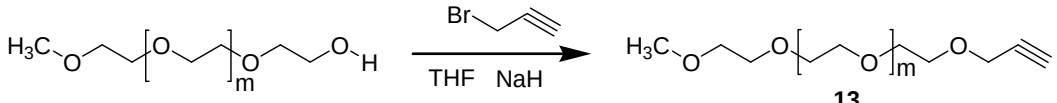

7 **13**

13a m = 3

13b m = 12

13c m = 48

NaH (1.2 equivalent 0.348 g, 0.014 mol) was washed three times with dry THF under an argon atmosphere to remove the mineral oil and cooled down to 0 °C in an ice bath. A solution of triethylene-glycol monomethyl ether (**7a**) (2 g, 0.012 mol) in 20 mL of THF was added at 0 °C under stirring. After stirring for 30 min, propargyl bromide (80% in toluene, 1.58 g, 0.01331 mol) was added slowly, and the mixture was stirred at 0°C for 2 h and then warmed to room temperature and stirred with a magnetic stirrer. After 22 h THF was removed; then the crude product was extracted with DCM and washed with water two times. DCM extract was evaporated, and the yellow oil was vacuum-dried at room temperature to yield (**13**) 85% product, 1.7 g.

13a: ^{1}**H-NMR** (400 MHz, $CDCl_3$) δ ppm 4.16 (d, J = 3.05 Hz, 2H), 3.60 (m, 12H), 3.34 (s, 3H), 2.39 (t, J = 2.38 Hz, 1H); ^{13}**C-NMR** (400 MHz, $CDCl_3$) δ ppm 79.7 (s, 1C), 74.4 (s, 1C), 71.9 (s, 1C), 70.7-70.3 (m, 4C), 69.1 (s, 1C), 58.9 (s, 1C), 58.3 (s, 1C).

13b: ^{1}**H-NMR** (400 MHz, $CDCl_3$) δ ppm 4.16 (d, J = 3.05 Hz, 2H), 3.6 (m, 48H), 3.3 (s, 3H), 2.3 (t, J = 2.38 Hz, 1H); ^{13}**C-NMR** (400 MHz, $CDCl_3$) δ ppm 79.7, 74.4, 71.9, 70.7-70.3, 69.1, 58.9, 58.3.

13c, ^{1}**H-NMR** (400 MHz, $CDCl_3$) δ ppm 4.16 (d, J = 3.05 Hz, 2H), 3.60 (m, 192H), 3.34 (s, 3H), 2.39 (t, J = 2.38 Hz, 1H); ^{13}**C-NMR** (400 MHz, $CDCl_3$) δ ppm 79.7 (s, 1C), 74.4 (s, 1C), 71.9 (s, 1C), 70.7-70.3, 69.1, 58.9 (s, 1C), 58.3.

7.4.7 Synthesis of ~-TEO-μ-bromo telechelic PIB (14)[226]

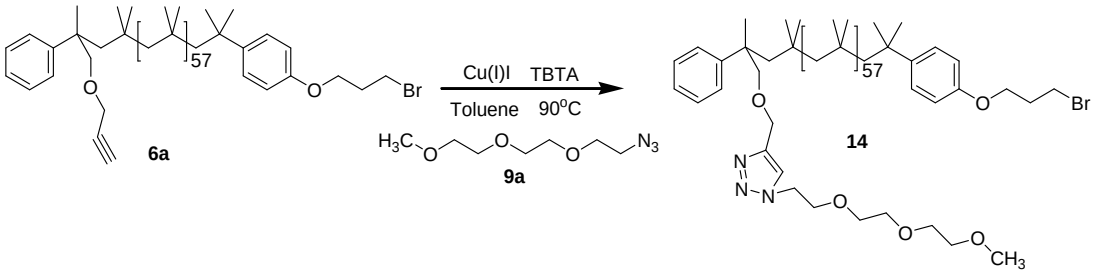

6a **9a** **14**

The click reaction between α-methoxy-ω-azido telechelic triethylene oxide **(9a)** and α-alkyne-ω-bromo telechelic PIB (**6a**) was conducted under Cu(I) iodide mediated conditions

as follows: α-alkyne-ω-bromo telechelic PIB (**6a**) (1 equiv.), monoazido-telechelic triethylene oxide **(9a)** (1 equiv.), tris-(benzyltriazolylmethyl) amine (TBTA) (0.1 equiv.) and Cu^{I} iodide were dissolved in toluene and bubbled with argon for 1 hour and subsequently stirred at 90 °C with an oil bath. After 48 h, the solvent was removed with a rotary evaporator and the crude product was purified by column chromatography on silica gel (chloroform to remove the unreacted α-alkyne-ω-bromo telechelic PIB (**6a**), R_f = 1 and then chloroform/methanol = 30:1, R_f = 0.2 to furnish the α-TEO-ω-bromo telechelic PIB (**14**) in 50% yield , 1 g.

^{1}H-NMR (400 MHz, $CDCl_3$) δ ppm 7.47 (s, 1H), 6.82 (d, J = 8.41 Hz, 2H), 4.64-4.46 (m, 2H), 4.08 (t, J = 5.78 Hz, 2H), 3.86 (t, J = 4.76, 4.76 Hz, 1H), , 3.72-3.47 (m, 12H), 3.37 (s, 3H), 2.29 (p, J = 6.23 Hz, 2H); **^{13}C-NMR** (400 MHz, $CDCl_3$) δ ppm 154.4, 158.8, 145.4, 42.8, 128.8, 125.7, 125.1, 120.9, 114.2, 81.3, 71.8, 70.6, 69.8, 64.8, 63.5, 59.3, 52.9, 43.1, 29.3, 27.6

7.4.8 Synthesis of ~-TEO-μ-azido telechelic PIB (15)[230]

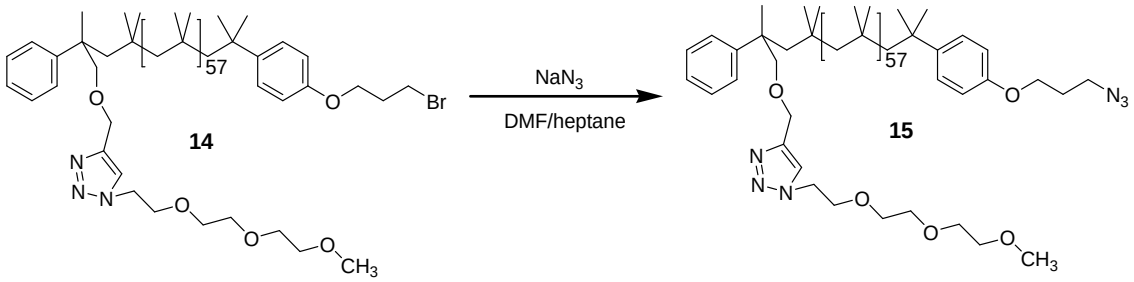

α-Triethyleneglycol-ω-bromo telechelic PIB (**14**) (1 g) was dissolved in 100 ml of 50/50 (v/v) mixture of heptane and DMF. To this biphasic mixture sodium azide (2.5 equiv.) was added, and the mixture was heated to 90 °C upon which it became monophasic and was allowed to react for 5 h. After cooling and phase separation, the heptane layer was washed with deionized water and the polymer was precipitated into methanol. The residual solvent was removed under vacuum to yield 90% of **(15)**, 900 mg.

^{1}H-NMR (400 MHz, $CDCl_3$) δ ppm 7.47 (s, 1H), 6.82 (d, J = 8.41 Hz, 2H), 4.64-4.46 (m, 2H), 4.08 (t, J = 5.78 Hz, 2H), 3.86 (t, J = 4.76, 4.76 Hz, 1H), , 3.72-3.47 (m, 12H), 3.37 (s, 3H); **^{13}C-NMR** (400 MHz, $CDCl_3$) δ ppm 154.4, 158.8, 145.4, 142.8, 128.8, 125.7, 125.1, 120.9, 114.2, 81.3, 71.8, 70.6, 69.8, 64.8, 63.5, 59.3, 52.9, 44.3, 43.1, 29.3, 27.6; **FT-IR:** ν (cm^{-1}) 3000-2700 (C-H), 2110 (N_3).

7.4.9 Synthesis of ~-TEO-μ-TEO telechelic PIB (16)

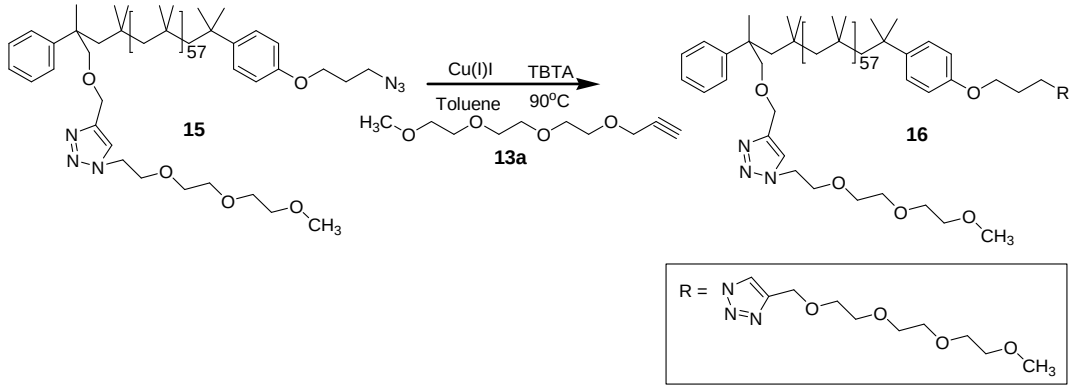

The click reaction between α-TEO-ω-azido telechelic PIB (**15**) (500 mg) and α-methoxy-ω-alkyne telechelic triethylene oxide (**13a**) was conducted under Cu^{I} mediated conditions as follows: α-TEO-ω-azido telechelic PIB (**15**) (1 equiv.), α-methoxy-ω-alkyne telechelic triethylene oxide (**13a**) (1.3 equiv.), (TBTA) (0.1 equiv.) and Cu(I) iodide (catalytic amount) were dissolved in toluene (20 mL). The mixture was bubbled with argon for 1 h and then heated at 85 °C. After 48 h, the solvent was removed with a rotary evaporator and the crude product was purified by column chromatography on silica gel (chloroform/methanol = 30:1, R_f = 0.1) to furnish the α-TEO-ω-TEO telechelic PIB (**16**) (98%), 480 mg.

^{1}H-NMR (400 MHz, $CDCl_3$) δ ppm 8.12 (s, 1H), 7.47 (2, 1H), 6.81 (d, J = 8.41 Hz, 2H), 4.66-4.45 (m, 8H), 3.97 (t, J = 5.78 Hz, 2H), 3.86 (t, J = 4.76, 4.76 Hz, 2H), , 3.69-3.47 (m, 20H), 3.37 (s, 3H). 2.41 (p, J= 6.23); **^{13}C-NMR** (400 MHz, $CDCl_3$) δ ppm 154.4, 150.0, 142.4, 141.6, 128.8, 125.7, 125.1, 120.9, 114.2, 83.1, 72.8, 70.6, 69.2, 66.4, 59.3, 55.8, 53.4, 49.9, 48.8, 41.6, 32.6, 29.8, 28.8,23,9, 20.8.

7.4.10 Synthesis of ~-PEO$_{13}$-μ-Br telechelic PIB (17)

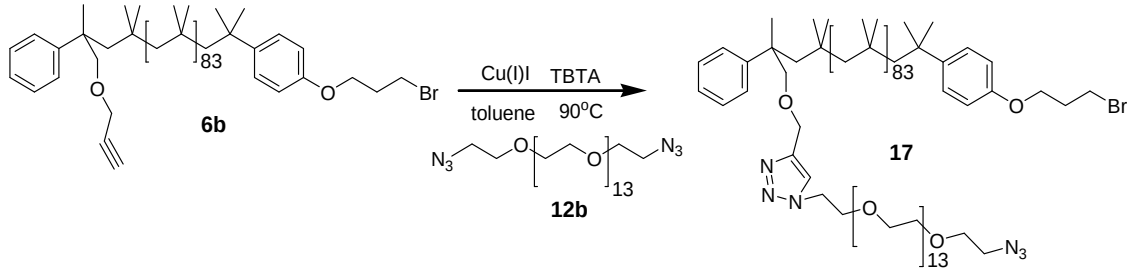

The click reaction between α,ω-azido telechelic polyethylene oxide **(12b)** and α-alkyne-ω-bromo telechelic PIB (**6b**) (1 g) was conducted under Cu^{I} mediated conditions as follows: α-alkyne-ω-bromo telechelic PIB (**6b**) (1 equiv.), diazido-telechelic polyethylene oxide **(12b)** (1.5 equiv.), tris-(benzyltriazolylmethyl) amine (TBTA) (0.1 equiv.) and Cu(I) iodide were

dissolved in an argon-sparged toluene (40 mL) and stirred at 90 °C. After 48 h the solvent was removed with a rotary evaporator and the crude product was purified by column chromatography on silica gel: (chloroform to remove the unreacted α-alkyne-ω-bromo telechelic PIB (**6b**), R_f = 1 and then chloroform/methanol = 30:1, R_f = 0.2 to furnish the α-PEO_{13}-ω-bromo telechelic PIB (**17**) (70%), 700 mg.

^{1}H-NMR (400 MHz, $CDCl_3$) δ ppm 7.46 (s, 1H), 6.81 (d, J = 8.83 Hz, 2H), 4.62-4.45 (m, 4H), 4.08 (t, J = 5.81, 5.81 Hz, 2H), 3.85 (t, J = 5.22, 5.22 Hz, 2H), 3.39 (t, J = 5.04, 5.04 Hz, 2H), 2.31 (P, p, J = 6.20, 6.20, 6.18, 6.18 Hz, 2H); **^{13}C-NMR** (400 MHz, $CDCl_3$) δ ppm 154.4, 150.0, 142.4, 142.6, 128.4, 125.7, 125.1, 120.9, 114.0, 83.1, 70.2, 69.2, 67.3, 55.8, 53.4, 50.0, 41.6, 32.6, 30.0, 29.8, 28.8, 23.9, 20.8, 20.5. **FT-IR:** ν (cm^{-1}) 3000-2700 (C-H), 2110 (N_3).

7.4.11 Synthesis of a-TEO-ω-thymine telechelic PIB (18)

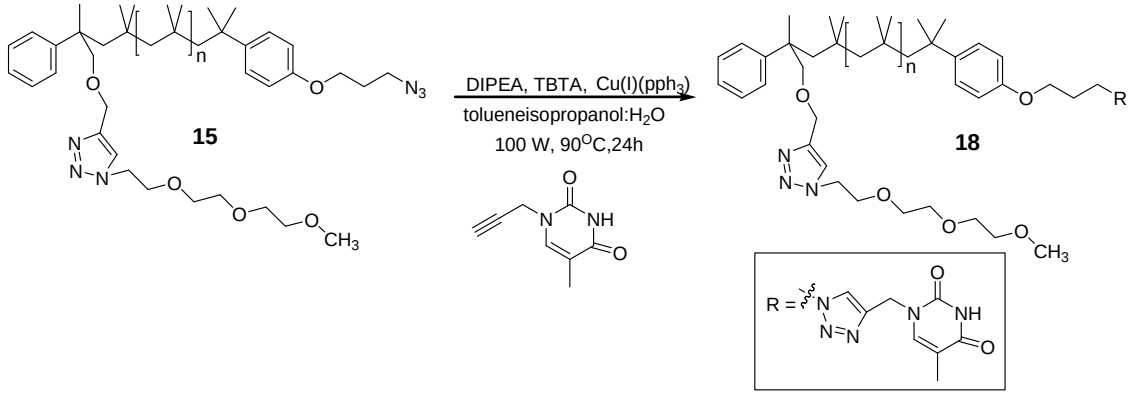

The click reaction between α-triethyleneglycol-ω-azido telechelic PIB (**15**) (500 mg) and the alkyne-substituted thymine was conducted under Cu^I mediated conditions as follows: α-triethyleneglycol-ω-azido telechelic PIB (**15**) (1 equiv.), the thymine (1.3equiv.), TBTA (0.1 equiv.), N,N-diisopropylethylamine (DIPEA; 5 equiv.), and Cu(I) iodide triphenyl phosphine (catalytic amount) were dissolved in toluene, water, and isopropanol (2:1:1) (20 mL) in a predried microwave vial. The mixture was bubbled with argon for 1 h and the vial was transferred into microwave CEM Discover system (CEM Corporation, Kamp-Lintfort) in connection with Synergy controlling software (version 1.37). The system parameters were adjusted as follows: running time 2 h; power 100 W; temperature 90 °C; method: SPS; and set points: 20 bar. Thereafter, the solvent was evaporated and n-hexane was added. The polymer was precipitated into 10-fold excess of methanol. The crude product was purified by silica chromatography (SiO_2, chloroform/methanol 20:1, R_f = 0.1) to furnish (**18**) with a yield of 70%, 350mg.

^{1}H-NMR (500 MHz, $CDCl_3$) δ ppm 7.90 (s, 1H), 7.61 (s, 1H), 7.40 (s, 1H), 6.71 (d, J ¼ 8.79 Hz, 2H), 4.87 (s, 2H), 4.56–4.39 (m, 6H), 3.90 (t, J = 5.68 Hz, 2H), 3.78 (t, J = 5.68 Hz, 2H), 3.57–3.38 (m, 12H), 3.30 (s, 3H), 2.29 (t, J = 6.23 Hz, 2H); **^{13}C-NMR** (400 MHz, $CDCl_3$) δ ppm 177.2, 160.6, 144.3, 130.8, 127.6, 126.7, 113.5, 73.1, 62.6, 60.8, 67.8, 19.3, 14.6.

7.4.12 Synthesis of a-TEO-ω-2,4-diaminotriazine telechelic PIB (19)

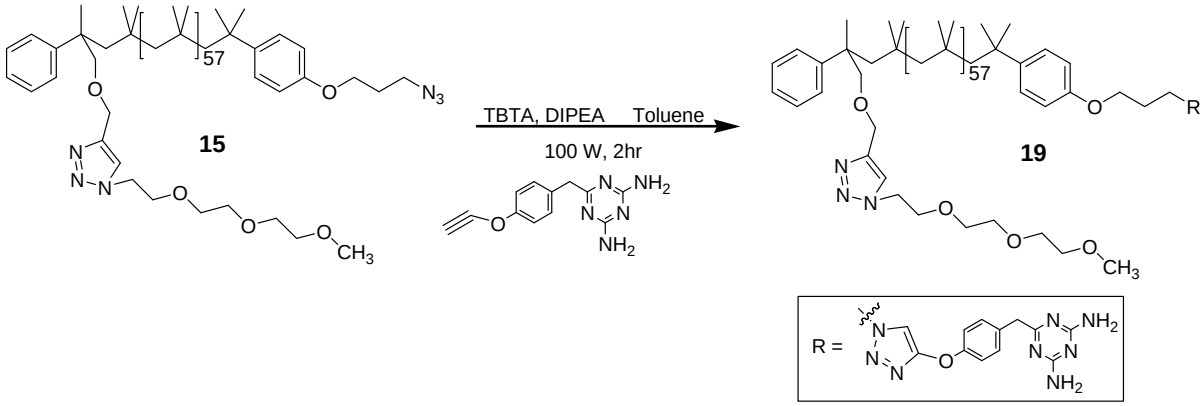

The click reaction between α-TEO-ω-azido telechelic PIB (**15**) (500 mg) and the alkyne-substituted diaminotriazine was also conducted under Cu^{I} mediated conditions in a similar manner as for (**17**), but the 5-methyl-1-(prop-2-ynyl)-1-pyrimidine-2,4-dione was replaced with 6-(4-ethynylbenzyl)-1,3,5-triazine-2,4-diamine to furnish α-triethyleneglycol-ω-2,4-aminotriazine telechelic PIB (**19**) in 80% yield, 400 mg.

^{1}H-NMR (400 MHz, $CDCl_3$) δ ppm 7.78–7.68 (m, 4H), 6.80 (d, J = 8.85 Hz, 2H), 5.47 (bs, 2H), 5.05 (bs, 1H), 4.69–4.44 (m, 6H), 3.98 (t, J = 5.67 Hz, 2H), 3.63–3.47 (m, 12H), 3.37 (s, 3H), 2.29 (t, J = 6.23 Hz, 2H); **^{13}C-NMR** (400 MHz, $CDCl_3$) δ ppm 154.4, 158.8, 145.4, 142.8, 128.8, 125.7, 125.1, 120.9, 114.2, 81.3, 71.8, 70.6, 69.8, 64.8, 63.5, 59.3, 52.9, 44.3, 43.1, 29.3, 27.6.

7.4.13 Synthesis of diaminotriazine functionalized TRI-PEO$_{13}$-b-PIB$_{83}$ diblock copolymer (20)

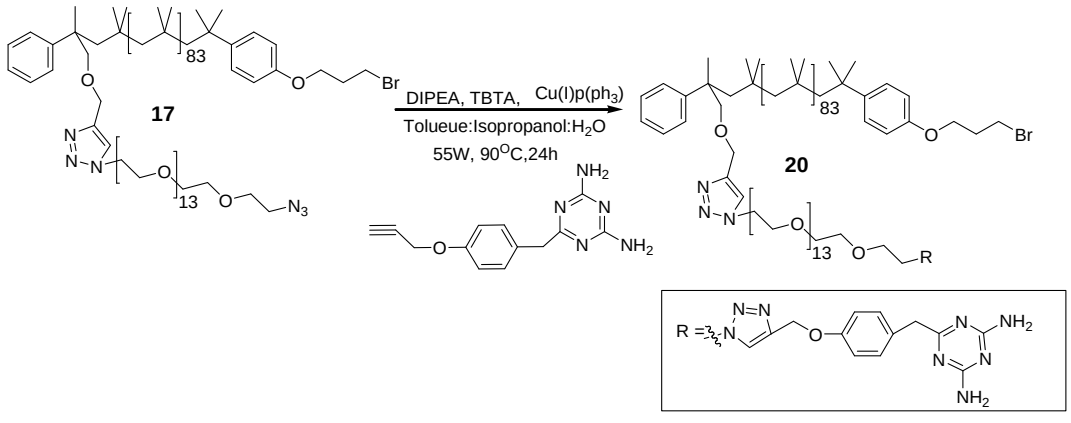

The click reaction between α-azido polyethyleneoxide-ω-bromide-telechelic PIB (**17**) (200mg) and alkyne-substituted diaminotriazine was conducted under Cu^{I} mediated conditions: α-azidopolyethyleneoxide-ω-bromide-telechelic PIB (**17**) (1 equiv.), alkyne-substituted diaminotriazine (1.3 equiv.), TBTA (0.1 equiv.), DIPEA (5 equiv.) and Cu(I) iodode triphenyl phosphine were dissolved in toluene, water and isopropanol (2:1:1) (15 mL) in a predried microwave vial. The mixture was bubbled with argon for 1 h, and the vial was transferred into microwave CEM Discover system (CEM Corporation, Kamp-Lintfort) in connection with Synergy controlling software (vers. 1.37). The system parameters were adjusted as follows: running time 24h; power 55 W; temperature 90 °C; method, SPS; set points, 20 bar. Thereafter 24 hours, the solvent was evaporated and n-hexane was added. The polymer was precipitated into 10-fold excess of methanol. The crude product was purified by silica chromatography (SiO_2, chloroform/methanol 20:1, R_f = 0.1) to furnish **(20)** with a yield of 95%, 190 mg.

^{1}H NMR (400 MHz, $CDCl_3$) δ ppm 7.82 (s, 1H), 7.46 (s, 1H), 6.91 (d, J = 8.61 Hz, 2H), 6.81 (d, J = 8.79 Hz, 2H), 5.19 (bs, 4H), 4.63-4.47 (m, 6H), 4.08 (t, J = 5.82, 5.82 Hz, 2H), 3.85 (t, J = 4.95, 4.95 Hz, 4H), 3.73 (s, 2H), 3.69-3.47 (m, 52H), 2.31 (p, J = 6.20, 6.20, 6.18, 6.18 Hz, 2H); **^{13}C-NMR** (400 MHz, $CDCl_3$) δ ppm 178.4, 176.7, 157.7, 154.4, 150.0, 142.4,141.6, 130.1, 128.6, 128.4, 125.7, 125.1, 120.9, 114.2, 83.1, 72.3, 70.2, 69.2, 67.3, 55.8, 53.9, 53.4, 49.9, 41.6, 32.5, 30.0, 29.8, 28.8, 23.9, 20.5.

7.4.14 Synthesis of 1-octylphosphinoyl-octan (22)[189]

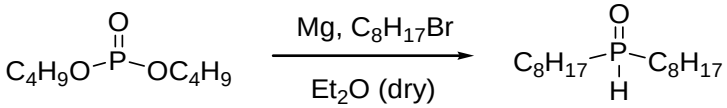

21 **22**

A solution of Grignard reagent was prepared under Ar atmosphere, using n-octylbromide (98.69 g, 0.51 mol) and magnesium (11.27 g, 0.46 mol) in 250 ml of anhydrous diethyl ether. After all the magnesium has been consumed, the mixture was added to a solution of di-n-butyl phosphite (30 g, 0.15 mol) in 75 ml of anhydrous diethyl ether cooled to 15 °C. The mixture was refluxed for 30 mins to complete the reaction. The reaction was then destroyed with ice cubes followed by the drop wise addition of 200 ml of 25% sulfuric acid. The organic phase was separated and washed three times with 100 ml H_2O, three times with 50 ml 15% potassium carbonate solution, and finally three times with distilled H_2O. After drying

over Na_2SO_4 the organic phase was concentrated in a rotary evaporator. Recrystallization of the crude product from *n*-hexane gave (**22**) as a white solid with 80% yield, 24 g

^{1}H-NMR (400 MHz, $CDCl_3$) δ ppm 6.84 (t, J = 446.5 Hz, 1H), 1.90-1.25 (m, 28H), 0.86 (t, J = 6.3 Hz, 6H); **^{13}C-NMR** (400 MHz, $CDCl_3$) δ ppm 31.7, 30.6, 29.0, 28.9, 28.1, 22.56, 21.71, 14.0; **^{31}P-NMR** (400 MHz, $CDCl_3$) δ ppm δ 36.31.

7.4.15 Synthesis of 3-(dioctyl-phosphinoyl)-propan-1-ol (23)[189]

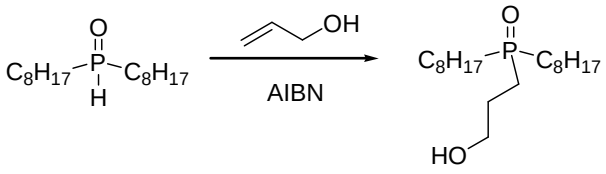

22 **23**

(**22**) (1.0 g, 3.64 mmol) was heated in a round bottom flask at 100 °C until molten. A solution of AIBN (0.017 g, 0.10 mmol) in allylalcohol (0.73 g, 12.57 mmol) was added dropwise under magnetic stirring. After 10 hours the reaction mixture was cooled to room temperature followed by purification by column chromatography on silica gel (chloroform/methanol = 60:1) furnishing the alcohol (**23)** as a colorless oil with 60% yield, 600 mg.

^{1}H-NMR (400 MHz, $CDCl_3$) δ ppm 4.14 (s, 1H), 3.66 (t, J = 5.2 Hz, 2H), 2.00-1.10 (m,32H), 0.86 (t, J = 6.7 Hz, 6H); **^{13}C-NMR** (400 MHz, $CDCl_3$) δ ppm 62.4, 31.7,31.0, 29.0, 29.0, 27.7, 25.7, 25.6, 22.5, 21.7, 14.0; **^{31}P-NMR** (400 MHz, $CDCl_3$) δ ppm δ 52.80.

7.4.16 Synthesis of 1-(3-bromo-propyl)-octyl-phosphinoyl-octane (24)[189]

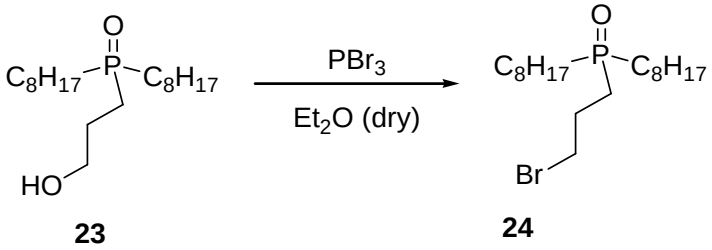

23 **24**

PBr_3 (0.25 g, 0.9 mmol) was added dropwise to a solution of (**23**) (600 mg, 1.8 mmol) in 10 ml of dry diethylether. The mixture was stirred for 10 hours at room temperature and finally quenched by the slow addition of 3 mL of methanol. Next, the mixture was washed twice

with 10 ml of a 1 M solution of $NaHCO_3$, and the organic phase was dried over Na_2SO_4, filtered and concentrated in using a rotary evaporator. Purification was done by column chromatography on silica gel (chloroform/methanol = 60:1) to furnish bromide (**24**) as a colorless oil with a yield of 76%, 456 mg.

^{1}H-NMR (400 MHz, $CDCl_3$) δ ppm 3.45 (t, J = 6.2Hz, 2H), 2.25-2.00 (m, 2H), 1.90-1.00 (m, 30H), 0.83 (t, J = 6.4 Hz, 6H); **^{13}C-NMR** (400MHz, $CDCl_3$) δ ppm 34.2, 31.6, 31.0, 28.9, 28.8, 28.1, 26.5, 25.0, 22.4, 21.5, 13.9; **^{31}P-NMR** (400 MHz, $CDCl_3$) δ ppm 50.28.

7.4.17 Synthesis of 1-(3-Azido-propyl)-octyl-phosphinoyl-octane (25)[189]

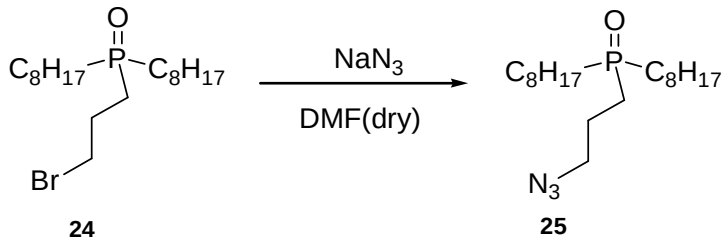

24 **25**

Sodium azide (0.5 g, 7.69 mmol) was added to a mixture of (**24**) (900 mg, 2.43 mmol) in 10 mL of anhydrous DMF and was stirred for 20 h at 50°C. After evaporation of the solvent, the residue was diluted with 25 ml of dichloromethane and extracted with 3 x 15 mL of water. The organic phase was dried over Na_2SO_4, filtered and concentrated in vacuum. Purification was done by column chromatography on silica gel (chloroform/methanol = 60:1) to furnish the azide (**25**) as a pale yellow oil with a yield of 93%, 837 mg.

^{1}H-NMR (400 MHz, $CDCl_3$) δ ppm 3.36 (t, J = 5.5 Hz, 2H), 1.95-1.10 (m, 32H), 0.83 (t, J = 5.2Hz, 6H); **^{13}C-NMR** (400 MHz, $CDCl_3$) δ ppm 52.0, 31.6, 31.0, 28.9, 28.9, 28.0, 24.9, 22.5, 21.6, 21.5, 13.9; **^{31}P-NMR** (400 MHz, $CDCl_3$) δ ppm 49.21. **FT-IR:** ν (cm^{-1}) 2958-2853, 2100 (N_3), 1305-1247

7.4.18 Synthesis of Hex-5-ynoic acid 3-(dioctyl-phosphinoyl)-propyl ester (26)[189]

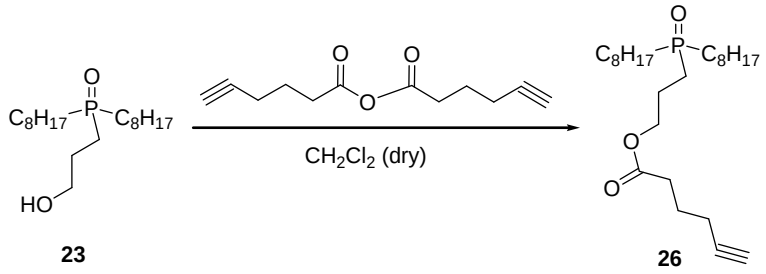

23 **26**

A solution of (**23**) (1.3 g, 3.85 mmol), DMAP (N,N-dimethylaminopyridine) (120 mg, 0.96 mmol) and pyridine (120 mg, 1.50 mmol) in 10 ml anhydrous CH_2Cl_2 was added dropwise to a solution of hex-5-ynoic acid anhydride (1.19 g, 5.77 mmol) in 2 ml anhydrous CH_2Cl_2. After 20 hours excess anhydride was quenched with water. The solution was diluted with 150 ml CH_2Cl_2 and washed twice with 50 mL Na_2CO_3 (10%) and twice with 50 ml $NaHSO_4$ (10%). The organic phase was dried over Na_2SO_4, filtered and concentrated in vacuo. Purification was performed by column chromatography on silica gel (chloroform/methanol = 50:1) to furnish alkyne (**26**) as a colorless oil with a yield of 90%, 1 g.

^{1}H-NMR (400 MHz, $CDCl_3$) δ ppm 4.09 (t, 2H), 2.42 (t, J = 6.3 Hz, 2H), 2.21 (t, J =6.4 Hz), 2.00-1.00 (m, 35H), 0.83 (t, 6H); **^{13}C-NMR** (400 MHz, $CDCl_3$) δ ppm 172.7, 82.9, 69.0, 64.3, 32.5, 31.6, 31.0, 28.9, 28.8, 27.8, 24.3, 23.3, 22.4, 21.5, 21.1, 17.6, 13.9; **^{31}P-NMR** (400 MHz, $CDCl_3$) δ ppm d 49.19.

7.4.19 Synthesis of ~-phosphineoxide-μ-bromo telechelic PIB (27)

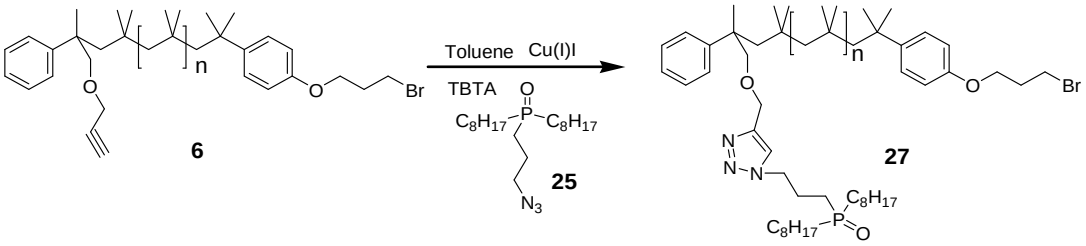

The click reaction between 1-(3-azidopropyl)octylphosphinoyloctane (**25**) and α-alkyne-ω-bromo-telechelic PIB (**6**) (1 g) was conducted under Cu^I mediated conditions as follows: α-alkyne-ω-bromo-telechelic PIB (**6**) (1 equiv.), 1-(3-azidopropyl)octylphosphinoyl-octane (**25**), TBTA (0.1 equiv.) DIPEA (0.1 equiv.) and Cu(I) iodide were dissolved in an argon-sparged THF (40 mL) and stirred at 50 °C. After 48 h the solvent was removed and the crude product was purified by column chromatography on silica gel ($CHCl_3$ to remove the unreacted α-alkyne-ω-bromo-telechelic PIB (**5**) (R_f = 1) and then chloroform/methanol = 30:1, R_f = 0.1 to furnish (**27**) in 65% yield, 650 mg.

^{1}H-NMR (400 MHz, $CDCl_3$) δ ppm 6.79 (d, J = 8.81 Hz, 2H), 4.55 (dd, J = 31.39, 12.94 Hz, 2H), 4.40 (t, J = 6.84 Hz, 2H), 4.06 (t, J = 5.79 Hz, 2H), 3.58 (t, J = 6.84 Hz, 2H), 3.47 (s, 2H), 2.29 (t, J = 6.23 Hz, 2H), 2.15 (bs, 2H); **^{13}C-NMR** (400 MHz, $CDCl_3$) δ ppm 156.1, 146.7, 142.8, 127.7, 127.0, 126.7, 113.6, 81.5, 64.3, 52.8, 43.2, 30.6, 21.7, 14.2; **^{31}P-NMR** (400 MHz, $CDCl_3$) δ ppm 48.91

7.4.20 Synthesis of α-phosphineoxide-ω-azido telechelic PIB (28)

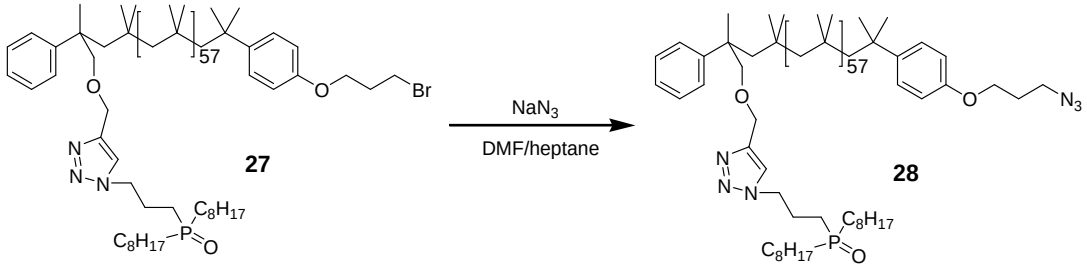

α-Phosphineoxide-ω-azido telechelic PIB (**27**) was synthesized according to the same procedure used for the synthesis of α-TEO-ω-azido telechelic PIB (**15**) to furnish (**28**) with 90% yield, 540 mg.

^{1}H-NMR (400 MHz, $CDCl_3$) δ ppm 6.79 (d, J = 8.81 Hz, 2H), 4.55 (dd, J = 31.39, 12.94 Hz, 2H), 4.40 (t, J = 6.84 Hz, 2H), 4.06 (t, J = 5.79 Hz, 2H), 3.58 (t, J = 6.84 Hz, 2H), 3.47 (s, 2H), 2.15 (bs, 2H); **^{13}C-NMR** (400 MHz, $CDCl_3$) δ ppm 156.1, 146.7, 142.8, 127.7, 127.0, 126.7,113.6, 81.5, 64.3, 52.8, 48.3, 43.2, 30.6, 21.7, 14.2; **^{31}P-NMR** (400 MHz, $CDCl_3$) δ ppm 47.72 **FT-IR:** ν (cm^{-1}) 3000-2700 (C-H), 2110 (N_3).

7.4.21 Synthesis of ~-phosphineoxide-μ-PEO$_{12}$ telechelic PIB (29)

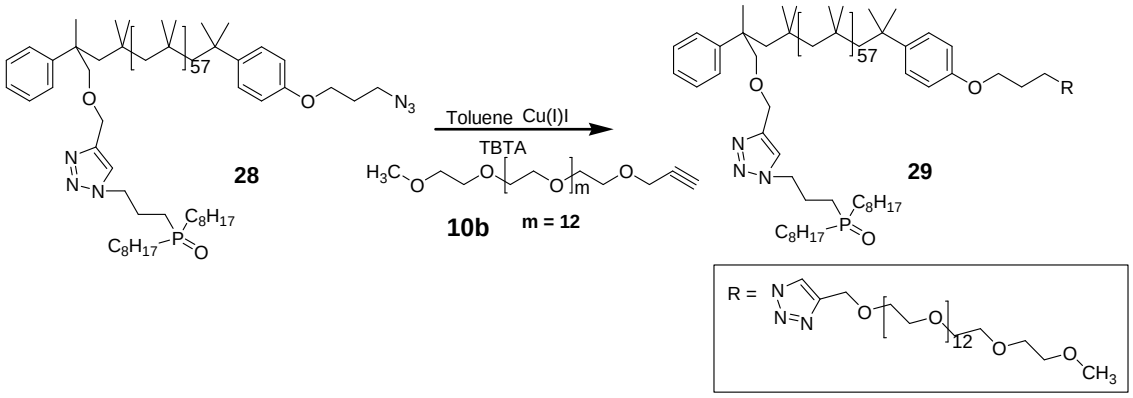

The click reaction between α-phosphineoxide-ω-azido telechelic PIB (**28**) (550 mg) and α-methoxy-ω-alkyn telechelic triethylene oxide (**10b**) was conducted under Cu^{I} mediated conditions: α-phosphineoxide-ω-azido telechelic PIB (**28**) (1 equiv.), α-methoxy-ω-alkyne telechelic triethylene oxide (**10b**) (1.3 equiv.), (TBTA) (0.1 equiv.) and Cu(I) iodide were dissolved in toluene (20 mL). The mixture was sparged with argon for 1 h and then heated at 85 °C. After 48 h, the solvent was removed with a rotary evaporator, and the crude product was purified by column chromatography on silica gel (chloroform/methanol = 30:1, R_f = 0.1

to remove the unreacted α-methoxy-ω-alkyne telechelic triethylene oxide (**10b**)) to furnish the α-phosphineoxide-ω-PEO_{12} telechelic PIB (**29**) in 98% yield, 530 mg.

^{1}H-NMR (400 MHz, $CDCl_3$) δ ppm 7.51 (s, 1H), 6.79 (d, J = 8.81 Hz, 2H), 4.60 (s, 2H), 4.56 – 4.43 (m, 6H), 4.34 (t, J = 6.84 Hz, 2H), 3.96 (t, J = 5.79 Hz, 2H), 3.70 – 3.49 (m, 56H), 3.30 (s, 3H), 2.38 (t, J = 6.23 Hz, 2H), 2.20 (m, 2H); **^{13}C-NMR** (400 MHz, $CDCl_3$) δ ppm 154.1, 140.7, 142.8, 128.4, 127.7, 125.0, 120.7, 114.6, 83.5, 72,5, 70.7, 68,4, 66,6, 59.3, 55.5, 53.8, 48.3, 41.2, 31.6, 29.4, 28.7, 25.7, 23.8, 22.5, 19.3, 14.2; **^{31}P-NMR** (400 MHz, $CDCl_3$) δ ppm 47.67.

7.4.22 Synthesis of ~-phosphineoxide-μ-thymine telechelic PIB (30)

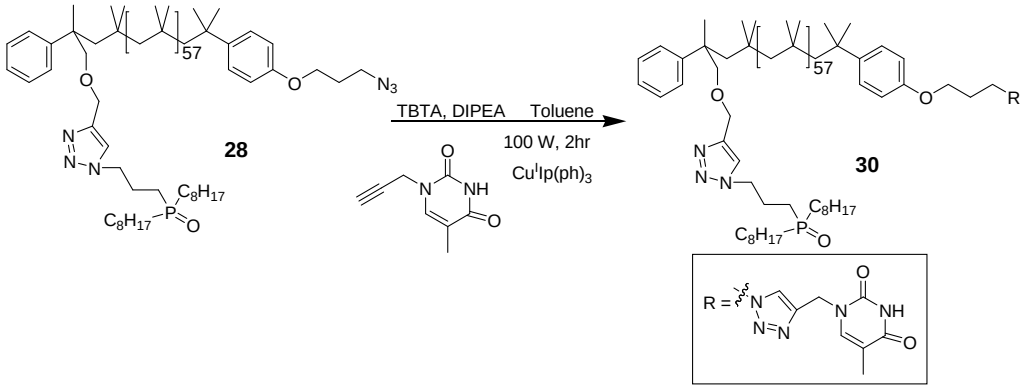

The click reaction between α-phosphineoxide-ω-azido-telechelic PIB (**28**) (500 mg) and alkyne-substituted thymine was conducted under Cu^I mediated conditions: α-phosphineoxide-ω-azido-telechelic PIB (**28**), alkyne-substituted thymine (1.3 equiv.), TBTA (0.1 equiv.), DIPEA (5 equiv.) and Cu(I) iodide triphenyl phosphine (0.1 equiv.) were dissolved in toluene, water and isopropanol (2:1:1) in a predried microwave vial. The mixture was bubbled with argon for 1 h, and the vial was transferred into microwave CEM Discover system (CEM Corporation, Kamp-Lintfort) in connection with Synergy controlling software (vers. 1.37). The system parameters were adjusted as follows: running time 2 h; power 100 W; temperature 90 °C; method, SPS; set points, 20 bar. Thereafter the solvent was evaporated and n-hexane was added. The polymer was precipitated into a 10-fold excess of methanol. The crude product was purified by silica chromatography (SiO_2, chloroform/methanol 20:1, R_f = 0.1) to furnish **(30)** with a yield of 80%, 400 mg.

^{1}H-NMR (400 MHz, $CDCl_3$) δ ppm 7.86 (s, 1H), 7.61 (s, 1H), 6.71 (d, J = 8.83 Hz, 2H), 4.87 (s, 2H), 4.59-4.42 (m, 4H), 4.34 (t, J =5.69 Hz, 2H), 3.97 (t, J = 5.79 Hz, 2H), 3.42 (s, 1H),

2.32 (t, J = 5.69 Hz, 2H), 2.15 (bs, 4H); **^{13}C-NMR** (400 MHz, $CDCl_3$) δ ppm 163.8, 151.8, 154.5, 148.4, 128.4, 125.7, 83.1, 25.6, 14.5. **^{31}P-NMR** (400 MHz, $CDCl_3$) δ ppm 49.43.

7.4.23 Synthesis of ~-phosphineoxide-μ-methoxy telechelic PEO (31)

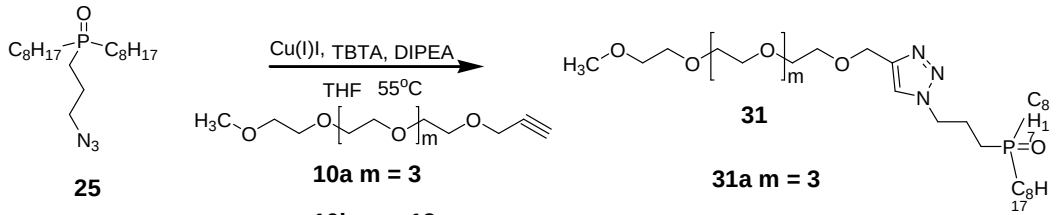

The click reaction between 1-(3-azidopropyl)octylphosphinoyl-octane (**25**) and α-methoxy-ω-alkyn telechelic triethylene oxide (**10**) was conducted under Cu^I mediated conditions as follows: α-methoxy-ω-alkyne telechelic triethylene oxide (**10**) (1 equiv.), 1-(3-azidopropyl) octylphosphinoyl-octane (**25**), TBTA (0.1 equiv.) DIPEA (0.1 equiv.) and Cu(I) iodide (0.1 equiv.) were dissolved in 20 mL of argon sparged THF and stirred at 50 °C. After 48 h the solvent was removed and the crude product was purified by column chromatography on silica gel (chloroform/methanol = 30:1, R_f = 0.3 to remove Cu(I) iodide and the unreacted phosphine oxide ligand (**25**)) and furnish (**31**) with 95% yield, 500 mg.

30a: ^{1}H-NMR (400 MHz, $CDCl_3$) δ ppm 7.60 (s, 1H), 4.65 (s, 2H), 4.44 (t, J = 6.77, 2H), 3.63 – 3.55 (m, 14H), 3.30 (s, 3H), 2.16 (m, 2H), 1.62 – 1.96 (m, 32H), 0.86 (3, 3H) ; **^{13}C-NMR** (400 MHz, $CDCl_3$) δ ppm 145.0, 122.0, 71.7, 70.4, 69.6, 64.5, 58.8, 50.3, 50.5, 31.6, 30.9, 30.1, 28.8, 28.4, 27.7, 24.9, 24.3, 22.8, 22.4, 21.5, 13.9; **^{31}P-NMR** (400 MHz, $CDCl_3$) δ ppm 47.67.

30b: ^{1}H-NMR (400 MHz, $CDCl_3$) δ ppm 7.60 (s, 1H), 4.65 (s, 2H), 4.44 (t, J = 6.77, 2H), 3.63 – 3.55 (m, 48H), 3.30 (s, 3H), 2.16 (m, 2H), 1.62 – 1.96 (m, 32H), 0.86 (3, 3H) ; **^{13}C-NMR** (400 MHz, $CDCl_3$) δ ppm 145.0, 122.0, 71.7, 70.4, 69.6, 64.5, 58.8, 50.3, 50.5, 31.6, 30.9, 30.1, 28.8, 28.4, 27.7, 24.9, 24.3, 22.8, 22.4, 21.5, 13.9; **^{31}P-NMR** (400 MHz, $CDCl_3$) δ ppm 47.67.

30c: ^{1}H-NMR (400 MHz, $CDCl_3$) δ ppm 7.60 (s, 1H), 4.65 (s, 2H), 4.44 (t, J = 6.77, 2H), 3.63 – 3.55 (m, 189H), 3.30 (s, 3H), 2.16 (m, 2H), 1.62 – 1.96 (m, 32H), 0.86 (3, 3H) ; **^{13}C-NMR** (400 MHz, $CDCl_3$) δ ppm 145.0, 122.0, 71.7, 70.4, 69.6, 64.5, 58.8, 50.3, 50.5, 31.6,

30.9, 30.1, 28.8, 28.4, 27.7, 24.9, 24.3, 22.8, 22.4, 21.5, 13.9; **^{31}P-NMR** (400 MHz, $CDCl_3$) δ ppm 47.67.

7.4.24 Synthesis of amphiphilic α-PO-ω-THY telechelic PEO_{47} (35a)

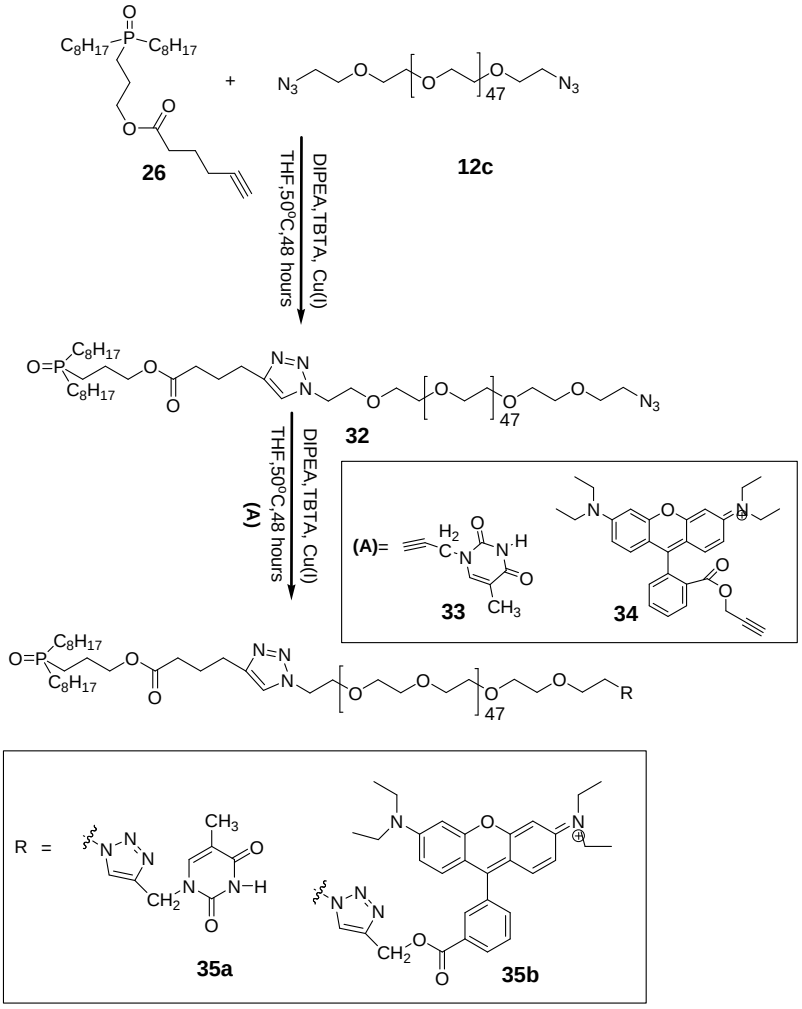

The first click reaction between hex-5-ynoic acid 3-(dioctyl-phosphinoyl)-propyl ester (**26**) and α, ω–azido polyethyleneoxide telechelic PEO_{47} (**12c**) was conducted in the presence of Cu(I) iodide as follows: hex-5-ynoic acid 3-(dioctyl-phosphinoyl)-propyl ester (**26**) (1 equiv.), α, ω–azido telechelic polyethyleneoxide PEO_{47} (**12c**) (2 equiv.), TBTA (0.1 equiv.), DIPEA (5 equiv.) and Cu(I) iodide (0.1 equiv.) were dissolved in THF and degassed at room temperature for 1 hour then heated to 60 °C. After 48 h THF was removed with a rotary evaporator, and the crude product was purified by column chromatography on silica gel $CHCl_3/CH_3OH$ = 20:1, R_f = 0.4 to elute α-phosphineoxide-ω-azido-telechelic PEO_{47} (**32**)

with a yield of 85%, 850 mg. The second click reaction between α-phosphineoxide-ω-azido-telechelic PEO_{47} (**32**) and alkyne-substituted thymine was also conducted under Cu^{I} mediated conditions as follows: α-phosphineoxide-ω-azido-telechelic PEO_{47} (**32**) (1 equiv.), alkyne-substituted thymine (1.3 equiv.), TBTA (0.1 equiv.), DIPEA (5 equiv.) and Cu(I) iodide triphenyl phosphine (0.1 equiv.) were dissolved in toluene in a predried microwave vial. The mixture was bubbled with argon for 1 h, and the vial was transferred into microwave CEM Discover system (CEM Corporation, Kamp-Lintfort) in connection with synergy controlling software (vers. 1.37). The system parameters were adjusted as follows: running time 2h; power 100 Watt; temperature 90 °C; method, SPS; set points, 20 bar. Thereafter 2 hours, toluene was evaporated and n-hexane was added. The polymer was precipitated into 10-fold excess of methanol. The crude product was purified by silica chromatography (SiO_2, chloroform/methanol 20:1, R_f = 0.5 to remove the unreacted thymine and thereafter 20:5, R_f = 0.1 to furnish (**35a**) with a yield of 80%, 800 mg.

^{1}H NMR (400 MHz, $CDCl_3$) δ ppm 11.25 (s, 1H), 8.01 (s, 1H), 7.80 (s, 1H), 7.58 (s, 1H), 4.89 (s, 2H), 4.46 (td, J = 15.62, 5.28, 5.28 Hz, 2H), 4.31 (t, J = 5.08, 5.08 Hz, 2H), 4.10-3.95 (m, 2H), 3.78 (dd, J = 9.84, 5.00 Hz, 2H),3.40-3.31 (m, 186H), 2.61 (t, J = 7.55, 7.55 Hz, 2H), 2.34 (t, J = 7.40, 7.40 Hz, 2H), 1.89-1.12 (m, 36H), 1.04 (t, J = 6.99, 6.99 Hz, 3H), 0.83 (t, J = 6.84, 6.84 Hz, 6H).); **^{13}C-NMR** (400 MHz, CDCl3) δ ppm 173.8, 163.8, 150.9, 143.2, 137.5, 123.2, 110.9, 70.2, 70.5, 66.8, 53.9, 49.6, 30.0, 29.4, 28.2, 25.2, 22.5, 15.5, 14.1.

7.5 Nanoparticle Synthesis

7.5.1 Preparation of TOPO-covered CdSe nanoparticles (TOPO NP)

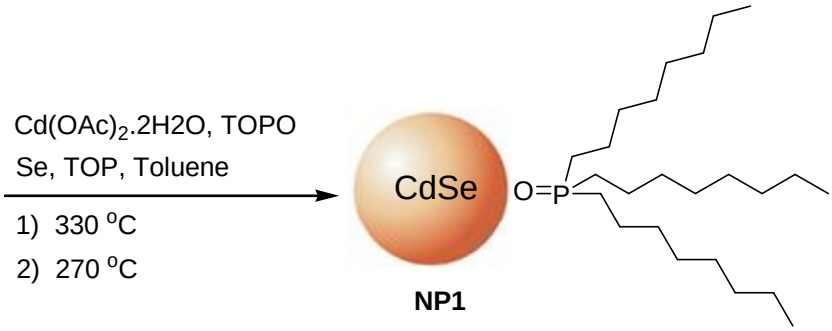

Trioctylphosphine oxide-covered CdSe NPs (**NP1**) were synthesized by the conventional hot injection method[186] as follows: A selenium stock solution was prepared by mixing selenium (0.3 g, 3.8 mmol), TOP (7.5 g, 18 mmol), and anhydrous toluene (0.135 g) in a dried and

sealed round bottom flask under a nitrogen atmosphere. The selenium stock solution was swiftly injected into a pre-heated (330 °C) mixture of TOPO (15 g, 35 mmol) and 0.35 g of cadmium acetate.$2H_2O$ (0.195 g, 0.73 mmol) in a reaction vessel under argon flow. After injection the reaction temperature was immediately adjusted to 270 °C to continue particle growth and to achieve a narrow size distribution. The reaction was stopped 1 min after the injection, and heat was immediately removed. The reaction mixture was allowed to cool to room temperature, and then methanol (100 mL) was added to precipitate the nanocrystals. The supernatant was decanted, and the precipitate was centrifuged to remove remaining solvent. The TOPO covered CdSe nanocrystals were then stored in dark conditions under argon to prevent oxidation until further use. The size of the nanocrystals synthesized by the above procedure was ~ 2.4 nm measured via UV-VIS (with the first exciton absorption peak at about 512 nm), according to the size and wavelength equation proposed by Peng *et al.*[260] DLS measurements showed an average size of 2.3±0.21 nm. DLS measurements and FTIR were used to probe for the presence of TOPO on the nanoparticle surface. The nanoparticle spectrum had peaks matching all of the TOPO peaks in frequency and relative intensity, except for the P-O stretch, which was shifted lower by ~ 50 cm^{-1} as a result of the bulkiness to the TOPO molecule. This is in good agreement with IR measurements performed on triphenylphosphine oxides complexing to CdI_2 and other metal salts,[264] which typically show shifts in P-O frequency of between 20 and 60 cm^{-1} upon complexation. The ^{1}H-NMR showed broad peaks between 2.40 and 1.00 ppm corresponding to 42 aliphatic protons and of the 9 methyl protons at 0.85 ppm. The broadness of the peaks in the ^{31}P-NMR at about 25 ppm is due to the inhomogeneous distribution of magnetic environments found on the nanoparticle surface.

7.5.2 Pyridine treatment of TOPO-covered CdSe nanoparticles (TOPO NP)

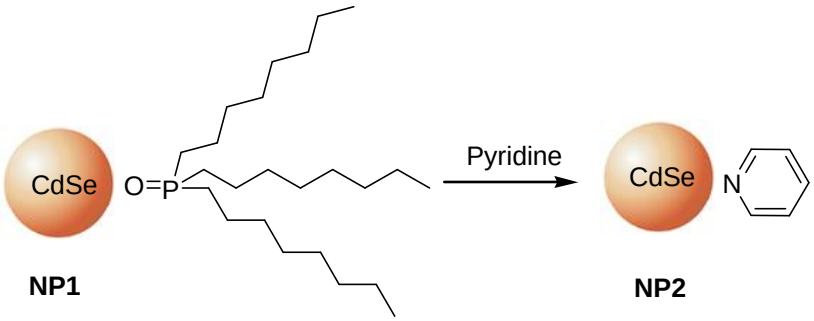

Pyridine is known to form a weak and reversible bond with the surface cadmium ions of cadmium chalcogenide nanocrystals.[263] The TOPO ligands in **NP1** were replaced with a relatively weak pyridine ligand in other to facilitate their use for ligand exchange with polymers **27, 29, 31,** and **35**. The purified TOPO covered nanocrystals (100 mg) were re-dissolved in pyridine (5 mL) and heated for 24 h at 50 °C under continuous stirring in an argon atmosphere. The excess pyridine was removed with a rotary evaporator to yield a viscous solution. The resulting pyridine covered nanocrystals were then precipitated in n-hexane and the nanocrystal precipitate was isolated by centrifugation and decantation. The precipitation procedure was repeated twice in order to remove all of the free pyridine and TOPO-ligands.

UV-Vis measurement of CdSe QDs (mean diameter 2.47 nm, 512 nm) after pyridine treatment maintained the original optical spectra of the TOPO covered NPs (*i.e.* the position and the width of the first exciton did not change) indicating no aggregation of the NPs during the pyridine treatment. In NMR, three broad peaks at 7.30, 7.68 and 8.62 ppm correspond to the signals of pyridine.

7.5.3 Synthesis of polymer covered CdSe nanoparticles (NP3, NP4, andNP5) [193, 258]

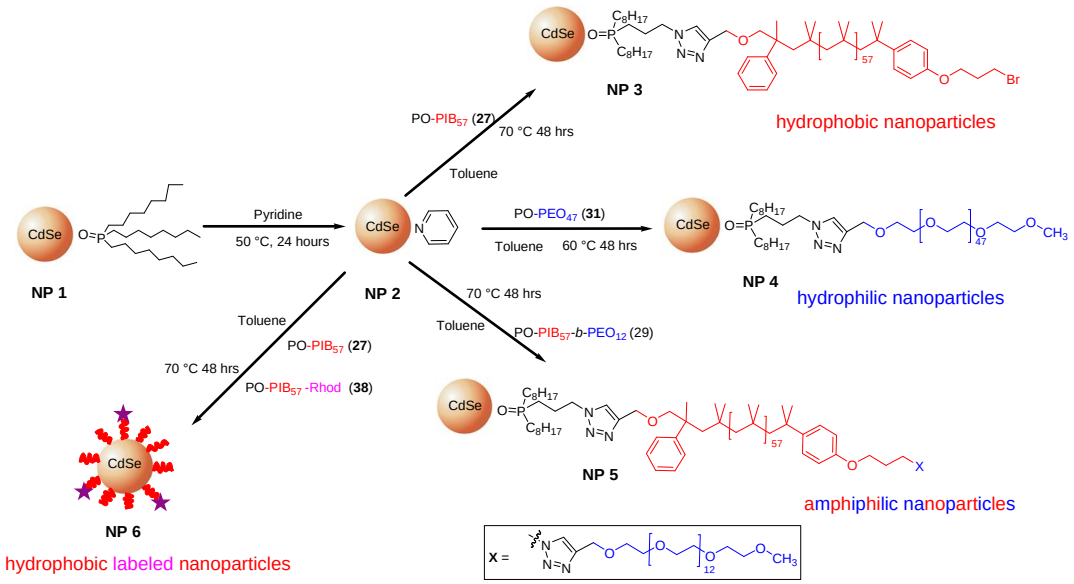

Ligand exchange of the relatively stable passivating TOPO on the CdSe nanoparticle surface with polymers **27**, **29**, and **31c** was conducted according to Emrick *et al.*[193] yielding the nanoparticles **NP3**, **NP4**, and **NP5**, as follows: After replacing the TOPO ligand in **NP1** with a relatively weak pyridine ligand in other to facilitate the ligand exchange, the pyridine-

covered CdSe nanoparticles **NP2** (50 mg) were subsequently treated with α-phosphineoxide-ω-bromo telechelic polyisobutylene (**27**) PO-PIB_{57}-Br (M_n (GPC) = 3200 g·mol^{-1}; M_w/M_n = 1.3) (273 mg,) to generate hydrophobic PIB-covered CdSe nanoparticle (**NP3**). The hydrophilic water-soluble PEO covered CdSe nanoparticle (**NP4**) and amphiphilic PIB_{57}-*b*-PEO_{12}-covered CdSe nanoparticle (**NP5**) were synthesized in a similar manner using α-phosphineoxide-ω-methylene telechelic PEO (**31c**) PO-PEO_{47} (180 mg) and α-phosphineoxide-ω-polyethylene oxide telechelic polyisobutylene (**29**) PO-PIB_{57}-$_b$-PEO_{12} (292 mg) respectively. The nanoparticles and the polymer were dissolved in 10 mL of freshly distilled anhydrous toluene. The resulting mixture was stirred for 48 h at 70 °C. Toluene was evaporated under reduced pressure, and the polymer-covered NPs (**NP3, NP4,** and **NP5**), were precipitated three times in 20 mL of hexane followed by centrifugation to separate the free unbound polymer from the polymer-covered nanoparticles. In the NMR spectra it is known that the signals from ligands bound to the surface are usually broadened; some of them can disappear or they can be shifted.[263] NMR spectroscopy showed that the signals coming from the part of the ligands being in the direct neighborhood or bound to the NP surface were strongly broadened or shifted in comparison to the free unbounded ligand. This can especially be observed in the broadening of the proton peak at 1.6 - 2.2 ppm in the phosphine oxide ligand bound to the NP surface, which is in agreement with literature values.[261-263]

7.6 Labelling of CdSe nanoparticles for fluorescence microscopy

7.6.1 Synthesis of alkyne-functionalized rhodamine-B (37)

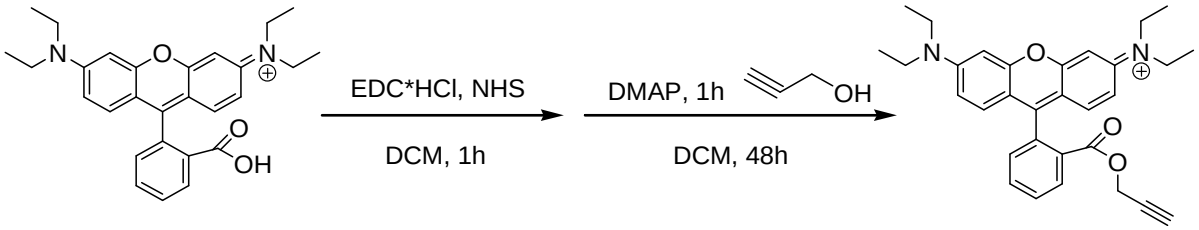

36 **37**

According to the literature,[331] the synthesis of alkyne-functionalized rhodamine-B (**37**) was conducted under a dry atmosphere of nitrogen in a two-step reaction as follows: a two-necked round bottom flask equipped with a magnetic stirring bar, a stop cock and a septum was dried by heating under vacuo and flushed with nitrogen several times. Under a stream of nitrogen, rhodamin-B (1.16 mmol, 500 mg) was added and was dissolved in dry DCM (5.0 mL).

EDC·HCl (2 mmol, 400 mg) and NHS (1.3 mmol, 165.0 mg) were added under a stream of nitrogen, and the reaction mixture was stirred at room temperature for one hour. A solution of DMAP (0.1 mmol, 17.0 mg) and propargyl alcohol (5.5 mmol, 328.0 µL) in dry DCM (2.0 mL) was added dropwise to the reaction mixture. After stirring the reaction mixture at room temperature for 48 hours, the reaction mixture was poured into diethylether to precipitate the alkyne-functionalized rhodamine-B. Further purification was carried out by column chromatograph starting with a mixture of ethyl acetate and MeOH (v/v = 20 / 1, R_f = 0.25) as eluent. Finally the desired product was collected by using MeOH yielding 90 % of pure (**37**).
^{1}H-NMR (400 MHz, $CDCl_3$) δ ppm 8.31 (dd J = 7.8 Hz, J = 0.9 Hz, 1H,), 7.84 (dt, J = 7.6 Hz, J= 1.3 Hz 1H), 7.75 (dt, J = 7.7 Hz, J= 1.2 Hz 1H), 7.34 (dd, J = 7.6 Hz, J = 0.9 Hz 1H), 7.05 (d J = 9.4 Hz, 2H), 6.88 (dd, J = 9.5 Hz, J = 2.4 Hz, 2H), 6.83 (d, J = 2.4 Hz, 2H), 4.61 (d, J= 2.5 Hz, 2H), 3.62 (q, J = 7.1 Hz, 8H), 2.41 (t, J= 2.4 Hz, 1H), 1.32 (t, J = 7.1 Hz, 12H)

7.6.2 Synthesis of ~-phosphine oxide-µ- rhodamine-B telechelic PIB (38)

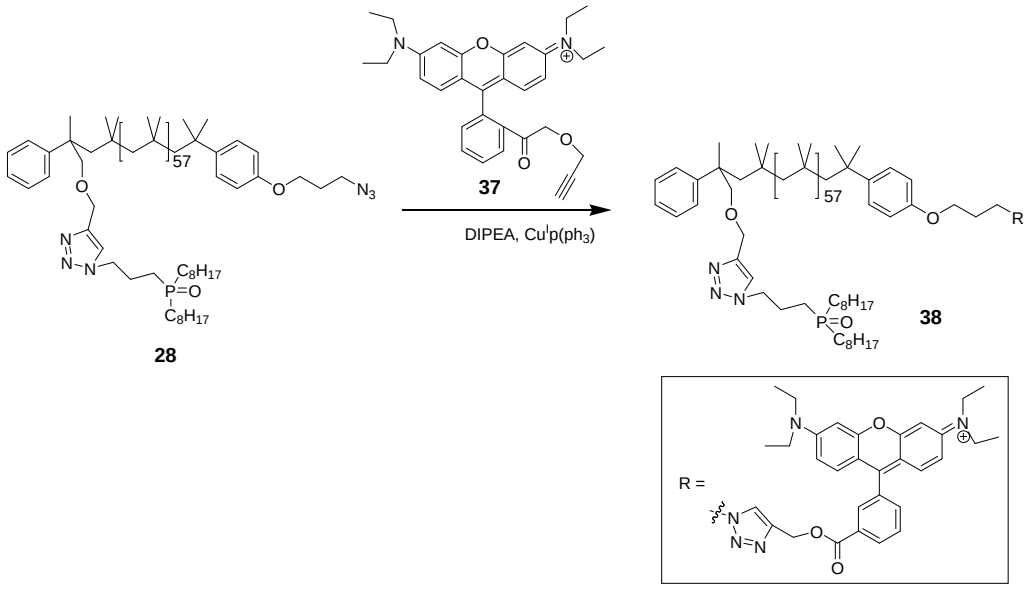

α-Phosphine oxide-ω-rhodamine-B telechelic PIB_{57} (**38**) was synthesized in order to be utilized for fluorescence labeling of the CdSe-nanoparticles. α-Phosphineoxide-ω-azido-telechelic PIB (**28**) (1 equiv.), alkyne substituted rhodamine-B (1.3 equiv.), TBTA (0.1 equiv.), DIPEA (5 equiv.) and Cu(I) iodode triphenyl phosphine (0.1 equiv.) were dissolved in THF. The mixture was bubbled with argon for 1 h and then heated 40 °C for 48 hours in the dark. Thereafter the solvent was evaporated, and the polymer was precipitated into 10-

fold excess of methanol. The crude product was purified by silica chromatography (SiO_2, chloroform/methanol 20:1, R_f = 0.1) to furnish (**38)** with a yield of 80%. The excess alkyne-functionalized rhodamine-B was removed by dialysis against methanol for four days (1000 $g{\cdot}mol^{-1}$ M_w cut-off dialysis tubing).

^{1}H-NMR (400 MHz, $CDCl_3$) δ ppm 8.32-8.28 (m, 1H), 7.80-7.68 (m, 1H), 7.07-7.02 (m, 1H), 7.33 (s, 1H), 7.19-7.13 (m, 1H), 6.90-6.76 (m, 1H), 5.13-5.09 (m, 1H), 4.44-4.39 (m, 1H), 4.67-4.49 (m, 1H), 4.04 -3.93 (m, 1H), 3.67-3.59 (m, 1H), 3.49 (s, 1H), 3.36-3.29 (m, 1H), 2.42-2.33 (m, 1H), 2.26-2.18 (m, 1H), , 4.85-4.74 (m, 1H).

*7.6.3 Synthesis of ~-phosphine oxide-*μ*- rhodamine-B telechelic PEO (35b)*

α-Phosphine oxide-ω-rhodamine-B telechelic PEO_{47} (**35b**) was also synthesized in order to utilize it for fluorescence labeling the CdSe nanoparticles. Firstly alkyne-functionalized rhodamine-B (**35**) was synthesized according to literature.[332] The first click reaction between hex-5-ynoic acid 3-(dioctyl-phosphinoyl)-propyl ester (**26**) and α,ω–azido polyethyleneoxide telechelic PEO_{47} (**12c**) was conducted in a similar fashion to that of α-phosphineoxide-ω-azido-telechelic PEO_{47} **(32)** reported above. The second click reaction to attach the alkyne-functionalized rhodamine-B to the α-phosphineoxide-ω-azido-telechelic PEO_{47} (**32**) was conducted in a Cu^I mediated condition in the presence of TBTA and DIPEA. 1.3 molar equivalent of alkyne-functionalized rhodamine-B was used with respect to α-phosphineoxide-ω-azido-telechelic PEO_{47} (**33**). The excess alkyne-functionalized rhodamine-B was removed by dialysis against methanol for four days (1000 g/mol M_w cut-off dialysis tubing).

^{1}H-NMR (400 MHz, $CDCl_3$) δ ppm 8.28 (d, J = 7.2 Hz, 1H,), 7.87-7.64 (m, 3H), 7.48 (s, 1H), 7.08-6.97 (d, 7.2 Hz, 2H), 6.89-6.81 (d, 9.5 Hz, 2H), 6.42-6.33 (m, 2H), 5.13 (s, 1H), 4.49 (t, J = 5.12, 5.12 Hz, 2H), 4.11 (t, J = 5.12, 5.12 Hz, 2H), 3.91-3.23 (m, 189H), 2.61 (t, J = 7.55, 7.55 Hz, 2H), 2.34 (t, J = 7.40, 7.40 Hz, 2H), 1.89-1.12 (m, 36H), 1.04 (t, J = 6.99, 6.99 Hz, 3H), 0.83 (t, J = 6.84, 6.84 Hz, 6H); **^{13}C-NMR** (400 MHz, CDCl3) δ ppm 210.8, 166.1, 154.7, 149.5, 142.5, 142.4, 139.9, 133.5, 130.1, 128.6, 126.4, 123.2, 120.9, 115.2, 108.4, 105.4, 100.3, 92.6, 75.6, 70.5, 69.2, 63.4, 53.9, 52.0, 49.4, 44.7, 42.3, 40.1, 31.2, 29.4, 24.9, 22.5, 20.3, 14.1.

7.6.4 Synthesis of polymer covered and rhodamine-B labeled CdSe nanoparticles (NP6)

In order to easily locate hydrophobic PIB-covered CdSe NPs (**NP3**) in the DPPC:PEO_{17}-*b*-PIB_{87} mixed monolayer at the air/water interface using fluorescence spectroscopy, NPs were labeled with rhodamine-B as follows: a 80 to 20 wt % mixture of ligand **27** and **38** was dissolved in toluene and subsequently added to 50 mg of **NP2**. The mixture was heated at 70 °C for 48 h. Toluene was evaporated under reduced pressure, and the rhodamine-B-labeled NPs (**NP6**) were precipitated three times in 20 mL of hexane followed by centrifugation to separate the free polymer from the polymer-covered nanoparticle.

7.6.5 Synthesis of hydrophilic water soluble PEO_{47}-THY covered CdSe-nanoparticles (NP7)

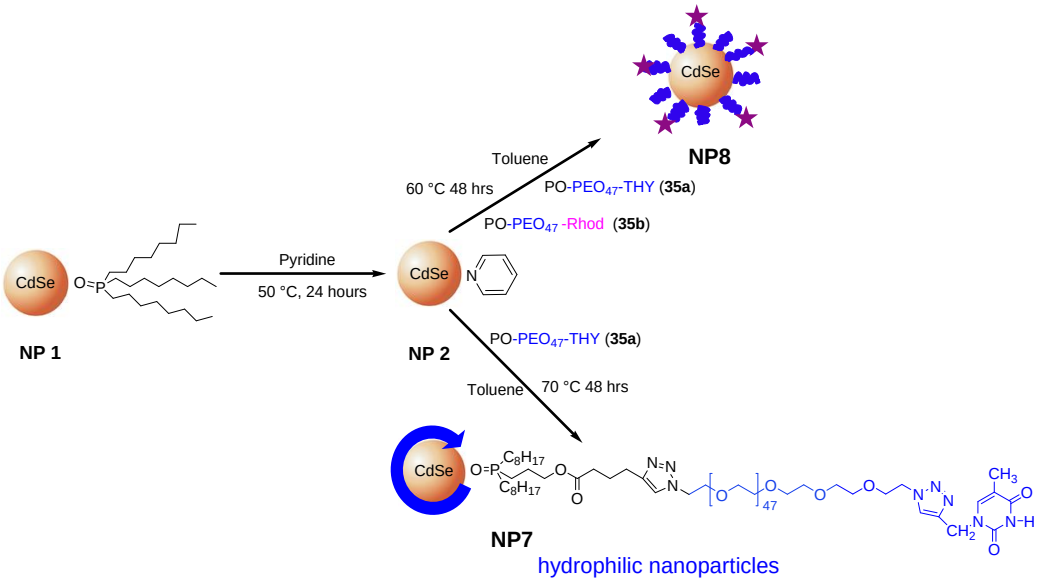

The TOPO ligand in **NP1** was replaced with a relatively weak pyridine ligand in order to facilitate the ligand exchange, and subsequently the pyridine covered CdSe nanoparticles **NP2** (50 mg) were treated with α-phosphineoxide-ω-thymine telechelic polyethylene oxide (**35a**) PO-PEO_{47}-THY ($M_{n(GPC)}$ = 2100 g·mol^{-1}; M_w/M_n = 1.3) (179 mg). The nanoparticles were dissolved in 10 mL of freshly distilled anhydrous toluene, and then the resulting mixture was stirred for 48 hours at 70 °C. Toluene was evaporated under reduced pressure, and the PO-PEO_{47}-THY (**35a**) covered NPs (**NP7**) were precipitated three times in 20 mL of hexane followed by centrifugation to separate the free unbounded polymer from the PEO_{47} covered nanoparticles. The grafting density of the final **NP7** was determined via TGA to be 0.7 chains·nm^{-2}.

7.6.6 Synthesis of polymer covered rhodamine-B labeled CdSe-nanoparticles (NP8)

In order to render the hydrophilic water soluble PEO-covered CdSe NPs (**NP7**) amenable to fluorescence microscopy studies as they undergo supramolecular recognition with mixed lipid (DPPC or DOPC) and TRI-PEO_{13}-*b*-PEO_{83} bilayers, they were fluorescently labeled with rhodamine-B as follows: a 50 to 50 mol% mixture of ligands **35a** and **35b** were dissolved in toluene and subsequently added to 50 mg of **NP2**. The mixture was heated at 60 °C for 48 hours. Toluene was evaporated under reduced pressure and the rhodamine-B labeled NPs (**NP8**) were precipitated three times in 20 mL of hexane followed by centrifugation to separate the free polymer from the polymer covered nanoparticle.

8.0 Summary

The aim of this thesis was to investigate and control the selective interaction and location of surface functionalized CdSe nanoparticles within mixed or phase separated hybrid lipid/polymer membranes utilizing monolayer- and bilayer- techniques.

A prerequisite for the selective localization and interaction of the CdSe NPs with mixed and hybrid lipid/polymer membrane is the defined functionalization of their surfaces with either hydrophobic, hydrophilic or amphiphilic moieties. The approach towards the specific surface modification of CdSe NPs with hydrophobic, hydrophilic and amphiphilic moieties involves the design of α,ω- telechelic polyisobutylenes (PIBs) carrying different functional moieties on their chain ends. Thus, on one chain end of the polymer, a phosphine oxide ligand is attached (through which the polymer may be connected to the surface of the nanoparticles); whereas the other chain end is functionalized with either hydrogen bonding moieties (thymine/2,4-diaminotriazine) (to enable their use in selective supramolecular recognition), rhodamine-B (to enable easy visualization of the nanoparticles) or poly(ethylene oxide) (to generate an amphiphilic block copolymer) (see compounds **27, 29, 30, 31** and **38)**.

PIBs (with molecular weights M_n between 2,000 and 10,000 $g \cdot mol^{-1}$ and low polydispersities (M_w/M_n = 1.3) carrying different functional groups on their chain end (*i.e* hydroxyl on one end and bromide on the other end; see compound **5**) were synthesized via living carbocationic polymerization using methyl-styrene epoxide as initiator, followed by a quenching reaction with 3-bromopropoxybenzene. Subsequent bromide/azide exchange and the use of the azide/alkyne click reaction allowed the synthesis of the nonsymmetric α, ω- functionalized polyisobutylenes (PIBs) as shown in **Scheme 3**. The chemical identity of the final structures was proven by extensive ^{1}H-NMR, ^{13}C-NMR and matrix-assisted laser desorption-ionization mass spectroscopy (MALDI) investigations.

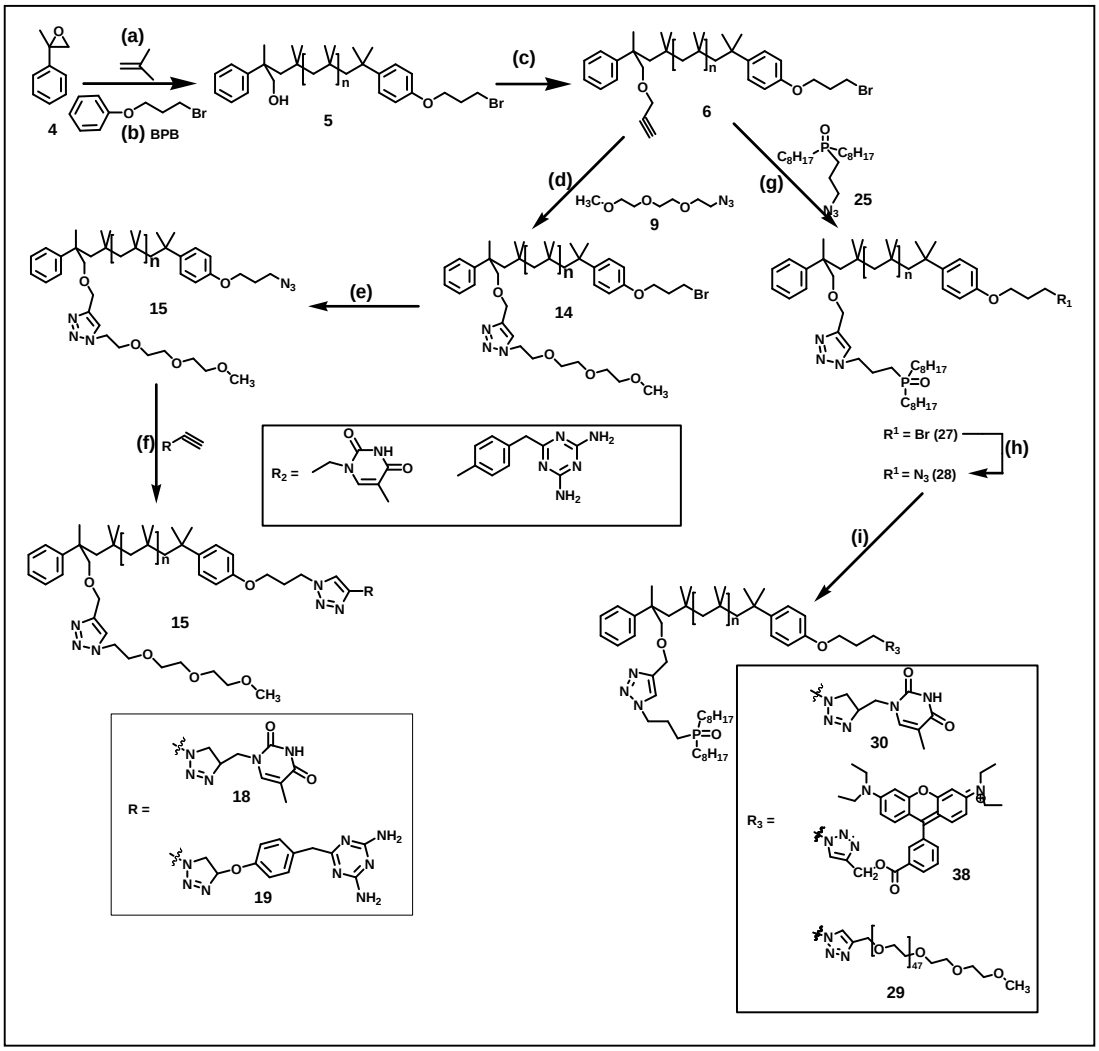

Scheme 3. Synthesis of nonsymmetric α-ω-functionalized poly(isobutylenes) bearing two different functional moieties at either chain end by initiation with styrene-epoxide and quenching reaction with 3-bromopropyloxy-benzene (BPB), followed by subsequent azide/alkyne-"click"-reactions. (a) polymerization : hexane/dichloromethane = 60/40, T = (-60 °C), [isobutylene] = 1 mol/L, [$TiCl_4$] = 0.034 mol/L; [**I**] = 0.049 mol/L, time = 30 min; [di-*tert.*butyl-pyridine] = 0.005 mol/L (b) quenching reaction : [BPB] = 0.026 mol/L, time = 2.5 hours, yield (a, b) = 98%; (c) propargylation reaction : NaH (1.2 equiv.), 15-crown-5 (1 equiv.), propargyl bromide (2 equiv.), T = (35 °C), time = 48 hours, yield 95%; (d) Cu(I)iodide (0.1 equiv.), TBTA (0.1 equiv.), toluene, yield 50%; (e, h) NaN_3 (2.5 equiv.), DMF:heptane (1:1) yield 90%; (g) Cu(I)iodide (0.1 equiv.), TBTA (0.1 equiv.), toluene, yield 50%; (f, i) Cu(I) iodide triethylphosphate (0.1 equiv.), TBTA/DIPEA (0.1 equiv.), toluene:H_2O:isopropanol (2:1:1), yield (f) = 80, (i) = 75%.

Since surface hydrophobicity plays a significant role in controlling the specific localization and interaction between nanoparticles and lipid membranes, nanoparticle (depending on its surface hydrophobicity) can be encapsulated into a liposome, either being incorporated into the hydrophobic bilayer interior or trapped within the aqueous vesicle core. The synthesized α,ω- functionalized polymers **27, 29, 30** and **38** (see **Scheme 3**) were utilized in functionalizing the surface of CdSe nanoparticles (~2 nm). This approach for surface modification of NPs combines a ligand exchange and its subsequent chemical reaction *i.e* α-phosphineoxide-ω-bromo telechelic polyisobutylene (PO-PIB_{57} **(27)**), α-phosphineoxide-ω-methoxy-telechelic polyethylene oxide (PO-PEO_{47} **(31c)**), α-phosphineoxide-ω-PEO_{12} telechelic polyisobutylene (PO-PIB_{57}-*b*-PEO_{12} **(29)**) and α-phosphineoxide- ω-thymine telechelic poly(ethylene oxide) (PO-PEO_{47}-*b*-THY **(35a)**) ligands were attached to the NP surface to generate NPs **3, 4, 5** and **7** respectively (see **Scheme 4**).

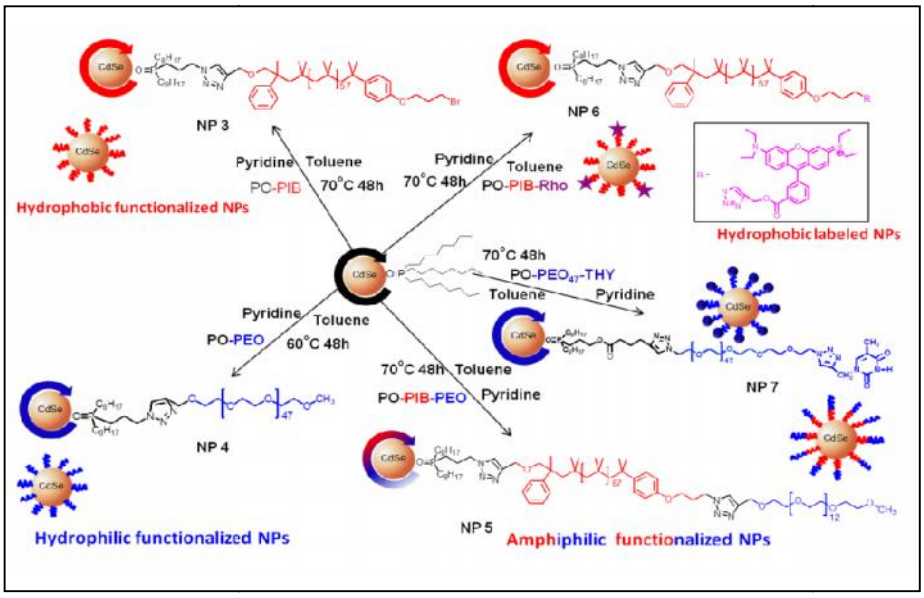

Scheme 4. Schematic diagram showing the functionalization of CdSe nanoparticles with α, ω- functionalized polymers **27, 31c**, **29, 38** and **35a** to generate **NP3, NP4, NP5, NP6** and **NP7.**

Investigating the specific localization of these polymer functionalized CdSe nanoparticles having different surface hydrophobicity in hybrid lipid/polymer membrane of 1,2-dipalmitoyl-sn-glycero-3-phophocholine (DPPC) as the lipid component and PEO_{17}-*b*-PIB_{87} block copolymer as the polymer component (in a BCP ratio which leads to a phase separated hybrid lipid/polymer membrane) was therefore monitored.

Hydrophobic PIB_{57}-modified CdSe NPs (**NP3**) were selectively located within polymer domains in a hybrid lipid/polymer monolayer at the air/water interface thereby changing their typical domain morphology from a cylindrical like structure to cone like structure; while amphiphilic PIB_{57}-*b*-PEO_{12} modified CdSe NPs showed no specific localization in phase-separated lipid/polymer films; see **Figure 31**. In addition, hydrophilic water-soluble PEO-modified CdSe NPs can readily adsorb onto spread monolayers, showing deeper penetration ability into pure lipid films than into mixed monolayers, based on attractive interactions between their polymer shell and the hydrophilic block copolymer parts. Monitoring of fluorescently labeled PIB_{57}-CdSe NPs (**NP6**) embedded into phase-separated vesicles demonstrated that the nanoparticles were enriched in one specific phase (polymer domain), thus probing their selective incorporation into the hydrophobic portion of PIB_{57}-*b*-PEO_{17} BCP rich domains.

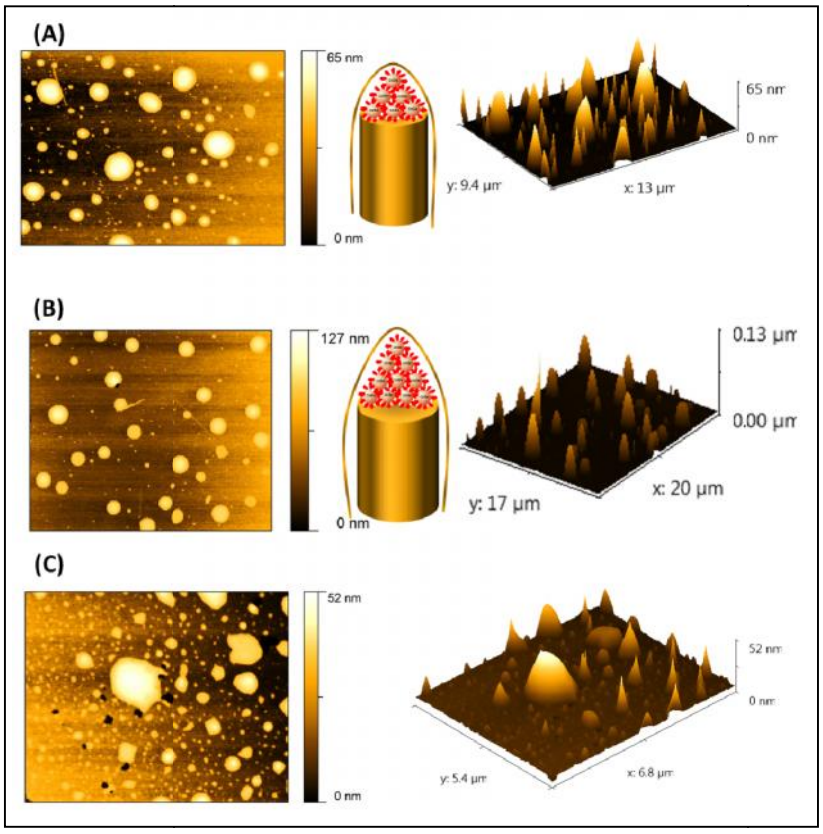

Figure 31. AFM height image of a (A) mixed DPPC:PEO_{17}-*b*-PIB_{87} monolayer in the ratio 80:20 mol% transferred at a surface pressure of 30 mNm^{-1} with hydrophobic PIB covered CdSe NPs **(NP3)** showing the specific localization of the NPs on top of the PIB columns. (B) mixed DPPC:PEO_{17}-*b*-PIB_{87} monolayer in the ratio 60:40 mol% transferred at a surface pressure of 30 mNm^{-1} with

hydrophobic PIB covered CdSe NPs (**NP3**) showing the specific localization of the NPs on top of the PIB columns. (C) mixed DPPC:PEO_{17}-*b*-PIB_{87} monolayers in the ratio 80:20 mol% transferred at a surface pressure of 30 mNm^{-1} with amphiphilic PIB_{57}-*b*-PEO_{12} covered CdSe NPs (**NP5**) showing the unspecific localization of the NPs.

To further study the specific localization of polymer functionalized nanoparticles in hybrid lipid/polymer membrane, the supramolecular interaction between a water soluble nanoparticle **(NP8)** engineered to carry a long PEO_{47}-thymine polymer on the surface (making it water soluble), and a bi and mono-layer composed of a lipid/polymer mixture was studied. The lipid/polymer membrane was constructed from DPPC or DOPC and a biocompatible amphiphilic block copolymer carrying a triazine moiety (TRI-PEO_{13}-*b*-PIB_{83}). The thymine moiety attached onto the surface of the nanoparticles can recognize the triazine moiety covalently connected to the block copolymer which is incorporated into the mixed lipid/polymer membrane. Bilayer experiment with GUVs fabricated from mixed DPPC/TRI-PEO_{13}-*b*-PIB_{83} showed that the supramolecular recognition between the PEO_{47}-thymine functionalized nanoparticles **(NP8)** and the triazine functionalized polymer **(20)** in the mixed membrane induced the removal of the polymer in the mixed GUVs, thereby resulting into facetation of the originally round and smooth vesicles see **Figure 32A** to **D.**

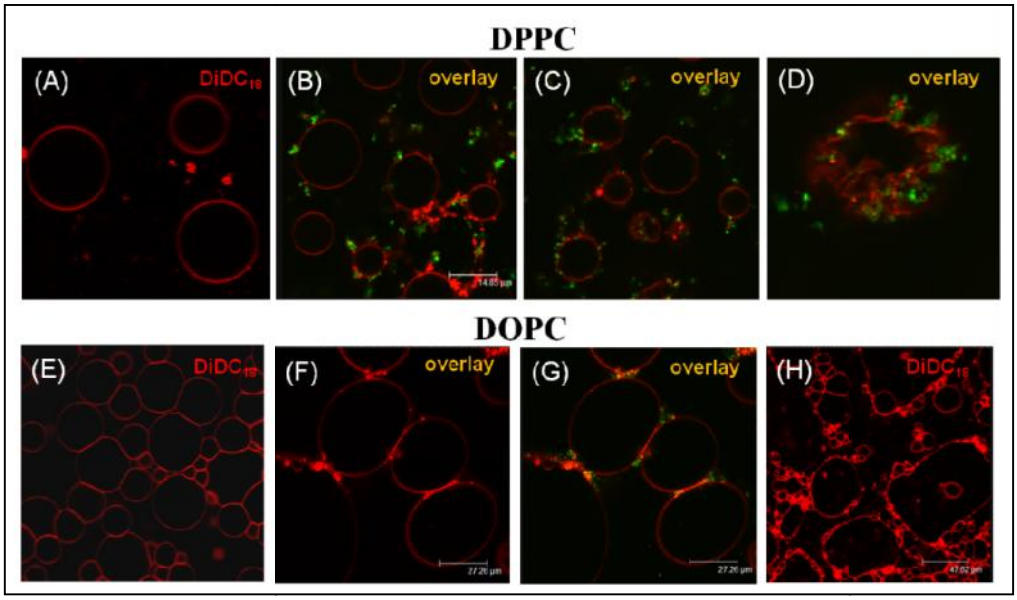

Figure 32. Confocal microscopy images of freshly prepared hybrid GUVs composed of DOPC/DPPC and TRI-PEO_{13}-*b*-PIB_{83} BCP (**20**) showing the facetation effect of the vesicles upon addition of **NP8**. Panel (A) shows an overview of hybrid GUVs, which were obtained from DPPC and 16 mol% TRI-

PEO_{13}-*b*-PIB_{83} BCP (**20**) labeled with $DiDC_{18}$. Panel (B), (C) overlay images showing the fluorescence of (**NP8**) as they bind to the GUVs after **NP8** addition. Panel (D) single faceted GUV after 24 h of **NP8** addition (red; excited at 633 nm) showing the fluorescence of (**NP8**) as they bind to the GUVs. Panel (E) shows an overview of hybrid GUVs, which were obtained from DOPC and TRI-PEO_{13}-*b*-PIB_{83} BCP (**20**) labeled with $DiDC_{18}$. Panel (F), (G) overlay images showing the fluorescence of (**NP8**) as they bind to the GUVs after **NP8** addition. Panel (H) destruction of the vesicles (via membrane rupture).

GUVs fabricated from mixed DOPC/TRI-PEO_{13}-*b*-PIB_{83} also showed that the PEO_{47}-thymine functionalized nanoparticles (**NP8**) can interact with the TRI-PEO_{13}-*b*-PIB_{83} block copolymer, and as a consequence induce their removal from the membrane, thereby leading to the destruction of the vesicles as a result of their fluid nature at room temperature; see **Figure 32F** to **H**. Monolayer adsorption experiment revealed that the water soluble PEO_{47}-thymine functionalized nanoparticles (**NP7**) can recognize the TRI-PEO_{13}-*b*-PIB_{83} block copolymer in DPPC/TRI-PEO_{13}-*b*-PIB_{83} mixture at the air/water interface leading to a much higher increase in the surface pressure when compared to a mixture of DPPC and PEO_{17}-*b*-PIB_{87} block copolymer which does not consist of any hydrogen bonding moiety.

Thus, the formation of biocompatible hybrid GUVs with selectively localization nanoparticles opens a new perspective for subtle engineering of membranes together with their (nano-) phase structure serving as a model system in designing functional nanomaterials for effective nanomedicine or drug delivery. The selective recognition and removal of one membrane component from the mixed mono- or bilayer membrane by externally added multivalent nanoparticles via a relatively simple (supramolecular) interaction, can be applicable to a large number of receptor molecules of similar or even stronger association constants between receptor and ligand. Thus it is hoped that this basic investigation can spur *e.g.* the selective capturing and detection of cancer cells via similar principles.

9.0 References

1. Gennis, R. B., *Biomembranes: molecular structure and function New*. Springer-Verlag: New York, 1989.
2. Discher, B. M.; Won, Y.-Y.; Ege, D. S.; Lee, J. C.-M.; Bates, F. S.; Discher, D. E.; Hammer, D. A., Polymersomes: Tough Vesicles Made from Diblock Copolymers. *Science* **1999,** 284, 1143-1146.
3. Discher, D. E.; Eisenberg, A., Polymer Vesicles. *Science* **2002,** 297, 967-973.
4. Helfand, E.; Wasserman, Z. R., In Developments in Block Copolymers. In New York, 1982.
5. Gopalakrishnan, G.; Danelon, C.; Izewska, P.; Prummer, M.; Yves Bolinger, P.; Geissbhler, I.; Demurtas, D.; Dubochet, J.; Vogel, H., Multifunctional Lipid/Quantum Dot Hybrid Nanocontainers for Controlled Targeting of Live Cells. *Angew. Chem. Int. Ed.* **2006,** 45, 5478-5483.
6. Binder, W. H.; Sachsenhofer, R.; Farnik, D.; Blaas, D., Guiding the location of nanoparticles into vesicular structures: a morphological study. *Phys.Chem.Chem.Phys.* **2007,** 9, 6435-6441.
7. Binder, W. H.; Sachsenhofer, R., Polymersome/Silica Capsules by 'Click'-Chemistry. *Macromol. Rapid Commun.* **2008,** 29, 1097-1103.
8. Israelachvili, J. N.; Mitchell, D. J.; Ninham, B. W., Theory of self-assembly of hydrocarbon amphiphiles into micelles and bilayers. *J. Chem. Soc. Faraday Trans.* **1976,** 72, 1525-1568.
9. van Dongen, S. F. M.; Verdurmen, W. P. R.; Peters, R. J. R. W.; Nolte, R. J. M.; Brock, R.; van Hest, J. C. M., Cellular Integration of an Enzyme-Loaded Polymersome Nanoreactor. *Angew. Chem. Int. Ed.* **2010,** 49, 7213-7216.
10. Lomas, H.; Canton, I.; MacNeil, S.; Du, J.; Armes, S. P.; Ryan, A. J.; Lewis, A. L.; Battaglia, G., Biomimetic pH Sensitive Polymersomes for Efficient DNA Encapsulation and Delivery. *Adv. Mater.* **2007,** 19, 4238-4243.
11. Chithrani, B. D.; Ghazani, A. A.; Chan, W. C. W., Determining the Size and Shape Dependence of Gold Nanoparticle Uptake into Mammalian Cells. *Nano Letters* **2006,** 6, 662-668.
12. Jong, W. H. D.; Borm, P. J. A., Drug delivery and nanoparticles:Applications and hazards. *Int. J. Nanomedicine* **2008,** 3, 133-149.
13. Aranda-Espinoza, H.; Berman, A.; Dan, N.; Pincus, P.; Safran, S., Interaction Between Inclusions Embedded in Membranes. *Biophys. J.* **1996,** 71, 648-656.
14. Dan, N.; Berman, A.; Pincus, P.; Safran, S., *J. Phys. (Paris)* **1994,** 4, 1713.
15. Schmidt, U.; Guigas, G.; Weiss, M., Cluster Formation of Transmembrane Proteins Due to Hydrophobic Mismatching. *Phys. Rev. Lett.* **2008,** 101, 1281041-1281044.
16. Yu, Y.; Granick, S., Pearling of Lipid Vesicles Induced by Nanoparticles. *J. Am. Chem. Soc.* **2009,** 131, 14158-14159.
17. Schulz, M.; Olubummo, A.; Binder, W. H., Beyond the lipid-bilayer: interaction of polymers and nanoparticles with membranes. *Soft Matter* **2012,** 8, 4849-4864.
18. Hong, S.; Bielinska, A. U.; Mecke, A.; Keszler, B.; Beals, J. L.; Shi, X.; Balogh, L.; Orr, B. G.; Baker, J. R.; Banaszak Holl, M. M., Interaction of Poly(amidoamine) Dendrimers with Supported Lipid Bilayers and Cells: Hole Formation and the Relation to Transport. *Bioconjugate Chem.* **2004,** 15, 774-782.
19. Leroueil, P. R.; Berry, S. A.; Duthie, K.; Han, G.; Rotello, V. M.; McNerny, D. Q.; Baker, J. R.; Orr, B. G.; Banaszak Holl, M. M., Wide Varieties of Cationic Nanoparticles Induce Defects in Supported Lipid Bilayers. *Nano Letters* **2008,** 8, 420-424.
20. Nigavekar, S.; Sung, L.; Llanes, M.; El-Jawahri, A.; Lawrence, T.; Becker, C.; Balogh, L.; Khan, M., 3H Dendrimer Nanoparticle Organ/Tumor Distribution. *Pharm. Res.* **2004,** 21, 476-483.
21. Rozenberg, B. A.; Tenne, R., Polymer-assisted fabrication of nanoparticles and nanocomposites. *Prog. Polym. Sci.* **2008,** 33, 40-112.

22. Ginzburg, V. V.; Balijepalli, S., Modeling the Thermodynamics of the Interaction of Nanoparticles with Cell Membranes. *Nano Lett.* **2007,** 7, 3716-3722.
23. Alexeev, A.; Uspal, W. E.; Balazs, A. C., Harnessing Janus Nanoparticles to Create Controllable Pores in Membranes. *ACS Nano* **2008,** 2, 1117-1122.
24. Gopalakrishnan, G.; Danelon, C.; Izewska, P.; Prummer, M.; Yves Bolinger, P.; Geissbhler, I.; Demurtas, D.; Dubochet, J.; Vogel, H., Multifunctional Lipid/Quantum Dot Hybrid Nanocontainers for Controlled Targeting of Live Cells. *Angew. Chem. Int. Ed.* **2006,** 45, 5478-5483.
25. Chen, Y.; Bose, A.; Bothun, G. D., Controlled Release from Bilayer Decorated Magnetoliposomes via Electromagnetic Heating. *ACS Nano* **2010,** 4, 3215-3221.
26. Bothun, G. D., Hydrophobic silver nanoparticles trapped in lipid bilayers: Size distribution, bilayer phase behavior, and optical properties. *J. Nanobiotechnol.* **2008,** 6, 13-23.
27. Rasch, M. R.; Rossinyol, E.; Korgel, B. A.; Hueso, J. L.; Goodfellow, B. W.; Arbiol, J., Hydrophobic Gold Nanoparticle Self-Assembly with Phosphatidylcholine Lipid: MembraneLoaded and Janus Vesicles. *Nano Lett.* **2010,** 10, 3733-3739.
28. Rasch, M. R.; Rossinyol, E.; Hueso, J. L.; Goodfellow, B. W.; Arbiol, J.; Korgel, B. A., Hydrophobic Gold Nanoparticle Self-Assembly with Phosphatidylcholine Lipid: Membrane-Loaded and Janus Vesicles. *Nano Lett.* **2010,** 10, 3733-3739.
29. Jing, B.; Zhu, Y. E., Disruption of Supported Lipid Bilayers by Semi-Hydrophobic Nanoparticles. *J. Am. Chem. Soc.* **2011,** 133, 10983-10989.
30. Li, Y.; Chen, X.; Gu, N., Computational Investigation of Interaction between Nanoparticles and Membranes: Hydrophobic/Hydrophilic Effect. *J. Phys. Chem. B* **2008,** 112, 16647-16648.
31. Leroueil, P. R.; Berry, S. A.; Duthie, K.; Han, G.; Rotello, V. M.; McNerny, D. Q.; Baker, J. R.; Orr, B. G.; Banaszak Holl, M. M., Wide Varieties of Cationic Nanoparticles Induce Defects in Supported Lipid Bilayers. *Nano Lett.* **2008,** 8, 420-424.
32. Heller, W. T.; Waring, A. J.; Lehrer, R. I.; Harroun, T. A.; Weiss, T. M.; Yang, L.; Huang, H. W., Membrane Thinning Effect of the β-Sheet Antimicrobial Protegrin. *Biochemistry* **1999,** 39, 139-145.
33. Livadaru, L.; Kovalenko, A., Fundamental Mechanism of Translocation across Liquidlike Membranes: Toward Control over Nanoparticle Behavior. *Nano Letters* **2005,** 6, 78-83.
34. Hong, S.; Leroueil, P. R.; Janus, E. K.; Peters, J. L.; Kober, M.-M.; Islam, M. T.; Orr, B. G.; Baker, J. R.; Banaszak Holl, M. M., Interaction of Polycationic Polymers with Supported Lipid Bilayers and Cells: Nanoscale Hole Formation and Enhanced Membrane Permeability. *Bioconjugate Chem.* **2006,** 17, 728-734.
35. Li, Y.; Gu, N., Thermodynamics of Charged Nanoparticle Adsorption on Charge-Neutral Membranes: A Simulation Study. *J. Phys. Chem. B* **2010,** 114, 2749-2754.
36. Lin, J.; Zhang, H.; Chen, Z.; Zheng, Y., Penetration of Lipid Membranes by Gold Nanoparticles: Insights into Cellular Uptake, Cytotoxicity, and Their Relationship. *ACS Nano* **2010,** 4, 5421-5429.
37. Arvizo, R. R.; Miranda, O. R.; Bhattacharya, R.; Thompson, M. A.; Robertson, J. D.; Rotello, V. M.; Pabelick, C. M.; Prakash, Y. S.; Mukherjee, P., Effect of Nanoparticle Surface Charge at the Plasma Membrane and Beyond. *Nano Lett.* **2010,** 10, 2543-2548.
38. Laurencin, M.; Georgelin, T.; Malezieux, B.; Siaugue, J.-M.; Ménager, C., Interactions Between Giant Unilamellar Vesicles and Charged Core–Shell Magnetic Nanoparticle *Langmuir* **2010,** 26, 16025-16030.
39. Zhang, L.; Granick, S., How to Stabilize Phospholipid Liposomes (Using Nanoparticles). *Nano Lett.* **2006,** 6, 694-698.
40. Wang, B.; Zhang, L.; Bae, S. C.; Granick, S., Nanoparticle-induced surface reconstruction of phospholipid membranes. *Proc. Natl. Acad. Sci. U.S.A.* **2008,** 105, 18171-18175.

41. Roiter, Y.; Ornatska, M.; Heine, D. R.; Rammohan, A. R.; Minko, S.; Balakrishnan, J., Interaction of Nanoparticles with Lipid Membrane. *Nano Lett.* **2008,** 8, 941-944.
42. de Planque, M. R. R.; Aghdaei, S.; Roose, T.; Morgan, H., Electrophysiological Characterization of Membrane Disruption by Nanoparticles. *ACS Nano* **2011,** 5, 3599-3606.
43. Lipowsky, R.; Döbereiner, H. G., Vesicles in contact with nanoparticles and colloids. *Europhys. Lett.* **1998,** 43, 219-225.
44. Breidenich, M.; Netz, R. R.; Lipowsky, R., The influence of non-anchored polymers on the curvature of vesicles. *Mol. Phys.* **2005,** 103, 3169-3183.
45. Noguchi, H.; Takasu, M., Adhesion of Nanoparticles to Vesicles: A Brownian Dynamics Simulation. *Biophys. J.* **2002,** 83, 299-308.
46. Leroueil, P. R.; Orr, G. B.; Hong, S.; Banaszak Holl, M. M.; Mecke, A.; Baker Jr. , J. R., Nanoparticle Interaction with Biological Membranes. *Acc. Chem. Res.* **2007,** 40, 335–342.
47. Chen, J.; Hessler, J. A.; Khan, D. P.; Som, A.; Hong, S.; Tew, G. N.; Holl, M. M. B.; Putchakayala, K.; Mullen, D. G.; Lopatin, A. N.; Orr, G. B.; Panama, B. K.; DiMaggio, S. C.; Baker, J. R., Cationic Nanoparticles Induce Nanoscale Disruption in Living Cell Plasma Membranes. *J. Phys. Chem. B* **2009,** 113, 11179-11185.
48. Ionov, M.; Gardikis, K.; Wróbel, D.; Hatziantoniou, S.; Mourelatou, H.; Majoral, J.; Klajnert, B.; Bryszewska, M.; Demetzos, C., Interaction of cationic phosphorus dendrimers (CPD) with charged and neutral lipid membranes. *Colloids Surf. B* **2011,** 82, 8-12.
49. Kroto, H. W.; Heath, J. R.; O'Brien, S. C.; Curl, R. F.; Smalley, R. E., C60: Buckminsterfullerene. *Nature* **1985,** 318, 162-163.
50. Ashcroft, J. M.; Tsyboulski, D. A.; Hartman, K. B.; Zakharian, T. Y.; Marks, J. W.; Weisman, R. B.; Rosenblum, M. G.; Wilson, L. J., Fullerene (C60) immunoconjugates: interaction of water-soluble C60 derivatives with the murine anti-gp240 melanoma antibody. *Chem. Commun.* **2006**, 28, 3004-3006.
51. Ryan, J. J.; Bateman, H. R.; Stover, A.; Gomez, G.; Norton, S. K.; Zhao, W.; Schwartz, L. B.; Lenk, R.; Kepley, C. L., Fullerene Nanomaterials Inhibit the Allergic Response. *J. Immunol.* **2007,** 179, 665-672.
52. Nakashima, N.; Nonaka, Y.; Nakanishi, T.; Sagara, T.; Murakami, H., A C60-Embedded Artificial Bilayer Membrane Film Electrode Device: Phase-Transition-Dependent Electrochemistry. *J. Phy. Chem. B* **1998,** 102, 38, 7328-7330.
53. Wharton, T.; Wilson, L. J., Toward fullerene-based X-ray contrast agents: design and synthesis of non-ionic, highly-iodinated derivatives of C60. *Tetrahedron Lett.* **2002,** 43, 561-564.
54. Wong-Ekkabut, J.; Baoukina, S.; Triampo, W.; Tang, I. M.; Tieleman, D. P.; Monticelli, L., Computer simulation study of fullerene translocation through lipid membranes. *Nat Nano* **2008,** 3, 6, 363-368.
55. D'Rozario, R. S. G.; Wee, C. L.; Wallace, E. J.; Sansom, M. S. P., The interaction of C_{60} and its derivatives with a lipid bilayer via molecular dynamics simulations. *Nanotechnol.* **2009,** 20, 115102-115109.
56. Qiao, R., Translocation of C_{60} and Its Derivatives Across a Lipid Bilayer. *Nano Lett.* **2007,** 7, 614-619.
57. Jeng, U. S.; Hsu, C.-H.; Lin, T.-L.; Wu, C.-M.; Chen, H.-L.; Tai, L.-A.; Hwang, K.-C., Dispersion of fullerenes in phospholipid bilayers and the subsequent phase changes in the host bilayers. *Physica B (Amsterdam, Neth.)* **2005,** 357, (1-2), 193-198.
58. Li, L.; Davande, H.; Bedrov, D.; Smith, G. D., A Molecular Dynamics Simulation Study of C60 Fullerenes Inside a Dimyristoylphosphatidylcholine Lipid Bilayer. *J. Phys. Chem. B* **2007,** 111, 4067-4072.

59. Lecommandoux, S.; Sanson, C.; Diou, O.; Thelì venot, J.; Ibarboure, E.; Soum, A.; Bruì,let, A.; Miraux, S.; Thiaudière, E.; Tan, S.; Brisson, A.; Dupuis, V.; Sandre, O., Doxorubicin Loaded Magnetic Polymersomes: Theranostic Nanocarriers for MR Imaging and Magneto-Chemotherapy. *ACS Nano* **2011,** 5, 1122-1140.
60. Lin, Y.; Boker, A.; He, J.; Sill, K.; Xiang, H.; Abetz, C.; Li, X.; Wang, J.; Emrick, T.; Long, S.; Wang, Q.; Balazs, A.; Russell, T. P., Self-directed self-assembly of nanoparticle/copolymer mixtures. *Nature* **2005,** 434, 55-59.
61. Haryono, A.; Binder, W. H., Controlled Arrangement of Nanoparticle Arrays in Block-Copolymer Domains. *Small* **2006,** 2, 600-611.
62. Sanchez-Gaytan, B. L.; Cui, W.; Kim, Y.; Mendez-Polanco, M. A.; Duncan, T. V.; Fryd, M.; Wayland, B. B.; Park, S., Interfacial Assembly of Nanoparticles in Discrete Block-Copolymer Aggregates. *Angew. Chem. Int. Ed.* **2007,** 119, 9395-9398.
63. Hickey, R. J.; Haynes, A. S.; Kikkawa, J. M.; Park, S., Controlling the Self-Assembly Structure of Magnetic Nanoparticles and Amphiphilic Block-Copolymers: From Micelles to Vesicles. *J. Am. Chem. Soc.* **2011,** 133, 1517-1525.
64. Chan, Y. N. C.; Craig, G. S. W.; Schrock, R. R.; Cohen, R. E., Synthesis of palladium and platinum nanoclusters within microphase-separated diblock copolymers. *Chem. Mater.* **1992,** 4, 885-894.
65. Förster, S.; Antonietti, M., Amphiphilic Block Copolymers in Structure-Controlled Nanomaterial Hybrids. *Adv. Mater.* **1998,** 10, 195-217.
66. Sachsenhofer, R.; Binder, W. H.; Farnik, D.; Zirbs, R., Polymersome-Embedded Nanoparticles. *Macromol. Symp.* **2007,** 254, 375-377.
67. Mueller, W.; Pierrat, S.; Koynov, K.; Basche, T.; Fischer, K.; Hartmann, S.; Maskos, M., Hydrophobic Shell Loading of PB-b-PEO Vesicles. *Macromolecules* **2009,** 42, 357-361.
68. Li, H.; Sachsenhofer, R.; Binder, W. H.; Henze, T.; Thurn-Albrecht, T.; Busse, K.; Kressler, J., Hierarchical Organization of Poly(ethylene oxide)-block-poly(isobutylene) and Hydrophobically Modified Fe_2O_3 Nanoparticles at the Air/Water Interface and on Solid Supports. *Langmuir* **2009,** 25, 8320-8329.
69. Binder, W. H.; Sachsenhofer, R., Polymersome/Silica Capsules by 'Click'-Chemistry. *Macromol. Rapid Commun.* **2008,** 29, 1097-1103.
70. Mai, Y.; Eisenberg, A., Controlled Incorporation of Particles into the Central Portion of Vesicle Walls. *J. Am. Chem. Soc.* **2010,** 132, 10078-10084.
71. Krack, M.; Hohenberg, H.; Weller, H.; Kornowski, A.; Förster, S.; Lindner, P., Nanoparticle-Loaded Magnetophoretic Vesicles. *J. Am. Chem. Soc.* **2008,** 130, 7315-7320.
72. Lecommandoux, S.; Sandre, O.; Chécot, F.; Perzynski, R., Smart hybrid magnetic self-assembled micelles and hollow capsules. *Prog. Solid State Chem.* **2006,** 34, 171-179.
73. Hickey, R. J.; Sanchez-Gaytan, B. L.; Cui, W.; Composto, R. J.; Fryd, M.; Bradford, B. W.; Park, J., Morphological Transitions of Block-Copolymer Bilayers via Nanoparticle Clustering. *Small* **2010,** 6, 48-51.
74. Martinez-Hurtado, J. L., Metallic Nanoparticle Block Copoloymer Vesicles with Enhanced Optical Properties. *Nanomaterials* **2011,** 1, 20-30.
75. Chen, R.; Pearce, D. J. G.; Fortuna, S.; Cheung, D. L.; Bon, S. A. F., Polymer Vesicles with a Colloidal Armor of Nanoparticles. *J. Am. Chem. Soc.* **2011,** 133, 2151-2153.
76. Verma, A.; Stellacci, F., Effect of Surface Properties on Nanoparticle–Cell Interactions. *Small* **2010,** 6, 12-21.
77. Brayner, R., The toxicological impact of nanoparticles. *Nanotoday* **2008,** 3, 48-55.
78. Yang, Z.; Liu, Z. W.; Allaker, R. P.; Reip, P.; Oxford, J.; Ahmad, Z.; Ren, G., A review of nanoparticle functionality and toxicity on the central nervous system. *J. R. Soc. Interface* **2010,** 7, S411-S422.
79. Lewinski, N.; Colvin, V.; Drezek, R., Cytotoxicity of Nanoparticles. *Small* **2008,** 4, 26-49.

80. Pan, Y.; Neuss, S.; Leifert, A.; Fischler, M.; Wen, F.; Simon, U.; Schmid, G.; Brandau, W.; Jahnen-Dechent, W., Size-Dependent Cytotoxicity of Gold Nanoparticles. *Small* **2007,** 3, 1941-1949.
81. Donaldson, K.; Stone, V.; Clouter, A.; Renwick, L.; MacNee, W., Ultrafine particles. *Occup. Environ. Med.* **2001,** 58, 211-216.
82. Zhang, L. W.; Yang, J.; Barron, A. R.; Monteiro-Riviere, N. A., Endocytic mechanisms and toxicity of a functionalized fullerene in human cells. *Toxicol. Lett.* **2009,** 191, 149-157.
83. Windschiegl, B.; Orth, A.; Römer, W.; Berland, L.; Stechmann, B.; Bassereau, P.; Johannes, L.; Steinem, C., Lipid Reorganization Induced by Shiga Toxin Clustering on Planar Membranes. *PLoS ONE* **2009,** 4, e6238.
84. Napierska, D.; Thomassen, L. C. J.; Rabolli, V.; Lison, D.; Gonzalez, L.; Kirsch-Volders, M.; Martens, J. A.; Hoet, P. H., Size-Dependent Cytotoxicity of Monodisperse Silica Nanoparticles in Human Endothelial Cells. *Small* **2009,** 5, 846-853.
85. Lin, I. C.; Liang, M.; Liu, T.-Y.; Ziora, Z. M.; Monteiro, M. J.; Toth, I., Interaction of Densely Polymer-Coated Gold Nanoparticles with Epithelial Caco-2 Monolayers. *Biomacromolecules* **2011,** 12, 1339-1348.
86. Deng, Z. J.; Liang, M.; Monteiro, M.; Toth, I.; Minchin, R. F., Nanoparticle-induced unfolding of fibrinogen promotes Mac-1 receptor activation and inflammation. *Nat. Nanotechnol.* **2011,** 6, 39-44.
87. Colvin, V. L.; Schlamp, M. C.; Alivisatos, A. P., Light-emitting diodes made from cadmium selenide nanocrystals and a semiconducting polymer. *Nature* **1994,** 370, 354-357.
88. Mueller, A. H.; Petruska, M. A.; Achermann, M.; Werder, D. J.; Akhadov, E. A.; Koleske, D. D.; Hoffbauer, M. A.; Klimov, V. I., Multicolor Light-Emitting Diodes Based on Semiconductor Nanocrystals Encapsulated in GaN Charge Injection Layers. *Nano Lett.* **2005,** 5, 1039-1044.
89. Schlamp, M. C.; Peng, X.; Alivisatos, A. P., Improved efficiencies in light emitting diodes made with CdSe(CdS) core/shell type nanocrystals and a semiconducting polymer. *J. Appl. Phys.* **1997,** 82, 5837-5842.
90. Zhao, J.; Bardecker, J. A.; Munro, A. M.; Liu, M. S.; Niu, Y.; Ding, I. K.; Luo, J.; Chen, B.; Jen, A. K. Y.; Ginger, D. S., Efficient CdSe/CdS Quantum Dot Light-Emitting Diodes Using a Thermally Polymerized Hole Transport Layer. *Nano Lett.* **2006,** 6, 463-467.
91. Bivas-Benita, M.; Romeijn, S.; Junginger, H. E.; Borchard, G., PLGA–PEI nanoparticles for gene delivery to pulmonary epithelium. *Eur. J. Pharm. Biopharm.* **2004,** 58, 1-6.
92. Wim, H. D. J.; Paul, J. A. B., Drug delivery and nanoparticles:Application and hazards. *Int. J. Nanomedicine* **2008,** 3, 133-149.
93. Sahoo, S. K.; Labhasetwar, V., Nanotech approaches to drug delivery and imaging. *Drug discovery today* **2003,** 8, 1112-1120.
94. Lai, C.-Y.; Trewyn, B. G.; Jeftinija, D. M.; Jeftinija, K.; Xu, S.; Jeftinija, S.; Lin, V. S. Y., A Mesoporous Silica Nanosphere-Based Carrier System with Chemically Removable CdS Nanoparticle Caps for Stimuli-Responsive Controlled Release of Neurotransmitters and Drug Molecules. *J. Am. Chem. Soc.* **2003,** 125, 4451-4459.
95. Adam, P. Z.; Peng, X., Formation of High-Quality CdTe, CdSe, and CdS Nanocrystals Using CdO as Precursor. *J. Am. Chem. Soc.* **2001,** 123, 183-184.
96. Hines, M. A.; Guyot-Sionnest, P., Synthesis and Characterization of Strongly Luminescing ZnS-Capped CdSe Nanocrystals. *J. Phys. Chem.* **1996,** 100, 468-471.
97. Lippens, P. E.; Lannoo, M., Calculation of the band gap for small CdS and ZnS crystallites. *Phys. Rev. B* **1989,** 39, 10935-10942.
98. Weller, H., Colloidal Semiconductor Q-Particles: Chemistry in the Transition Region Between Solid State and Molecules. *Angew. Chem. Int. Ed.* **1993,** 32, 41-53.

99. Bawendi, M. G.; Steigerwald, M. L.; Brus, L. E., The Quantum Mechanics of Larger Semiconductor Clusters ("Quantum Dots"). *Annu. Rev. Phys. Chem.* **1990,** 41, 477-496.
100. Fontes, A.; Lira, R. B. d.; Seabra, M. A. B. L.; Silva, T. G. d.; Gomes, d. C. N. A.; Santos, B. S., *Quantum Dots in Biomedical Research*. 2012.
101. Yu, W. W.; Peng, X., Formation of High-Quality CdS and Other II–VI Semiconductor Nanocrystals in Noncoordinating Solvents: Tunable Reactivity of Monomers. *Angew. Chem. Int. Ed.* **2002,** 41, 2368-2371.
102. Henglein, A., Photochemistry of colloidal cadmium sulfide. 2. Effects of adsorbed methyl viologen and of colloidal platinum. *J. Phys. Chem.* **1982,** 86, 2291-2293.
103. Ohtani, T.; Motoki, M.; Koh, K.; Ohshima, K., Synthesis of binary copper chalcogenides by mechanical alloying. *Mater. Res. Bull.* **1995,** 30, 1495-1504.
104. Ohtani, T.; Maruyama, K.; Ohshima, K., Synthesis of copper, silver, and samarium chalcogenides by mechanical alloying. *Mater. Res. Bull.* **1997,** 32, 343-350.
105. Wang, J.; Grocholl, L.; Gillan, E. G., Facile Azidothermal Metathesis Route to Gallium Nitride Nanoparticles. *Nano Lett.* **2002,** 2, 899-902.
106. Lian, G.; Zhang, X.; Zhu, L.; Tan, M.; Cui, D.; Wang, Q., A facile solid state reaction route towards nearly monodisperse hexagonal boron nitride nanoparticles. *J. Mater. Chem.* **2010,** 20, 3736-3742.
107. Mu, J.; Gao, X., Synthesis of CdSe Nanocrystals through a Reaction of H2Se Gas and Cd2+ Ions in Aqueous Medium and Their Optical and Structural Properties. *J. Dispersion Sci. Technol.* **2005,** 26, 763-767.
108. Tian, Y.; Newton, T.; Kotov, N. A.; Guldi, D. M.; Fendler, J. H., Coupled Composite CdS−CdSe and Core−Shell Types of (CdS)CdSe and (CdSe)CdS Nanoparticles *J. Phys. Chem.* **1996,** 100, 8927-8939.
109. Gutierrez-Wing, C.; Esparza, R.; Vargas-Hernandez, C.; Fernandez Garcia, M. E.; Jose-Yacaman, M., Microwave-assisted synthesis of gold nanoparticles self-assembled into self-supported superstructures. *Nanoscale* **2012,** 4, 2281-2287.
110. Zhu, J.; Koltypin, Y.; Gedanken, A., General Sonochemical Method for the Preparation of Nanophasic Selenides: Synthesis of ZnSe Nanoparticles. *Chem. Mater.* **1999,** 12, 73-78.
111. Han, H.-y.; Sheng, Z.-h.; Liang, J.-g., A novel method for the preparation of water-soluble and small-size CdSe quantum dots. *Mater. Lett.* **2006,** 60, 3782-3785.
112. Dong, S.; Tang, C.; Zhou, H.; Zhao, H., Photochemical synthesis of gold nanoparticles by the sunlight radiation using a seeding approach. *Gold Bull* **2004,** 37, 187-195.
113. Sau, T.; Pal, A.; Jana, N. R.; Wang, Z. L.; Pal, T., Size Controlled Synthesis of Gold Nanoparticles using Photochemically Prepared Seed Particles. *J. Nanopart. Res.* **2001,** 3, 257-261.
114. Steigerwald, M. L.; Alivisatos, A. P.; Gibson, J. M.; Harris, T. D.; Kortan, R.; Muller, A. J.; Thayer, A. M.; Duncan, T. M.; Douglass, D. C.; Brus, L. E., Surface derivatization and isolation of semiconductor cluster molecules. *J. Am. Chem. Soc.* **1988,** 110, 3046-3050.
115. Murray, C. B.; Norris, D. J.; Bawendi, M. G., Synthesis and characterization of nearly monodisperse CdE (E = sulfur, selenium, tellurium) semiconductor nanocrystallites. *J. Am. Chem. Soc.* **1993,** 115, 8706-8715.
116. Peng, Z. A.; Peng, X., Formation of High-Quality CdTe, CdSe, and CdS Nanocrystals Using CdO as Precursor. *J. Am. Chem. Soc.* **2000,** 123, 183-184.
117. Mekis, I.; Talapin, D. V.; Kornowski, A.; Haase, M.; Weller, H., One-Pot Synthesis of Highly Luminescent CdSe/CdS Core−Shell Nanocrystals via Organometallic and “Greener” Chemical Approaches. *J. Phys. Chem. B* **2003,** 107, 7454-7462.
118. Yu, W. W.; Qu, L.; Guo, W.; Peng, X., Experimental Determination of the Extinction Coefficient of CdTe, CdSe, and CdS Nanocrystals. *Chem. Mater.* **2003,** 15, 2854-2860.

119. Peng, X.; Manna, L.; Yang, W.; Wickham, J.; Scher, E.; Kadavanich, A.; Alivisatos, A. P., Shape control of CdSe nanocrystals. *Nature* **2000,** 404, 59-61.
120. Xia, Y.; Xiong, Y.; Lim, B.; Skrabalak, S. E., Shape-Controlled Synthesis of Metal Nanocrystals: Simple Chemistry Meets Complex Physics. *Angew. Chem. Int. Ed.* **2009,** 48, 60-103.
121. Xiao, J.; Qi, L., Surfactant-assisted, shape-controlled synthesis of gold nanocrystals. *Nanoscale* **2011,** 3, 1383-1396.
122. Gill, R.; Zayats, M.; Willner, I., Semiconductor Quantum Dots for Bioanalysis. *Angew. Chem. Int. Ed.* **2008,** 47, 7602-7625.
123. Frankamp, B. L.; Uzun, O.; Ilhan, F.; Boal, A. K.; Rotello, V. M., Recognition-Mediated Assembly of Nanoparticles into Micellar Structures with Diblock Copolymers. *J. Am. Chem. Soc.* **2002,** 124, 892-893.
124. Olubummo, A.; Schulz, M.; Lechner, B.-D.; Scholtysek, P.; Bacia, K.; Blume, A.; Kressler, J.; Binder, W. H., Controlling the Localization of Polymer-Functionalized Nanoparticles in Mixed Lipid/Polymer Membranes. *ACS Nano* **2012,** 6, 8713-8727.
125. Peng, Z. A.; Peng, X., Mechanisms of the Shape Evolution of CdSe Nanocrystals. *J. Am. Chem. Soc.* **2001,** 123, 1389-1395.
126. Yu, W. W.; Falkner, J. C.; Shih, B. S.; Colvin, V. L., Preparation and Characterization of Monodisperse PbSe Semiconductor Nanocrystals in a Noncoordinating Solvent. *Chem. Mater.* **2004,** 16, 3318-3322.
127. Landi, B. J.; Castro, S. L.; Ruf, H. J.; Evans, C. M.; Bailey, S. G.; Raffaelle, R. P., CdSe quantum dot-single wall carbon nanotube complexes for polymeric solar cells. *Sol. Energy Mater. Sol. Cells* **2005,** 87, 733-746.
128. Dubois, F.; Mahler, B.; Dubertret, B.; Doris, E.; Mioskowski, C., A Versatile Strategy for Quantum Dot Ligand Exchange. *J. Am. Chem. Soc.* **2006,** 129, 482-483.
129. Zhu, M.-Q.; Chang, E.; Sun, J.; Drezek, R. A., Surface modification and functionalization of semiconductor quantum dots through reactive coating of silanes in toluene. *J. Mater. Chem.* **2007,** 17, 800-805.
130. Heinemann, M. D.; von Maydell, K.; Zutz, F.; Kolny-Olesiak, J.; Borchert, H.; Riedel, I.; Parisi, J., Photo-induced Charge Transfer and Relaxation of Persistent Charge Carriers in Polymer/Nanocrystal Composites for Applications in Hybrid Solar Cells. *Adv. Funct. Mater.* **2009,** 19, 3788-3795.
131. Oluwafemi, S. O.; Revaprasadu, N., Study on growth kinetics of hexadecylamine capped CdSe nanoparticles using its electronic properties. *Physica B: Condensed Matter* **2009,** 404, 1204-1208.
132. Fahmi, A.; Pietsch, T.; Appelhans, D.; Gindy, N.; Voit, B., Water-soluble CdSe nanoparticles stabilised by dense-shell glycodendrimers. *New J. Chem.* **2009,** 33, 703-706.
133. Wisher, A. C.; Bronstein, I.; Chechik, V., Thiolated PAMAM dendrimer-coated CdSe/ZnSe nanoparticles as protein transfection agents. *Chem. Commun.* **2006,** 0, 1637-1639.
134. Cooper, D. R.; Suffern, D.; Carlini, L.; Clarke, S. J.; Parbhoo, R.; Bradforth, S. E.; Nadeau, J. L., Photoenhancement of lifetimes in CdSe/ZnS and CdTe quantum dot-dopamine conjugates. *Phys. Chem. Chem. Phys.* **2009,** 11, 4298-4310.
135. Hezinger, A. F. E.; Teßmar, J.; Göpferich, A., Polymer coating of quantum dots – A powerful tool toward diagnostics and sensorics. *Eur. J. Pharm. Biopharm.* **2008,** 68, 138-152.
136. Shen, L., Biocompatible Polymer/Quantum Dots Hybrid Materials: Current Status and Future Developments. *J. Funct. Biomater.* **2011,** 2, 355-372.
137. Mattoussi, H.; Mauro, J. M.; Goldman, E. R.; Anderson, G. P.; Sundar, V. C.; Mikulec, F. V.; Bawendi, M. G., Self-Assembly of CdSe−ZnS Quantum Dot Bioconjugates Using an Engineered Recombinant Protein. *J. Am. Chem. Soc.* **2000,** 122, 12142-12150.
138. Roux, S.; Garcia, B.; Bridot, J.-L.; Salomé, M.; Marquette, C.; Lemelle, L.; Gillet, P.; Blum, L.; Perriat, P.; Tillement, O., Synthesis, Characterization of Dihydrolipoic Acid Capped Gold

Nanoparticles, and Functionalization by the Electroluminescent Luminol. *Langmuir* **2005,** 21, 2526-2536.

139. Pathak, S.; Choi, S.-K.; Arnheim, N.; Thompson, M. E., Hydroxylated Quantum Dots as Luminescent Probes for in Situ Hybridization. *J. Am. Chem. Soc.* **2001,** 123, 4103-4104.
140. Lundgren, A. O.; Björefors, F.; Olofsson, L. G. M.; Elwing, H., Self-Arrangement Among Charge-Stabilized Gold Nanoparticles on a Dithiothreitol Reactivated Octanedithiol Monolayer. *Nano Letters* **2008,** 8, 3989-3992.
141. Wilson, K. S.; Goff, J. D.; Riffle, J. S.; Harris, L. A.; St Pierre, T. G., Polydimethylsiloxane-magnetite nanoparticle complexes and dispersions in polysiloxane carrier fluids. *Polym. Adv. Technol.* **2005,** 16, 200-211.
142. Li, X.; Zhang, J.; Xu, W.; Jia, H.; Wang, X.; Yang, B.; Zhao, B.; Li, B.; Ozaki, Y., Mercaptoacetic Acid-Capped Silver Nanoparticles Colloid: Formation, Morphology, and SERS Activity. *Langmuir* **2003,** 19, 4285-4290.
143. Misra, T.; Liu, C.-Y., Surface-functionalization of spherical silver nanoparticles with macrocyclic polyammonium cations and their potential for sensing phosphates. *J. Nanopart. Res.* **2009,** 11, 1053-1063.
144. Misra, T. K.; Liu, C.-Y., Synthesis of 28-membered macrocyclic polyammonium cations functionalized gold nanoparticles and their potential for sensing nucleotides. *J. Coll. Interface Sci.* **2008,** 326, 411-419.
145. H. T. Yang; C. M. Shen; Y. G. Wang; Y. K . Su; T. Z. Yang; Gao., H. J., Stable cobalt nanoparticles passivated with oleic acid and triphenylphosphine *Nanotechnology* **2004,** 15, 70-74.
146. Green, M.; Rahman, P.; Smyth-Boyle, D., Ionic liquid passivated CdSe nanocrystals. *Chem. Commun.* **2007**, 6, 574-576.
147. Zhang, L.; He, R.; Gu, H.-C., Oleic acid coating on the monodisperse magnetite nanoparticles. *Appl. Surf. Sci.* **2006,** 253, 2611-2617.
148. Mohamed, M. B.; AbouZeid, K. M.; Abdelsayed, V.; Aljarash, A. A.; El-Shall, M. S., Growth Mechanism of Anisotropic Gold Nanocrystals via Microwave Synthesis: Formation of Dioleamide by Gold Nanocatalysis. *ACS Nano* **2010,** 4, 2766-2772.
149. Zou, S.; Hong, R.; Emrick, T.; Walker, G. C., Ordered CdSe Nanoparticles within Self-Assembled Block Copolymer Domains on Surfaces. *Langmuir* **2007,** 23, 1612-1614.
150. Hou, Y.; Yu, J.; Gao, S., Solvothermal reduction synthesis and characterization of superparamagnetic magnetite nanoparticles. *J. Mater. Chem.* **2003,** 13, 1983-1987.
151. Zhuravleva, N. G.; Sapoletova, N. A.; Eliseev, A. A.; Lukashin, A. V.; Tretyakov, Y. D.; Kynast, U., The synthesis of monodisperse trioctylphosphine oxide-capped EuF3 nanoparticles. *Opt. Mater.* **2006,** 28, 606-609.
152. Mejías, R.; Pérez-Yagüe, S.; Gutiérrez, L.; Cabrera, L. I.; Spada, R.; Acedo, P.; Serna, C. J.; Lázaro, F. J.; Villanueva, Á.; Morales, M. d. P.; Barber, D. F., Dimercaptosuccinic acid-coated magnetite nanoparticles for magnetically guided in vivo delivery of interferon gamma for cancer immunotherapy. *Biomaterials* **2011,** 32, 2938-2952.
153. Sevinc, E.; Ertas, F. S.; Ulusoy, G.; Ozen, C.; Acar, H. Y., Meso-2,3-dimercaptosuccinic acid: from heavy metal chelation to CdS quantum dots. *J. Mater. Chem.* **2012,** 22, 5137-5144.
154. Niidome, T.; Nakashima, K.; Takahashi, H.; Niidome, Y., Preparation of primary amine-modified gold nanoparticles and their transfection ability into cultivated cells. *Chem. Commun.* **2004**, 17, 1978-1979.
155. Yu, W. W.; Chang, E.; Drezek, R.; Colvin, V. L., Water-soluble quantum dots for biomedical applications. *Biochem. Biophys. Res. Commun.* **2006,** 348, 781-786.
156. Torimoto, T.; Tsumura, N.; Miyake, M.; Nishizawa, M.; Sakata, T.; Mori, H.; Yoneyama, H., Preparation and Photoelectrochemical Properties of Two-Dimensionally Organized CdS Nanoparticle Thin Films. *Langmuir* **1999,** 15, 1853-1858.

157. E. Guerrero; M. A. Muñoz-Márquez; M. A. García; P. Crespo; E. Fernández-Pinel; A. Hernando; Fernández., A., Surface plasmon resonance and magnetism of thiol-capped gold nanoparticles. *Nanotechnology* **2008,** 19, 175701.
158. Kulikova, V. S.; Shestakov, A. F., Functionalization of alkanes by gold nanoparticles stabilized by 1-dodecanethiol in organic media. *Russ. J. Phys. Chem. B* **2007,** 1, 507-511.
159. Kyrychenko, A.; Karpushina, G. V.; Bogatyrenko, S. I.; Kryshtal, A. P.; Doroshenko, A. O., Preparation, structure, and a coarse-grained molecular dynamics model for dodecanethiol-stabilized gold nanoparticles. *Comp. Theor. Chem.* **2011,** 977, 34-39.
160. Peterle, T.; Leifert, A.; Timper, J.; Sologubenko, A.; Simon, U.; Mayor, M., Multidentate thioether ligands coating gold nanoparticles. *Chem. Commun.* **2008**, 29, 3438-3440.
161. Petryayeva, E.; Krull, U. J., Quantum Dot and Gold Nanoparticle Immobilization for Biosensing Applications using Multidentate Imidazole Surface Ligands. *Langmuir* **2012,** 28, 13943-13951.
162. Thomas, L. A.; Dekker, L.; Kallumadil, M.; Southern, P.; Wilson, M.; Nair, S. P.; Pankhurst, Q. A.; Parkin, I. P., Carboxylic acid-stabilised iron oxide nanoparticles for use in magnetic hyperthermia. *J. Mater. Chem.* **2009,** 19, 6529-6535.
163. Ankireddy, K.; Vunnam, S.; Kellar, J.; Cross, W., Highly conductive short chain carboxylic acid encapsulated silver nanoparticle based inks for direct write technology applications. *J. Mater.Chem C* **2013,** 1, 572-579.
164. Hanaki, K.-i.; Momo, A.; Oku, T.; Komoto, A.; Maenosono, S.; Yamaguchi, Y.; Yamamoto, K., Semiconductor quantum dot/albumin complex is a long-life and highly photostable endosome marker. *Biochem. Biophys. Res. Commun.* **2003,** 302, 496-501.
165. Kaufman, E. D.; Belyea, J.; Johnson, M. C.; Nicholson, Z. M.; Ricks, J. L.; Shah, P. K.; Bayless, M.; Pettersson, T.; Feldotö, Z.; Blomberg, E.; Claesson, P.; Franzen, S., Probing Protein Adsorption onto Mercaptoundecanoic Acid Stabilized Gold Nanoparticles and Surfaces by Quartz Crystal Microbalance and ζ-Potential Measurements. *Langmuir* **2007,** 23, 6053-6062.
166. Poderys, V.; Matulionyte, M.; Selskis, A.; Rotomskis, R., Interaction of Water-Soluble CdTe Quantum Dots with Bovine Serum Albumin. *Nanoscale Res. Lett.* **2010,** 6, 1-6.
167. Rogach, A. L.; Kornowski, A.; Gao, M.; Eychmüller, A.; Weller, H., Synthesis and Characterization of a Size Series of Extremely Small Thiol-Stabilized CdSe Nanocrystals. *The J. Phys. Chem. B* **1999,** 103, 3065-3069.
168. Chen, C.-C.; Yet, C.-P.; Wang, H.-N.; Chao, C.-Y., Self-Assembly of Monolayers of Cadmium Selenide Nanocrystals with Dual Color Emission. *Langmuir* **1999,** 15, 6845-6850.
169. Chang, R.-L. J.; Yang, J., para-Mercaptobenzoic acid-modified silver nanoparticles as sensing media for the detection of ammonia in air based on infrared surface enhancement effect. *Analyst* **2011,** 136, 2988-2995.
170. Wang, Y. A.; Li, J. J.; Chen, H.; Peng, X., Stabilization of Inorganic Nanocrystals by Organic Dendrons. *J. Am. Chem. Soc.* **2002,** 124, 2293-2298.
171. Smith, A. M.; Nie, S., Minimizing the Hydrodynamic Size of Quantum Dots with Multifunctional Multidentate Polymer Ligands. *J. Am. Chem. Soc.* **2008,** 130, 11278-11279.
172. Potapova, I.; Mruk, R.; Hübner, C.; Zentel, R.; Basché, T.; Mews, A., CdSe/ZnS Nanocrystals with Dye-Functionalized Polymer Ligands Containing Many Anchor Groups. *Angew. Chem. Int. Ed.* **2005,** 44, 2437-2440.
173. Nikolic, M. S.; Krack, M.; Aleksandrovic, V.; Kornowski, A.; Förster, S.; Weller, H., Tailor-Made Ligands for Biocompatible Nanoparticles. *Angew. Chem. Int. Ed.* **2006,** 45, 6577-6580.
174. Wang, M.; Oh, J. K.; Dykstra, T. E.; Lou, X.; Scholes, G. D.; Winnik, M. A., Surface Modification of CdSe and CdSe/ZnS Semiconductor Nanocrystals with Poly(N,N-dimethylaminoethyl methacrylate). *Macromolecules* **2006,** 39, 3664-3672.

175. Lee, J.; Yang, B.; Li, R.; Seery, T. A. P.; Papadimitrakopoulos, F., Poly(allylamine)-Encapsulated Water-Soluble CdSe Nanocrystals. *J. Phys. Chem. B* **2006,** 111, 81-87.
176. Duan, H.; Nie, S., Cell-Penetrating Quantum Dots Based on Multivalent and Endosome-Disrupting Surface Coatings. *J. Am. Chem. Soc.* **2007,** 129, 3333-3338.
177. Shen, L.; Pich, A.; Fava, D.; Wang, M.; Kumar, S.; Wu, C.; Scholes, G. D.; Winnik, M. A., Loading quantum dots into thermo-responsive microgels by reversible transfer from organic solvents to water. *J. Mater. Chem.* **2008,** 18, 763-770.
178. Generalova, A. N.; Oleinikov, V. A.; Sukhanova, A.; Artemyev, M. V.; Zubov, V. P.; Nabiev, I., Quantum dot-containing polymer particles with thermosensitive fluorescence. *Biosensors and Bioelectronics* **2013,** 39, 187-193.
179. Esteves, A. C. C.; Bombalski, L.; Trindade, T.; Matyjaszewski, K.; Barros-Timmons, A., Polymer Grafting from CdS Quantum Dots via AGET ATRP in Miniemulsion. *Small* **2007,** 3, 1230-1236.
180. Skaff, H.; Emrick, T., Reversible Addition Fragmentation Chain Transfer (RAFT) Polymerization from Unprotected Cadmium Selenide Nanoparticles. *Angew. Chem. Int. Ed.* **2004,** 43, 5383-5386.
181. Sill, K.; Emrick, T., Nitroxide-Mediated Radical Polymerization from CdSe Nanoparticles. *Chem. Mater.* **2004,** 16, 1240-1243.
182. Glogowski, E.; Tangirala, R.; Russell, T. P.; Emrick, T., Functionalization of nanoparticles for dispersion in polymers and assembly in fluids. *J. Polym. Sci. A Polym. Chem.* **2006,** 44, 5076-5086.
183. Skaff, H.; Sill, K.; Emrick, T., Quantum Dots Tailored with Poly(para-phenylene vinylene). *J. Am. Chem. Soc.* **2004,** 126, 11322-11325.
184. Skaff, H.; Ilker, M. F.; Coughlin, E. B.; Emrick, T., Preparation of Cadmium Selenide−Polyolefin Composites from Functional Phosphine Oxides and Ruthenium-Based Metathesis. *J. Am. Chem. Soc.* **2002,** 124, 5729-5733.
185. Carrot, G.; Rutot-Houzé, D.; Pottier, A.; Degée, P.; Hilborn, J.; Dubois, P., Surface-Initiated Ring-Opening Polymerization: A Versatile Method for Nanoparticle Ordering. *Macromolecules* **2002,** 35, 8400-8404.
186. Binder, W. H.; Lomoschitz, M.; Friedbacher, G.; Sachsenhofer, R., Reversible and Irreversible Binding of Nanoparticles to Polymeric Surfaces. *J. Nanomat.* **2009,** ID 613813, doi:10.1155/2009/613813.
187. Guo, W.; Li, J. J.; Wang, Y. A.; Peng, X., Conjugation Chemistry and Bioapplications of Semiconductor Box Nanocrystals Prepared via Dendrimer Bridging. *Chem. Mater.* **2003,** 15, 3125-3133.
188. Lokteva, I.; Radychev, N.; Witt, F.; Borchert, H.; Parisi, J. r.; Kolny-Olesiak, J., Surface Treatment of CdSe Nanoparticles for Application in Hybrid Solar Cells: The Effect of Multiple Ligand Exchange with Pyridine. *J. Phys. Chem. C* **2010,** 114, 12784-12791.
189. Binder, W. H.; Sachsenhofer, R.; Straif, C. J.; Zirbs, R., Surface-modified nanoparticles via thermal and Cu(i)-mediated "click" chemistry: Generation of luminescent CdSe nanoparticles with polar ligands guiding supramolecular recognition. *J. Mater. Chem.* **2007,** 17, 2125-2132.
190. Essa, S.; Rabanel, J. M.; Hildgen, P., Characterization of rhodamine loaded PEG-g-PLA nanoparticles (NPs): Effect of poly(ethylene glycol) grafting density. *Int. J. Pharm.* **2011,** 411, 178-187.
191. Farmer, S. C.; Patten, T. E., Photoluminescent Polymer/Quantum Dot Composite Nanoparticles. *Chem. Mater.* **2001,** 13, 3920-3926.
192. Chiefari, J.; Chong, Y. K.; Ercole, F.; Krstina, J.; Jeffery, J.; Le, T. P. T.; Mayadunne, R. T. A.; Meijs, G. F.; Moad, C. L.; Moad, G.; Rizzardo, E.; Thang, S. H., Living Free-Radical Polymerization by Reversible Addition−Fragmentation Chain Transfe The RAFT Process. *Macromolecules* **1998,** 31, 5559-5562.

193. Skaff, H.; Ilker, M. F.; Coughlin, E. B.; Emrick, T., Preparation of Cadmium Selenide−Polyolefin Composites from Functional Phosphine Oxides and Ruthenium-Based Metathesis. *J. Am. Chem. Soc.* **2002,** 124, 5729-5733.
194. Binder, W. H.; Zirbs, R.; Machl, D.; Gahleitner, M., Grafting Polyisobutylene from Nanoparticle Surfaces: Concentration and Surface Effects on Livingness. *Macromolecules* **2009,** 42, 7379-7387.
195. Zhou, L.; Gao, C.; Xu, W., Amphibious polymer-functionalized CdTe quantum dots: Synthesis, thermo-responsive self-assembly, and photoluminescent properties. *J. Mater. Chem.* **2009,** 19, 5655-5664.
196. Dubertret, B.; Skourides, P.; Norris, D. J.; Noireaux, V.; Brivanlou, A. H.; Libchaber, A., In Vivo Imaging of Quantum Dots Encapsulated in Phospholipid Micelles. *Science* **2002,** 298, 1759-1762.
197. Fan, H.; Leve, E. W.; Scullin, C.; Gabaldon, J.; Tallant, D.; Bunge, S.; Boyle, T.; Wilson, M. C.; Brinker, C. J., Surfactant-Assisted Synthesis of Water-Soluble and Biocompatible Semiconductor Quantum Dot Micelles. *Nano Lett.* **2005,** 5, 645-648.
198. Lala, N.; Lalbegi, S. P.; Adyanthaya, S. D.; Sastry, M., Phase Transfer of Aqueous Gold Colloidal Particles Capped with Inclusion Complexes of Cyclodextrin and Alkanethiol Molecules into Chloroform. *Langmuir* **2001,** 17, 3766-3768.
199. Wang, Y.; Wong, J. F.; Teng, X.; Lin, X. Z.; Yang, H., "Pulling" Nanoparticles into Water: Phase Transfer of Oleic Acid Stabilized Monodisperse Nanoparticles into Aqueous Solutions of α-Cyclodextrin. *Nano Lett.* **2003,** 3, 1555-1559.
200. Tinguely, J.; Charron, G.; Lau-Truong, S.; Hohenau, A.; Grand, J.; Félidj, N.; Aubard, J.; Krenn, J. R., Template-assisted deposition of CTAB-functionalized gold nanoparticles with nanoscale resolution. *J. Coll. Interface Sci.* **3013,** 394, 237-242.
201. Yu, W. W.; Chang, E.; Falkner, J. C.; Zhang, J.; Al-Somali, A. M.; Sayes, C. M.; Johns, J.; Drezek, R.; Colvin, V. L., Forming Biocompatible and Nonaggregated Nanocrystals in Water Using Amphiphilic Polymers. *J. Am. Chem. Soc.* **2007,** 129, (10), 2871-2879.
202. Schabas, G.; Yusuf, H.; Moffitt, M. G.; Sinton, D., Controlled Self-Assembly of Quantum Dots and Block Copolymers in a Microfluidic Device. *Langmuir* **2008,** 24, 637-643.
203. Smith, A. M.; Duan, H.; Rhyner, M. N.; Ruan, G.; Nie, S., A systematic examination of surface coatings on the optical and chemical properties of semiconductor quantum dots. *Phys. Chem. Chem. Phys.* **2006,** 8, 3895-3903.
204. Wang, M.; Felorzabihi, N.; Guerin, G.; Haley, J. C.; Scholes, G. D.; Winnik, M. A., Water-Soluble CdSe Quantum Dots Passivated by a Multidentate Diblock Copolymer. *Macromolecules* **2007,** 40, 6377-6384.
205. Anderson, R. E.; Chan, W. C. W., Systematic Investigation of Preparing Biocompatible, Single, and Small ZnS-Capped CdSe Quantum Dots with Amphiphilic Polymers. *ACS Nano* **2008,** 2, 1341-1352.
206. Luccardini, C.; Tribet, C.; Vial, F.; Marchi-Artzner, V.; Dahan, M., Size, Charge, and Interactions with Giant Lipid Vesicles of Quantum Dots Coated with an Amphiphilic Macromolecule. *Langmuir* **2006,** 22, 2304-2310.
207. Potapova, I.; Mruk, R.; Prehl, S.; Zentel, R.; Basché, T.; Mews, A., Semiconductor Nanocrystals with Multifunctional Polymer Ligands. *J. Am. Chem. Soc.* **2002,** 125, 320-321.
208. Sanchez, S.; Gunther, G.; Tricerri, M.; Gratton, E., Methyl-β-Cyclodextrins Preferentially Remove Cholesterol from the Liquid Disordered Phase in Giant Unilamellar Vesicles. *J. Membrane Biol.* **2011,** 241, 1-10.
209. Ordentlich dynamisch: Supramolekulare Polymere. *Nachrichten aus der Chemie* **2010,** 58, 734-739.

210. Binder, W.; Zirbs, R., Supramolecular Polymers and Networkswith Hydrogen Bonds in the Main- and Side-Chain. In *Hydrogen Bonded Polymers*, Binder, W., Ed. Springer Berlin Heidelberg: **2007**, 207, 1-78.
211. Erdödi, G.; Iván, B., Novel Amphiphilic Conetworks Composed of Telechelic Poly(ethylene oxide) and Three-Arm Star Polyisobutylene. *Chem. Mater.* **2004,** 16, 959-962.
212. Domján, A.; Erdödi, G.; Wilhelm, M.; Neidhöfer, M.; Landfester, K.; Iván, B.; Spiess, H. W., Structural Studies of Nanophase-Separated Poly(2-hydroxyethyl methacrylate)-l-polyisobutylene Amphiphilic Conetworks by Solid-State NMR and Small-Angle X-ray Scattering. *Macromolecules* **2003,** 36, 9107-9114.
213. Süvegh, K.; Domján, A.; Vankó, G.; Iván, B.; Vértes, A., Free Volume and Swelling Dynamics of the Poly[(2-dimethylamino)ethyl methacrylate]-l-polyisobutylene Amphiphilic Network by Positron Annihilation Investigations. *Macromolecules* **1998,** 31, 7770-7775.
214. Gragert, M.; Schunack, M.; Binder, W. H., Azide/Alkyne-"Click"-Reactions of Encapsulated Reagents: Toward Self-Healing Materials. *Macromol. Rapid. Commun.* **2011,** 32, 419-425.
215. Binder, W. H.; Petraru, L.; Roth, T.; Groh, P. W.; Pálfi, V.; Keki, S.; Ivan, B., Magnetic and Temperature-Sensitive Release Gels from Supramolecular Polymers. *Adv. Funct. Mater.* **2007,** 17, 1317-1326.
216. Herbst, F.; Schröter, K.; Gunkel, I.; Gröger, S.; Thurn-Albrecht, T.; Balbach, J.; Binder, W. H., Aggregation and Chain Dynamics in Supramolecular Polymers by Dynamic Rheology: Cluster Formation and Self-Aggregation. *Macromolecules* **2010,** 43, 10006-10016.
217. Binder, W. H.; Kunz, M. J.; Kluger, C.; Hayn, G.; Saf, R., Synthesis and Analysis of Telechelic Polyisobutylenes for Hydrogen-Bonded Supramolecular Pseudo-Block Copolymers. *Macromolecules* **2004,** 37, 1749-1759.
218. Hackethal, K.; Döhler, D.; Tanner, S.; Binder, W. H., Introducing Polar Monomers into Polyisobutylene by Living Cationic Polymerization: Structural and Kinetic Effects. *Macromolecules* **2010,** 43, 1761-1770.
219. Kim, I. J.; Faust, R., Synthesis and Characterization of Novel Silicon-Functional Polyisobutylenes and Their Applications: Polyisobutylene Brushes on Silicate Substrates via Living Cationic Polymerization. *J. Macromol. Sci. A* **2003,** 40, 991-1008.
220. Kwon, Y.; Faust, R., Synthesis of Polyisobutylene-Based Block Copolymers with Precisely Controlled Architecture by Living Cationic Polymerization. *Adv. Polym. Sci.* **2004,** 167, 107-135.
221. Breland, L. K.; Storey, R. F., Polyisobutylene-based miktoarm star polymers via a combination of carbocationic and atom transfer radical polymerizations. *Polym. J.* **2008,** 49, 1154-1163.
222. Breland, L. K.; Murphy, J. C.; Storey, R. F., Poly(tert-butyl acrylate-b-isobutylene-b-styrene) terpolymer from a carbocationic initiator containing a latent radical initiating site. *Polym. J.* **2006,** 47, 1852-1860.
223. Puskas, J. E.; Chen, Y.; Tomkins, M., Investigation of the effect of epoxide structure on the initiation efficiency in isobutylene polymerizations initiated by epoxide/TiCl4 systems. *Eur. Polym. J.* **2003,** 39, 2147-2153.
224. Puskas, J. E.; Brister, L. B.; Michel, A. J.; Lanzendörfer, M. G.; Jamieson, D.; Pattern, W. G., Novel substituted epoxide initiators for the carbocationic polymerization of isobutylene. *J. Polym. Sci. A Polym. Chem.* **2000,** 38, 444-452.
225. Lange, A.; Rath, H.-P.; Lang, G., Telechelic Polyisobutenes with Asymmetrical Reactivity. *Macromol. Symp.* **2004,** 215, 209-214.
226. Binder, W. H.; Zirbs, R., "Click" Chemistry in Macromolecular Synthesis. In *Encyclopedia of Polymer Science and Technology*, John Wiley & Sons, Inc.: 2002.
227. Binder, W. H., "Click"-Chemistry in Polymer and Material Science: the Update. *Macromol. Rapid. Commun.* **2008,** 29, 951-981.

228. Binder, W. H.; Sachsenhofer, R., 'Click' Chemistry in Polymer and Materials Science. *Macromol. Rapid. Commun.* **2007,** 28, 15-54.
229. Binder, W. H.; Kluger, C., Azide/Alkyne-"Click" Reactions: Applications in Material Science and Organic Synthesis *curr.Org. Chem.* **2006,** 10, 1791.
230. Morgan, D. L.; Storey, R. F., End-Quenching of Quasi-Living Isobutylene Polymerizations with Alkoxybenzene Compounds. *Macromolecules* **2009,** 42, 6844-6847.
231. Bothun, G. D., Hydrophobic silver nanoparticles trapped in lipid bilayers: Size distribution, bilayer phase behavior, and optical properties. *J. Nanobiotechnol.* **2008,** 6, 13-23.
232. Zhang, L.; Hong, L.; Yu, Y.; Bae, S. C.; Granick, S., Nanoparticle-Assisted Surface Immobilization of Phospholipid Liposomes. *J. Am. Chem. Soc.* **2006,** 128, 9026-9027.
233. Li, N.; Binder, W. H., Click-chemistry for nanoparticle-modification. *J. Mater. Chem.* **2011,** 21, 16717-16734.
234. Barenholz, Y., Liposome application: problems and prospects. *Curr. Opin. Colloid Interface Sci.* **2001,** 6, 66-77.
235. Binder, W. H.; Barragan, V.; Menger, F. M., Domains and Rafts in Lipid Membranes. *Angew. Chem. Int. Ed.* **2003,** 42, 5802-5827.
236. Discher, D. E.; Ahmed, F., Polymersomes. *Annu. Rev. Biomed. Eng.* **2006,** 8, 323-341.
237. Egli, S.; Nussbaumer, M. G.; Balasubramanian, V.; Chami, M.; Bruns, N.; Palivan, C.; Meier, W., Biocompatible Functionalization of Polymersome Surfaces: A New Approach to Surface Immobilization and Cell Targeting Using Polymersomes. *J. Am. Chem. Soc.* **2011,** 133, 4476-4483.
238. Jeng, U. S.; Hsu, C. H.; Lin, T. L.; Wu, C. M.; Chen, H. L.; Tai, L. A.; Hwang, K. C., Dispersion of fullerenes in phospholipid bilayers and the subsequent phase changes in the host bilayers. *Physica B (Amsterdam, Neth.)* **2005,** 357, 193-198.
239. Chen, Y.; Bothun, G. D., Lipid-Assisted Formation and Dispersion of Aqueous and Bilayer-Embedded Nano-C60. *Langmuir* **2009,** 25, 4875-4879.
240. Park, S.-H.; Oh, S.-G.; Mun, J.-Y.; Han, S.-S., Loading of gold nanoparticles inside the DPPC bilayers of liposome and their effects on membrane fluidities. *Colloids Surf., B* **2006,** 48, 112-118.
241. Park, S.-H.; Oh, S.-G.; Mun, J.-Y.; Han, S.-S., Effects of silver nanoparticles on the fluidity of bilayer in phospholipid liposome. *Colloids Surf. B* **2005,** 44, 117-122.
242. Bothun, G. D., Hydrophobic silver nanoparticles trapped in lipid bilayers: Size distribution, bilayer phase behavior, and optical properties. *J. Nanobiotechnol.* **2008,** 6, 13-23.
243. El Rassy, H.; Belamie, E.; Livage, J.; Coradin, T., Onion Phases as Biomimetic Confined Media for Silica Nanoparticle Growth. *Langmuir* **2005,** 21, 8584-8587.
244. Al-Jamal, W. T.; Al-Jamal, K. T.; Bomans, P. H.; Frederik, P. M.; Kostarelos, K., Functionalized-Quantum-Dot-Liposome Hybrids as Multimodal Nanoparticles for Cancer. *Small* **2008,** 4, 1406-1415.
245. Al-Jamal, W. T.; Al-Jamal, K. T.; Tian, B.; Lacerda, L.; Bomans, P. H.; Frederik, P. M.; Kostarelos, K., Lipid-Quantum Dot Bilayer Vesicles Enhance Tumor Cell Uptake and Retention in Vitro and in Vivo. *ACS Nano* **2008,** 2, 408-418.
246. Bothun, G. D.; Rabideau, A. E.; Stoner, M. A., Hepatoma Cell Uptake of Cationic Multifluorescent Quantum Dot Liposomes. *J. Phys. Chem. B* **2009,** 113, 7725-7728.
247. Jing, B.; Zhu, Y. E., Disruption of Supported Lipid Bilayers by Semi-Hydrophobic Nanoparticles. *J. Am. Chem. Soc.* **2011,** 133, 10983-10989.
248. Breidenich, M.; Netz, R. R.; Lipowsky, R., The influence of non-anchored polymers on the curvature of vesicles. *Mol. Phys.* **2005,** 103, 3169-3183.
249. Noguchi, H.; Takasu, M., Adhesion of Nanoparticles to Vesicles: A Brownian Dynamics Simulation. *Biophys. J.* **2002,** 83, 299-308.

250. Sanchez-Gaytan, B. L.; Cui, W.; Kim, Y.; Mendez-Polanco, M. A.; Duncan, T. V.; Fryd, M.; Wayland, B. B.; Park, S., Interfacial Assembly of Nanoparticles in Discrete Block-Copolymer Aggregates. *Angew. Chem. Int. Ed.* **2007,** 119, 9395-9398.
251. Lecommandoux, S.; Sandre, O.; Chécot, F.; Perzynski, R., Smart hybrid magnetic self-assembled micelles and hollow capsules. *Prog. Solid State Chem.* **2006,** 34, 171-179.
252. Schulz, M.; Glatte, D.; Meister, A.; Scholtysek, P.; Kerth, A.; Blume, A.; Bacia, K.; Binder, W. H., Hybrid lipid/polymer giant unilamellar vesicles: effects of incorporated biocompatible PIB-PEO block copolymers on vesicle properties. *Soft Matter* **2011,** 7, 8100-8110.
253. Binder, W. H., Polymer-Induced Transient Pores in Lipid Membranes. *Angew. Chem. Int. Ed.* **2008,** 47, 3092-3095.
254. Meier, W.; Ruysschaert, T.; Sonnen, A. F. P.; Haefele, T.; Winterhalter, M.; Fournier, D., Hybrid Nanocapsules: Interactions of ABA Block Copolymers with Liposomes. *J. Am. Chem. Soc.* **2005,** 127, 6242-6247.
255. Meier, W.; Kita-Tokarczyk, K.; Itel, F.; Grzelakowski, M.; Egli, S.; Rossbach, P., Monolayer Interactions between Lipids and Amphiphilic Block Copolymers. *Langmuir* **2009,** 25, 9847-9856.
256. Nam, J.; Beales, P. A.; Vanderlick, T. K., Giant Phospholipid/Block Copolymer Hybrid Vesicles: Mixing Behavior and Domain Formation. *Langmuir* **2011,** 27, 1-6.
257. Chemin, M.; Brun, P.-M.; Lecommandoux, S.; Sandre, O.; Le Meins, J.-F., Hybrid polymer/lipid vesicles: fine control of the lipid and polymer distribution in the binary membrane. *Soft Matter* **2012,** 8, 2867-2874.
258. Binder, W. H.; Lomoschitz, M.; Friedbacher, G.; Sachsenhofer, R., Reversible and Irreversible Binding of Nanoparticles to Polymeric Surfaces. *J. Nanomater.* **2009,** ID 613813, doi:10.1155/2009/613813.
259. Alivisatos, A. P., Semiconductor Clusters, Nanocrystals, and Quantum Dots. *Science* **1996,** 271, 933-937.
260. Yu, W. W.; Qu, L.; Guo, W.; Peng, X., Experimental Determination of the Extinction Coefficient of CdTe, CdSe, and CdS Nanocrystals. *Chem. Mater.* **2003,** 15, 2854-2860.
261. Sachleben, J. R.; Wooten, E. W.; Emsley, L.; Pines, A.; Colvin, V. L.; Alivisatos, A. P., NMR studies of the surface structure and dynamics of semiconductor nanocrystals. *Chem. Phys. Lett.* **1992,** 198, 431-436.
262. Li, H. H.; Yabuuchi, N.; Meng, Y. S.; Kumar, S.; Breger, J.; Grey, C. P.; Shao-Horn, Y., Changes in the Cation Ordering of Layered O3 $Li_xNi_{0.5}Mn_{0.5}O_2$ during Electrochemical Cycling to High Voltages: An Electron Diffraction Study. *Chem. Mater.* **2007,** 19, 2551-2565.
263. Ji, X.; Copenhaver, D.; Sichmeller, C.; Peng, X., Ligand Bonding and Dynamics on Colloidal Nanocrystals at Room Temperature: The Case of Alkylamines on CdSe Nanocrystals. *J. Am. Chem. Soc.* **2008,** 130, 5726-5735.
264. Cotton, F. A.; Barnes, R. D.; Bannister, E., The effect of complex-formation by phosphine oxides on their P-O stretching frequencies. *J. Chem. Soc. (Resumed)* **1960**, 2199-2203.
265. Sunday, D.; Curras-Medina, S.; Green, D. L., Impact of Initiator Spacer Length on Grafting Polystyrene from Silica Nanoparticles. *Macromol.* **2010,** 43, 4871-4878.
266. Ma, G.; Allen, H. C., DPPC Langmuir Monolayer at the Air−Water Interface: Probing the Tail and Head Groups by Vibrational Sum Frequency Generation Spectroscopy. *Langmuir* **2006,** 22, 5341-5349.
267. El Kirat, K.; Besson, F.; Prigent, A.-F.; Chauvet, J.-P.; Roux, B., Role of Calcium and Membrane Organization on Phospholipase D Localization and Activity. *J. Biol. Chem.* **2002,** 277, 21231-21236.
268. Xia, T.; Li, N.; Nel, A. E., Potential Health Impact of Nanoparticles. *Annu. Rev. Public Health* **2009,** 30, 137-150.

269. Angelova, M. I.; Dimitrov, D. S., Liposome electroformation. *Faraday Discuss. Chem. Soc.* **1986,** 81, 303-311.
270. Nam, J.; Vanderlick, T. K.; Beales, P. A., Formation and dissolution of phospholipid domains with varying textures in hybrid lipo-polymersomes. *Soft Matter* **2012,** 8, 3982-3988.
271. Jiang, H.; Smith, B. D., Dynamic molecular recognition on the surface of vesicle membranes. *Chem. Commun.* **2006,** 0, 1407-1409.
272. Leblanc, R. M., Molecular recognition at Langmuir monolayers. *Curr. Opin. Chem. Biol.* **2006,** 10, 529-536.
273. Oshovsky, G. V.; Reinhoudt, D. N.; Verboom, W., Supramolecular Chemistry in Water. *Angew. Chem. Int. Edit.* **2007,** 46, 2366-2393.
274. Voskuhl, J.; Ravoo, B. J., Molecular recognition of bilayer vesicles. *Chemical Society Reviews* **2009,** 38, 495-505.
275. Uzun, O.; Sanyal, A.; Jeong, Y.; Rotello, V. M., Molecular Recognition Induced Self-Assembly of Diblock Copolymers: Microspheres to Vesicles. *Macromolecular Bioscience* **2010,** 10, 481-487.
276. Binder, W. H.; Enders, C.; Herbst, F.; Hackethal, K., *Synthesis and Self-Assembly of Hydrogen-Bonded Supramolecular Polymers*. John Wiley & Sons (Asia) Pte Ltd: **2011**, 53-95.
277. Binder, W. H., *Hydrogen Bonded Polymers*. **2007**, 207, 1-78.
278. Binder, W. H.; Sachsenhofer, R., 'Click' Chemistry in Polymer and Materials Science. *Macromol. Rapid Commun.* **2007,** 28, 15-54.
279. Fan, E.; Van Arman, S. A.; Kincaid, S.; Hamilton, A. D., Molecular recognition: hydrogen-bonding receptors that function in highly competitive solvents. *J. Am. Chem. Soc.* **1993,** 115, 369-370.
280. Kurihara, K.; Ohto, K.; Honda, Y.; Kunitake, T., Efficient, complementary binding of nucleic acid bases to diaminotriazine-functionalized monolayers on water. *J. Am. Chem. Soc.* **1991,** 113, 5077-5079.
281. Sasaki, D. Y.; Kurihara, K.; Kunitake, T., Specific, multiple-point binding of ATP and AMP to a guanidinium-functionalized monolayer. *J. Am. Chem. Soc.* **1991,** 113, 9685-9686.
282. Ariga, K.; Nakanishi, T.; Hill, J. P., A paradigm shift in the field of molecular recognition at the air-water interface: from static to dynamic. *Soft Matter* **2006,** 2, 465-477.
283. Ariga, K.; Ito, H.; Hill, J. P.; Tsukube, H., Molecular recognition: from solution science to nano/materials technology. *Chem. Soc. Rev.* **2012,** 41, 5800-5835.
284. Ariga, K.; Kunitake, T., Molecular Recognition at Air–Water and Related Interfaces: Complementary Hydrogen Bonding and Multisite Interaction. *Acc. Chem. Res.* **1998,** 31, 371-378.
285. Kawahara, T.; Kurihara, K.; Kunitake, T., Cooperative Binding of Adenine via Complementary Hydrogen Bonding to an Imide Functionalized Monolayer at the Air-Water Interface. *Chem. Lett.* **1992,** 21, 1839-1842.
286. Hasegawa, T.; Hatada, Y.; Nishijo, J.; Umemura, J.; Huo, Q.; Leblanc, R. M., Hydrogen Bonding Network Formed between Accumulated Langmuir–Blodgett Films of Barbituric Acid and Triaminotriazine Derivatives. *J. Phys. Chem. B* **1999,** 103, 7505-7513.
287. Kong, X.; Du, X., In Situ IRRAS Studies of Molecular Recognition of Barbituric Acid Lipids to Melamine at the Air–Water Interface. *J. Phys. Chem. B* **2011,** 115, 13191-13198.
288. Xin, Y.; Kong, X.; Zhang, X.; Lv, Z.; Du, X., Self-Assembly and Molecular Recognition of Adenine- and Thymine-Functionalized Nucleolipids in the Mixed Monolayers and Thymine-Functionalized Nucleolipids on Aqueous Melamine at the Air–Water Interface. *Langmuir* **2012,** 28, 11153-11163.
289. Oishi, Y.; Torii, Y.; Kato, T.; Kuramori, M.; Suehiro, K.; Ariga, K.; Taguchi, K.; Kamino, A.; Koyano, H.; Kunitake, T., Molecular Patterning of a Guanidinium/Orotate Mixed Monolayer

through Molecular Recognition with Flavin Adenine Dinucleotide. *Langmuir* **1997,** 13, 519-524.

290. Onda, M.; Yoshihara, K.; Koyano, H.; Ariga, K.; Kunitake, T., Molecular Recognition of Nucleotides by the Guanidinium Unit at the Surface of Aqueous Micelles and Bilayers. A Comparison of Microscopic and Macroscopic Interfaces. *J. Am. Chem. Soc.* **1996,** 118, 8524-8530.
291. Duan, P.; Qin, L.; Liu, M., Langmuir−Blodgett Films and Chiroptical Switch of an Azobenzen - Containing Dendron Regulated by the in Situ Host−Guest Reaction at the Air/Wa Interface. *Langmuir* **2010,** 27, 1326-1331.
292. Sanchez, S.; Gunther, G.; Tricerri, M.; Gratton, E., Methyl-β-Cyclodextrins Preferentially Remove Cholesterol from the Liquid Disordered Phase in Giant Unilamellar Vesicles. *J Membrane Biol.* **2011,** 241, 1-10.
293. Taneva, S.; Ariga, K.; Okahata, Y.; Tagaki, W., Association between amphiphilic cyclodextrins and cholesterol in mixed insoluble monolayers at the air-water interface. *Langmuir* **1989,** 5, 111-113.
294. Ohvo, H.; Slotte, J. P., Cyclodextrin-Mediated Removal of Sterols from Monolayers: Effects of Sterol Structure and Phospholipids on Desorption Rat *Biochemistry* **1996,** 35, 8018-8024.
295. Beseničar, M. P.; Bavdek, A.; Kladnik, A.; Maček, P.; Anderluh, G., Kinetics of cholesterol extraction from lipid membranes by methyl-β-cyclodextrin—A surface plasmon resonance approach. *BBA-Biomembranes* **2008,** 1778, 175-184.
296. Veatch, S. L.; Polozov, I. V.; Gawrisch, K.; Keller, S. L., Liquid Domains in Vesicles Investigated by NMR and Fluorescence Microscopy. *Biophys. J.* **2004,** 86, 2910-2922.
297. Mascetti, J.; Castano, S.; Cavagnat, D.; Desbat, B., Organization of β-Cyclodextrin under Pure Cholesterol, DMPC, or DMPG and Mixed Cholesterol/Phospholipid Monolayers. *Langmuir* **2008,** 24, 9616-9622.
298. Veatch, S. L.; Keller, S. L., Separation of Liquid Phases in Giant Vesicles of Ternary Mixtures of Phospholipids and Cholesterol. *Biophys. J.* **2003,** 85, 3074-3083.
299. Ariga, K.; Kamino, A.; Koyano, H.; Kunitake, T., Recognition of aqueous flavin mononucleotide on the surface of binary monolayers of guanidinium and melamine amphiphiles. *J. Mater. Chem.* **1997,** 7, 1155-1161.
300. Taguchi, K.; Ariga, K.; Kunitake, T., Multi-site Recognition of Flavin Adenine Dinucleotide by Mixed Monolayers on Water. *Chem. Lett.* **1995,** 24, 701-702.
301. Sasaki, D. Y.; Kurihara, K.; Kunitake, T., Self-assembled multifunctional receptors for nucleotides at the air-water interface. *J. Am. Chem. Soc.* **1992,** 114, 10994-10995.
302. Cha, X.; Ariga, K.; Kunitake, T., Molecular Recognition of Aqueous Dipeptides at Multiple Hydrogen-Bonding Sites of Mixed Peptide Monolayers. *J. Am. Chem. Soc.* **1996,** 118, 9545-9551.
303. Ariga, K.; Kamino, A.; Cha, X.; Kunitake, T., Multisite Recognition of Aqueous Dipeptides by Oligoglycine Arrays Mixed with Guanidinium and Other Receptor Units at the Air−Water Interface. *Langmuir* **1999,** 15, 3875-3885.
304. Berndt, P.; Kurihara, K.; Kunitake, T., Adsorption of poly(styrenesulfonate) onto an ammonium monolayer on mica: a surface forces study. *Langmuir* **1992,** 8, 2486-2490.
305. Swairjo, M. A.; Seaton, B. A.; Roberts, M. F., Effect of vesicle composition and curvature on the dissociation of phosphatidic acid in small unilamellar vesicles - a ^{31}P-NMR study. *BBA-Biomembranes* **1994,** 1191, 354-361.
306. Smart, J. L.; McCammon, J. A., Surface Titration: A Continuum Electrostatics Model. *J. Am. Chem. Soc.* **1996,** 118, 2283-2284.

307. Sakurai, M.; Tamagawa, H.; Inoue, Y.; Ariga, K.; Kunitake, T., Theoretical Study of Intermolecular Interaction at the Lipid−Water Interface. 1. Quantum Chemical Analysis Using a Reaction Field Theory. *J. Phys. Chem. B* **1997,** 101, 4810-4816.
308. Tamagawa, H.; Sakurai, M.; Inoue, Y.; Ariga, K.; Kunitake, T., Theoretical Study of Intermolecular Interaction at the Lipid−Water Interface. 2. Analysis Based on the Poisson−Boltzmann Equation. *J. Phys. Chem. B* **1997,** 101, 4817-4825.
309. Ma, M.; Bong, D., Directed Peptide Assembly at the Lipid−Water Interface Cooperatively Enhances Membrane Binding and Activity. *Langmuir* **2010,** 27, 1480-1486.
310. Binder, W. H., Polymer-Induced Transient Pores in Lipid Membranes. *Angew. Chem . Int. Ed.* **2008,** 47, 3092-3095.
311. Schulz, M.; Glatte, D.; Meister, A.; Scholtysek, P.; Kerth, A.; Blume, A.; Bacia, K.; Binder, W. H., Hybrid lipid/polymer giant unilamellar vesicles: effects of incorporated biocompatible PIB-PEO block copolymers on vesicle properties. *Soft Matter* **2011,** 7, 8100-8110.
312. Lecommandoux, S.; Sandre, O.; Chécot, F.; Perzynski, R., Smart hybrid magnetic self-assembled micelles and hollow capsules. *Prog. Solid State Chem.* **2006,** 34, 171-179.
313. Schulz, M.; Werner, S.; Bacia, K.; Binder, W. H., Controlling Molecular Recognition with Lipid/Polymer Domains in Vesicle Membranes. *Angew. Chem. Int. Ed.* **2013,** 52, 1829-1833.
314. Schulz, M.; Olubummo, A.; Binder, W. H., Beyond the Lipid-Bilayer: Interaction of Polymers and Nanoparticles with Membranes. *Soft Matter* **2012,** 8, 4849–4864.
315. Olubummo, A.; Schulz, M.; Lechner, B.-D.; Scholtysek, P.; Bacia, K.; Blume, A.; Kressler, J.; Binder, W. H., Controlling the Localization of Polymer-Functionalized Nanoparticles in Mixed Lipid/Polymer Membranes. *ACS Nano* **2012,** 6, 8713–8727.
316. Sachsenhofer, R.; Binder, W. H.; Farnik, D.; Zirbs, R., Polymersome-Embedded Nanoparticles. *Macromol. Symp.* **2007,** 254, 375-377.
317. Binder, W. H.; Sachsenhofer, R.; Farnik, D.; Blaas, D., Guiding the location of nanoparticles into vesicular structures: a morphological study. *Phys. Chem. Chem. Phys.* **2007,** 9, 6435-6441.
318. Binder, W. H.; Kerschner, H.; Georgopoulos, A.; Barragan-Montero, V.; Einzmann, M., Chemistry with liposomes: controlling membrane-structure by macromolecules. *Joint Meeting on Medicinal Chemistry, Proceedings, Vienna, Austria, June 20-23* **2005,** 2005, 113.
319. Binder, W. H., Supramolecular Assembly of Nanoparticles at Liquid-Liquid Interfaces. *Angew. Chem. Int. Ed.* **2005,** 44, 5172-5175.
320. Binder, W. H.; Einzmann, M.; Knapp, M.; Köhler, G., Domain Formation in Lipid Bilayer Membranes: Control of Membrane Nanostructure by Molecular Architecture. *Monatsh. Chem./Chemical Monthly* **2004,** 135, 1, 13-21.
321. Binder, W. H.; Barragan, V.; Menger, F. M., Domains and Rafts in Lipid Membranes. *Angew. Chem. Int. Ed.* **2003,** 42, 5802-5827.
322. Schulz, M.; Werner, S.; Bacia, K.; Binder, W. H., Controlling Molecular Recognition with Lipid/Polymer Domains in Vesicle Membranes. *Angew. Chem. Int. Edit.* **2013,** 52, 1829-1833.
323. Attwood, S.; Choi, Y.; Leonenko, Z., Preparation of DOPC and DPPC Supported Planar Lipid Bilayers for Atomic Force Microscopy and Atomic Force Spectroscopy. *Int. J. Mol. Sci.* **2013,** 14, 3514-3539.
324. Breslow, R.; Zhang, B., Cholesterol Recognition and Binding by Cyclodextrin Dimers. *J. Am. Chem. Soc.* **1996,** 118, 8495-8496.
325. Walde, P.; Cosentino, K.; Engel, H.; Stano, P., Giant Vesicles: Preparations and Applications. *Chem. Bio. Chem* **2010,** 11, 848-865.
326. Sackmann, E., Membrane bending energy concept of vesicle- and cell-shapes and shape-transitions. *FEBS Letters* **1994,** 346, 3-16.

327. Baumgart, T.; Hess, S. T.; Webb, W. W., Imaging coexisting fluid domains in biomembrane models coupling curvature and line tension. *Nature* **2003,** 425, 6960, 821-824.
328. Camps, F.; Coll, J.; Messeguer, A.; Pujol, F., m-Chloroperoxybenzoic acid-potassium fluoride system: study of its stability and reaction with alpha-methylstyrene. *J. Org. Chem.* **1982,** 47, 5402-5404.
329. Song, J.; Bódis, J.; Puskas, J. E., Direct functionalization of polyisobutylene by living initiation with α-methylstyrene epoxide. *J. Polym. Sci. A Polym. Chem.* **2002,** 40, 1005-1015.
330. Gruškienė, R.; Čiuta, G.; Makuška, R., Grafting of poly(ethylene glycol) to chitosan at c(6) position of glucosamine units via "click chemistry" reactions. *chemija.* **2009,** 20, 241-249.
331. Liu, X.-M.; Thakur, A.; Wang, D., Efficient Synthesis of Linear Multifunctional Poly(ethylene glycol) by Copper(I)-Catalyzed Huisgen 1,3-Dipolar Cycloaddition. *Biomacromolecules* **2007,** 8, 2653-2658.
332. Wu, J.; Gao, C., Click Chemistry Approach to Rhodamine B-Capped Polyrotaxanes and their Unique Fluorescence Properties. *Macromol. Chem. Physic.* **2009,** 210, 1697-1708.

10.0 Appendix

10.1 Appendix 1

10.1.1 Synthesis of nonsymmetric chain end functionalized poly(isobutylene)

This supplementary was published in the Journal of Polymer Science Part A: Polymer Chemistry Volume 49, Issue 13, pages 2931–2940, 1 July 201. DOI: 10.1002/pola.24729

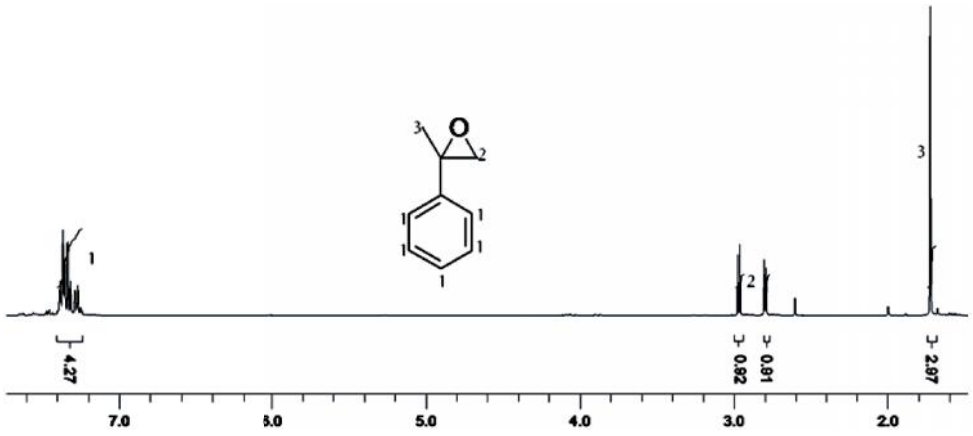

Figure S1. ^{1}H NMR spectrum of methyl styrene epoxide initiator (**4**).

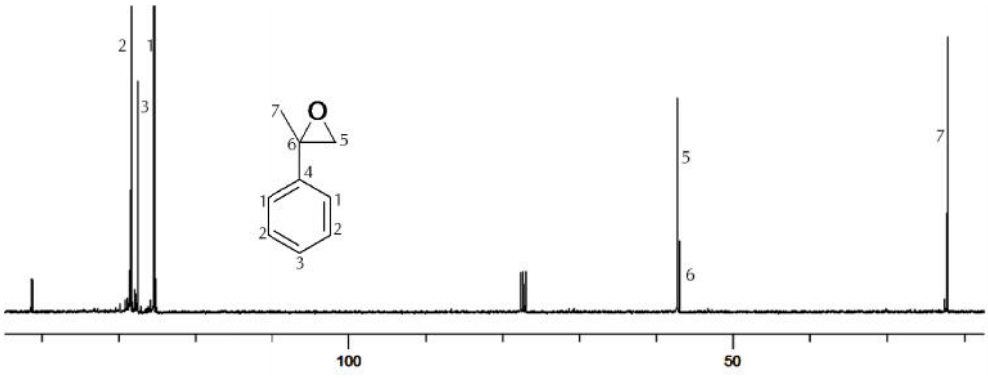

Figure S2. ^{13}C NMR spectrum of methyl styrene epoxide initiator (**4**).

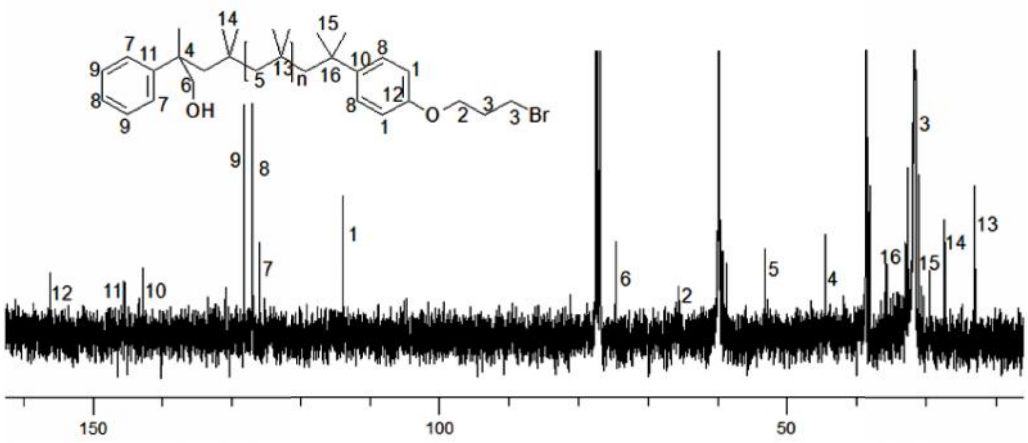

Figure S3. ^{13}C NMR spectrum of α-hydroxymethyl-ω-bromo telechelic PIB (**5**).

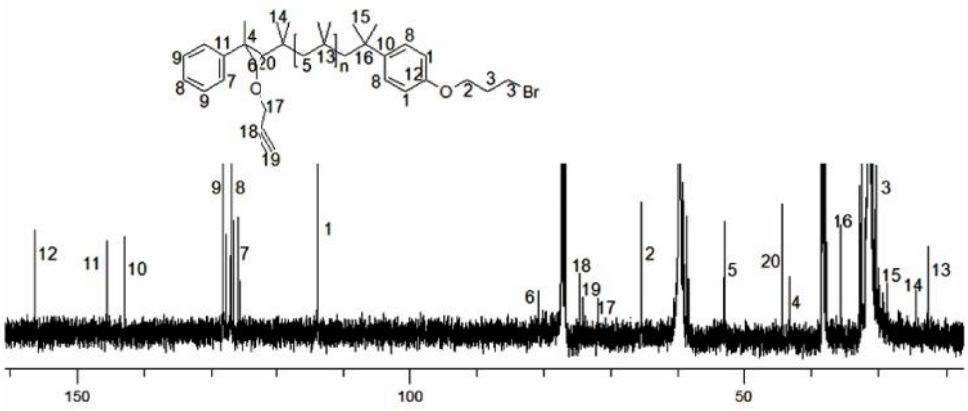

Figure S4. ^{13}C NMR spectrum of α-alkinyl-ω-bromo telechelic PIB (**6**).

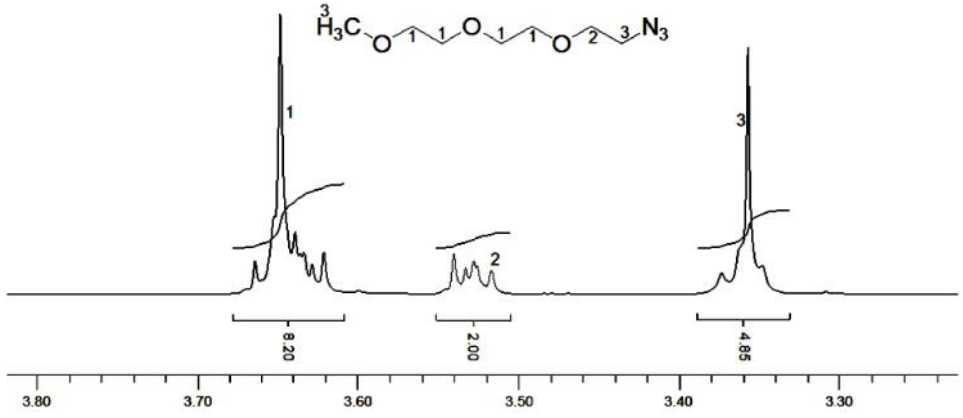

Figure S5. ^{1}H NMR spectrum of α- methoxy -ω- azido telechelic triethylene oxide (**9a**).

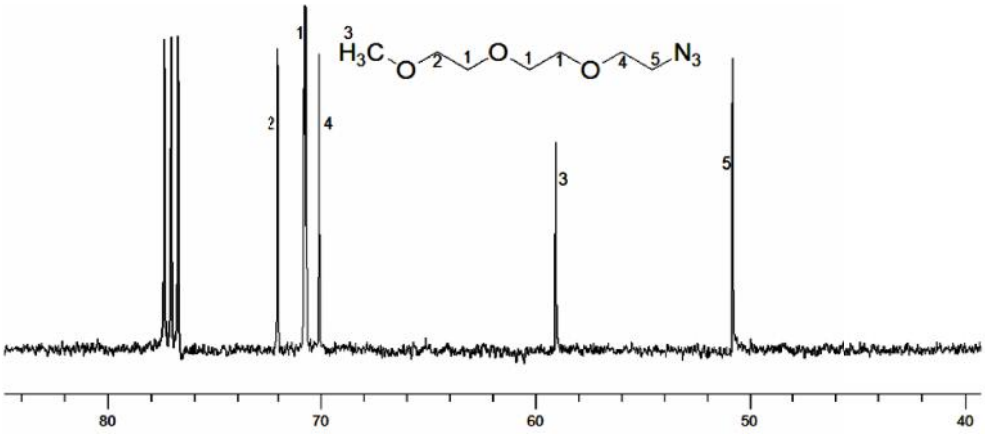

Figure S6. ^{13}C NMR spectrum of α- methoxy-ω-azido telechelic triethylene oxide (**9a**).

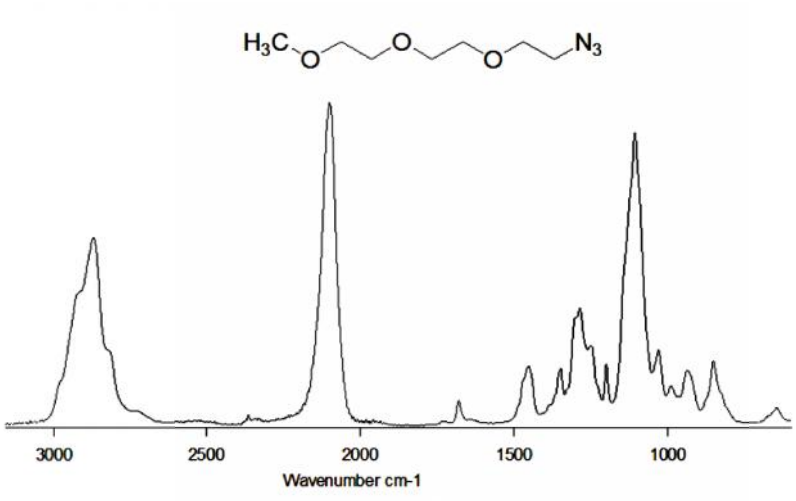

Figure S7. IR spectrum of monoazido-telechelic triethylene oxide (**9a**).

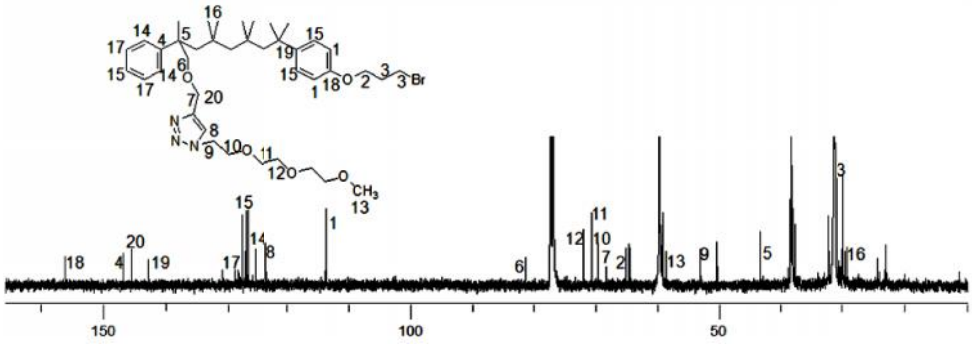

Figure S8. ^{13}C NMR spectrum of α-TEO-ω-bromo telechelic PIB (**14**).

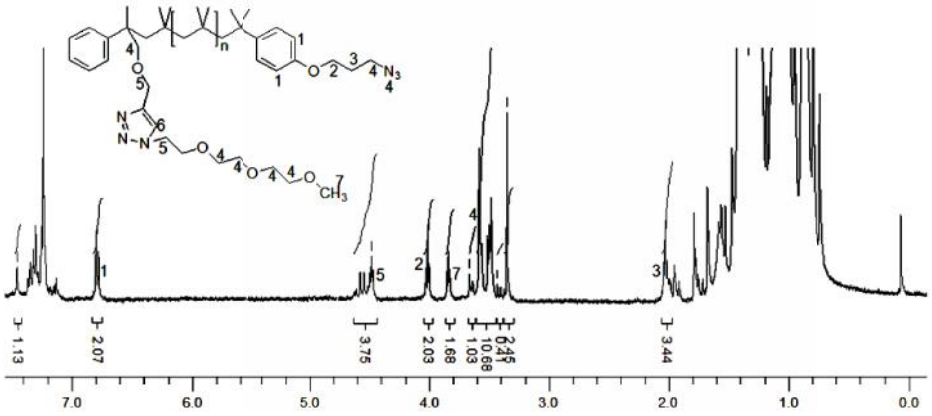

Figure S9. ^{1}H NMR spectrum of α-TEO-ω-azido telechelic PIB (**15**).

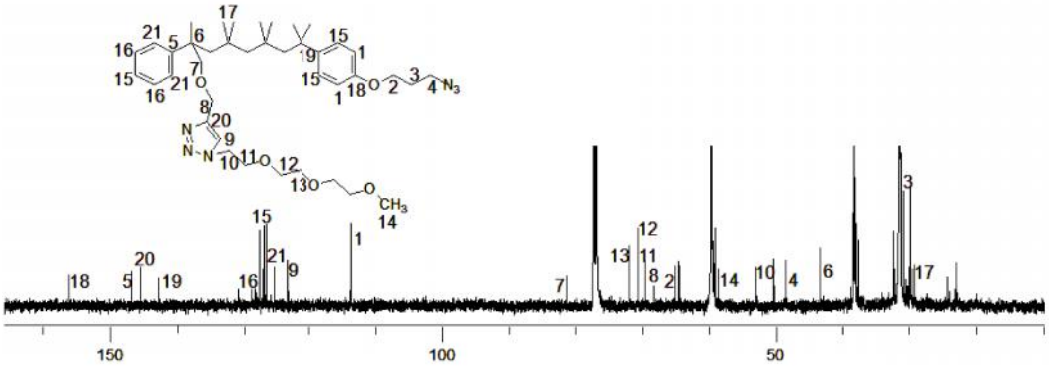

Figure S10. ^{13}C NMR spectrum of α-TEO-ω-azido telechelic PIB (**15**).

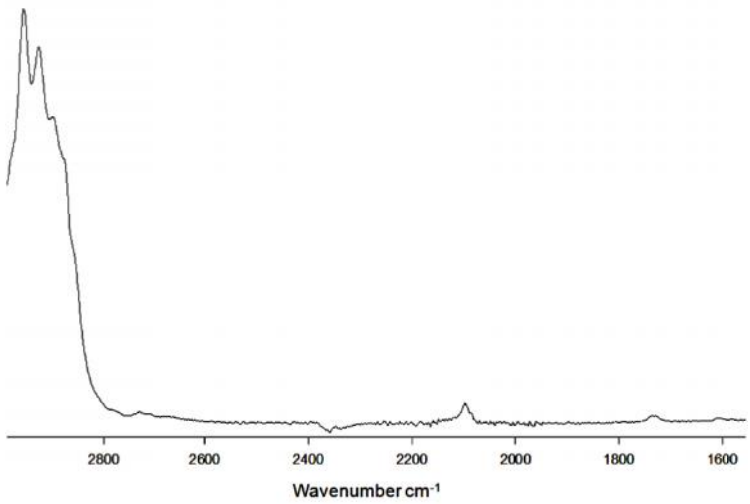

Figure S11. IR spectrum of α-TEO-ω-azido telechelic PIB (**16**).

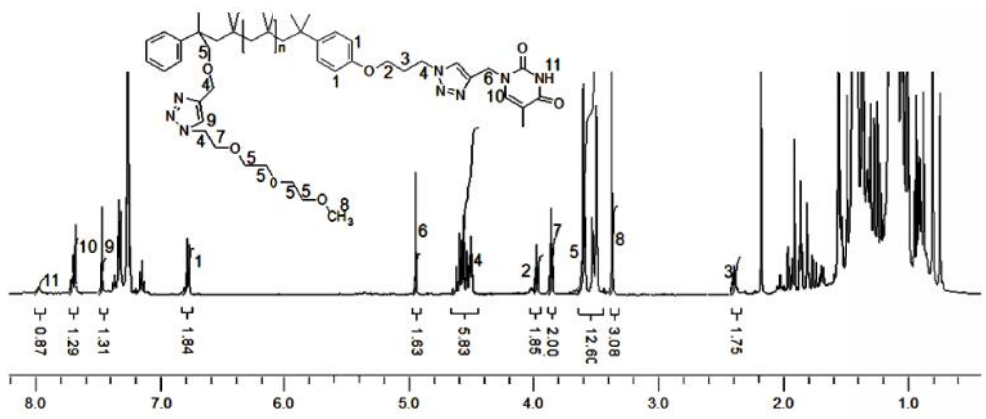

Figure S12. ^{1}H NMR spectrum of α-TEO-ω-thymine telechelic PIB (**18**).

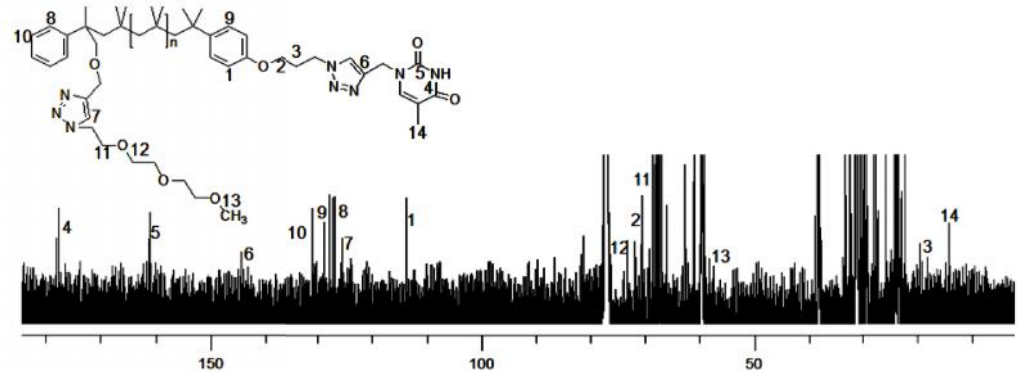

Figure S13. ^{13}C NMR spectrum of α-TEO-ω-thymine telechelic PIB (**18**).

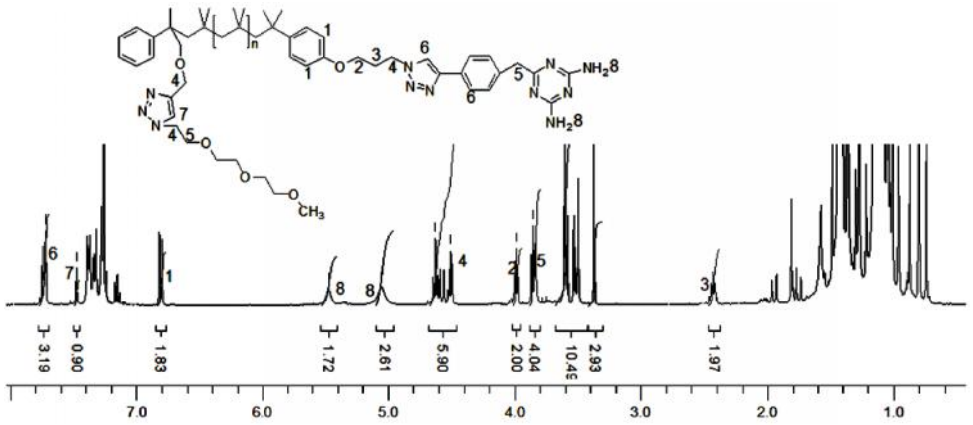

Figure S14. ^{1}H NMR spectrum of α-TEO-ω-thymine telechelic PIB (**19**).

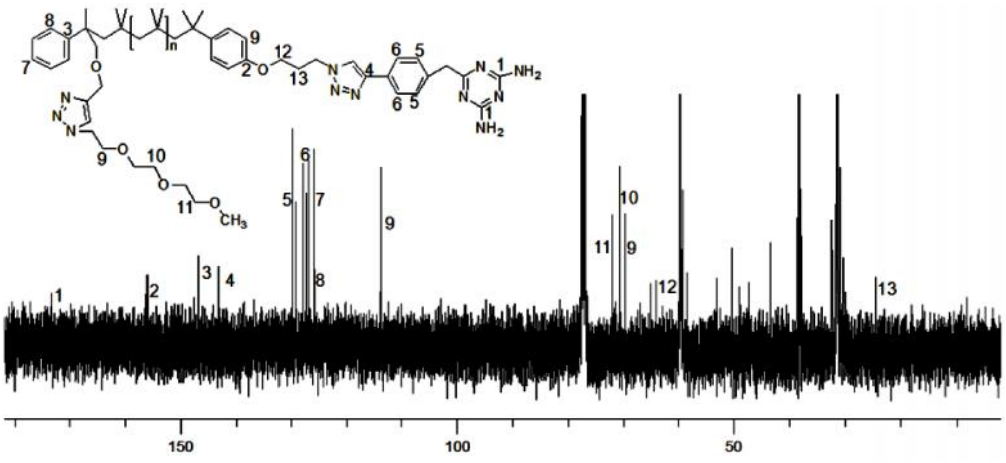

Figure S15. ^{13}C NMR spectrum of α-TEO-ω-2,6-diaminotriazine telechelic PIB (**19**).

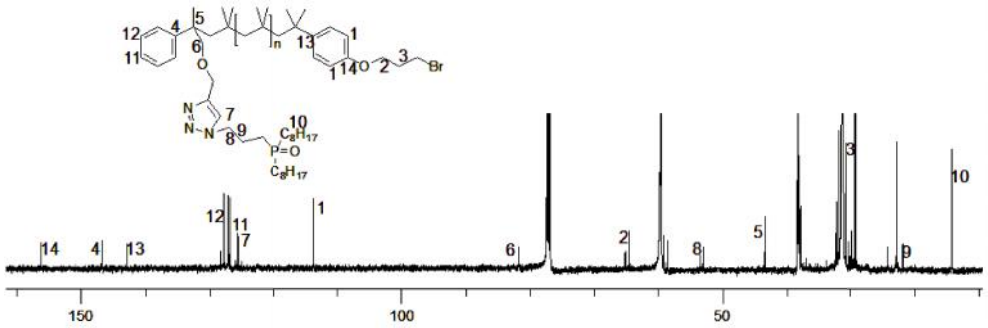

Figure S16. ^{13}C NMR spectrum of α-phosphineoxide-ω-bromo-telechelic (**27**).

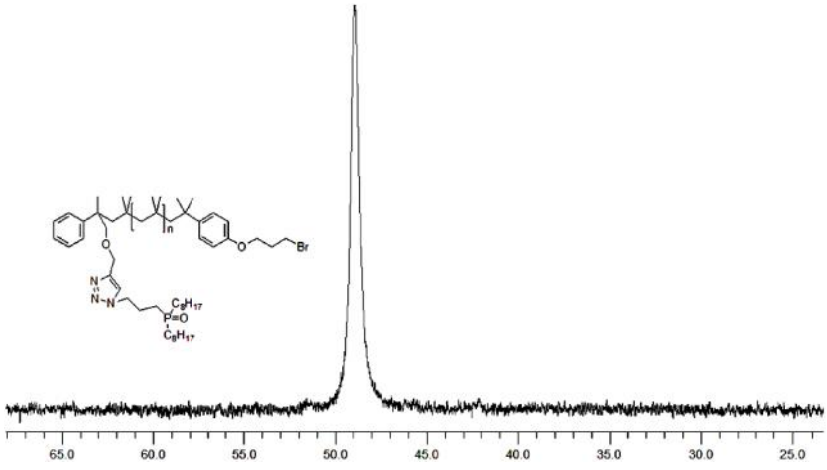

Figure S17. ^{31}P NMR spectrum of α-phosphineoxide-ω-bromo-telechelic (**27**).

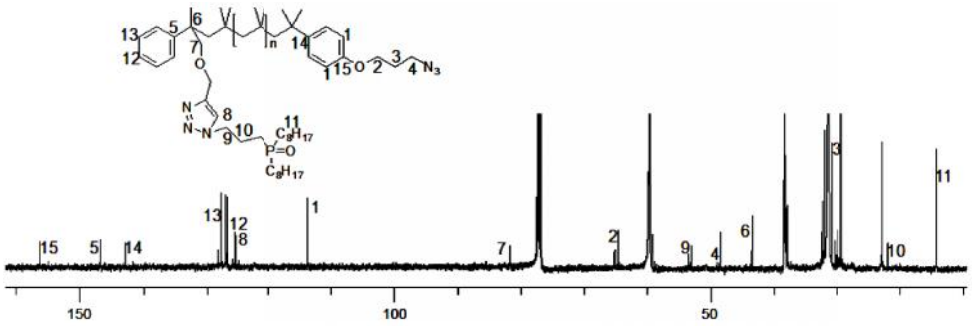

Figure S18. ^{13}C NMR spectrum of α-phosphineoxide-ω-azido-telechelic (**28**).

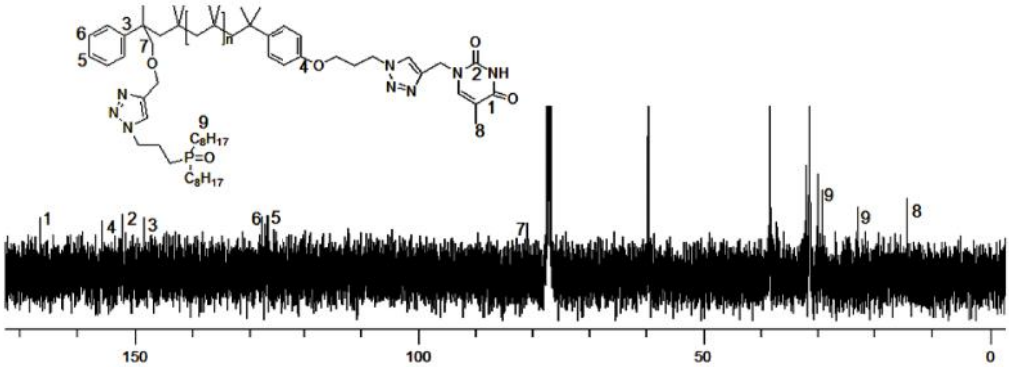

Figure S19. ^{13}C NMR Spectrum of α-phosphineoxide-ω-thymine-telechelic PIB (**30**).

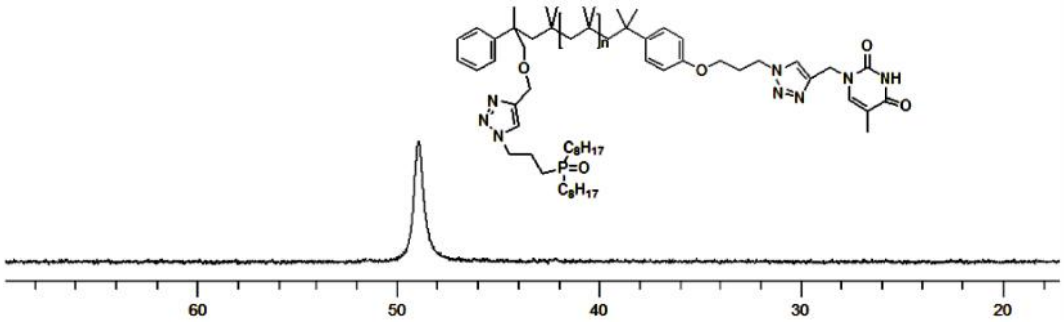

Figure S20. ^{31}P NMR Spectrum of α-phosphineoxide-ω-thymine-telechelic PIB (**30**).

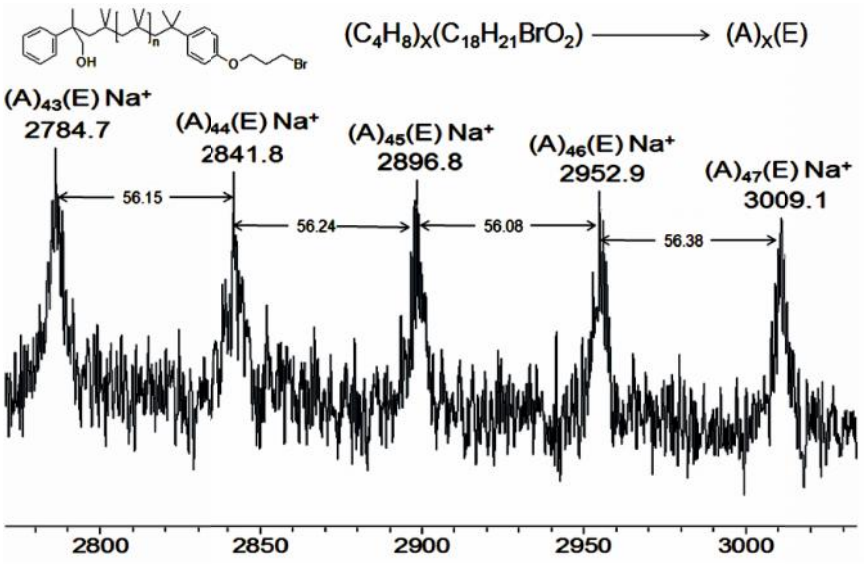

Figure S21. MALDI-TOF-MS of α-hydroxymethyl-ω-bromo-telechelic PIB (**5**).

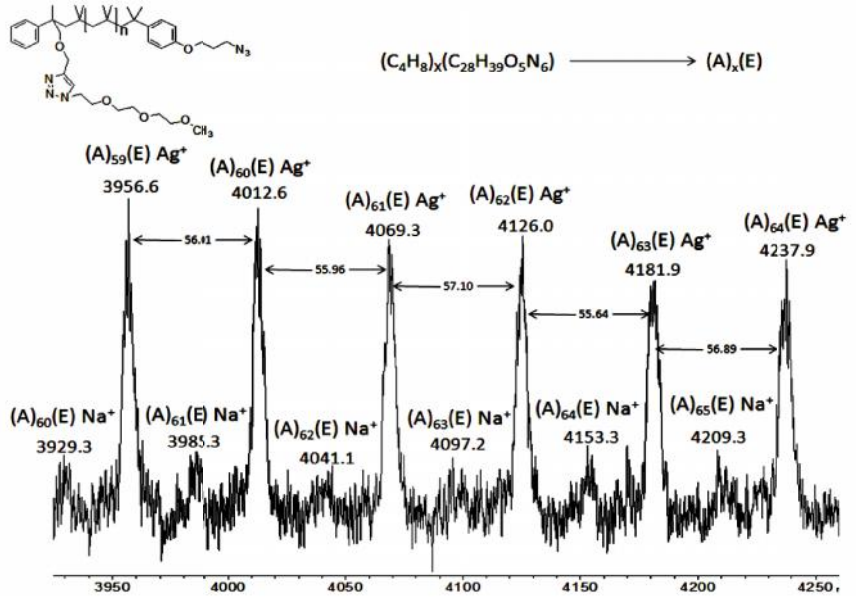

Figure S22. MALDI-TOF-MS of α-TEO-ω-azido-telechelic PIB (**15**).

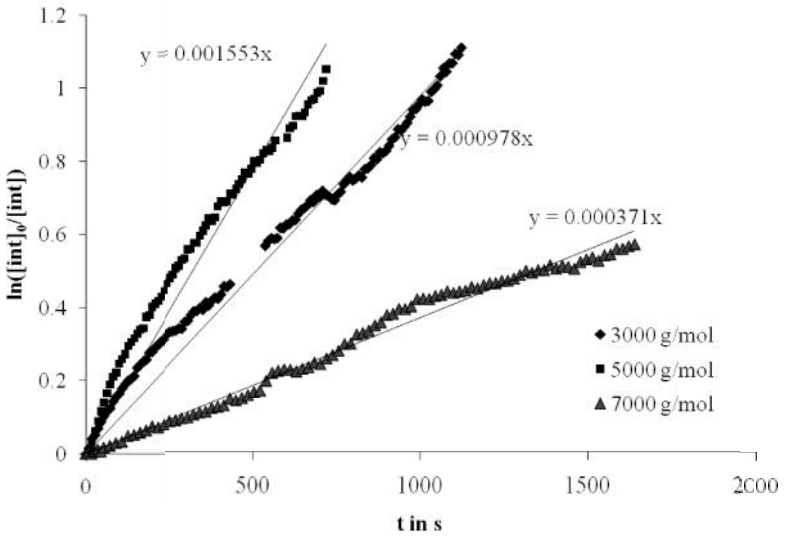

Figure S23. Kinetic measurement of polymerization using MSE as initiator for 3000, 5000 and 7000 g/mol.

Table S1. Kinetic measurements of polymerization using MSE as initiator for 3000, 5000 and 7000 g/mol.

entry	$M_{n(theor)}$	M_n [a] [g/mol]	M_w/M_n	k_{app} (10^{-4} s^{-1})	k_p [b] (10^7 s^{-1} M^{-1})
1	3 000	4 000	1.3	9.83	3.21
2	5 000	5900	1.4	15.84	28.4
3	7 000	7 300	1.3	3.71	19.1

[a]Mn determined by GPC measurement in THF as solvent, calibration with PIB standards ($g \cdot mol^{-1}$).

[b]Determination by eq 2 (k_{-i} =7.5 _ 107 1/s, k_i=15 1/(s M2)[1] a combination of eqs 1 and 2 ($K_{eq}=k_i/k_{-i}$) with respect to the dimeric form of the LA($[LA]_0$[2]).

10.2 Appendix 2

10.2.1 Controlling the localization of polymer-functionalized nanoparticles in mixed lipid/polymer membranes

This supplementary was published in the ACS Nano, 2012, Volume 6, Issue 10, Pages 8713–8727. DOI: 10.1021/nn3023602

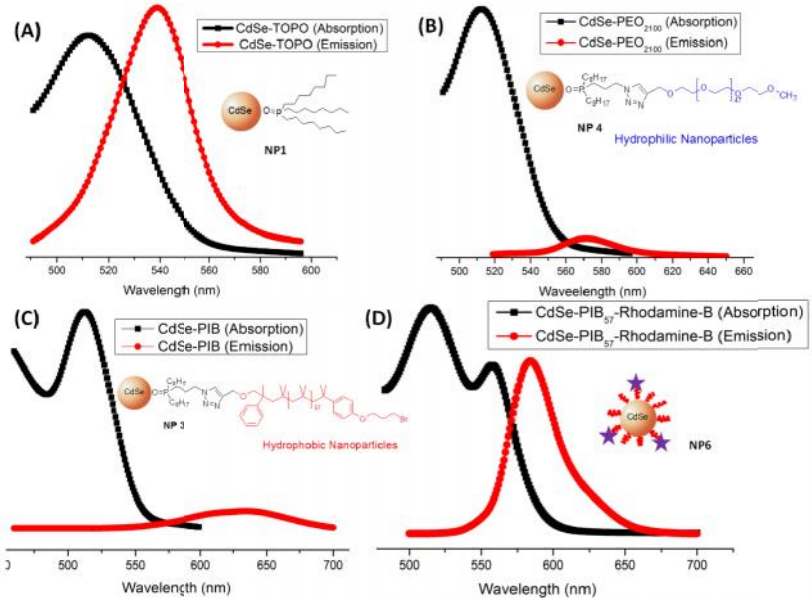

Figure S24. Absorption and emission spectra of (A) TOPO covered (**NP1**) (B) PEO covered (**NP4**) (C) PIB covered (**NP3**) and (D) Rhodamine-B labeled PIB (**NP6**) CdSe nanoparticles.

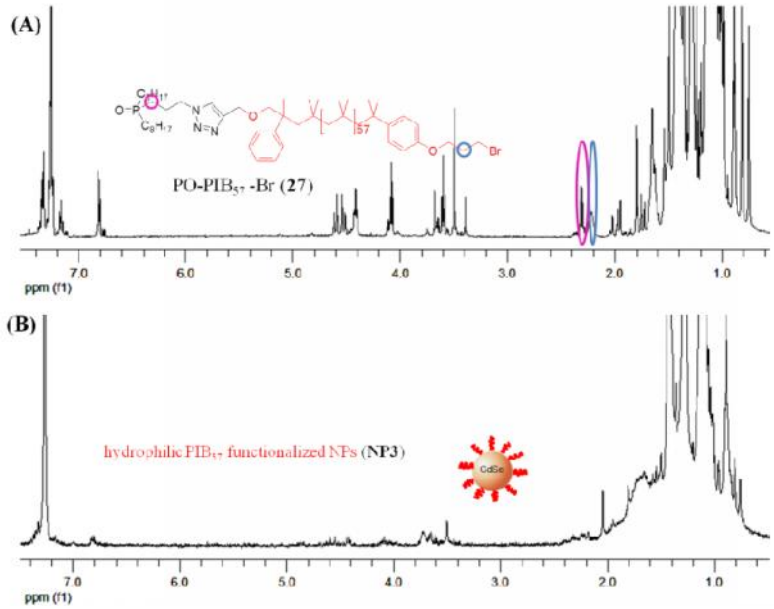

Figure S25. ^{1}H-NMR spectra of (A) α-phosphineoxide-γ-bromo telechelic polyisobutylene (**1**) PO-PIB_{57}-Br and (B) Hydrophobic PIB_{57} covered CdSe NPs (**NP3**).

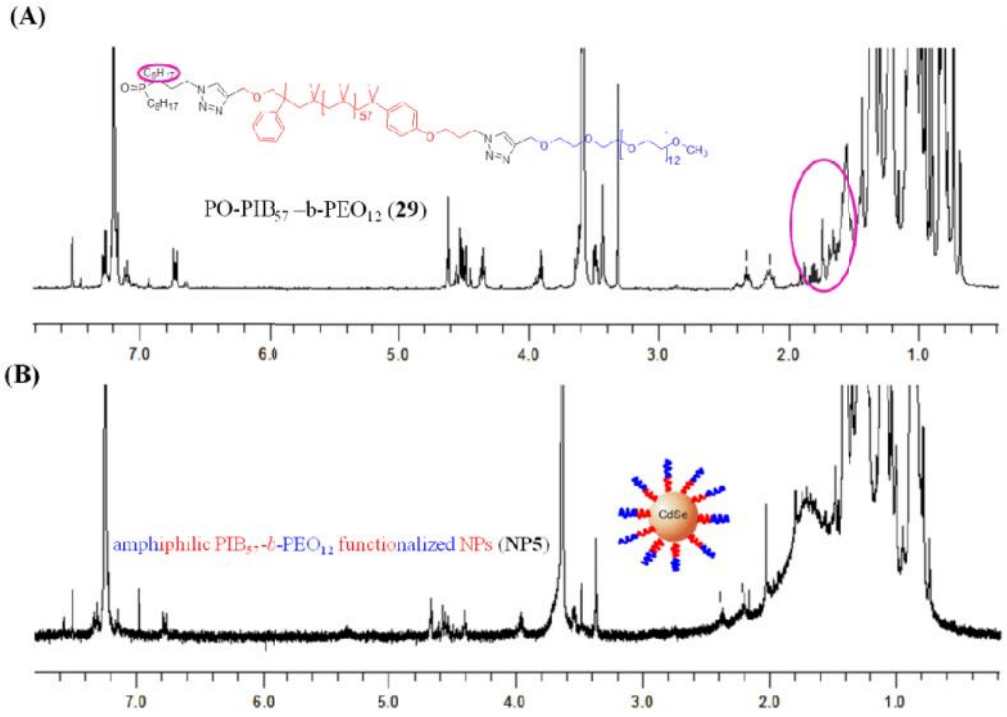

Figure S26. ^{1}H NMR spectra of (A) α-phosphineoxide-γ-polyethylene oxide telechelic PIB PO-PIB$_{57}$-*b*-PEO$_{12}$ (**29**) and (B) amphiphilic PIB$_{57}$-*b*-PEO$_{12}$ covered CdSe NPs (**NP5**).

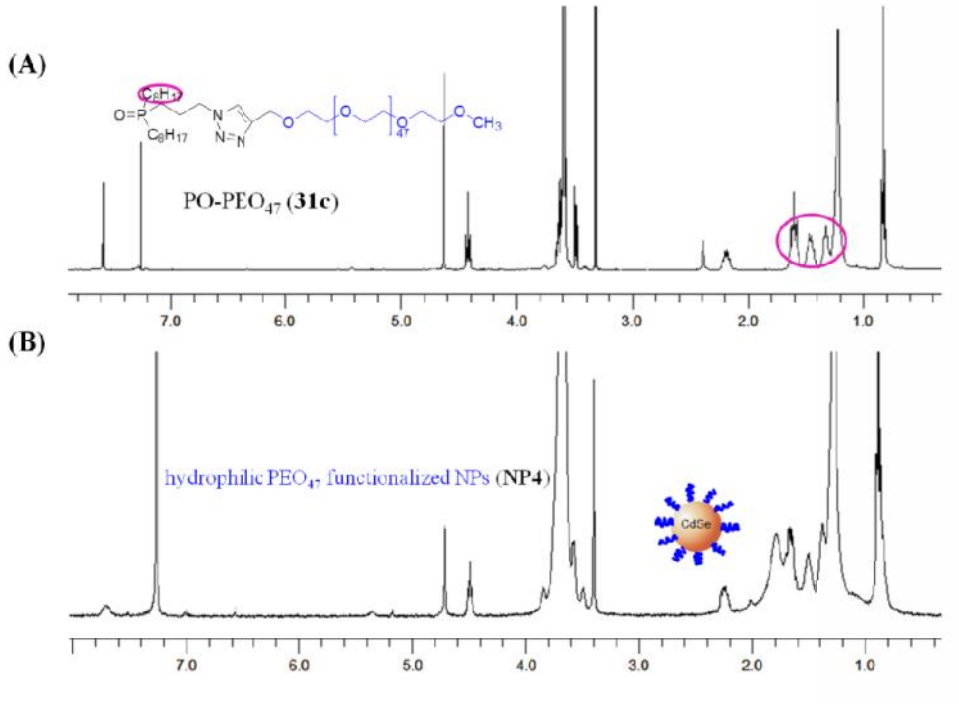

Figure S27. ^{1}H NMR of (A) α-phosphineoxide-γ-methylene telechelic PEO (PO-PEO$_{47}$) (**31c**) and (B) amphiphilic PIB$_{57}$-*b*-PEO$_{12}$ covered CdSe NPs (**NP4**).

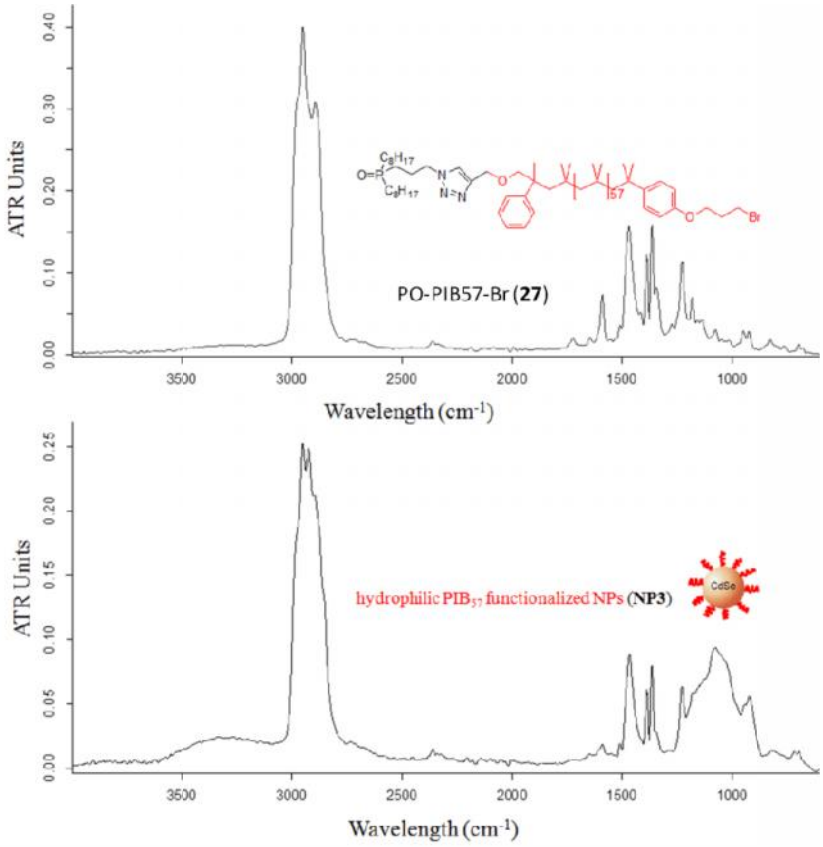

Figure S28. IR spectra of (A) α-phosphineoxide-γ-bromo telechelic polyisobutylene (PO-PIB_{57}-Br) (**27**) and (B) hydrophobic PIB_{57} covered CdSe NPs (**NP3**).

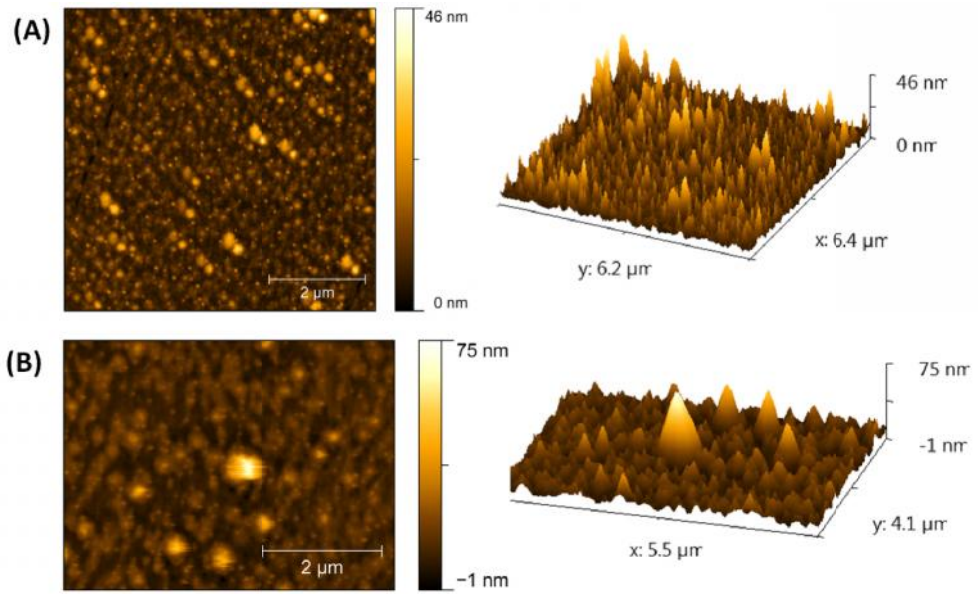

Figure S29. AFM height image of hydrophobic PIB covered NPs (**NP3**) transferred at a surface pressure of (A) 20 mN/m and (B) 30 mN/m.

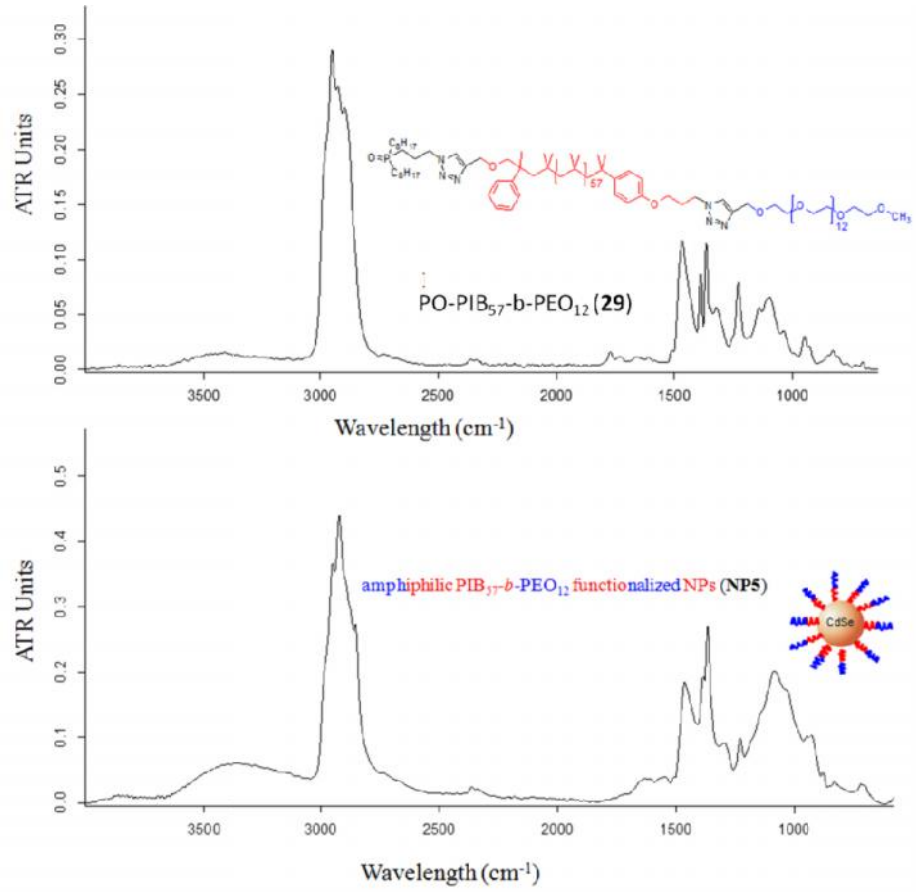

Figure S30. IR spectra of (A) α-phosphineoxide-γ-polyethylene oxide telechelic PIB (PO-PIB_{57}-*b*-PEO_{12}) (**29**) and (B) amphiphilic PIB_{57}-*b*-PEO_{12} covered CdSe NPs (**NP5**).

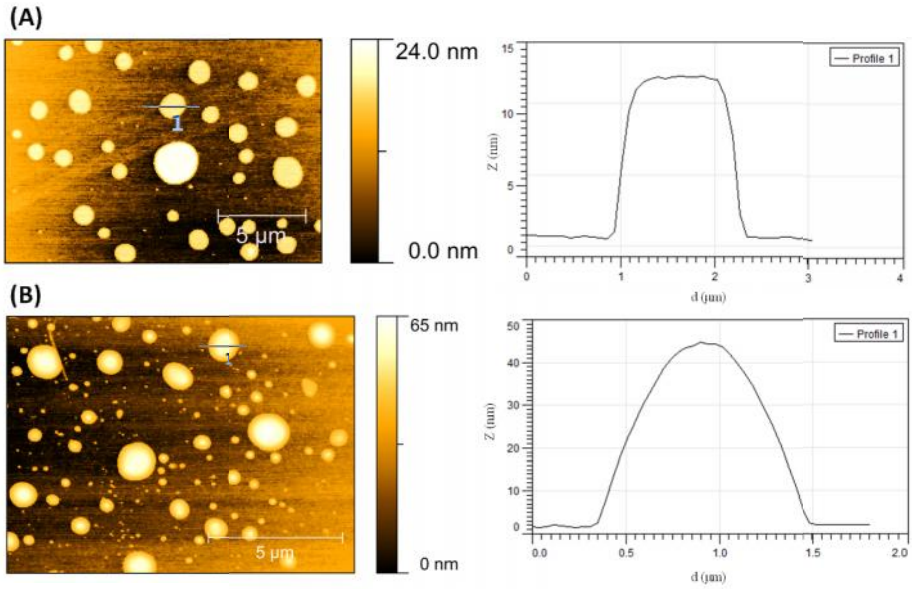

Figure S31. AFM height image and cross section measurement of mixed DPPC:PIB_{87}-*b*-PEO_{17} 80:20 mol% transferred at surface pressure of 30 mNm^{-1} (A) without NPs. (B) with hydrophobic PIB covered CdSe NPs (**NP3**).

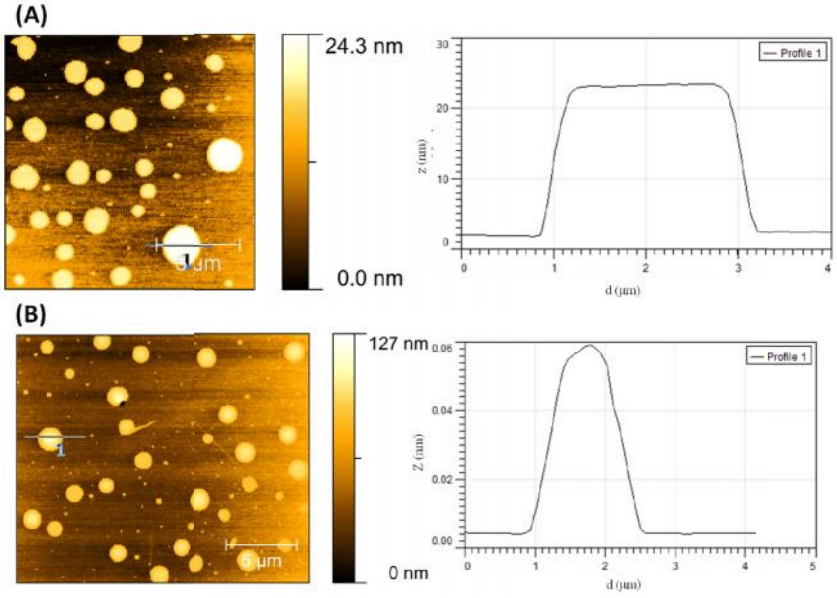

Figure S32. AFM height image and cross section measurement of mixed DPPC:PIB_{87}-*b*-PEO_{17} 60:40 mol% transferred at surface pressure of 30 mNm^{-1} (A) without NPs. (B) with hydrophobic PIB covered CdSe NPs (**NP3**).

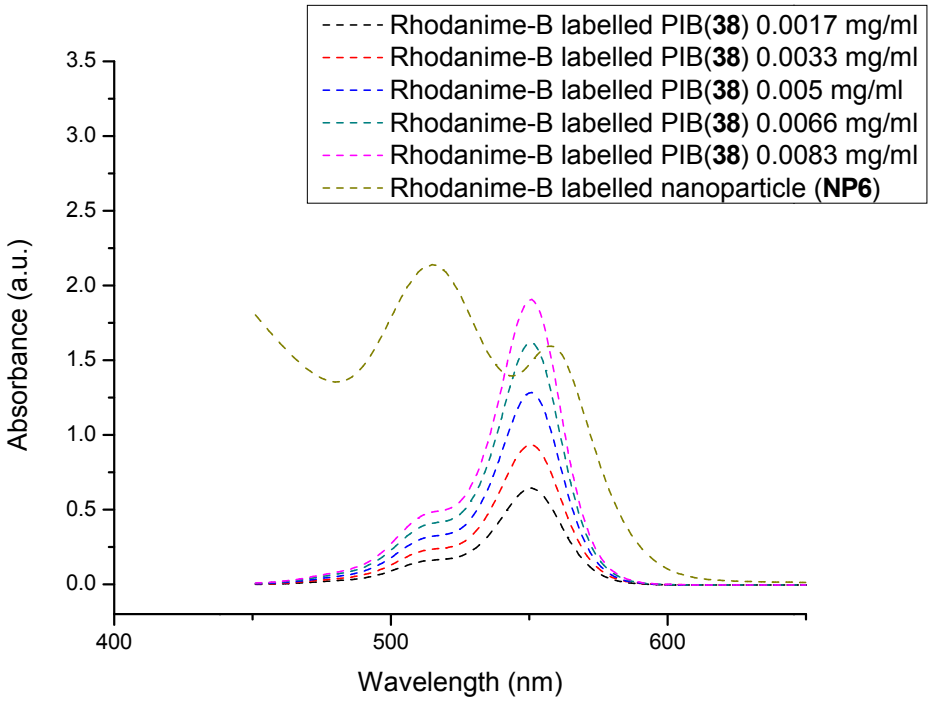

Figure S33. Absorption spectra of rhodamine-B labeled PIB (**2**) and rhodamine-B labeled PIB CdSe nanoparticles (**NP6**) at different concentrations.

Table S2. Change in surface pressure of pure DPPC, pure PIB_{87}-*b*-PEO_{17} and binary mixture of DPPC and PIB_{87}-*b*-PEO_{17} with addition of hydrophilic PEO47 covered CdSe NPs at varying initial surface pressure π_0

substance	targeted surface pressure (mNm^{-1})	starting surface pressure (π_0) (mNm^{-1})	equilibrium surface pressure (π_{eq}) (mNm^{-1})	change in surface pressure ($\Delta\pi = \pi_{eq} - \pi_0$) ($mNm^{-1}$)
pure DPPC	10	9.58	20.29	10.71
pure PIB_{87}-*b*-PEO_{17}		9.62	12.91	3.29
DPPC: PIB_{87}-*b*-PEO_{17} 80 : 20		9.62	17.06	7.44
DPPC: PIB_{87}-*b*-PEO_{17} 60 : 40		9.62	14.64	5.02
pure DPPC	20	19.64	27.13	7.49
pure PIB_{87}-*b*-PEO_{17}		19.63	20.79	1.16
DPPC: PIB_{87}-*b*-PEO_{17} 80 : 20		19.63	24.31	4.68
DPPC: PIB_{87}-*b*-PEO_{17} 60 : 40		19.63	23.22	3.59
pure DPPC	30	27.87	31.87	3.74
pure PIB_{87}-*b*-PEO_{17}		29.04	~29.0	0
DPPC: PIB_{87}-*b*-PEO_{17} 80 : 20		28.95	31.36	2.41
DPPC: PIB_{87}-*b*-PEO_{17} 60 : 40		29.13	30.64	1.51

Calculation of NPs surface coverage via TGA

$$\rho\left(\frac{chains}{nm^2}\right) = \frac{\Delta weight\ X\ 6.022.10^{23}}{M_{w_{Polymer}} X\ A_{NP}} \qquad (\boldsymbol{equation\ S1})$$

where ρ(chains·nm^{-2}) is the immobilized polymer chains density, Δ weight is the weight loss due to the organic material decomposition, $Mw_{polymer}$ is the molecular weight of the polymer and A_{NP} is the surface area of nanoparticles. Inserting this into the above expression gave a chain density of 0.5 chains/nm^2 for the hydrophobic PIB_{57} covered CdSe nanoparticles 0.47 chains·nm^{-2} for the hydrophilic PEO_{47} covered CdSe NPs and 0.53 chains·nm^{-2} for the PO-PIB_{57}-*b*-PEO_{12} covered nanoparticles.

10.3 Appendix 3

10.3.1 Phase changes in mixed lipid/polymer membranes by multivalent nanoparticle recognition

This supplementary was published in Langmuir, 2013, DOI: 10.1021/la403763v

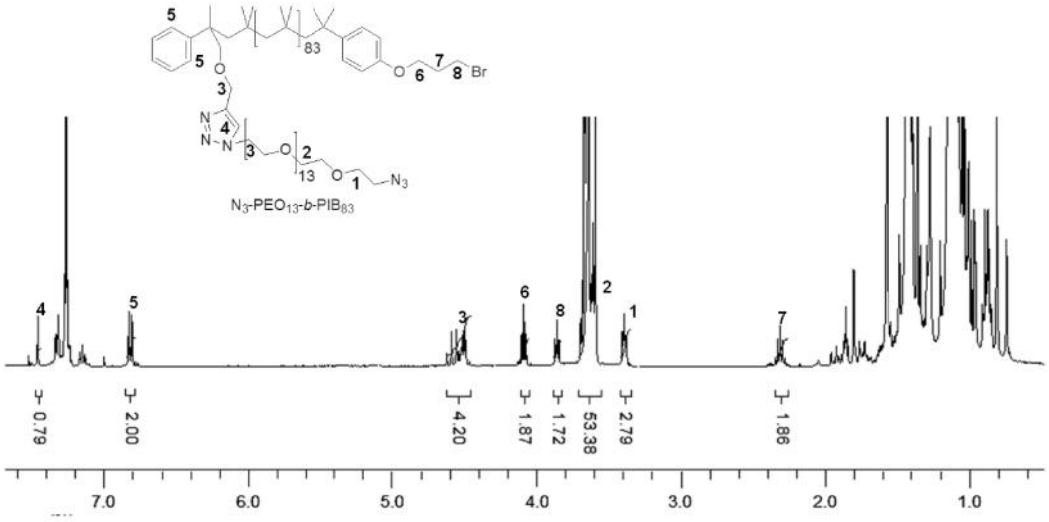

Figure S34. Proton NMR spectrum of compound (**17**).

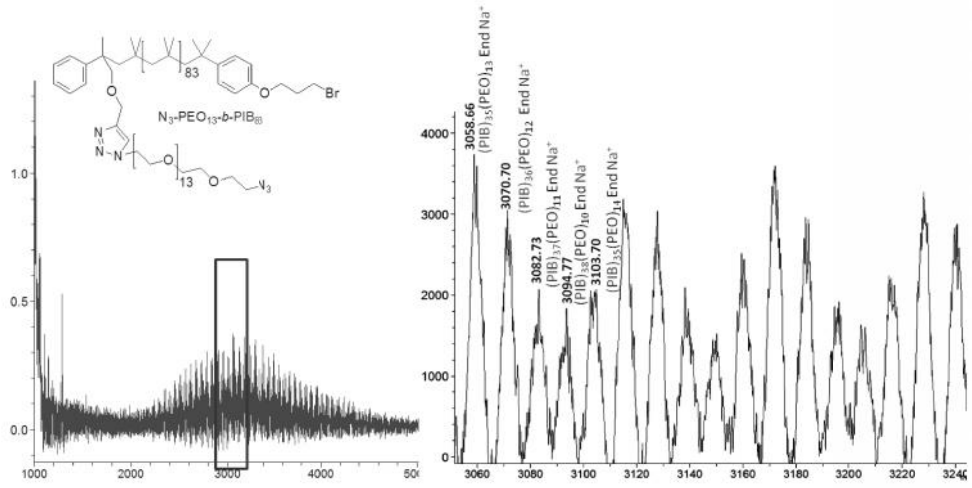

Figure S35. MALDI-TOF mass spectrum of compound (**17**).

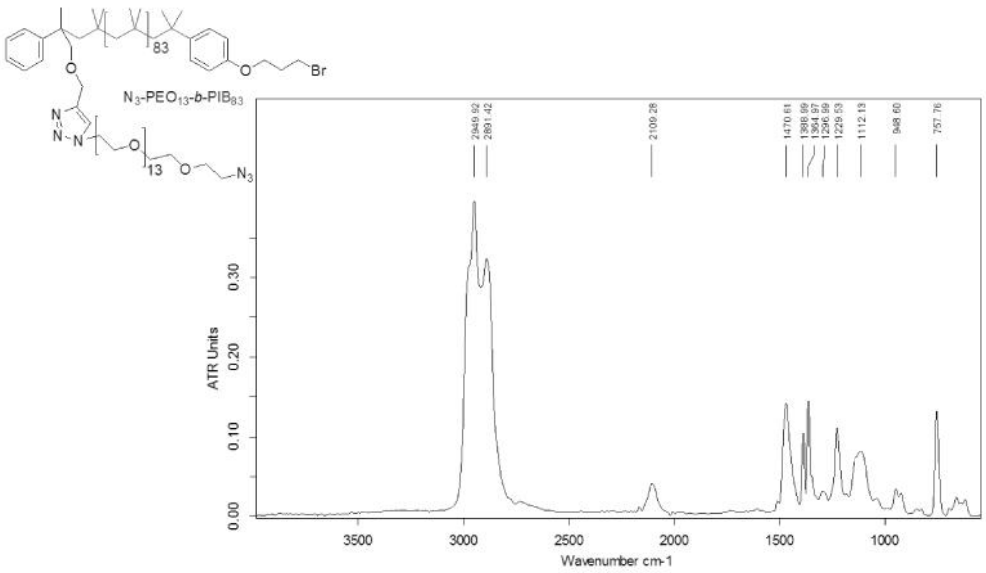

Figure S36. FT-IR spectrum of compound (**17**) with the characteristic adsorption band of the azide chain end at ~2100 cm^{-1}.

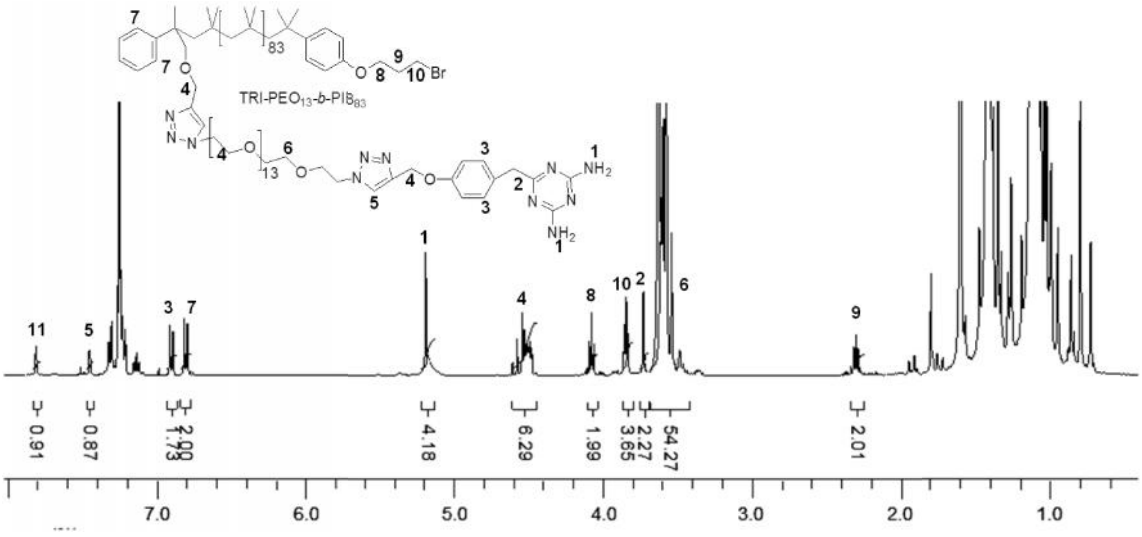

Figure S37. Proton NMR spectrum of compound (**20**).

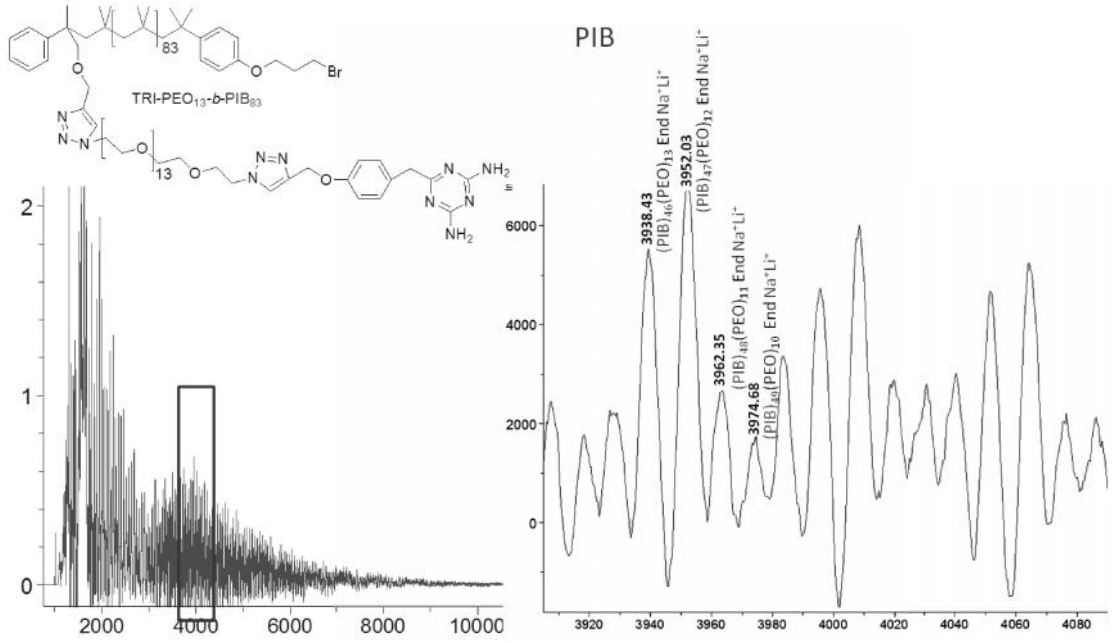

Figure S38. MALDI-TOF mass spectrum of compound (**20**).

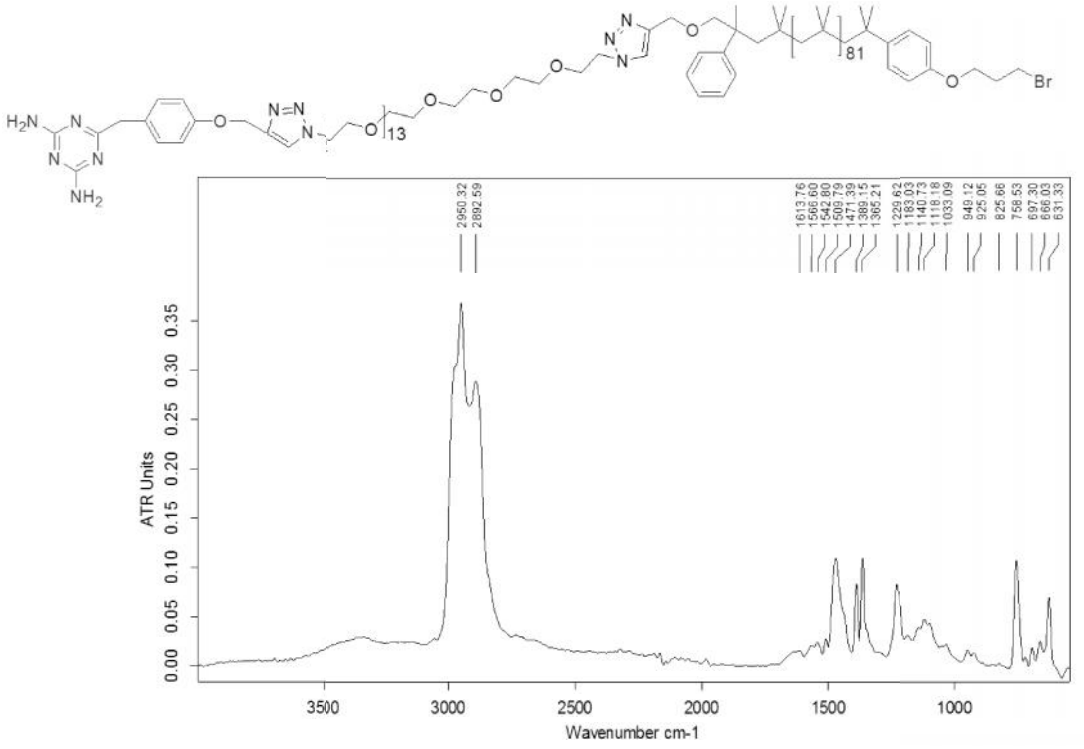

Figure S39. FT-IR spectrum of compound (**20**) showing no residual azide content.

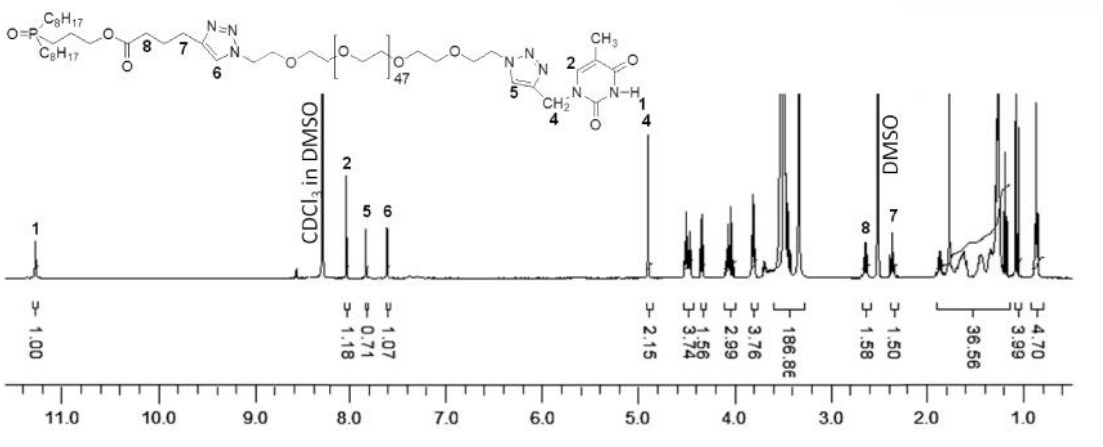

Figure S40. Proton NMR spectrum of compound (**35a**).

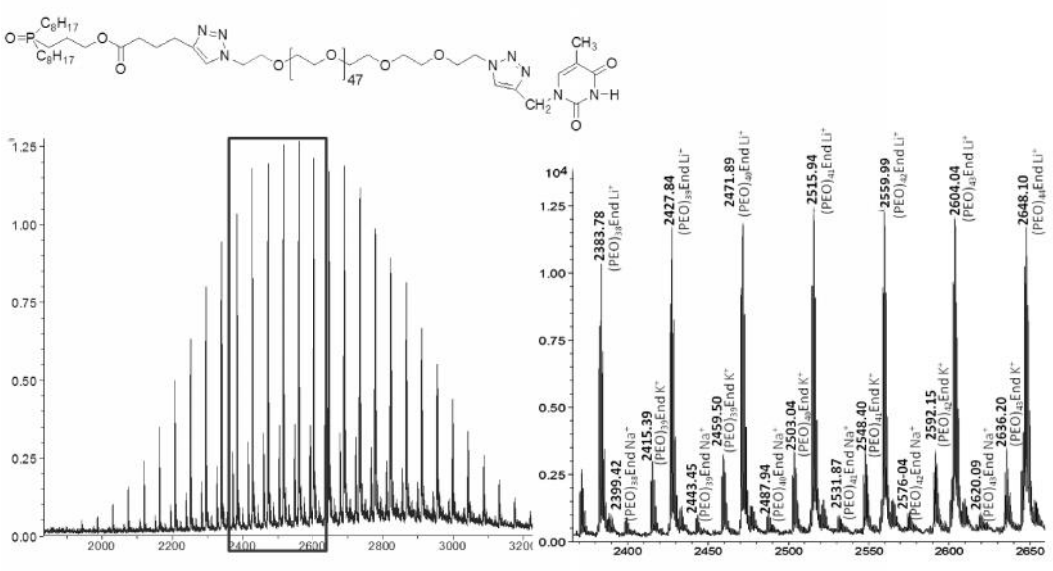

Figure S41. MALDI-TOF mass spectrum of compound (**35a**)

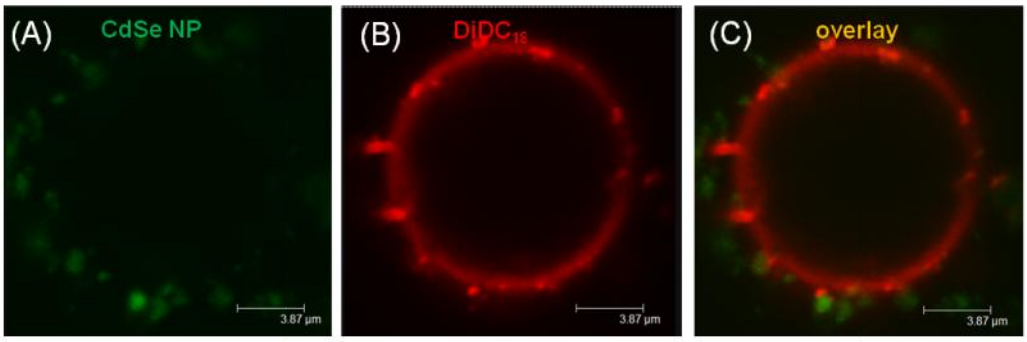

Figure S42. Confocal microscopy images of freshly prepared hybrid GUVs composed of DPPC and 16 mol% TRI-PEO_{13}-*b*-PIB_{83} BCP (**20**) showing the binding of the NPs to the membrane in the first 5 to 10 mins of NP addition (**NP8**).

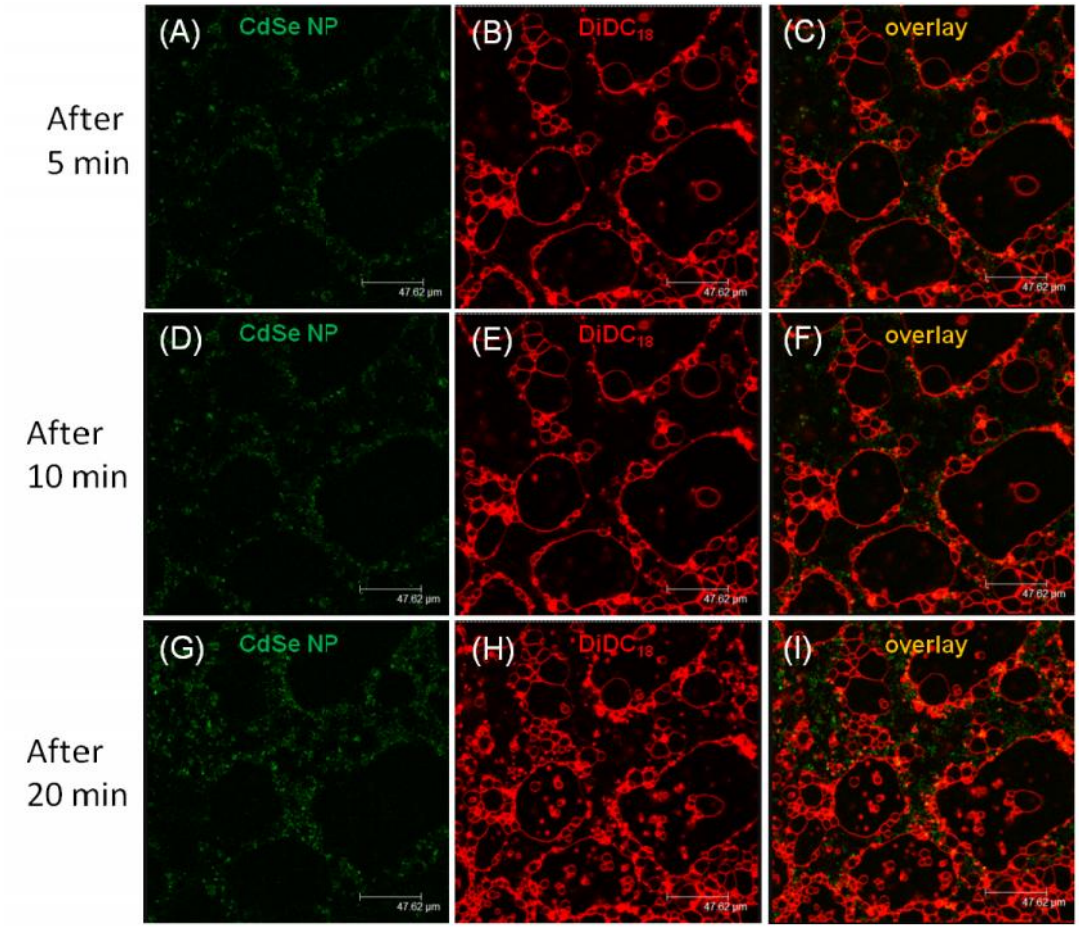

Figure S43. Hybrid GUVs prepared from mixtures of DOPC and 10 mol % of TRI-PEO_{13}-*b*-PIB_{83} BCP (**20**) showing a destruction of the vesicles (via membrane rupture) with time, which was induced by NP addition (**NP8**).

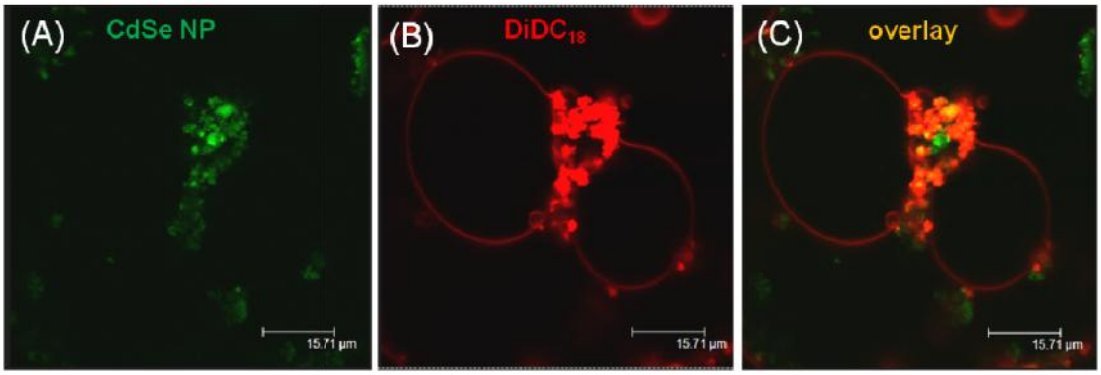

Figure S44. Hybrid GUVs prepared from mixtures of DOPC and 10 mol % of TRI-PEO_{13}-*b*-PIB_{83} BCP (**20**). Panel (A-C) shows the specific attraction of **NP8** into the polymer rich areas of the vesicles inducing membrane rupture.

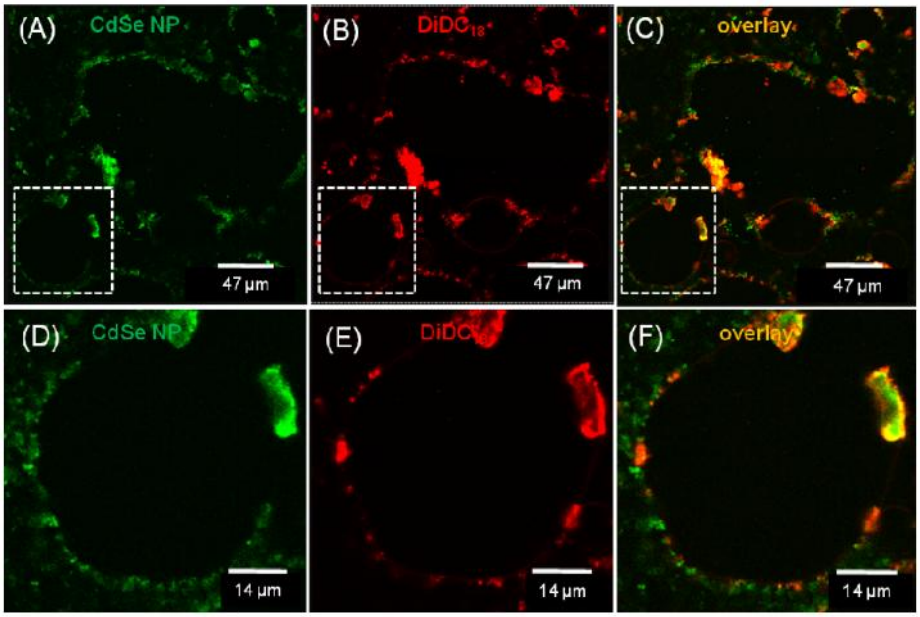

Figure S45. Hybrid GUVs prepared from mixtures of DOPC and 10 mol % of TRI-PEO_{13}-*b*-PIB_{83} BCP (**20**). Panel (A-C) shows overview of destroyed vesicles, Panel (D-F) depicts a magnification of a single destroyed GUV (after ~30 mins of NP addition) displaying no intact bilayer membrane.

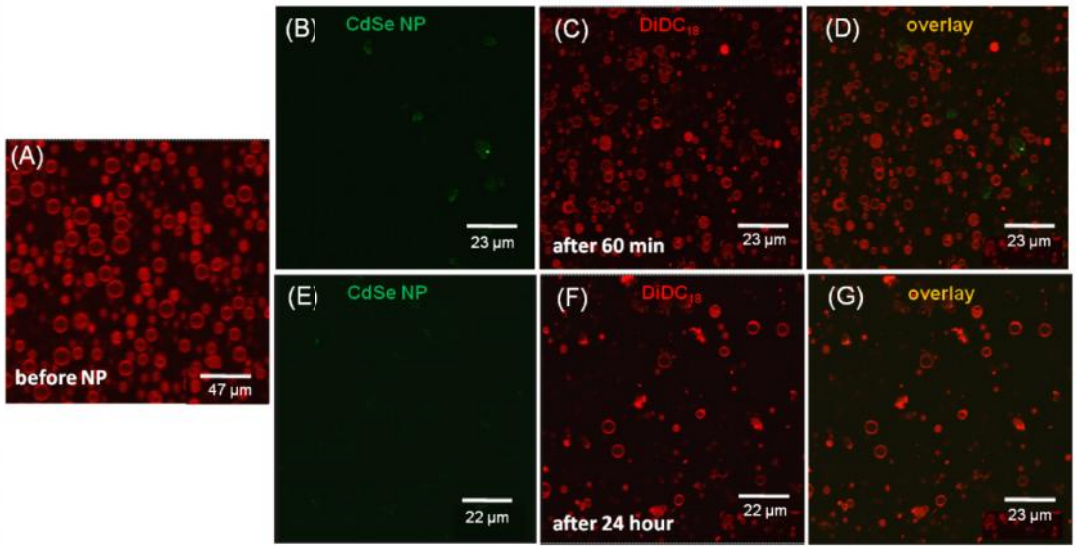

Figure S46. Hybrid GUVs prepared from a ternary mixture of DOPC with 15 mol% of PEO_{17}-*b*-PIB_{87} BCP (**1**) and 5 mol% of TRI-PEO_{13}-*b*-PIB_{83} BCP (**20**). Panel (A) shows an overview image of hybrid GUVs before NP addition. Panel (B-D) shows an over view after 60 mins of **NP8** addition. Panel (E-G) depicts an over view after 24 hours of **NP8** addition.

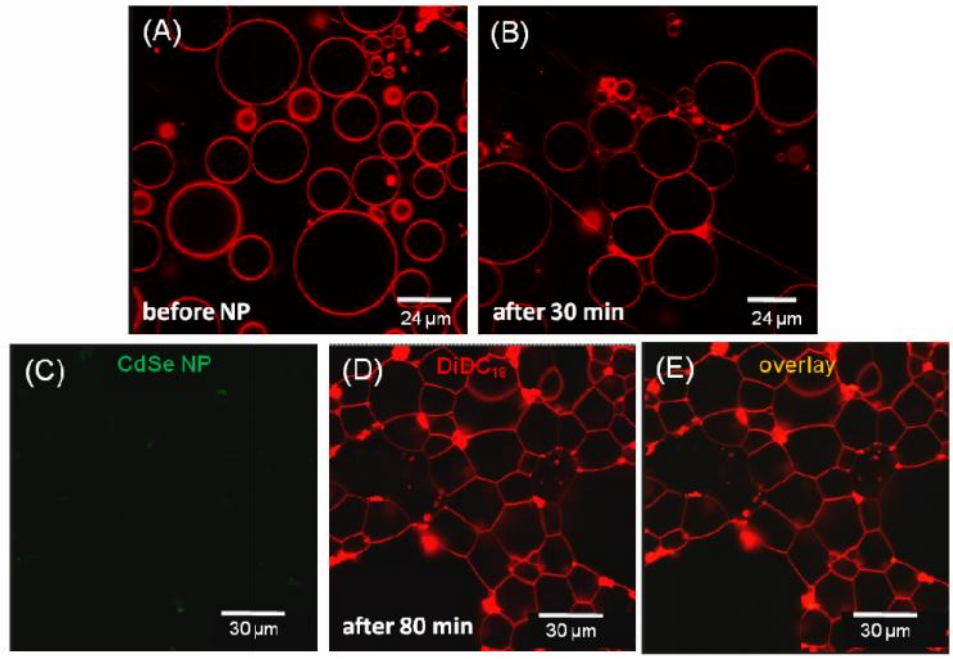

Figure S47. Confocal microscopy images of GUVs prepared from pure DOPC showing stable GUVs after addition of **NP8** (monitored over several hours).

Acknowledgment

I would like to express my sincere gratitude to my supervisor Prof. Dr. Wolfgang Binder, for the opportunity he gave me to work on this interesting topic, his guidance, patience, encouragements and positive suggestions throughout my PhD thesis.

Special thank goes to the Forschergruppe FOR 1145 for the financial support.

I would like to say thank you to Frau Anke and my colleagues in the Arbeitgruppe Binder, it was a real pleasure to work with them in an enjoyable environment. Special thanks to Matthias Schulz for his friendship and help.

I extend my sincere thanks to Prof. Jörg Kressler for giving me the permission to conduct experiments on his Langmuir film-balance and fluorescence microscope, and for providing me with a friendly environment in his laboratory.

I express my thanks to the group of Prof. Alfred Blume for the discussion about my results and for measurements conducted on the fluorescence spectrophotometer and the Langmuir adsorption film-balance.

A number of people made my stay in Halle a pleasant one. I would like to take the opportunity to thank all my friends.

Special thanks to my mother for her prayers, my sister and brothers who are always there for me, and for their constant support and encouragement.

And above all, my eternal gratitude goes to Almighty God for carrying me on His wings of love.

OLUBUMMO ADEKUNLE AYODELE

An der Feuerwache 3, 06124. Halle-Saale Germany.
Telephone: +491626472164
E-Mail: olubummo.adekunle-ayodele@student.uni-halle.de

SUMMARY AND GOAL

A highly talented and enthusiastic polymer material scientist with great deal of experience in the synthesis, characterization, testing and processing of polymers.

Looking to expand upon my years of research and production experience in polymer science and contribute to the development of new products in a leading polymer institution.

EDUCATIONAL QUALIFICATION

2010 to Date	**Doctorate Degree (PhD) Macromolecular Chemistry (In view)** **Martin Luther University Halle-Wittenberg, Germany**
Dissertation	Interaction of polymers and nanoparticles with cell membrane - *Institute of chemistry,* Macromolecular Chemistry Martin Luther University Halle-Wittenberg, Germany.
Area of concentration	Synthesis of amphiphilic block copolymer and nanoparticles. The functionalization of nanoparticles surface with polymers and investigating their location and interaction within lipid membranes.
2007- 2009	**Master of Science Degree (Msc) in Applied Polymer Science,** **Martin Luther University Halle-Wittenberg, Germany.**
Master-thesis	Synthesis and crossover reaction of TEMPO containing block Copolymers via ROMP - *Department of Engineering Sciences* Martin Luther University Halle-Wittenberg, Germany.
Area of concentration	The synthesis of block copolymers using ring opening methathesis polymerization and their analysis using NMR, GPC, WAXS, MALDI-TOF, XRD, TEM, TGA and DSC.
1998-2003	**Bachelor of Technology Degree (B.Tech) in Industrial Chemistry, Federal University of Technology Akure, Ondo - State, Nigeria.**

SPECIALIZED SKILLS

Data processing	MS Office, MS PowerPoint, Origin Pro, Corel Draw, Chem Office, Scifinder, ISIS Draw, Materials Studio, Beilstein, Gwyddion and Matlab.
Analytical methods	NMR, GPC, AFM, SAXS, DSC, MALDI-TOF, WASX, XRD, TGA,HPLC, UV-VIS,IR,ESI-TOF,DLS, DMA FTIR, Langmuir monolayer, fluorescence monolayer and Laser scannining microscopy.
Polymerization Methods	Living Carbocationic Polymerization (LCCP), Living Anionic Polymerization, Living Radical Polymerization (NMP, ATRP, RAFT), Ring Opening Metathesis polymerization (ROMP) and Polycondensation
Languages	English (Very good) and German (Intermediate).

PERSONAL INTERESTS

Driving, Traveling, Sport (Football, Basketball and Table-Tennis), Music (playing the bass guitar), Walking and Reading.

PUBLICATIONS

Olubummo, A.; Tanner, S.; Binder, W. H.	**Synthesis and crossover reaction of TEMPO containing block copolymer via ROMP** *Beilstein J. Org. Chem.* **2010**, 6, 59.
Olubummo, A.; Herbst, F., Hackethal, K.; Binder, W. H.	**Synthesis of Non-symmetrically Chain End Functionalized Polyisobutylene** *J. Polym. Sci. Part A: Polymer Chemistry,* **2011,** 49, 2931-2940.
Schulz, M.; **Olubummo, A.;** Binder, W. H.	**Beyond the Lipid-Bilayer: Interaction of Polymers and Nanoparticles with Membranes** *Soft Matter,* **2012**, 8, 4849-4864.
Olubummo, A.; Schulz, M.; Lechner, B.-D.; Scholtysek, P.; Bacia, K.; Blume, A.; Kressler, J.; Binder, W. H.	**Controlling the Localization of Polymer-Functionalized Nanoparticles in Mixed Lipid/Polymer Membranes** *ACS Nano,* **2012**, *6*, 8713–8727.
Barqawi, H.; Schulz, M.; **Olubummo, A.**; Sauerland, V.; Binder, W. H.	**2D-LC/SEC-(MALDI-TOF)-MS characterization of symmetric and nonsymmetric biocompatible PEOm-PIB-PEOn block copolymers** *Macromolecules*, **2013**, 46, 7638-7649.
Schulz, M.; **Olubummo, A.** Bacia, K. and Binder, W. H.	**Lateral surface engineering of hybrid lipid/BCP vesicles and selective nanoparticle embedding** *Soft Matter,* **2014,** 10, 831-839
Olubummo, A.; Schulz, M.; Regina Schöps; Kressler, J.; Binder, W. H.	**Phase Changes in mixed lipid/polymer membranes by multivalent nanoparticle recognition** *Langmuir,* **2014**, *30, 1, 259-267*

PERSENTATION AND INTERNATIONAL CONFERENCES

Olubummo A.; Binder W. H.; Pulamagatta B.; Schulz M.; Sachsenhofer R.	*Interaction of polymer and nanoparticles with lipid membranes* **EUROMAT 2011** Montpellier, France. 12 – 15 Sept. 2011 (Oral presentation)
Olubummo A.; Schulz M.; Lechner B.-D.,Kressler J.; Binder W. H.	*Localization of polymer-functionalized nanoparticles in mixed lipid/polymer membranes –Variation of the NP hydrophobicity* **15th international conference of polymeric materials** Halle-Saale Germany 12 - 14 Sept. 2012 (Oral presentation)
Olubummo A.	*The International Plastics Showcase* **ANTEC 2012** Orange County Convention Center Orlando, Florida USA 1 – 5 April 2012 (Attendee)

AWARD

2009: DOW (Chemical Company) Olefinverbund GMBH Scholarship	For above average achievements and for demonstrating a particular commitment to science.

REFEREES

1. Prof. Dr. Wolfgang Binder
   Martin-Luther University Halle-Wittenberg
   Institute of Chemistry
   Von-Danckelmann-Platz 4
   D-06120 Halle
   Phone: +49-(0)345/55-25930
   E-mail: wolfgang.binder@chemie.uni-halle.de

2. Prof. Dr. Jörg Kressler
   Martin-Luther-University Halle-Wittenberg
   Department of Engineering Sciences
   Von-Danckelmann-Platz 4
   D-06120 Halle
   Phone: +49-(0) 345/55-25800
   E-mail: joerg.kressler@chemie.uni-halle.de

Eigenständigkeitserklärung

Hiermit erkläre ich an Eides statt, dass ich die vorliegende Dissertation („Controlling the location of polymer functionalized (CdSe) nanoparticles in mixed lipid/polymer membranes“) selbständig und ohne fremde Hilfe verfasst, andere als die von mir angegebenen Quellen und Hilfsmittel nicht benutzt und die den zitierten Werken wörtlich oder inhaltlich entnommenen Stellen als solche gekennzeichnet habe. Weiterhin versichere ich, dass die vorliegende Arbeit noch an keiner anderen Einrichtung zur Begutachtung vorgelegt wurde.

Halle (Saale),

.....

Adekunle Olubummo